Production of Bioelectricity from Chlamydomonas reinhardtii Microalgae and Quinones

Marc Arderiu I Romero

Sorbonne Université

Ecole Doctorale de Chimie Physique et Analytique de Paris Centre

ED388

UMR 8640 : Laboratoire P.A.S.T.E.U.R

Groupe « Chimie Physique et Biologique de la Matière Vivante »

Production of Bioelectricity from *Chlamydomonas reinhardtii* Microalgae and Quinones

Par Marc ARDERIU I ROMERO

Thèse de doctorat de Physico-Chimie Analytique

Dirigée par Frédéric LEMAÎTRE

Présentée et soutenue publiquement le 27 Septembre 2023

Devant un jury composé de :

Mme Marie ERARD, PR, Université Paris-Saclay	Rapportrice
M. Stéphane ARBAULT, DR, Université de Bordeaux	Rapporteur
M. Emmanuel MAISONHAUTE, Professeur des Universités	Examinateur
M. Frédéric LEMAITRE, PR, Sorbonne Université	Directeur de Thèse
M. Benjamin BAILLEUL, CR, Institut Biologie Physico-Chimique	Co-Encadrant (Invité)

TABLE DES MATIÈRES

REMERCIEMENTS

J'ai toujours su que je voulais contribuer à trouver des sources alternatives d'énergie. Or, je n'aurais jamais deviné que je finirais pour défendre cette thèse à Paris. Je tiens à remercier en tout premier lieu **Frédéric Lemaître**, mon directeur de thèse, et aussi la personne qui m'a fait la confiance de m'accueillir au sein l'UMR8640 pendant la période difficile de la pandémie. Ça n'a pas été toujours facile, et co-diriger une thèse entre deux unités reste toujours un défi, mais il a toujours tenu à garder le calme, et redresser le chemin quand il fallait pendant ces trois années pour aboutir à ce manuscrit. Je le remercie aussi pour m'avoir transmis sa rigueur scientifique et nos discussions ainsi que pour le privilège de me laisser explorer le monde des quinones et des algues et ses enseignements au-delà du scientifique. Je veux aussi le remercier pour m'avoir appris sur la nécessité de s'écouter soi-même.

Je tiens également à remercier **Benjamin Bailleul**, car c'est grâce à lui que j'ai rencontré les électrochimistes de l'ENS. Je le remercie d'avoir été mon co-directeur malgré le fait d'être tiraillé de tous les côtés par ses multiples engagements et sa facilité de distiller des sujets aussi complèxes. Depuis ces 5 dernières années, il m'a instillé la curiosité de rentrer dans le monde de la fluorescence et de faire de l'IBPC un espace bienveillant même sans lumière extérieure.

Je remercie de même **Manon Guille-Collignon**, pour son temps d'encadrement, ses commentaires et apports a mes textes et présentations, et pour les chocolats dans mon bureau quand je me sentais écrouler.

Je remercie aussi **Marie Erard**, **Stéphane Arbault** et **Emmanuel Maisonhaute** pour la relecture du manuscrit et d'avoir fait partie du jury.

A l'IBPC, je remercie **Sandrine Bujaldon**, qui a sauvé mes cultures de Chlamydomonas à plusieurs reprises et pour animer la paillasse avec la meilleure sélection des hits musicaux de l'année. Je remercie aussi **Sophie Landier** pour le stockage en continu des milieux de culture, **Suzanne Ferté** pour m'avoir montré comment utiliser les « Joliot » et son enthousiasme contagieux pour le partage de la connaissance scientifique. **Julien Sellés** et **Marcio Rodrigues** merci de m'avoir aidé à interpréter mes résultats et **Olivier Vallon** pour sa connaissance de « Chlamy ». A **Erik Jensen** hacerme sentir en Barcelona estando a 835km de distancia, actuar casi como un mentor y volver menos solitarias las manips en horas intempestivas. **Eliora**, **Marcelo**, **Amel**, **Katia**, **Alessandro**, **Sofia**,

Clotilde, **Oliver**, **Hugo** et autant d'autres étudiants en stage, doctorants et postdocs pour animer le sous-sol et le jardin de l'IBPC.

A l'ENS, je voudrais remercier **Jêrome Delacotte** de m'avoir aidé avec les couplages fluorescence-électrochimie. Merci aussi encore a tous ceux avec qui j'ai partagé des hauts et des bas dans un autre bureau au sous-sol, la « mezzanine ». En particulier, **Aliénor**, **Yoan**, **Majohly**, **Ian**, **Pierre Louis**, **Valentine** et **Fayrouz**. Je tiens à les remercier pour tout ce temps ensemble rempli des discussions sur l'avenir, des journées masquées (covid oblige et non masquées et tous les moments de partage). Je n'oublie pas non plus notre mezzanine jumelle et les couloirs de l'ENS avec **Léonard, Chems, Scott**, **Laura**, **Lucas**, **Marie Aude**, **Lucie**, **Emma**, **Mrinal**, **Hélène**, **Thomas**, **Glen** etc. Merci d'avoir maintenu l'idée d'un esprit collectif au laboratoire.

Partir pour Paris a supposé la rencontre de multitude de gens qui ont fini pour intégrer un tissu de liens d'amitié, amour et connaissances et le gain de deux dioptries et le droit de porter des lunettes à l'allure de savant. Merci infiniment pour ces 5 années **Albin**, **Giulio**, **Fanny**, **Guillermo**, **Camila**, **Mariana**, **Miranda**, **Lilas**, **Jonathan**, **Miguel**, **Alicia**, **Shubham**, **Chiara**, **Paula**, **Sonia**, **Natalia**, **Zahra**, **Santino**, **Akhsay**, **Neus**, **Hamid**, **Hannes**… Merci à **Shéryl**, qui était la dés le début et que j'ai aimé de tout mon coeur.

Enfin mes remerciements vont vers toutes mes autres familles qui sont restées à Barcelone ou ailleurs. Tot i que cadascun dels Lehninguers hagi acabat en un cantó diferent d'Europa, gràcies per encoratjar-me a arribar fins aquí i poder gaudir de les vostres defenses de tesi al llarg d'aquests darrers anys. A ma mare, mon pare, mon germà i tota la família perquè sense ells jo no ho sóc.

LISTE DES PRINCIPALES ABRÉVIATIONS

ATP : adénosine triphosphate

2,6-DCBQ : 2,6-Dichlorobenzoquinone

2,5-DCBQ : 2,5-Dichlorobenzoquinone

2,6-DMBQ : 2,6-Diméthylbenzoquinone

2,5-DMBQ : 2,5-Diméthylbenzoquinone

DCMU : Diuron (3-(3,4-DiChlorophenyl)-1,1-diMethylUrea)

E° : potential standard d'un couple redox (en V / ESH)

E°' : potential standard apparent (à pH 7.4) d'un couple redox (en V / ESH)

ITO : indium tin oxide (oxyde d'indium dopé à l'oxyde d'étain)

JTS : Joliot Type Spectrometer

LHC : Light Harvesting Complex

µE : µmol photons

NADPH : Nicotinamide Adénine Dinucléotide Phosphate réduit

NBQ : Naphtobenzoquinone

PETC : photosynthetic electron transport chain

Pmf : proton motive force

PPBQ : Phényl-para-Benzoquinone

PQ : Plastoquinone

PQH_2 : Plastoquinol

PSI/PSII : photosystème I/ photosystème II

Q : forme oxydée des quinones

QH_2 : forme réduite des quinones

RC : reaction center

ROS : reactive oxygen species

WOEC : water Oxidizing Evolving Complex

WT : wild Type

GENERAL INTRODUCTION

Within the current energy context, using photosynthetic organisms as relays for light-to-electricity transformation is both a hope and a potentially environmentally-friendly approach, while taking advantage of solar energy, an infinite resource on a human scale. Who wouldn't dream of buildings and complexes covered in plants that, in perfect synergy with them, would deliver the electrical energy we need while at the same time respecting nature and its biodiversity?

The principle would then be to use the photosynthetic apparatus as a photoconverter, diverting part of the endogenous electron flow circulating along the photosynthetic chain. Ideally, this harvesting would be performed in a non-invasive and beneficial way, alleviating the chain of the damaging electron excess resulting from the presence of kinetically determining steps and electron bottlenecks. This idea, first developed in the early 2000s, has encountered an unresolved issue: embedded within the photosynthetic organism, the electron transfer chain is difficult to access from the collecting electrode. This challenge can only be overcome by working on organism-derived fragments (PSII, thylakoid membrane... which have difficulties in functioning outside their natural environment) or by using redox mediators (quinones, $Fe(CN)_6^{3-}$, electroactive polymers...) which ensure formal electron transport to the electrode (but which may themselves have access difficulties or present side effects on the organism).

Within the framework of the LABEX DYNAMO project led by the Institut de Biologie Physico-Chimique in 2012, the "Bioelectrochemistry" team of UMR 8640 (Department of Chemistry, Ecole Normale Supérieure) began a collaboration with IBPC's UMR 7141 ("Biologie du chloroplaste et perception de la lumière chez les micro-algues") on the subject of "photosynthetic electron extraction", with the idea of testing a strategy involving the microalga Chlamydomonas reinhardtii as a model photosynthetic organism and benzo-1,4-quinone-type structures (commonly known as "quinones" in the vocabulary of molecular electrochemists). The work carried out from the beginning of the project to date has demonstrated the efficiency of quinones as redox mediators and photocurrent production agents from microalgae suspensions. However, the interactions between quinones and the photosynthetic organism are far from unambiguous, and raise the question of side effects related to their molecular structures. It is therefore necessary to study these interactions in detail, using relevant observables to draw up a "fingerprint" or identity card for each quinone considered, which is the main aim of this thesis.

The 1st chapter presents and summarizes the state of the art. The basics of natural photosynthesis will be outlined in order to better understand the complexity of this fundamental natural phenomenon. The various pathways for the extraction of photosynthetic electrons will then be discussed, followed by a presentation of the main results obtained as part of the LABEX DYNAMO project.

The 2nd chapter will include a first article published in the journal ChemElectroChem, dealing with the screening of several quinones in terms of bioelectrochemical performance, i.e. photocurrent

production from suspensions of Chlamydomonas reinhardtii microalgae. The question of poisoning (in the meaning of decreased and/or unstable bioelectricity production) is also at the heart of this article, which shows that "reading" an electric current is insufficient to fully capture the complexities of quinone effects. It shows how difficult is to understand the structure-activity relationship and that finding other observables along the photosynthetic chain are needed.

The 3rd chapter is based on a second article on how best to quantify and analyze PSI activity. This work then leads on to the application of this methodology to interactions between quinones and PSI in particular.

The 4th chapter corresponds to a 3rd article which focuses on the effect of two model quinones (2,6-dichloro-1,4-benzoquinone or 2,6-DCBQ and 2,6-dimethyl-1,4-benzoquinone or 2,6-DMBQ) on the photosynthetic chain, using various observables (PSII, ATPSynthase, PSI, respiratory chain) as a basis for investigation.

Finally, **a general conclusion** summarizes the main points of this work and outlines future prospects and follow-up.

Chapter I

Introduction to Natural Photosynthesis and The Harvesting of Photosynthetic Electrons

1. A brief energy context

Humanity is facing a polycrisis, with not evenly distributed rapid growth of populations needing to electrify their lives to improve their life standard conditions, rising global energy demands, scarcity of natural resources and slow pace decarbonization of human activities. Accordingly, it is imperative to move away from non-renewable energies and close the accumulative energy demand gap [1]. In this context, with Earth receiving (about 24x1020 kJ/year, or 120000 TW) on average 10.000 times more energy from the sun on any given time than energy is needed for current (and expected) human demands, almost none of it being used by nature, solar power is one of the most promising alternative energy sources with already record efficiencies. Therefore, developing a wide array of solar energy harvesting technologies must be fostered.

Currently, the fastest growing, solar energy-using technology is photovoltaics (PV), which directly converts solar energy into a potential difference between two layers of oppositely polarized semiconductor materials, leading to the production of electrical current ("photovoltaic effect"). In 2022, the PV electricity generation capacity exceeded 1000 GW (>3,6% global electricity generation) [2]. However, even as PV installation needs to be accelerated, toxic components of the panels including limited lifespans, toxicity concerns of chemicals involved in producing them, and the vast amounts of scarce minerals needed to produce them [3], opens the space to use the natural occurring phenomena of photosynthesis as a way to produce renewable energy.

2. What is photosynthesis ?

2.1. Generalities on photosynthesis

Photosynthesis underpins almost all form of life on Earth [4], either directly or indirectly. It is complex a process of several energetically unfavorable, (ΔG° = 2867 kJ/mol), physico-chemical reactions in the biosphere conducted by plants, algae and some bacteria, that transforms the energy from sunlight (photons) onto chemical energy by the form of highly energetic bonds in organic molecules. These sugars can subsequently be used by the organism as a source of energy. More particularly, oxygenic photosynthesis (first appeared around 3,5By ago), conducted by cyanobacteria, algae and plants and accomplishes the transformation of carbon dioxide and water into organic molecules (sugars, glucose, starch) with sunlight as energy source, thus releasing oxygen from water oxidation [5] into the atmosphere.

$$6CO_2 + 12H_2O \xrightarrow{h\nu} C_6H_{12}O_6 + 6O_2 + 6H_2O \qquad (\boldsymbol{1})$$

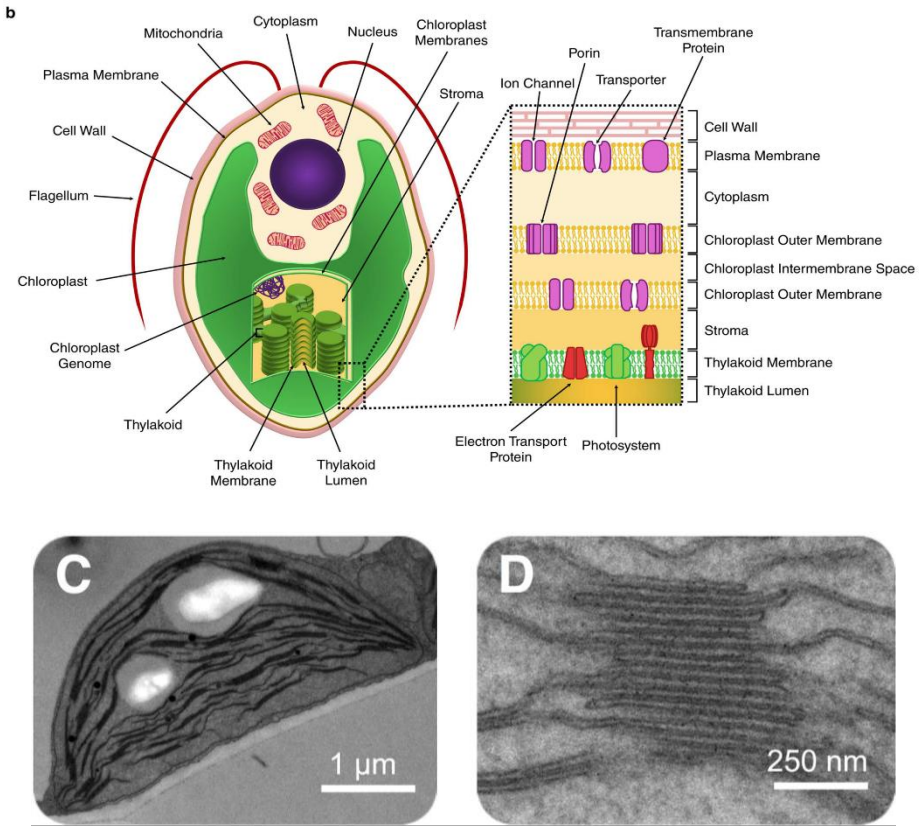

Figure 1. Location of the photosynthetic machinery. *Adapted from references* [6] *and* [7]*. B) Organization of the photosynthetic thylakoid membranes of the eukaryotic microalgae Chlamydomonas reinhardtii (including ATP synthases). C) An electron micrograph of an Arabidopsis chloroplast within the leaf. D) Close-up region of the chloroplast showing the stacked structure of the thylakoid membrane. The grana/lamella organization is found in plants, whereas Chlamydomonas displays only lamellae and loose stacking of thylakoids but no ultrastructure resembling plant grana.*

It is worth mentioning that photosynthesis is a process tightly associated with membranes. Indeed, the vast part of photosynthetic activity on Earth occurs in chloroplasts, intracellular phospholipidic double membrane-bound organelles (see *Figure 1*). The inner space they delimit is filled with a liquid fluid named stroma. Chloroplasts share similarities to cyanobacteria, simpler than eukaryotes gram-negative bacteria, which are thought to be the origin of modern chloroplasts. Both present arrays of membranes where photosynthesis takes place. Those structures are called thylakoids, which are lipidic double membrane structures delimiting an interior called lumen (see *Figure 2*), that can be tightly packed and stacked, ("grana" for they can be seen as granules on an optic microscope) or unstacked as thin layers or "lamellae".

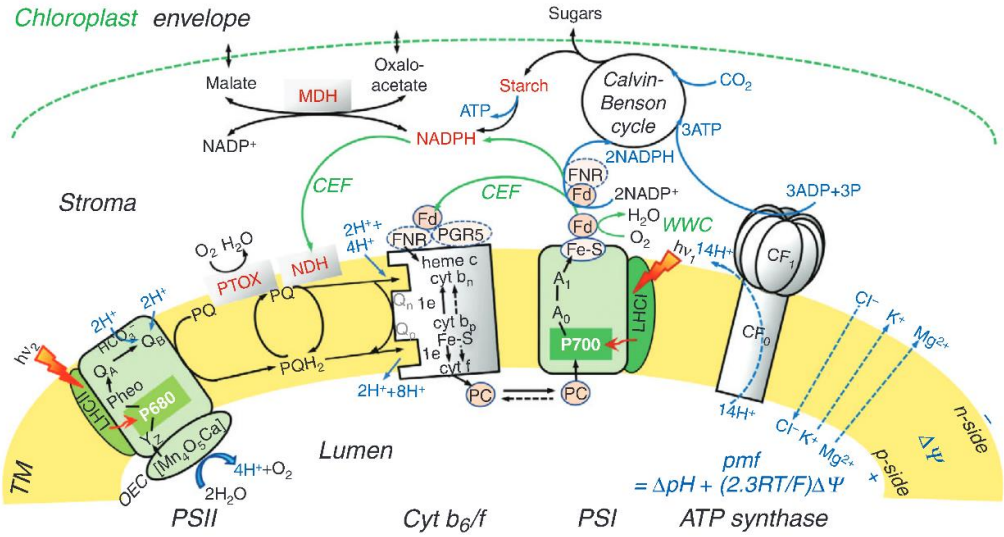

Figure 2. Schematic representation of a photosynthetic electron transport chain (PETC). *Adapted from reference* [8]*. In plants and algae, in the thylakoid membrane (TM) two photosystems (PSII and PSI) connected in series via the cytochrome (Cyt) b6 /f, and the ATP synthase) participate in the production of ATP and NADPH needed for the Calvin– Benson cycle to fix CO_2 to produce sugars. Black lines on the TM indicate linear electron transfer across the membrane to obtain reducing power. Alternative electron flows are indicated in green: cyclic electron flow (CEF) around PSI mediated by Fd (involving Fd-NADP⁺-reductase, FNR, and a proton gradient regulator, PGR5), or NADPH (via NADPH dehydrogenase, NDH); water–water cycle (WWC); chlororespiration (through the plastid terminal oxidase, PTOX); and the malate valve (through malate dehydrogenase, MDH). In the proton motive force formula (pmf), R is the gas constant, F is the Faraday constant, and T is the absolute temperature (in K).*

In plants and algae, the photosynthesis starts at the thylakoid membranes (TM) in the chloroplast organelles as we can see on *Figure 2*. These membranes contain 4 main protein complexes; multimeric photosystems II and I [PSII/PSI), cytochrome b_6f and ATPsynthase. PSI and PSII will work together in series simultaneously within the whole electron transport chain; as it is easily visualized in the form of a Z-scheme [9] (see *Figure 3*), in a series of redox chemical reactions allowing for a linear electron transfer so as to produce reducing power (NADPH) and ATP. This defines the light phase, as compared to the dark phase which takes advantage of ATP and NADPH throughout the Calvin-Benson-Bassam cycle (CBB).

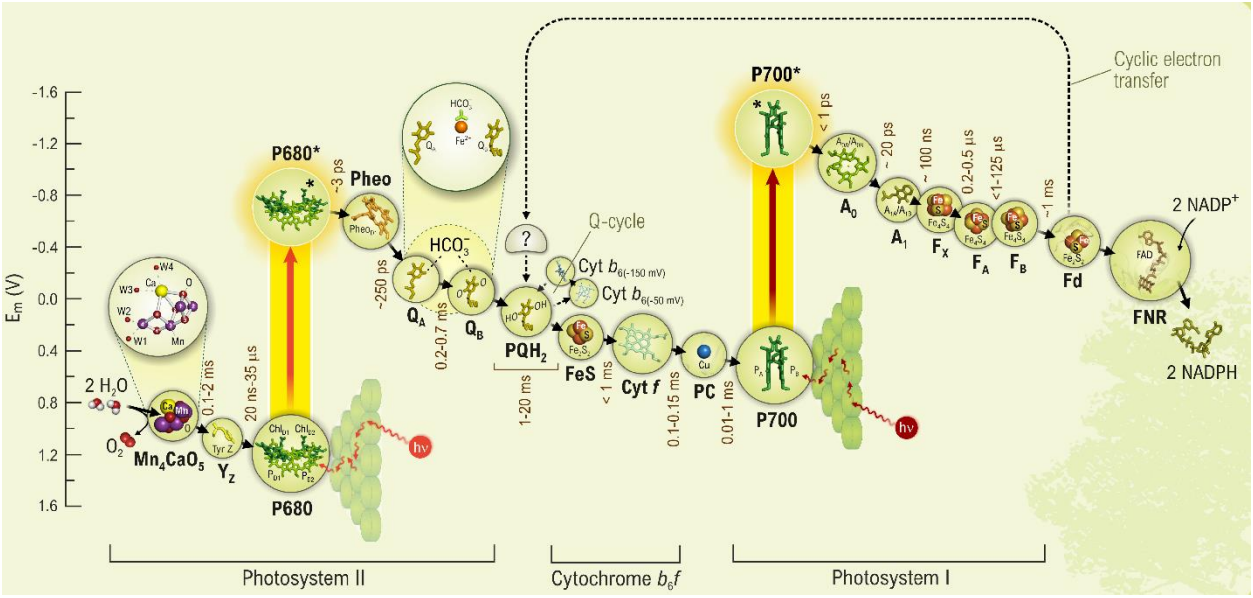

Figure 3. Z-scheme of the photosynthetic electron transport chain (PETC). *Adapted from reference* [10]*. The redox carriers were placed according to the accepted midpoint redox potentials (pH 7). Mn_4CaO_5, manganese – calcium-oxygen complex; W1-W4, metal bound water molecules; Y_z, redox active tyrosine (Tyr Z); P_{680} and P_{700}, primary electron donors of Photosystem I and Photosystem II (only their P_{D1} and Chl_{D1} molecules are shown); P_{680}* and P_{700}*, first singlet excited states of P_{680} and P_{700}; Pheo, pheophytin; Q_A and Q_B, primary and secondary quinone (plastoquinone) electron acceptors; bicarbonate ion (HCO_3^-); PQ, mobile plastoquinone molecules; FeS, Rieske iron-sulfur protein; Cyt f, cytochrome f; PC, mobile copper protein, plastocyanin; A_0, primary electron acceptor of PSI (a special pair of Chl a molecules); A_1, pair of phylloquinone (vitamin K) molecules; F_X/F_A and F_B, bound iron-sulfur clusters of PSI; Fd, ferredoxin; FNR, ferredoxin-NADP oxidoreductase. : reaction center chlorophyll (Chl) a of PSII, In this diagram, electron transfer through the redox components of plastoquinone pool and Cyt b_6f complex is shown.*

2.2. How oxygenic photosynthesis works- the main actors

Within the different types of photosynthesis, oxygenic photosynthesis is defined by the use of water as the initial electron donor and excludes photosynthetic organisms (e.g. heliobacteria, green sulfur bacteria or purple bacteria), using another molecule as an initial donor (e.g. hydrogen, sulfur, organic acids). In oxygenic photosynthesis, two types of photosystems with similar working concept yet with different terminal electron acceptors can be found (for detailed reviews on the structure and transfer of energy in photosynthesis [6,8,]).

Photosystem II (PSII) forms a super complex with its antenna (Light Harvesting Complex; LHCII). Together, they act as a water: plastoquinone (PQ) – oxidoreductase (see *Figure 4*). Its reaction center (RC), is the site of photochemistry where the special chlorophyll pair P_{680} [11] gets excited and performs charge separation. Once oxidized, P_{680}^+ is reduced by the electron donor side which encompasses a manganese (Mn_4O_5Ca) [12] oxygen evolving complex (OEC) (for a review on the functioning of the OEC and the atomic mechanism of water oxidation [13,14]), dubbed the 'engine of life' [15], and a D1 protein located tyrosine-161 (YZ) [16,17]. On the electron acceptor side of the reaction center, leading

to a final Q_A Q_B (non-heme iron, binding a hydrogen carbonate (HCO_3^-) [18]) plastoquinone electron transfer, side we have a pheophytin (Pheo, a chlorophyll molecule).

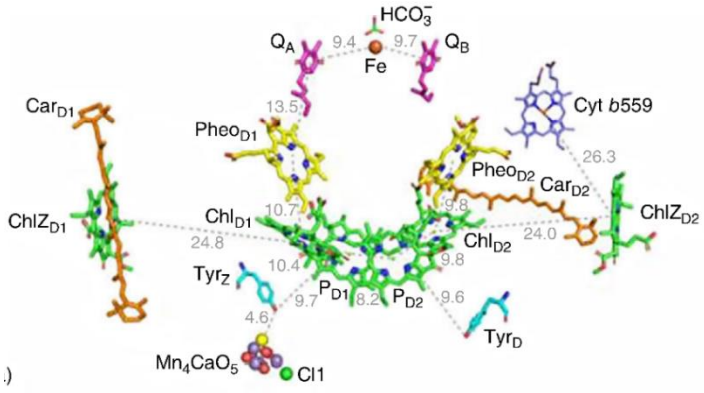

Figure 4. Structure of PSII from a thermophilic cyanobacterium Thermosynechocuus elongatus. *Adapted from reference* [19]. *This view is along the membrane plane, with the cytoplasm at the top and the lumen at the bottom. The catalytic site of water oxidation is the Mn_4CaO_5 cluster (magenta, yellow and red spheres). Cofactors are shown in green (chlorophylls), orange (carotenoids), blue (heme) and yellow (lipids), while water molecules are shown as blue dots.*

By contrast, photosystem I (PSI), forming a super complex with its antenna (LHCa) behaves as a plastocyanin (PC): ferredoxin (Fd) (photo)-oxidoreductase (see *Figure 5*). In PSI, the special pair is called P_{700} for its absorption peak [20] and performs charge separation, providing electrons to the electron acceptor side comprising a Chl a molecule (A_0) and vitamin K_1 [21] (A1), as well as three non-heme iron-sulfur centers on its acceptor side. PSI-reduced ferredoxin in turn provides the electrons for the Ferredoxin: $NADP^+$ oxidoreductase to form NADPH.

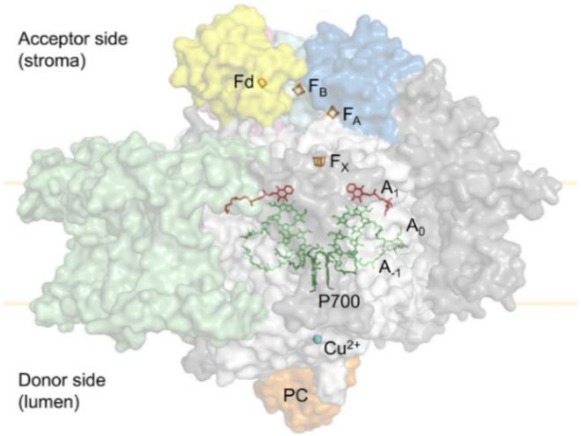

Figure 5. Simplified tertiary structure of the PSI: plastocyanin ferredoxin complex from plants (*PDB accession 6YEZ* [22]*). Adapted from reference* [23]*. Protein subunits PsaA and PsaB (white), PsaC (cyan), PsaD (blue), PsaE (pink) and LHCI subunits (green). Other PSI subunits are colored grey. Also shown are plastocyanin (orange) at the PSI donor side and ferredoxin (yellow) at the PSI acceptor side. Cofactors involved in electron transport are shown; Cu_2^+ (blue), P_{700} (dark green), A_{-1} and A_0 chlorophylls (lime), A_1 phylloquinone (red) in PSI, as well as the PSI 4Fe4S clusters F_X, F_A, F_B (orange) and the ferredoxin (Fd) 2Fe2S cluster (orange).*

Being part of the same super family of bc complexes, cytochrome b_6f (Cytb6f) dimeric complex, a plastoquinol (PQ): plastocyanin (PC) - oxidoreductase that catalyzes the rate-limiting step in linear electron transfer (LET), possesses a similar structure to that of cytochrome bc1 (Cytbc1) complex, which can be found in mitochondria as complex III (see [24] for a review on similarities and differences). Its electron transfer structure includes a Cyt f, an iron-sulfur (Fe-S) protein [25] and two cytochromes b (bn/bp) that are responsible for the Q cycle ([26], see [27] for a review). Following a bifurcated electron pathway, cytochromes bn/bp reduce and oxidize PQ (at Q_n- site) and PQH_2 (at Q_p-site), respectively, to finally reduce the acceptor, plastocyanin, (photo oxidized by the PSI) via the Fe-S/Cytf, and translocate protons from the stroma to the lumen, therefore contributing to the proton motive force. An additional heme, exclusively found in $Cytb_6f$ [28], could shine light on the current picture of oxygenic photosynthesis. Seemingly positioned between Qn-site and heme c (electron transfer ferredoxin to quinone [28,29], it is consistent with the finding of a new third plastoquinone (PQ3), which could be a quinone transitioning between Qn/Qp-sites of different dimers [29]. We will talk further in detail about cyclic electron flow (CEF), but it is proposed to represent a potential third pathway via the arrival from the stroma of electron donors to the $cytb_6f$ [30,31].

Chemical energy from the light phase arises from adenosine triphosphate (ATP) because the electron transfer is coupled to proton translocation across the thylakoidal membrane giving rise to a proton motive force (pmf) [32,33]. The pmf comprises both an electric ($\Delta\psi$) and an osmotic (ΔpH) component that will activate the production of ATP by the catalytic component CF1 of the ATPsynthase.

Responsible for making ATP from ADP and inorganic phosphate (Pi), the bipartite rotary machine enzyme ATP synthase catalyzes this endergonic reaction at the level of the F1 catalytic domain [34,35] powered by the pmf, while its second domain, the membrane-spanning F0, translocate protons to the stroma. Even as ATP production is dependent on the trans-thylakoid difference in proton concentration (ΔpH) component of pmf [36,37], the difference of electric potential across the thylakoid membrane (i.e. the membrane potential, $\Delta\Psi$) is equally important in producing ATP (see review in [38]), as F1 translocates protons independently of its driving force. Translocated protons to the lumen used by F0 subunit have been building up due to water splitting reactions at the OEC of PSII, and the translocation of protons to the lumen in both linear, cyclic electron flows at PSII plastoquinone and b_6f level, as seen beforehand. Furthermore, both photosystems I and II and b_6f contribute to the electrical component of the proton motive force.

Plastoquinone and plastocyanins are endogenous redox mediators that diffuse along the thylakoidal membrane and the lumen, respectively, to transfer electrons from PSII to cytochrome b6f, which will in turn complete the electron transfer between PSII and PSI. ATP and NADPH can then be used to fix CO_2 that notably involves the Calvin-Benson cycle (see [39] for an exhaustive list of alternative carbon fixation pathways). Apart from the transfer of electrons splitting from water NADP+ or linear electron flow (LEF), other alternative electron flows in the chloroplast (reviewed thoroughly in [40]), such as the commonly named water-water cycle [41] and the cyclic electron flow around PSI (CEF-PSI) exist [21]. CEF-PSI for instance, plays a crucial role in photosynthetic regulation by increasing the ATP/NADPH balance [35].

2.3. The linear electron transfer

2.3.1. Light absorption and charge separation

In a more detailed way, emitted photons coming from sunlight are captured by the collecting antenna, (i.e. the light-harvesting complex, LHC) a protein-pigment complex (chlorophyll and carotenoid pigments). LHC absorbs that energy by switching within femtoseconds to a different state (ground state S0 to excited S3 state) an electron of the closely associated (≤ 10 Å) chlorophyll. Relaxation (S3 state to S1 state) occurs after a 2ns state of excitation allowing for an excitation energy transfer (EET) to the next chlorophyll and the protein-pigment multimeric reaction center complex (RC) within 20-300 ps (see [42] for a light harvesting timeline). EET can be described as both electron hopping and electron oscillation between pigments as explained by Förster and Redfield theories [43]. However, if not occurring fast enough, excitation can decay. As seen before, for a simpler view, the primary donor of the reaction centre a chlorophyll a (pheophytin a, lacking Mn central atom). When the electron in excited state reaches the primary donor in the reaction center, stable charge separation occurs favorably with regards to decay or recombination of the charges (i.e. trapped). Then the electron is transferred to the primary acceptor (*see below*).

2.3.2. Electron transfer steps

The charge separation occurring at PSII RC (P_{680}), which transfers an excited electron to its primary acceptor, a chlorophyll magnesium central atom- lacking pheophytin (Pheo), is stabilized by a fast electron transfer to plastoquinone Q_A (an endogenous monoelectronic electron acceptor quinone from PSII). They give to the formation of a P_{680}+/Q_A^- according to the intermediate steps shown below.

$$P_{680} - Pheo - Q_A \xrightarrow{h\nu} {P_{680}}^{*} - Pheo - Q_A \quad (\textbf{2})$$

$${P_{680}}^{*} - Pheo - Q_A \xrightarrow{h\nu} {P_{680}}^{+\cdot} - Pheo^{-\cdot} - Q_A \quad (\textbf{3})$$

$${P_{680}}^{+\cdot} - Pheo^{-\cdot} - Q_A \xrightarrow{h\nu} {P_{680}}^{+\cdot} - Pheo - {Q_A}^{-\cdot} \quad (\textbf{4})$$

In a second time, as seen before, the OEC/Yz protein rereduce the $_{P680}$+/Q_A^- pair to P_{680}/Q_A, by virtue of the Kok cycle (see equation below) in a 5 steps catalytic oxidation of water and reduction of PSII.

$$4{P_{680}}^{+\cdot} - Pheo - {Q_A}^{-\cdot} \xrightarrow{Y_Z, OEC} 4P_{680} - Pheo - {Q_A}^{-\cdot} + O_2 + 4H^+ \quad (\textbf{5})$$

Immediately after, quinone Q_A^- reduces an exogenous plastoquinone anchored at the Q_B site, that is himself ligated to Q_A by an iron atom. After a second separation charge, the already reduced exogenous quinone at the Q_B site, PQ^-, is relayed a new electron, thus allowing for a protonation (which the first endogenous quinone, Q_A is not capable of) and the formation of plastoquinol PQH_2 (see equations below). Protons for this reaction are taken up from the stroma of the chloroplast. The newly formed plastoquinol, or reduced non polar plastoquinone, will then diffuse to the plastoquinone pool of the thylakoidal membrane, which will reduce cytb_6f.

$$P_{680} - Pheo - {Q_A}^{-\cdot} - Q_B \rightarrow P_{680} - Pheo - Q_A - {Q_B}^{-\cdot} \quad (\textbf{6})$$

$$P_{680} - Pheo - Q_A - Q_B{}^{-\cdot} \xrightarrow{h\nu} P_{680} - Pheo - Q_A{}^{-\cdot} - Q_B{}^{-\cdot} \quad (\textbf{7})$$

$$P_{680} - Pheo^{-\cdot} - Q_A{}^{-\cdot} - Q_B{}^{-\cdot} \rightarrow P_{680} - Pheo - Q_A - Q_B + PQH_2 \quad (\textbf{8})$$

As evidenced in the Z-Scheme (see *Figure 3*), each electron transfer downstream of PSII corresponds to an increase in the redox potential of the involved endogenous mediators. This goes hand in hand with a stable reduced form and therefore the impossibility to pursue the electron transfer. This is why a second light-induced charge separation is needed to significantly decrease the redox potential of the mediators. Such a charge separation occurs at PSI RC (P_{700}), which transfers an excited electron to its primary acceptors, A_0 and A_1, followed by an electron transfer towards bound iron-sulfur protein acceptors of PSI: FeSx/FeSB/FeSA, to finally transfer them to soluble ferredoxin and a ferredoxin-$NADP^+$ reductase (flavoprotein) to produce reducing power in the form of NADPH.

Of note, light energy absorbed by chlorophyll molecules in the thylakoid membranes of chloroplasts is not only involved for photosynthesis. Globally, three different competing pathways can be followed from PSII: photosynthesis (photochemistry) or dissipation either in form of heat (non photochemical quenching or NPQ) or radiative energy (fluorescence accounting for 2-10% of absorbed light [44]. It is worth mentioning that such competitive pathways may occur at a much lower level given a much longer time needed to occur (NPQ starting at 10^{-9}s [45] – (see [46] a review on the study of the main component of NPQ, qE) compared to 10^{-11}s needed for the chlorophyll-chlorophyll excitement transfer (for a review see [47]).

Measurements of fluorescence are particularly appropriate tools to investigate (see [48-50] for user-friendly reviews on chlorophyll fluorescence measurements) the state of the electron transport chain photochemistry and heat dissipation. Upon illumination after a period of dark adaptation, occurring in a time window under 1s [51], there appears to be an increase to the chlorophyll fluorescence yield. During this period, Q_A are reduced, leading to the 'closing' of the reaction centers. Because of that, the excited state of chlorophyll returns to its basal state via dissipation in form of heat or fluorescence in the chlorophyll antennae, as a rapid back transfer of excitons from the closed center to the bulk pigment [52]. However, the dissipation in form of heat is thought to be constant in the case of PSII. Hence, a lack of photochemistry results in an increase of fluorescence-mediated excitation decay and vice versa.

Following on, over several minutes, the fluorescence level starts to fall again until a steady-state is achieved, due to a photochemical quenching and a non-photochemical quenching.

It is generally assumed that at room temperature, photosystem I (PSI), unlike photosystem II (PSII), does not emit variable chlorophyll fluorescence (ChlF) after light-induced charge separation below 700 nm. In this context, it was calculated that PSI steady-state emission only represented about 20% of total constant (F_0) fluorescence [53] and 25% of the overall fluorescence yield at room temperature [54]. Even more so, variable ChlF coming from PSI *in vivo* (not isolated PSI) cannot be dissociated experimentally from PSII due to an overlap of their emission spectra [55]. Nevertheless, several experimental results under certain conditions show the appearance of a PSI ChlF variable component (see [56]). Lazar proposed a theoretical model based on the literature values and

information on PSI for fast ChlF, contributing a total of 8-17% to the maximal combined PSI/PSII ChlF signal. Recently, a significant contribution to ChlF in various organisms (*chlorella vulgaris*, *synecococcus leopoliensis* and a light-green ivy leaf), contrary to what is established, has been determined [57,58].

Notwithstanding the caveats of measuring variable fluorescence as a useful tool to observe the state of photosynthesis, PSII fluorescence yield is high enough to allow for chlorophyll fluorescence based calculations of a key parameter; the quantum yield of PSII centers photochemistry. (Φ_{PSII}) is thus the probability that an excitation induced by a photon will be deactived by photochemistry under continuous actinic light conditions. This is not to be confused to a very similar parameter, qP (photochemical quenching), which tells us the proportion of PSII reaction centers that are closed, or to the maximum efficiency of PSII (quantum efficiency if all PSII centers were open). Moreover, a linear correlation between the quantum yield of linear electron transport (CO_2 fixation rate under saturating CO_2 concentration) and PSII quantum yield can be found in the literature [59]. On top of that, oxygen evolution data cross validates fluorescence measurements of PSII energy conversion [60].

2.4. Photosynthesis. Limiting steps photoinhibition and photoprotection

2.4.1. Photoinhibition

In a previous section, we have discussed how competing different pathways for dissipation of light energy absorbed by chlorophyll coexist. Yet, it is fundamental to further discuss the role of light intensity and spectra in determining the regime of the photosynthetic electron transport chain and the balance between photon absorption and its final electron acceptors (photochemistry) in oxygen-evolving organisms. Under low-light conditions (see *Figure 6*), photochemistry is expectedly proportional to light intensity. However, under high-light conditions, rate-limiting steps take place. These are due to both inherent monoelectronic transfer processes (at the photosynthetic electron transport chain) [61] and chemical reactions (CBB cycle). Then, under very high-light conditions, exceeding excitation cannot be absorbed by chloroplasts, which can lead to the photoinhibition, i.e. the inactivation of both photosystems I and II or the light induced loss of photosynthetic activity.

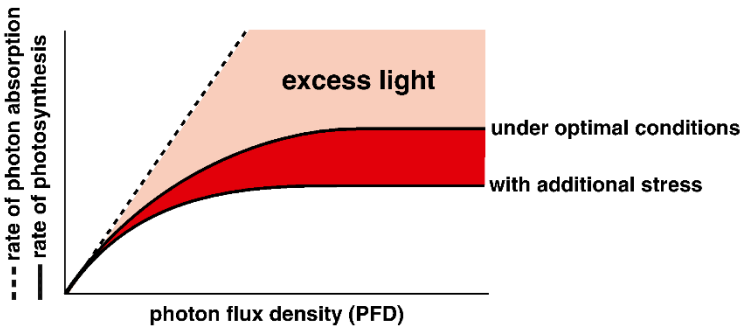

Figure 6. Efficiency of light absorption and utilization by photosynthetic chain.

Before we delve onto more consideration on photoinhibition, we first need to understand a key parameter; that is, *the NPQ or non-photochemical quenching* (see [62] for an in depth review of NPQ

in plants, algae and cyanobacteria), which describes the dissipation of emitted chlorophyll fluorescence by photosynthetic organisms, most probably at the level of the LHCII antenna [63]. It is in opposition to what is sometimes called photochemical quenching; electron transfer across the chain. From an experimental perspective, it represents thermal losses from an excited state under high light conditions.

NPQ can be deconvoluted onto several components: the energy dependent quenching [64] pH variation activated [65]; qE, photoinhibition [66]; qI and zeaxanthin-dependent quenching [67]; qZ. We do not consider state transitions to be one of these components of NPQ; it occurs due to a quenching by PSI. To the effect of this work, we will not consider qH as a genuine part of NPQ to be talked about.

qE quenching does act as a regulatory mechanism. Upon the acidification of the thylakoidal lumen, residues of the PSII antenna can become protonated, inducing conformational changes on the antenna facilitating a heat emitting return to the ground state from the excited state. qZ implies the activation also by a change of the pH of the thylakoid lumen of luminal enzymes. These will de-epixodate zeaxanthin, an antennae bound carotenoid. Violaxanthin, in turn, accepts the excitation energy from neighboring chlorophyll molecules thus acting as an efficient quencher. qI instead is activated once a high light-induced PSII damage occurs. This way, PSII active center is exposed to reactive oxidant species (ROS) - induced photodamage. However, this is short-lived, as upon photoinhibition PSII excited state is brought back to the ground state, preventing the formation of new ROS via the interaction of triplet states of chlorophylls with molecular oxygen.

To narrow down the meaning of photodamages [68], it is considered to be photochemical changes occurring in PSII structure, inactivating it. PSII photodamage occurs constantly, independent of inciding light intensity. In this regard, it has been longtime accepted that light induced turnover of D1 protein of PSII lead to its reaction center (RC) loss of activity [69]. Two non-mutually exclusive theories [70,71], if not a hybrid multifactorial frame [72], seem to explain photodamage on PSII (see *Figure 7*):

The first one of them, occurring on the donor side of PSII (WOEC Mn cluster inactivated) is induced by blue-ultraviolet light [73,74]. The special pair of chlorophyll of PSII reaction center (P_{680}) can be inactivated himself alone too. Upon an excess of excitation on the PETC (acceptor side limitation), the plastoquinone pool and Q_A get reduced, and subsequently the photochemical yield increases. Conversely, other relaxation pathways increase their yield (for instance NPQ qE and to simplify encompassing also qZ, which, as we will see later, can be distinguished by their fluorescence decay kinetics from photoinhibition quenching or qI). Several chemical agents have been proposed to explain photodamage. The excess of excitation we have referred to before, can dissipate by reversing P_{680} charge separation and moving chlorophyll to an excited triplet state (3Chl*) [75], which can attack O_2 [76] and form reactive oxygen species (ROS) like singlet oxygen. P_{680} in its oxidized form (P_{680}^+) can also be a radical species if given enough time to act [77] once the donor side of PSII (Mn) is inactivated reversibly or irreversibly. Finally, photons can be sufficient to act as reactive species by themselves by disassembling the Mn cluster [73,74].

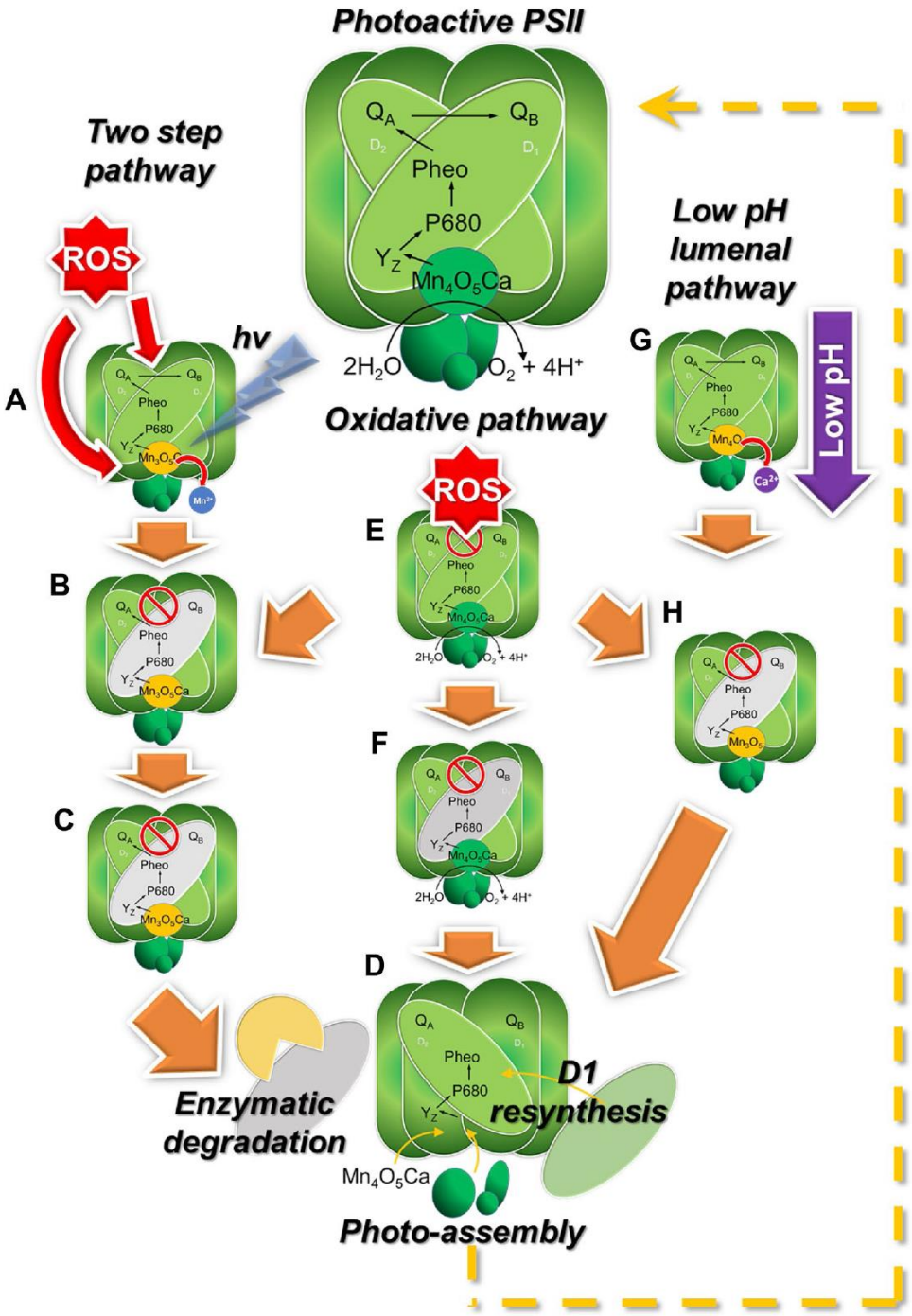

Figure 7. Pathways that lead to photodamage and repair of PSII. *Adapted from reference* [72]*. In the top is shown a fully functional PSII. The first one, namely the two-step pathway (a-d) begins by direct inactivation of the Mn cluster or by ROS production (a), followed by inactivation of the reaction center activity (b). Further steps (c, d) encompass degradation and repair of D1. The second one, or the photo-oxidative pathway (e-f-d), the reaction center is directly affected by ROS (e) and only D1 is targeted (f). Acidification of the lumen pathway (g-h-d) under very high light conditions depletes the Mn cluster (g) and inactivates its water splitting activity, leading to the inactivation of the reaction center by accumulation of highly reactive* P_{680}^{+} *(h).*

Unlike decades of study of PSII reaction centers photoinhibition [78], other light-harvesting reaction centers, like P_{700}, have been less well studied. Thanks to the development of methods to easily quantify P_{700} quantum yield and P_{700} equivalent electric field [79-82], a clear image of PSI photoinactivation has appeared.

PSI photoinhibition can be triggered by several phenomena that alter the electron flow in the PETC (see a review by [23]). This way, we can observe an overlapping for both PSI and PSII photoinhibition signals, as PSII electron sink capacity cannot held [83]. On its donor side, a limitation on CO_2 fixation can trigger PSI photoinhibition as well. This leads to a situation where either P_{700} gets excited to a triplet state ($3P_{700}$) [84], and whose reaction with O_2 will produce protein damage-dealing $O_2^-/^1O_2$ or to a use of O_2 as P_{700} final electron acceptor, instead of Fd. O_2 reduction happening at both A_1/acceptor side, it produces H_2O_2. The ROS species will then interact with PSI iron-sulfur (Fe-S) clusters, produce OH and inactivate PSI (reviewed in [85]). Even if not as vulnerable to photodamage as PSII or PSI, P_{700}, lacks of a repairing mechanism, and thus, photoinhibition is quite deleterious, taking days to recover, as it has to rely on almost entirely replacing PSI from scratch [86].

2.4.2. Photoprotection

Even as we have seen on the previous section, that excess light at varying spectra produces photo oxidative damage, i.e. photoinhibition, all photosynthetic organisms at the level of the PETC employ a variety of mechanisms to protect PSI from acceptor and donor side limitation, keep an ATP/reducing power balance and protect PSII from light-induced stress (for a review on photo protective mechanisms, see Bassi et al. [87]).

In this regard, the osmotic component (ΔpH) of the proton motive force activating the production of ATP by the ATP synthase regulates photoprotection [88]. To that effect, the relay space between both photosystems oxidizes [89] (Cytf/PC/P_{700}) due to a slowdown of cytb_6f at the Q_o- (previously referred as Qp or quinone oxidase site) site (see [90] for a review on PQH_2 cytb_6f interaction). This phenomenon, namely, the "photosynthetic control", occurs once there's a limitation on e- acceptors downstream of PSI. It results in an increase of the ATP/ (ADP + Pi) and ΔpH ratios driven by cyclic electron flow [91] (which we will not be analyzing in detail). It was determined in vivo by the dissipation of ΔpH by nigericin without affecting the pmf to increase photoinhibition in PSI [90]. As a result of more H^+ being pumped to the stroma, PQH_2 oxidation at b_6f will be more thermodynamically costly and slow down [90].

Cytochrome b_6f seems to be implicated in other photosynthetic acclimation mechanisms. On this matter, state transitions, a fast, readily reversible (occurring in minutes) process first discovered in *chlorella* [92], occurring in higher plants and algae to changes in light spectra, equilibrates PSI and PSII RC turnover when there's an imbalance of their activity, by remodeling events modifying the size of PSI and PSII antennas: part of the LHCII (chlorophyll b containing) antenna detaches from PSII by attacking itself to PSI's (see reviews on state transitions [93] and for *Chlamydomonas* specifically [94]). Here it is where cytb_6f plays its role, as once plastoquinone (PQ) pool sitting at cytb6f Qo- site [95] is over reduced (PQH_2>PQ) [96,97], STT7/STN7 protein quinases activates [96] and phosphorylates LHCII, stabilizing the redox activity of the PQ pool by an increase of PSI activity. If an excess of PSI was to

occur, the oxidized PQ pool is sensed by cytb_6f which will lead to kinases being deactivated, dephosphorylating and subsequent transition of LHCII towards PSII. The fast, reversible nature of the redox loop implies we will have an intermediate balance of LHCII-PSI/PSII multidimers [98].

Acidification of the lumen has been appreciated for a longtime, unlike the photosynthetic control, to prevent the inactivation of both PSI and PSII by activating non photochemical quenching NPQ events. As seen before, under an excess of light-induced excitation, on the PETC, dissipation will occur by form of heat (qE here accounting also for qZ) and photoinhibition (qI), resulting in the decrease of variable fluorescence. Fluorescence decay signal can be deconvoluted as it undergoes recovery in minutes for qE and hours for qI. The role of pH in controlling qE induction is established to work as either, by changes of pigments activity of xanthophyll cycles or by changes of conformation of PSII subunits (protonation of antenna) [99].

The commonly accepted model for the strongest NPQ component, qE in plants and green algae works as follows [99]. Under high-light conditions, ΔpH increase allows protonation of Psbs, a PSII LHC subunit displaying acidic sensors in the lumen [100], and somehow modify LHCII antenna proteins favoring heat dissipation [97,101]. In the case of *Chlamydomonas*, heat dissipation and pH sensing takes place at the same LHC protein, LHCRS3 [102]. Unlike qE, qZ induction only relies on ΔpH for its activation and is closely associated to qE. It is proposed that ΔpH activates the conversion of violaxanthin (Vio) into antheraxanthin (Ant) and zeaxanthin (Zea) [103] thanks to a violaxanthin de-epoxidase (VDE). Zea will then be able on itself to sustain qZ in plants, and in *Chlamydomonas* [104] and has a sort of positive feedback on the induction of qE in plants [99], although it is not the case for the latter in *Chlamydomonas* [99].

Acidification of the lumen by cyclic electron flow has been crucial in explaining both photosynthetic control and NPQ. Nevertheless, other alternative electron flows ("meta" water-water cycle, flavodiiron and ascorbate mediated w-w cycles, hydrogenase pathway) involve b_6f turnover increasing proton pumping to the lumen, thus activating ΔpH dependent processes, NPQ and photosynthetic control.

As outlined on the introductory paragraph on photoprotection, PSI needs to be shielded from acceptor and donor side limitations. Previously explained mechanisms directly involving PSII will not be discussed. One way for PSI to dissipate the pressure on its reaction centers is to use the stromal sinks available to him. The carbon fixating (CO_2) enzyme rubisco can alternatively evolve O_2, which will result in an oxidized PETC.

As a matter of fact, fluctuating light spectra and intensity lead to deleterious effects in higher plants and algae, even after taking into account multiple photo protective mechanisms as it has been exposed.

2.5. Conclusion

As seen above, photosynthetic organisms involve many endogenous electron transfers including an oxidation ($H_2O \rightarrow O_2$) and reductions ($NADP^+ \rightarrow NADPH$; $CO_2 \rightarrow$ sugars). From an electrochemical point of view, this somehow makes photosynthesis a photo electrochemical cell through which an

electron flow passes. Moreover, high light intensities lead to deleterious effects notably in line with the increase in yield of the other relaxation pathways.

This is mainly why the extraction of the photosynthetic electron excess from their PETC was considered as a way to obtain biophotoelectrochemical currents, which we will explore in the next section. First considerations on the prime access site for electron extraction will be discussed later on as well.

3. Producing electricity from photosynthesis

3.1. Artificial photosynthesis

As it has been mentioned before, photosynthetic organisms have been able to take profit from solar energy in one of the most efficient ways there is in nature, i.e. photosynthesis. To that end, multiple proposals, ranging from closest to least resembling biological photosynthesis have been elucidated to capture and transform energy from sunlight into useful chemical bonds as plants, green algae and cyanobacteria do. The concept of artificial photosynthesis, first proposed by Giacomo Ciamician in 1912, can be performed by homogenous solutions of molecules or molecular assemblies, by wireless combination of molecules and solid-state materials, by wireless combination of solid-state materials only, including nanoparticles in solution, by diverse material combinations including electrical wires and by a local combination of components exchanging electricity or/and chemical intermediated by wires and/and pipelines.[105].

In this regard, artificial photosynthesis is a way for the obtention of solar fuels, like hydrogen or hydrogen peroxide and O_2 from water splitting, as the products of a series of chemical reactions driving the harvesting of sunlight by mimicking the catalytic nature and structures of oxygen photosynthetic organisms [106]. We can categorize two types of devices to produce solar fuels: the photovoltaic coupled electrolyzer (PVE) and the photoelectrochemical cell (PEC) variants (either a photo anode, a photocathode or an entire cell). In PVE cells, solar energy is converted into chemical energy following an indirect two-step process [107].

The established lambda solar fuel artificial photosynthetic system is composed of the following parts: an antenna, which will harvest energy from sunlight and funnel down the excitation energy to the reaction centers. These charge-separation units are then in charge of producing enough redox potential to drive electron transfers to produce chemical energy that can be stored. To couple these chemical reactions, both electron donors and acceptors (mostly from organic materials) are needed, as well as catalysts to facilitate the evolution of final electron donors (for instance [$Rhcp^{*-}$] complexes for H_2 evolution, or CuO_x particles for CO_2 reduction), oxygen (iron, cobalt, manganese, copper, iron, cobalt, nickel, ruthenium, iridium complexes) and photosensitizers (molecular dyes, quantum dots, semiconductors) to facilitate light harvesting.

Good performances of artificial photosynthetic systems depend on them adopting basic structures and loosely adopting designs found in natural systems, in a similar fashion to the planes to birds. For instance, the longer the lifetime of charge-separated states is in the electron transfer apparatus after the antenna, the greater are the odds to accumulate the potential energy onto a final energy container. For that, basically constructing a sort of Z scheme artificial equivalent with multiple electron transfers

along well defined redox gradients, allows to achieve stable charge-separation of the artificial reaction centers. At the same time, seeing a parallel to natural photosynthesis, electron transfer efficiency can be greatly improved by modifying the distances and orientations of all the electron transport chain (linkers, solvants, final electron acceptors and electron donors). The improvement of electron transfer pathways allow also to diversify the redox reactions that can be coupled together. Also, artificial photosynthesis benefits from the long term developments of highly efficient light-harvesters for solid-state photovoltaics. This way, light absorbers with different profiles can be coupled together to maximize light absorption.

However simple, and tunable they are, these systems suffer from instability from both electrodes and catalysts, high cost due to their non-biological origin leading to low efficiency, limited scalability, limited choices for solar fuels products and partial imitation of nature's photosynthetic electron transport chain constrain their future commercial applications.

3.2. From natural photosynthesis to photocurrents

3.2.1. Choice of natural photosynthesis

To recapitulate, oxygenic photosynthesis is the chemical process by which algae, plants and cyanobacteria can transform the energy from sunlight onto chemical energy thereby releasing O_2 from water splitting as by product. The concept of biophotovoltaics (BPV) is to take benefits from such a water oxidation by means of photosynthetic organisms [107-111]. In other words, an outer collecting electrode will interfere with the photosynthetic chain by acting as a partial short- circuit. The advantage of using intact cells, and to a lesser degree, parts of the photosynthetic electron transport chain (PETC) is that their stability and lifetime can be enhanced by using their regulatory and replicative machinery. A scheme of differing stability, efficiency and current generation for different parts of photosynthetic microorganism can be seen at the end of this section. The different strategies employed to extract photosynthetic electrons go from PSII to ferredoxin through the collecting electrode. Therefore, we shall define an "enlarged" natural photosynthesis harvesting definition, i.e. using a photosynthetic chain/ fragments of it alone or combined obtained from a living organism, to produce an extracellular electrical current under illumination. The usual photo - electrochemical cell is often designed and investigated as a half cell configuration, that is a photobioanode. The photosynthetic organism/fragment is connected to a polarized electrode capable of oxidize and obtain a photocurrent. Microbial solar cells (MSC) involve an entire and complete battery with a whole photo electrochemical system: the photosynthetic organisms at the anode promote the water oxidation (or even organic compounds) using sunlight and delivers electrons to the anode. These electrons flow to the cathode, where electrons are delivered to reduce oxygen and produce electricity [112]. In a different scale, isolated PSII can work in a biophotoanode configuration called "semi-artificial photosynthesis" [107,111]. Attached to the surface of an electrode, compared to thylakoidal membranes or whole cell organisms, it increases current production but reduces its stability. Membranous compartments encapsulated within the chloroplast (plants, algae) or in the cytosol (cyanobacteria) can also beisolated. As such, direct electron transfer from thylakoid membranes to the electrode can be obtained by means of PSII, PSI, plastocyanin, plastoquinone and the b6f (see an extended review on [111]). Chloroplasts can also be isolated. Both single isolated and sub fractions of

whole cell organisms have similar performances but lack stability (see *Figure 2B*). Even as current generation still remains low compared to artificial photosynthesis, the field of natural photosynthesis remains quite recent [113], and important improvements are expected [114].

There is a width of literature on PSII high redox potential ($E^{0'}$ > 0,1V vs SHE) exogenous electron acceptors of quinone [115-137] and $K_3Fe(CN)_6$ [116,117-120,122,128-129,131,133-134,135-143] nature. Quinones are considered to be selective PSII acceptors, whereas $K_3Fe(CN)_6$ can also accept electrons at the level of PSI [122]. Nevertheless, as we will see further ahead, this is more complicated. For instance, exogenous electron acceptors can interact with the photosynthetic electron transport chain (PETC), mitochondria, other organelles and interact in different ways with PSII (plastoquinone pool, Q_B, further beyond), facilitated if it presents halogenated (electron withdrawing groups, EWG) substituents, or hindered if it has alkylated ones (electron donating groups, EDG) [144]. At the same time, given quinone couple high redox potential, we could incur in significant thermodynamic costs, either as a loss of energy in form of heat dissipation or leaving room for other redox couples to concur as electron acceptors.

In order for a mediated electron transport to be perpetuated over time, a reversible oxidized electron acceptor (M_{Ox}) that will recover electrons turning onto its reduced form (M_{Red}) is needed.

At the same time, once working with living organisms such as *Chlamydomonas reinhardtii* is considered, the exogenous mediator will have to cross a great amount of membranes to access the PETC. In this regard, Warburg and col. [145] had already determined by 1944 the lipophilicity of para-benzoquinones, and $Fe(CN)_6^{3-}$ seems not to be able to cross membranes [146,147], and be reduced before reaching the thylakoids [147-150].

As a conclusion, taking benefit from natural photosynthesis by exploiting all or part of the photosynthetic chain as a converter of photons into usable electrons is a field that has been growing exponentially since the beginning of the 21st century. It is not possible to mention herein all the publications related to this topic, as they are so many in number. That is why, with a few exceptions, the state of the art presented in this section will be focused on the most relevant and recent reviews [7,108,111,151,152].

3.2.2. The experimental set-up

From an electrochemical point of view, two experimental configurations are commonly used in the literature.

The first one is the standard electroanalytical setup, i.e. a 3-electrode system containing a working electrode whose potential is monitored with respect to a reference electrode. While cyclic voltammetry experiments are sometimes carried out to identify the relevant potential values involved, the most popular monitoring method is chronoamperometry. In this case, a constant potential is applied where the reduced form of the endogenous or exogenous mediators is oxidized, generating an increased current at the electrode from the photosynthetic target under illumination. An undeniable advantage is that the photobiode can be studied as such, i.e. by controlling all the parameters that can affect its intrinsic performance in terms of chronoamperogram intensity and

shape. The major drawback is that these experiments involve a forced transformation (i.e. electrolysis), so the system studied does not deliver energy but receives it.

The other configuration is that of a photobiopile in operation. The photobioanode compartment is connected to a cathode compartment. The voltage delivered is then measured using a voltmeter for different resistance values in the external circuit. As with a conventional battery, this provides the electromotive force, polarization curve (I = f(U)) and power density curve (P = UI = f(U)). The clear advantage is that the characterization of the "real" photobiosystem can be carried out because electrical energy is spontaneously generated. However, the kinetic study is not only more time-consuming than for a "simple" chronoamperogramm, but performance also depends on the choice of cathode, which can also be limiting and bias the effects caused by the photobioanode.

As a result, the efficiencies of these two configurations are basically incomparable, which raises the question of how to summarize the related trends in relation to the different strategies. Unfortunately, comparison is not simply a question of electrochemistry. Other criteria are crucial, such as light (intensity, wavelengths, etc.), "biological" parameters (nature of photosynthetic target, PSII and/or chlorophyll amount, concentration of organisms in the system or on the electrode surface), system stability or parameters to assess the collection efficiency (maximum current, maximum delivered voltage, quantum efficiency - % of incident photons converted to electrons at the collecting electrode).

3.2.3. Photosynthetic targets

The photosynthetic targets described here are those that allow electrons to be transferred by first being oxidized downstream of the photoconverter. In other words, photosynthesis acts as an electron donor and water is formally the electron source. This means that electrons are collected at the anode. Moreover, if the systems generate photocurrent from phototrophic organisms, the term "biophotovoltaics" is often employed. However, less complex systems such as isolated photosystems or sub-cellular fractions (isolated thylakoid membranes) can also be considered. In the approach adopted here, this excludes isolated photosystems I, as these are involved as electron acceptors, which means they have to operate with a cathode. As a result, only isolated photosystems II are to be considered, and this is sometimes referred to as "semi-artificial photosynthesis" [108].

Working with **isolated units** like PSII first involves extracting them from cyanobacteria and coating them on a collecting electrode from a solution of suspended PSII. Mesoporous electrodes made from ITO (Indium Tin Oxide) are frequently used because of their ability to be transparent and conductive. The mesoporous aspect facilitates PSII encapsulation, although other hydrogel-based techniques can also be considered, thereby providing the opportunity to work with more conventional electrode materials (Au, glassy carbon, etc.). Although electron transfer between the PSII under illumination and the collecting electrode is intrinsically favored [111], photosynthetic electron collection can be greatly enhanced by the addition of redox mediators. In this respect, exogenous quinones (see section on laboratory activities) are particularly well adapted to improve the current produced by at least an order of magnitude although such an addition decreases the stability. It should be noted that soluble mediators (notably $Fe(CN)_6^{3-}$) are not the only electron carriers. The use of conductive polymers (based

on osmium or quinones; see *Figure 8*) or carbon nanotubes (CNTs) is also efficient, acting as both electron relays and encapsulating materials.

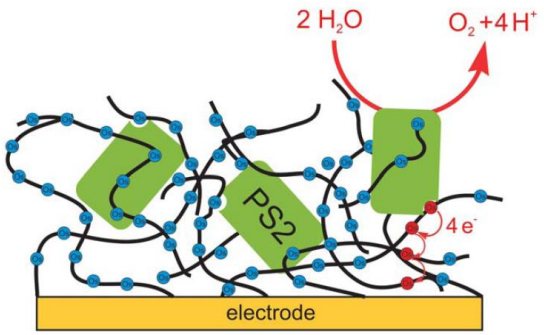

Figure 8. Example of PSII embedded within osmium polymers at the collecting electrode surface. *Adapted from reference* [153].

More recently, reaction centers from purple bacteria have been the subject of similar studies (see *Figure 9*). The general idea remains the same as for PSII, but in this case it involves isolated components extracted from organisms performing anoxygenic photosynthesis.

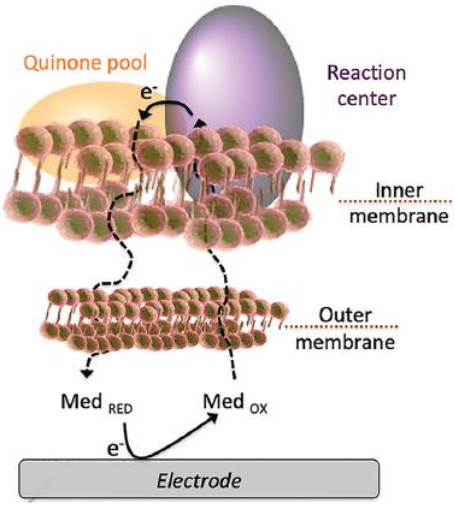

Figure 9. Principle of collecting electrons from an isolated reaction center. *Adapted from reference* [154].

An alternative strategy is to extract electrons **from thylakoid membranes**, typically from spinach leaves. Unlike photosystems or isolated reaction centers, thylakoid membranes can be used either by immobilization on the collecting electrode or as a suspension. Working with a thylakoid suspension is however less common, and requires the presence of a redox mediator (nanoparticles, again quinone or $Fe(CN)_6^{3-}$) to ensure electron transfer between the chain and the anode. The majority of research studies involving thylakoid membranes have focused on systems immobilized on the electrode (Au, carbon, CNTs...) with or without mediators (soluble or polymers), given that the mediators improve electron transfer efficiency, as expected. It is worth noting that thylakoid membranes can be used as

herbicide detectors, since these molecules will inhibit the photosynthetic chain and decrease the magnitude of the current collected.

The two above mentioned cases involve systems that are unable to divide (and thus be cultured) and are removed from their biological environment (i.e. potentially unstable). This is why many research groups work with **intact photosynthetic organisms**. The most popular organism is the cynaobacterium. Cyanobacteria can be immobilized on the collecting electrode either by deposition of a solution or by formation of a biofilm. Again, the presence of a redox mediator (quinone or phenazine) increases the efficiency of electron transfer to the electrode. More recently, similar studies have been extended to purple bacteria. Green microalgae (*Chlamydomonas reinhardtii*, *Chlorella vulgaris*) are also used, although they are not the most widely studied targets. Studies on immobilized microalgae exist, but many concern systems in suspension under stirring. The microalgae structure (additional barrier due to the chloroplast and/or phototactism) is probably the main reason for this.

It is worth mentioning that in recent years, the amplifying effect of the exogenous redox mediator has been found to be accompanied by a decrease in the performance of the photobioelectrochemical system over time (probably due to side-effects/toxicity induced by mediators especially exogenous quinones). Some groups are therefore focusing on investigating and improving direct transfer between cyanobacteria and electrodes by endogenous mediators (referred as exoelectrogenesis).

3.2.4. How can the different strategies be compared? The "PSII vs cyanobacteria" example [155].

This article is a rare example of an intrinsic comparison involving either cyanobacteria (Synechocystis sp. PCC 6803 cells) or PSII from these organisms (see *Figure 10*). The central idea is to immobilize photosynthetic targets on an inverse opal indium-tin oxide (IO-ITO) electrode whose pore size (pore diameter: 10 µm, channels: 3 µm) and thickness (40 µm) have been optimized. The authors work on the basis of the same irradiation (685 nm; 1 $mW.cm^{-2}$) in both cases, with a monitoring by chronoamperometry (0.3 V vs SHE). The Chla average loading of is 10.2 ± 0.4 µg Chl a per (geometrical) cm^2 for IO-ITO|PSII and 2.5 ± 0.5 µg $Chla.cm^{-2}$ for IO-ITO|biofilm

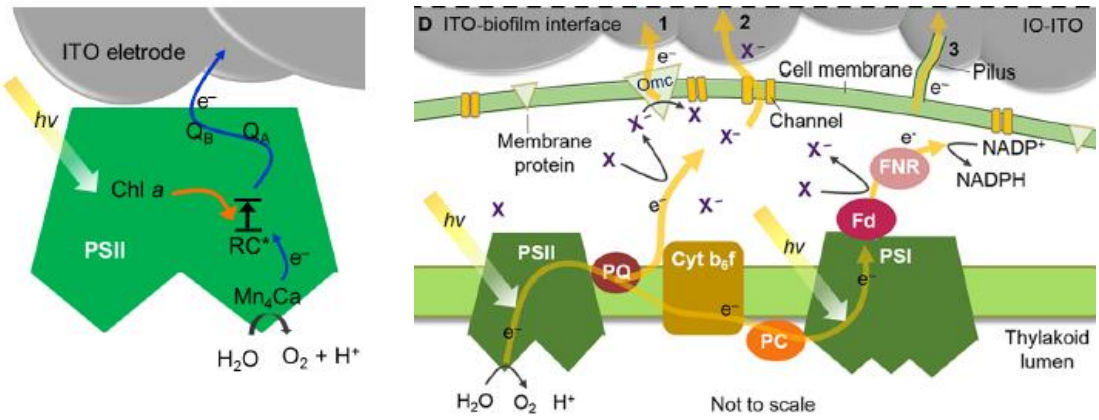

Figure 10. Scheme of the electron transfer between the photosynthetic target and the ITO collecting electrode. *Left: isolated PSII. Right: cyanobacteria biofilm. Adapted from reference* [155].

To compare IO-ITO|PSII and IO-ITO|biofilm, the photocurrents were scaled according to their Chl *a* content and normalized by the electrode geometric area. While current densities are thus quantified, other relevant parameters were calculated. First of all, EQE (external quantum efficiency) corresponds to the fraction of incident photons converted to collected electrons according to:

$$EQE(\%) = \frac{123.98 \times J(\mu A.cm^{-2})}{\lambda(nm) \times I°(mW.cm^{-2})} \quad (\textbf{9})$$

Second, the TOF (turnover frequency) corresponds to the number of electrocatalytic cycles assuming 100% faradaic yield (I = photocurrent; n = moles of PSII (dimer) or photosynthetic electron chain; e = charge of an electron; N_A = Avogadro number)

$$TOF(s^{-1}) = \frac{I(A)}{4 \times e(C) \times N_A(mol^{-1}) \times n(mol)} \quad (\textbf{10})$$

In addition to the studies performed for direct electron transfer (DET), a quinone-type mediator (2,6-DCBQ at 1 mmol. L^{-1}) can be used to perform mediated electron transfer (MET). The results are summarized in *Table 1*.

electrode	E_{app} (V_{SHE})	J (μA cm^{-2})	TOF (s^{-1})	EQE (%)
ITO|PSII (DET)	0.3	7.0 ± 0.3	7.2 ± 0.5 × 10^{-2}	1.3 ± 0.1
	0.5	13.7 ± 1.3	12.8 ± 0.5 × 10^{-2}	2.3 ± 0.2
ITO|PSII (MET)	0.3	164 ± 8	1.7 ± 0.1	29.7 ± 1.5
	0.5	185 ± 14	1.9 ± 0.2	33.5 ± 2.5
ITO|biofilm (DET)	0.3	0.21 ± 0.04	4.6 ± 0.9 × 10^{-2}	3.8 ± 0.7 × 10^{-2}
ITO|biofilm (MET)	0.3	8.9 ± 1.4	8.3 ± 0.5 × 10^{-1}	1.6 ± 0.3
	0.5	14.7 ± 0.5	1.1 ± 0.1	2.7 ± 0.1

Table 1. Performances resulting from ITO/PSII and ITO/cyanobacteria biofilm photoanodes. *Adapted from reference* [155].

These results show that:

⇒ An exogenous mediator significantly increases the amount of photosynthetic electrons collected per unit of time (current intensity, TOF) for both isolated PSII and biofilm.

⇒ A more detailed analysis of the article also shows that current stability is very poor in the absence of mediator in both cases. The presence of the mediator enhanced stability only in the case of biofilm.

⇒ Photon/amenable electrons conversion (EQE) is by far the best for PSII isolated in the presence of mediator. It is significantly improved in both cases when changing from a mediatorless system to one with a redox mediator. Efficiency is also much higher when comparing PSII isolated with biofilm.

3.2.5. Overview of the different strategies

The results described in the article above are reasonably representative of the overall trends in the literature, even if it remains difficult to strictly compare all biophotoelectrochemical systems (see *Figure 11*).

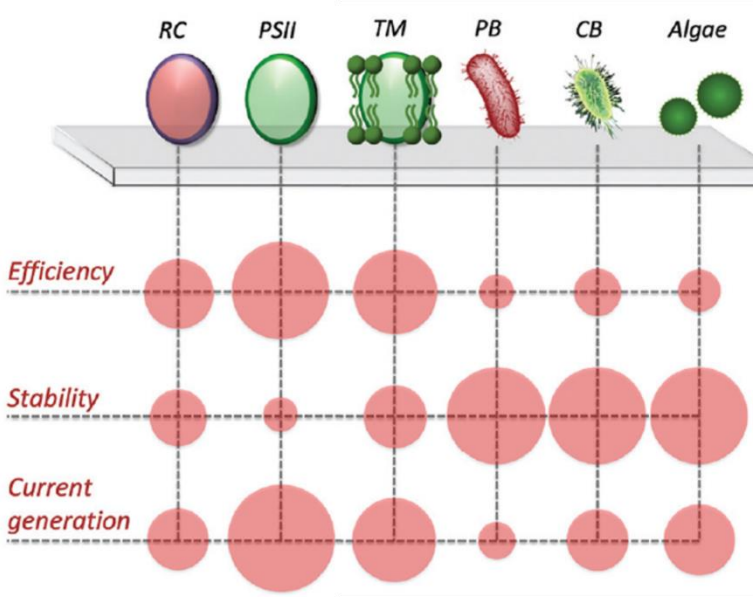

Figure 11. Tentative efficiencies, stabilities, and current generations for different photosynthetic targets*.Ii.e. isolated bacterial reaction centers (RC), photosystem II (PSII), thylakoid membranes (TM), purple bacteria (PB), cyanobacteria (CB), and algae. Adapted from reference* [111].

In this context, isolated photosynthetic fragments appear to lead to higher efficiency and electrical current than whole organisms. This is highly consistent with better connectivity between the anode and the photosynthetic electron transfer chain.

Conversely, intact photosynthetic organisms provide much more stable performance than isolated units which, lacking their environment, are more subject to photoinhibition, for example, and have no means of repair. Isolated PSII, for instance, is highly unstable outside its biological context.

This scientific and thematic framework is the basis for the research activities developed by the team led by Prs. F. Lemaître and M. Guille-Collignon (UMR 8640 "PASTEUR" – Département de Chimie, ENS) together with that of Drs. F.-A. Wollman and F. Rappaport and then B. Bailleul (UMR 7141 "Biologie du chloroplaste et perception de la lumière chez les micro-algues" - Institut de Biologie-Physico-Chimique). This scientific project on the diverting of photosynthetic electrons was conceived within the scope of LABEX DYNAMO, which provided support for this field through the Ph.D. of Guillaume Longatte (2012-15) and Adnan Sayegh (2015-18) as well as the post-doctoral internships of Han-Yi Fu (2015-17) and Léna Beauzamy (2017-19).

3.3. Prior to this work - Laboratory highlights

In the context of the LABEX DYNAMO project, the laboratory chose to explore ways of extracting photosynthetic electrons from living organisms, starting in late 2012. By focusing on the microalgae *Chlamydomonas reinhardtii*, the question was to find an electrochemical pathway for extracting electrons from the photosynthetic chain. In this respect, the principle of a mid-scale harvest limits the use of a direct collecting electrode, which would have to be nanometric in size.

Chlamydomonas reinhardtii, usually dubbed as the green yeast [156,157], is a ~10-µm, single cell, haploid, fast growing [158], soil-dwelling (first derived in 1945 in Amherst, Massachusetts) green alga. It has two anterior flagella for motility and mating and multiple mitochondria. Its photosynthetic apparatus is contained within the chloroplast. *Chlamydomonas reinhardtii* is a model for studying eukaryotic photosynthesis as it can grow in the dark on an organic carbon source (acetate) while keeping its photosynthetic apparatus intact [158]. Its potential as model organism has further been increased as it was established its full nuclear genome sequence [159,160], it could be transformed (chloroplast [161], nucleus [162], mitochondria [163]), has a genome-wide, indexed library of mapped insertion mutants [164,165] identifying gene functions [166], a CRISPR-mediated (first attained by [167] targeted gene modifications [168]) and an exhaustive repository of all knowledge on the algae; the Chlamydomonas Resource Center (University of Minnesota) and *Chlamydomonas Sourcebook* [169].

Consequently, mediated electron transfer appears to be the most suitable route: a redox mediator in its oxidized form is reduced by the photosynthetic chain under illumination, and the resulting reduced form is then oxidized at the surface of the collecting electrode. To be beneficial, this electrocatalytic cycle has moderately compete with endogenous electron flow. In this respect, the idea would be to use diverting as chain alleviation upstream of the kinetically determining step, namely the b_6f complex. Because the choice of mediator is not only related to its ability to accept electrons but also to "diffuse" into and out of the photosynthetic organism, a reasonable choice is to consider exogenous quinones as redox carriers. Indeed, electron transfer between PSII and the b_6f complex is carried out by the pool of plastoquinones, i.e. endogenous quinones sequestered in the thylakoid membranes. Exogenous quinones would then compete with the plastoquinone pool and be partially reduced instead.

3.3.1. Which quinones to choose? First investigations

The criteria for selecting the most suitable quinone are non-trivial. The acceptor capacity towards PSII could be understood in terms of the redox potential for the Q/QH_2 couple, but also in relation to steric hindrance or the ease of access of the quinone to the photosynthetic chain, or even of the hydroquinone to be released from the considered organism. An initial study has therefore been carried out to assess microalgae-quinone interactions using fluorescence measurements [170]. The key idea was to measure the effect of the addition of exogenous quinones on the fluorescence emitted by an algal suspension under actinic light. In this respect, and based on the literature [120], several "target" quinones were considered (see *Figure 12*):

⇒ two dichloroquinones (2,6-DCBQ and 2,5-DCBQ) which are PSII electron acceptors due to their electron-withdrawing Cl atoms (-I effect)

⇒ PPBQ which is a PSII acceptor due to the electron-withdrawing phenyl group (-M effect)

⇒ two dimethylquinones (2,6-DMBQ and 2,5-DMBQ) with moderate PSII accepting effect due to the electron-donating Me group (+I effect)

⇒ two "naked" quinones, namely benzoquinone (BQ) and naphthoquinone (NBQ)

Quinones with electrowithdrawing groups (high E° values)

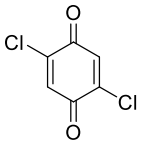

2,5-Dichlorobenzoquinone
(2,5-DCBQ)
E°(Q^-/Q) = 230 mV vs SHE
E°'(QH_2/Q) = 309 mV vs SHE

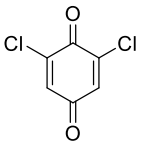

2,6-Dichlorobenzoquinone
(2,6-DCBQ)
E°(Q^-/Q) = 221 mV vs SHE
E°'(QH_2/Q) = 315 mV vs SHE

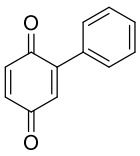

p-phenylbenzoquinone
(PPBQ)
E°(Q^-/Q) = 62 mV vs SHE
E°'(QH_2/Q) = 277 mV vs SHE

The "naked" quinone

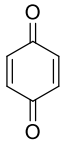

Benzoquinone
(BQ)
E°(Q^-/Q) = 90 mV vs SHE
E°'(QH_2/Q) = 286 mV vs SHE

Quinones with electrodonating groups (low E° values)

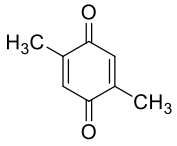

2,5-Dimethylbenzoquinone
(2,5-DMBQ)
E°(Q^-/Q) = -66 mV vs SHE
E°'(QH_2/Q) = 180 mV vs SHE

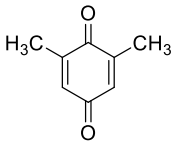

2,6-Dimethylbenzoquinone
(2,6-DMBQ)
E°(Q^-/Q) = -80 mV vs SHE
E°'(QH_2/Q) = 174 mV vs SHE

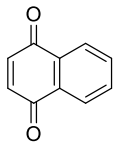

1,4-Naphthoquinone
(NBQ)
E°(Q^-/Q) = -140 mV vs SHE
E°'(QH_2/Q) = 143 mV vs SHE

Figure 12. Structure of quinones firstly considered in the LABEX DYNAMO project.

In this way, the fluorescence emitted (from excited PSIIs) by an illuminated algae suspension in the presence of the quinones mentioned above was monitored. In order to only consider interactions between PSII and exogenous quinones, the ΔPetA mutant was used (the chain is impaired at the b_6f complex). The principle of the experiment is that fluorescence emission is a de-excitation pathway that competes with PSII outgoing electron flow, i.e. the photochemical activity of the photosynthetic chain (see *Figure 13*). Actinic red light (λ = 640 nm) was considered with irradiances ranging from 150 to 1500 µmol photons.m^{-2}.s^{-1}.

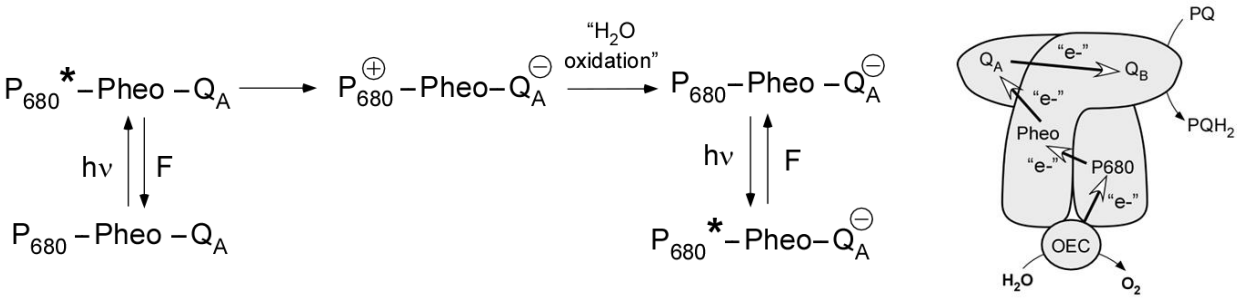

Figure 13. Simplified scheme of the different pathways taken within PSII after excitation of P680 with or without exogenous quinones.

Three levels of fluorescence are then measured: initial fluorescence (F_0; under actinic light with maximum photochemical capacity), steady state fluorescence (F_{stat}; under actinic light with a certain photochemical capacity) and maximum fluorescence (F_{max}; under supersaturating pulse which interrupts endogenous electron flow and leads to zero photochemical activity; see *Figure 14*).

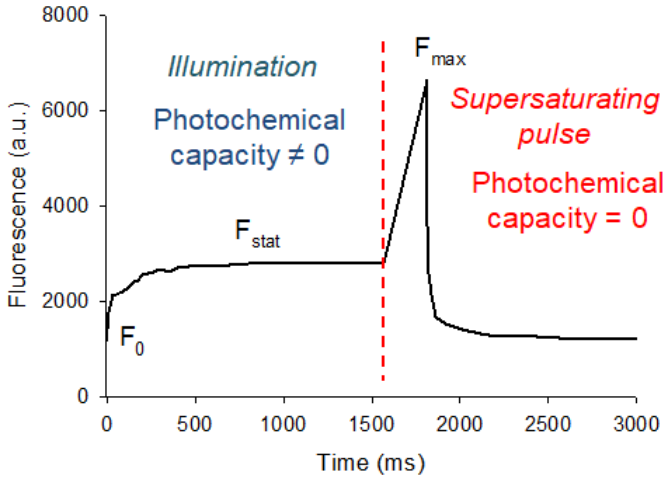

Figure 14. A representative fluorescence induction curve with a ΔPetA algae suspension. *(10^7 cells. mL^{-1}; actinic red light: I° = 340 µmol photons.m^{-2}.s^{-1} and then a supersaturating pulse) in presence of 30 µmol.L^{-1} 2,6-DCBQ.*

The percentage of open centers, i.e. the fraction of PSII centers where the quinone Q_A is oxidized, can be quantified. After substracting the value of this percentage in the absence of quinones, **a diverting parameter « D »** is obtained for each quinone concentration (see *Figure 14*).

$$D = \frac{F_{\max} - F_{stat}}{F_{\max} - F_0} - \frac{F_{\max,no\,Q} - F_{stat,no\,Q}}{F_{\max,no\,Q} - F_{0,no\,Q}} \qquad \textbf{(11)}$$

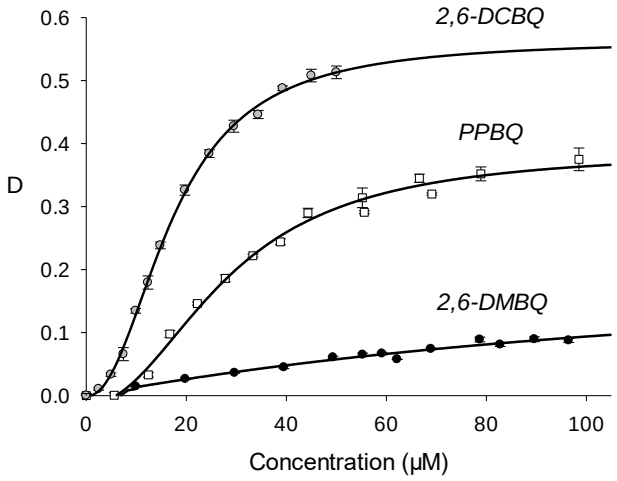

Figure 14. Examples of D = (quinone concentration) curves derived from fluorescence experiments. *(ΔPetA algae; similar conditions to the above figure).*

As expected, this extraction yield increases as a function of quinone concentration since the reduction of exogenous quinones at PSII "steals" electrons and promotes the $Q_A^- \rightarrow Q_A$ pathway. We also notice that the D = f(C) curves have a sigmoidal shape and that low quinone concentrations therefore lead to

D values approaching zero. This unexpected result, given an attended linear correlation, is confirmed by the study of non-photochemical quenching (NPQ). This reflects the non-radiative de-excitation of excited chlorophyll antennae and can be quantified from maximum fluorescence levels with and without exogenous quinones (see above and *Figure 15*).

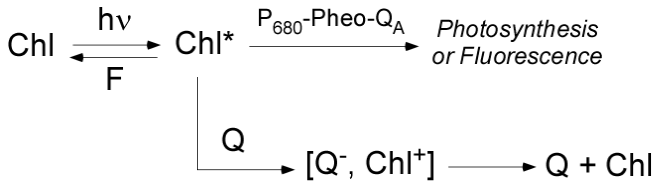

Figure 15. *Simplified scheme of NPQ resulting from exogenous quinones*

Moreover, NPQ is expected to obey the Stern-Volmer's law and be proportional to quinone concentration.

$$NPQ = \frac{F_{\max,no\,Q} - F_{\max}}{F_{\max}} = K_{SV} C_Q \qquad \textbf{(12)}$$

This behavior can be checked by calculating NPQ for each quinone concentration (see *Figure 16*). Once again, we observe a very low value for small concentrations and the expected straight line only for significant concentrations.

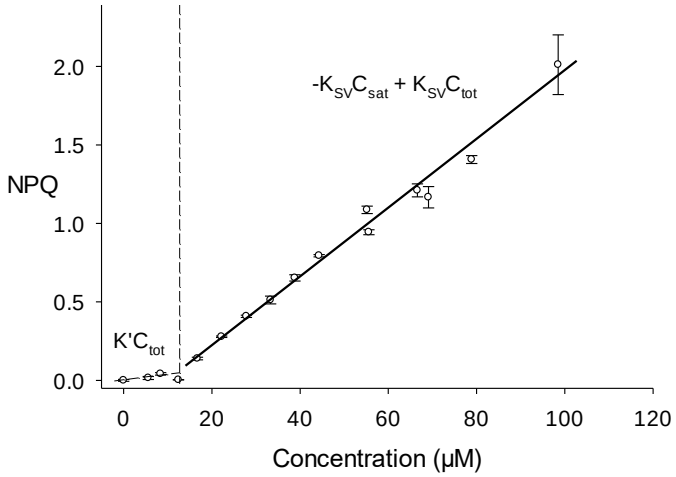

Figure 16. *Examples of NPQ = f (quinone concentration) curves derived from fluorescence experiments (ΔPetA algae + 2,6-DCBQ).*

One possible mechanism to explain this "lateness" is to consider an equilibrium between membranes and aqueous media, with a " loss " of lipophilic quinones. In this context, quinones could only interact with the photosynthetic chain or chlorophyll antennae once saturation had occurred. The mathematical formalism behind this mechanism is then experimentally confirmed, allowing the quenching constants (K_{SV}) and saturating quinone concentration (C_{sat}) to be determined according to the following treatments:

⇒ Low concentrations – Unsaturated membranes

$$k' = \frac{C_{quinones,\text{lost}}}{C_Q} \Rightarrow NPQ = K_{SV} C_Q = K_{SV} \frac{C_{tot}}{1+k'} \quad (\textbf{13})$$

⇒ High concentrations – Saturated membranes

$$C_{sat} = \frac{n_{quinones,membranes,\max}}{V_{total}} \Rightarrow NPQ = KC_Q = K(C_{tot} - C_{sat}) \quad (\textbf{14})$$

The D = f(C) curves can then be corrected to give only the effective quinone concentration as the x-axis. Two relevant parameters can then be identified to describe the efficiency of electron extraction by quinones: the value of D at infinite concentration and the initial slope (see *Figure 17*).

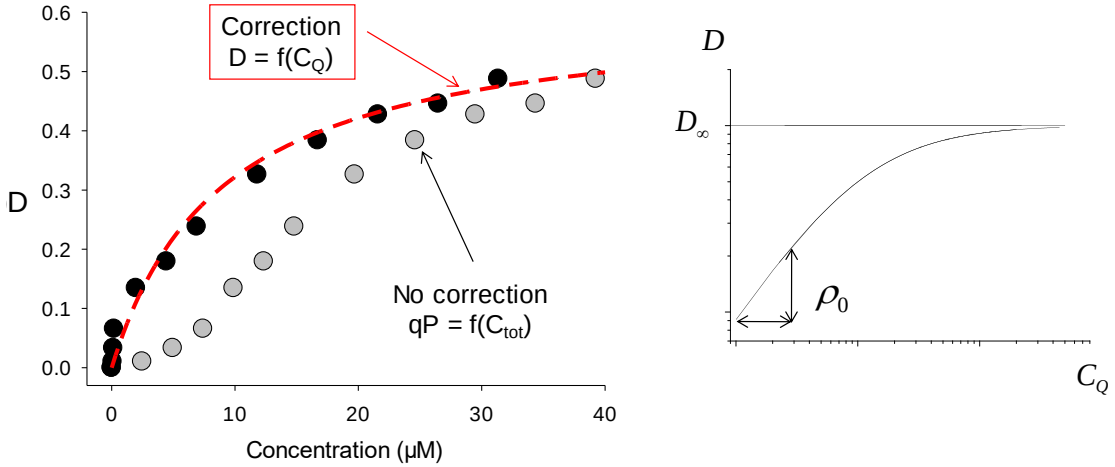

Figure 17. Data correction to take into account the unactive quinone concentration and defining appropriate parameters of electron harvesting/extraction yield. *Left: example of correction of a D = f(C) curve in the case of 2,6-DCBQ with ΔPetA algae. Right: parameters extracted from a representative corrected D = f(C) curve.*

All the results are summarized in *Table 2* and *Figure 18*. The results show that extraction is most efficient for dichloroquinones and DPPQ, which is broadly consistent with the values of the standard potentials at pH 7. It can also be seen that the most harvesting quinones are also those with the highest NPQ. Only BQ does not seem to have an activity in line with its redox potential. In any case, the most promising quinone is 2,6-DCBQ.

Quinone	D_∞	$10^2\rho_0$ ($L.\mu mol^{-1}$)	k'	C_{sat} ($\mu mol.L^{-1}$)	$10^{-4}.K_{SV}$ ($mol^{-1}.L$)
BQ	n.d. (too low)	0.08 ± 0.02	1.2 ± 0.6	36.6 ± 11.0	0.10 ± 0.01
NBQ	0.10 ± 0.03	0.40 ± 0.14	1.5 ± 0.8	5.0 ± 1.5	4.93 ± 0.52
PPBQ	0.48 ± 0.01	1.7 ± 0.1	10.5 ± 5.0	14.3 ± 4.9	2.37 ± 0.19
2,5-DCBQ	0.60 ± 0.08	5.9 ± 0.5	9.6 ± 4.0	12 ± 0.2	2.28 ± 0.40
2,6-DCBQ	0.58 ± 0.06	4.1 ± 1.4	38 ± 15	19.5 ± 6.6	1.84 ± 0.08
2,6-DMBQ	n.d. (too low)	0.10 ± 0.02	1.0 ± 0.5	11.9 ± 6.8	0.37 ± 0.04
2,5-DMBQ	n.d. (too low)	0.08 ± 0.02	1.0 ± 0.4	4.1 ± 0.8	0.45 ± 0.06

Table 2. Extracted parameters from fluorescence measurements except for E°' values *(ΔPetA algae suspension; 10^7 cells. $mL^{-1;}$ actinic red light: I° = 340 µmol photons.$m^{-2}.s^{-1}$).*

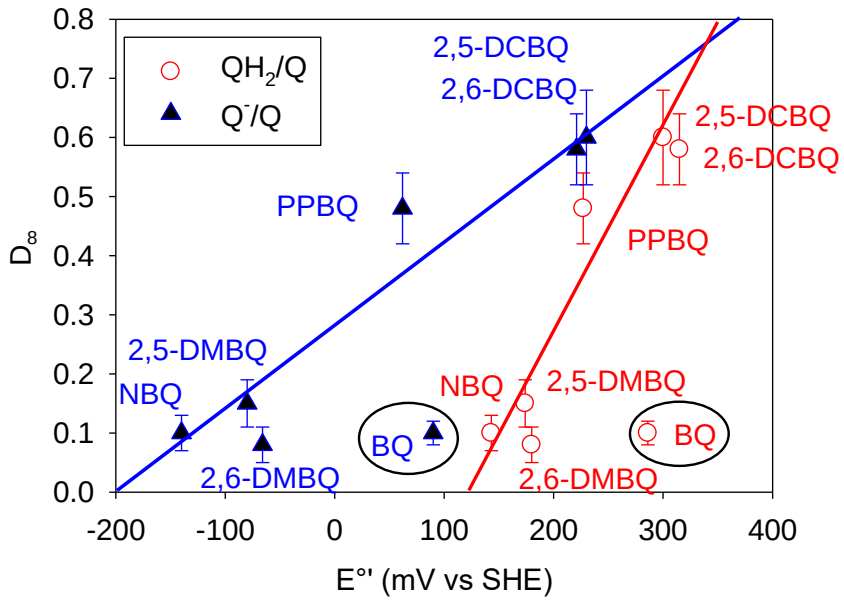

Figure 18. Maximum extraction yield from quinones toward ΔpetA algae as a function of standard redox potentials E°' *(for Q^-/Q and QH_2/Q redox couples at pH 7.4).*

3.3.2. Understanding the action of 2,6-DCBQ and developing the first photocurrent extraction/production device

Beyond the quinone partitioning phenomena, the question was raised of the shape of the D = f(C) curve, whose extraction yield by quinones rises and then reaches a constant value. Modeling studies were therefore carried out for 2,6-DCBQ based on an extraction mechanism at Q_A (see *Figure 19*) [171].

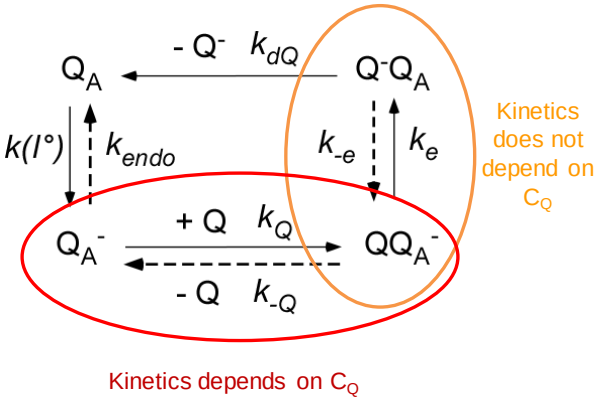

Figure 19. Whole scheme of the photosynthetic electron harvesting by quinones according to: $Q_A^- + Q = Q_A + Q^-$. *PSII light irradiance leads to a charge separation and the Q_A reduction. The exogenous quinone Q will arrive at the Q_B pocket (mass transfer step whose kinetics depends on Q concentration – red circle). The embedded Q will be then reduced by Q_A^- (charge transfer step whose kinetics does not depend on Q concentration – orange circle). Please note that this monoelectronic transfer corresponds to an oversimplified view. Indeed, a second electron step should occur but do not change the global mathematical expressions involved in the fluorescence experiments.*

From kinetic considerations (quasi-steady state approximation) on the stationary fluorence level Fstat, it could be shown that the photochemical quenching (named here qP, i.e. the value without any substraction of the value with no quinone) should follow a simple hyperbolic rectangular law (see *equation 14*), which is in agreement with the curves from the experiments.

$$qP = \frac{(qP)_0 + \rho_0 C_Q}{1 + \frac{\rho_0}{D_\infty} C_Q} \qquad (\textbf{15})$$

This model helps us to understand that the shape of the curve is governed by competition between two phenomena caused by the quinone: its arrival at the extraction site (concentration-dependent mass transfer - MT) and the efficiency of its reduction once in the Q_B pocket (concentration-independent charge transfer - CT). Thus (see *Figure 20*), the rising phase of the percentage of open centers as a function of quinone concentration corresponds to mass transfer limitation (slower than CT as concentrations remain moderate) while the constant phase corresponds to charge transfer limitation (as MT becomes faster at high concentrations).

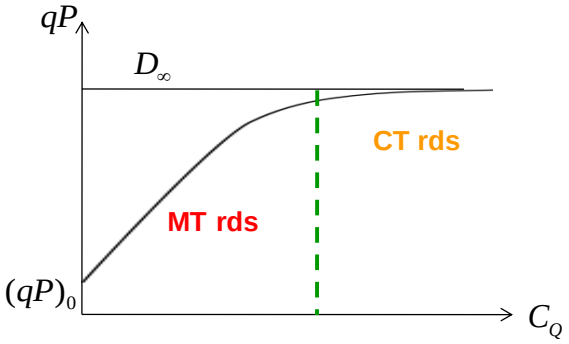

***Figure 20. Whole qP = f(C_Q) shape including the two important phases**: increasing where mass transfer is rate limiting and a constant qP value corresponding to a charge transfer kinetic limitation.*

This mechanism was confirmed by other experimental analyses, notably the effect of actinic light intensity or the nature of endogenous electron flow (wild-type vs. mutant algae). Interestingly, a possible pseudo-inverse Marcus zone was demonstrated for naphthoquinone (with a high affinity for the QB pocket and low electron acceptance), which acts as an inhibitor, reducing rather than increasing the percentage of open centers.

Based on these models, it was possible to construct a zone diagram simulating the value of the percentage of open centers as a function of effective quinone concentration (C_Q) and actinic light intensity (I°). This predicts the experimental conditions where electron harvesting is maximal and/or dependent on quinone concentration. Furthermore, this diagram shows that caution must be taken with regard to conditions generating MT-limiting extraction, as in this case the comparison of quinones according to their redox potential E°' becomes irrelevant.

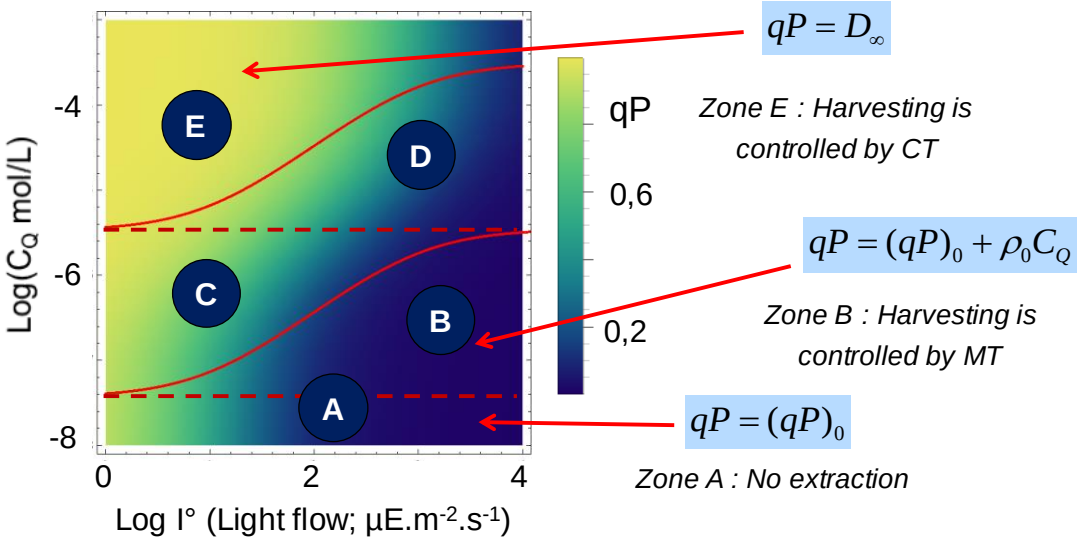

***Figure 21. 3D-Zone diagram (qP; I°; C_Q) calculated from fluorescence experiments for the tandem ΔpetA algae/2,6-DCBQ.** Considering light intensities and quinone concentration values, experimental conditions are defined where charge transfer governs electron extraction (maximum diverting and no C_Q effect) or mass transfer is rate determining (diverting depends on C_Q). I° in µE.m^{-2}.s^{-1} is equivalent to µmol photons.m^{-2}.s^{-1}.*

Based on these results, the experimental conditions for using 2,6-DCBQ were selected (I° = 340 µmol photons.m^{-2}.s^{-1}; C between 40 and 100 µmol.L^{-1} and therefore C_Q between 20 and 80 µmol.L^{-1} ; 10^7 cells.mL^{-1}) to be in a mixed region where CT, although prevailing, is not entirely limiting, ensuring significant but concentration-dependent extraction.

At this point, an early spectroelectrochemical device has been implemented to allow the hydroquinones resulting from interactions between microalgae and quinones to be oxidized and return to their original form [172]. To do so, an electrolysis cell (V ~20 mL containing a centimetric carbon gauze) sealed to a spectroscopy cuvette was built in the laboratory. Actinic light then passes through the cuvette, and stirring keeps the algae in suspension and moves them to the collecting electrode. Electrochemical conditions are therefore on a preparative scale and in half-cell configuration (3-electrode set-up). The potential of the electrode is set at a value (650 mV vs Ag/AgCl) allowing the reaction $QH_2 = Q + 2e^- + 2H^+$ and chronoamperometry measurements are then carried out (see *Figure 21*).

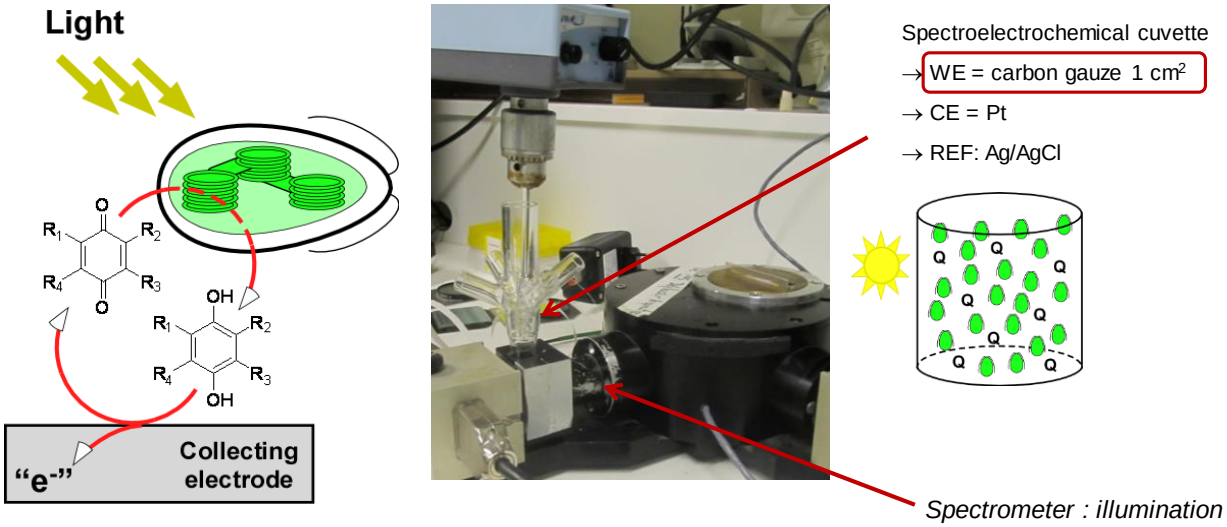

Figure 21. First generation spectroelectrochemical device for producing electricity from Chlamydomonas reinhardtii. *Left: principle of photocurrent production from microalgae and quinones through an electrocatalytic cycle involving Q reduction by algae and QH_2 oxidation at the collecting electrode surface. Top: first generation device with an electrolysis cell sealed to a spectrochemical cuvette.*

The first photocurrents (see *Figure 22*) were obtained from such an experimental set-up. The effect of 2,6-DCBQ concentration (between 40 and 100 µmol. L^{-1}) and light (between 135 and 340 µmol photons.m^{-2}.s^{-1}) was linear. Moreover, these photocurrents have reached a quasi-steady state for one hour before decreasing and disappearing after about 8 hours of illumination.

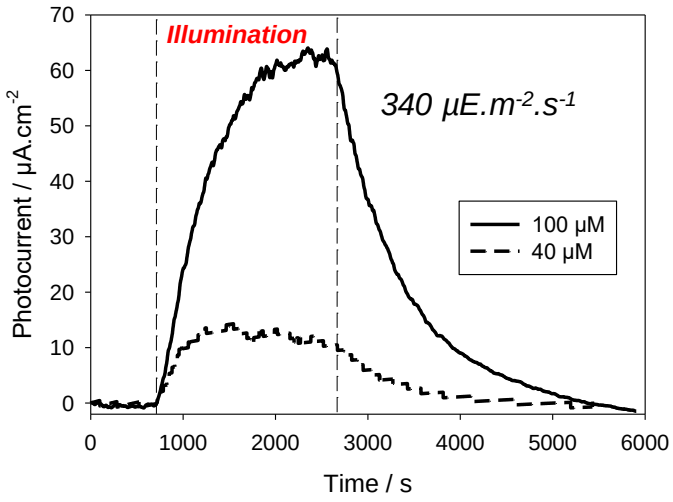

Figure 22. Chronoamperograms from a suspension of ΔPetA algae with 2,6-DCBQ *(E_{appl} = + 650 mV vs Ag/AgCl). I° in µE.m^{-2}.s^{-1} is equivalent to µmol photons.m^{-2}.s^{-1}.*

3.3.3. Analyzing the results - Investigating the shape of photocurrents

These initial encouraging results (current density ~ 60 µA.cm^{-2}) raise the question of how to optimize the biophotoelectrochemical system in terms of performance and stability. In this context, modelling has been performed to predict and understand the nature of the photocurrent produced [173]. Thus, the investigated electocatalytic cycle is in the form of an "EC" mechanism under electrolysis conditions (stirring + macroelectrode):

$$\begin{aligned} algae^{*} + h\nu + Q &\rightarrow algae + QH_2 \quad with\ rds = CT\ or\ MT \\ QH_2 &\xrightarrow{k_{el}} Q \quad with\ rds = CT\ or\ MT \end{aligned} \qquad \textbf{(16)}$$

In this context, a zone diagram (see *Figure 23*) can be used to determine the nature of the steps governing the steady state photocurrent on the basis of the following equations:

$$\frac{dC_Q}{dt} = k_{el} C_{QH_2} - \frac{v_{\max}}{V} \frac{D_\infty C_Q}{D_\infty / \rho_0 + C_Q} = 0 \qquad \textbf{(17)}$$

$$k = \frac{Electrochemical\ rate}{Harvesting\ rate} = \frac{k_{el} V}{v_{\max} \rho_0}; b = \frac{MT_{harvesting}}{CT_{harvesting}} = \frac{\rho_0 C}{D_\infty} \qquad \textbf{(18)}$$

$$\Psi = \frac{i}{2F k_{el} V C} = 1 - \frac{C_Q}{C} \qquad \textbf{(19)}$$

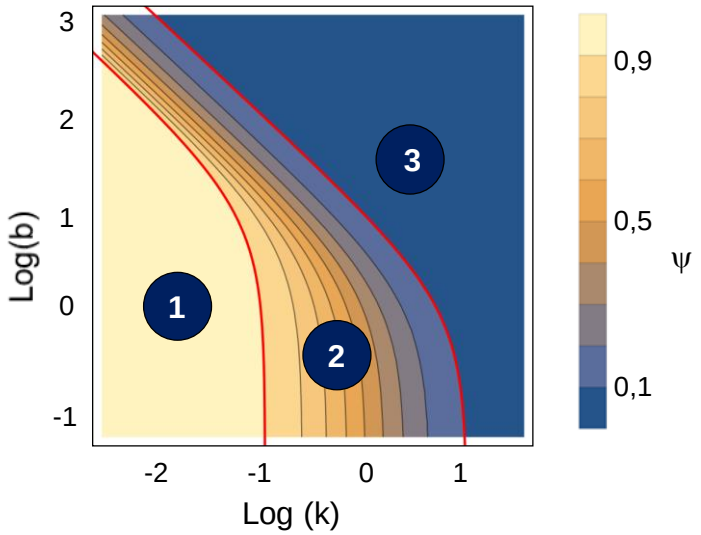

Figure 23. 3D-Zone diagram calculated from electrochemical experiments for the tandem ΔpetA algae/2,6-DCBQ. *ψ is the normalized steady state photocurrent. k is an undimensionnal parameter that compares the rates of Q reduction and QH_2 oxidation. b is related to the electron harvesting step and especially on the ratio of the mass to charge transfer rates.*

This shows that there are two boundary zones. The first, "1", is where the process at the electrode is kinetically limiting. Under these conditions, the steady-state current only depends on electrochemical conditions (C, V, k_{el}) and is expressed as:

$$i_{ss} = 2Fk_{el}VC \qquad (\textbf{20})$$

The second "3" is where photosynthetic electron extraction is the rate determining pathway (in which the rate determining step is charge transfer).

$$i_{ss} = 2Fv_{\max}D_{\infty}\rho^{\circ}\frac{C}{D_{\infty}+\rho^{\circ}C} \qquad (\textbf{21})$$

An intermediate zone, “2”, corresponds to a mix between the two behaviours. In any case, for a given volume of solution, zone 1 should lead to the best performance. Actually, it is not that simple, as this zone is obtained for low values of solution volume (V $\downarrow \Rightarrow$ k $\downarrow$), which reduces the intensity of the stationary current. In this context, it is preferable to focus on zone 3, which will lead to higher currents once the quinone diverting is efficient. Furthermore, it is this zone that is theoretically reached under the conditions of the experiment with 2,6-DCBQ and for which the model is used to simulate the experimental curve (see *Figure 24*).

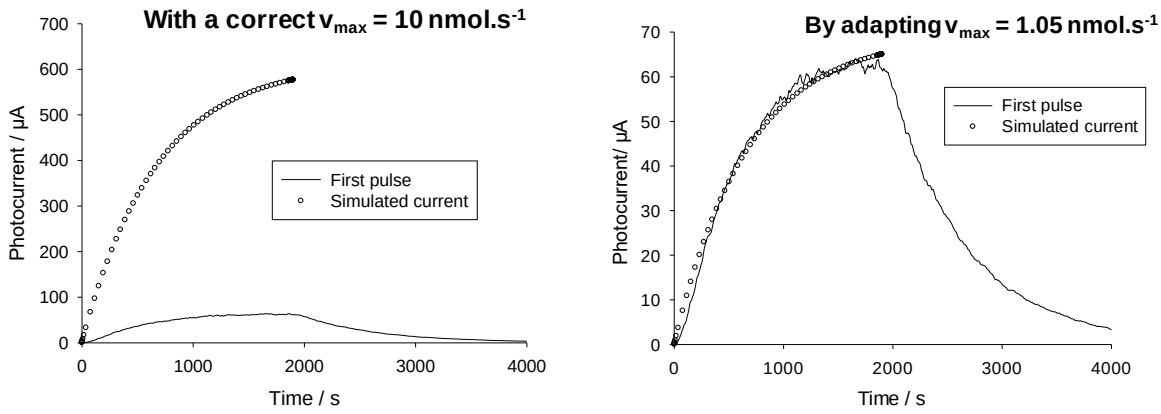

Figure 24. Comparison between experimental and simulated photocurrents from DpetA algae and 2,6-DCBQ from the first generation electrochemical device. *Left: simulations are achieved with the expected photochemical rate. Right: correlations between experimental and simulated curves are constrained thus resulting in a lower photochemical rate value.*

The simulation results are particularly interesting. On the one hand, the shape of the experimental curve is accurately reproduced and can be simulated with good agreement. On the other hand, this good correlation is only achieved by underestimating the value of the maximum photochemical rate vmax. In other words, with the correct value of this parameter, the expected current is 10 times higher than the experimental current. Finally, the model fails to explain why the current eventually drops (either under continuous light or after different light pulses). This shows that the model is not comprehensive and does not take into account poisoning and inhibition phenomena for instance.

For this reason, further investigations were carried out to monitor the evolution of the algae/quinone tandem over time [174]. Fluorescence measurements were performed for several quinones (2,6-DCBQ, 2,5-DCBQ, PPBQ, 2,6-DMBQ), showing that NPQ increases over time (see *Figure 27*).

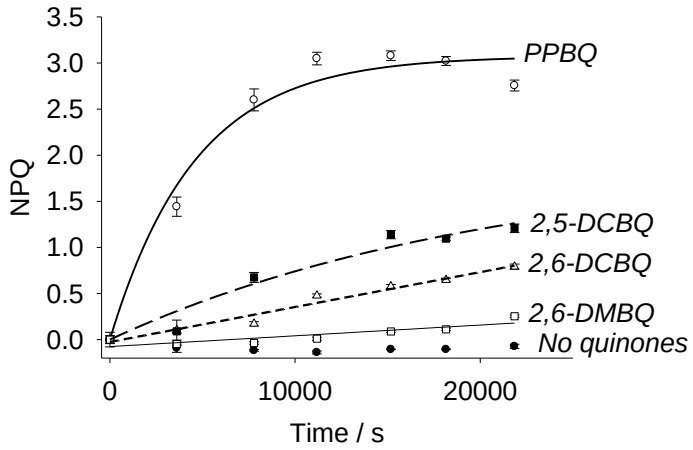

Figure 27. NPQ over time for a ΔPetA suspension in presence of 100 µmol.L^{-1} quinones.

3.3.4. Kinetic quenching from a suspension of ΔpetA algae with quinones

This more or less significant increase of NPQ over time, suggests kinetic quenching, which could be related to the decrease in photocurrent also occurring over time. This effect differs from one quinone to another, and the "diverting" quinones seem to be more involved in kinetic quenching than the low efficient quinones. An initial assumption for the decrease in current would therefore be linked to a side effect of the quinones, which would not act solely as acceptors of photosynthetic electrons. The origin of this kinetic quenching is unclear. On the basis of fluorescence measurements, this evolution could be modelled by a 1st order kinetic mechanism in which the quinones interact with a protein, which then releases an unknown molecule causing the fluorescence quenching (see *Figure 28)*.

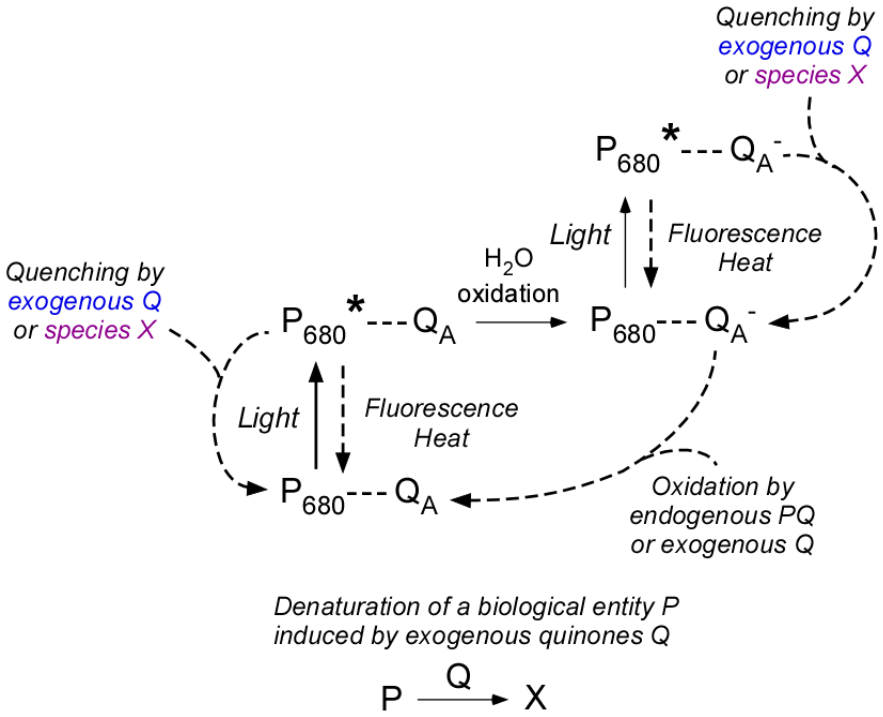

Figure 28. Tentative scheme summarizing the possible side effects of exogenous quinones towards non photochemical quenching (NPQ).

3.3.5. Overview of the quenching induced by exogenous quinones.

Furthermore, it cannot be ruled out that photoinhibition plays a role in the decrease in performance. For this reason, an experiment was carried out with PPBQ with green rather than red illumination. Under conditions where NPQ remains constant, the photocurrent thus becomes stable (see *Figure 29)*.

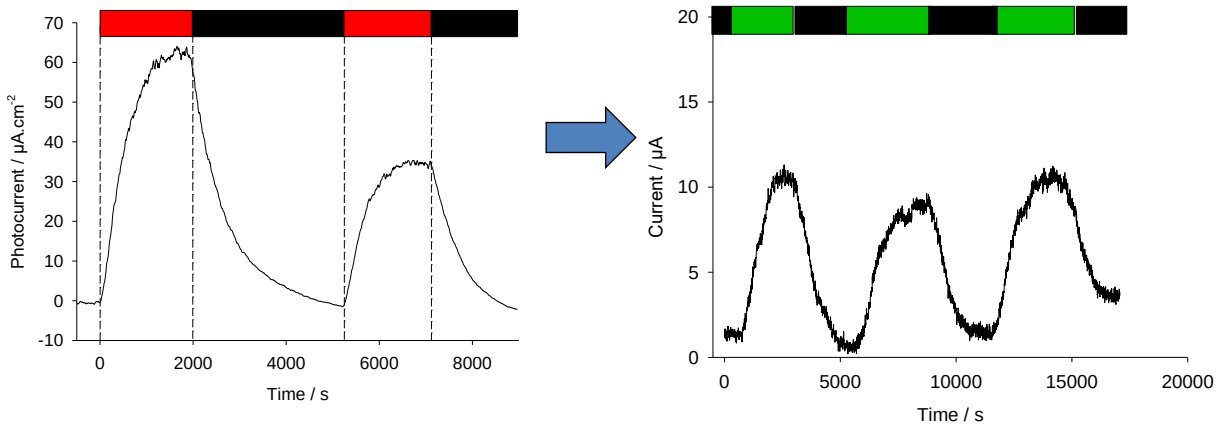

Figure 29. Effects of light/dark cycles on electrochemical experiments *(i.e. chronoamperometry measurements) from ΔpetA algae and quinones at +650 mV vs Ag/AgCl) carried out with the first generation device. Left: with 100 µmol.L^{-1} 2,6-DCBQ with an actinic red light (340 µmol photons.m^{-2}.s^{-1}).*

At this point in the research, it appears that the reasons for this fall in photocurrent have neither been elucidated nor fully understood. It cannot be ruled out that quinones may be involved in other side-effects such as oxidative stress, interactions with the respiratory chain or other types of reactivity, since quinones are identified as good electrophiles (see *Figure 30*).

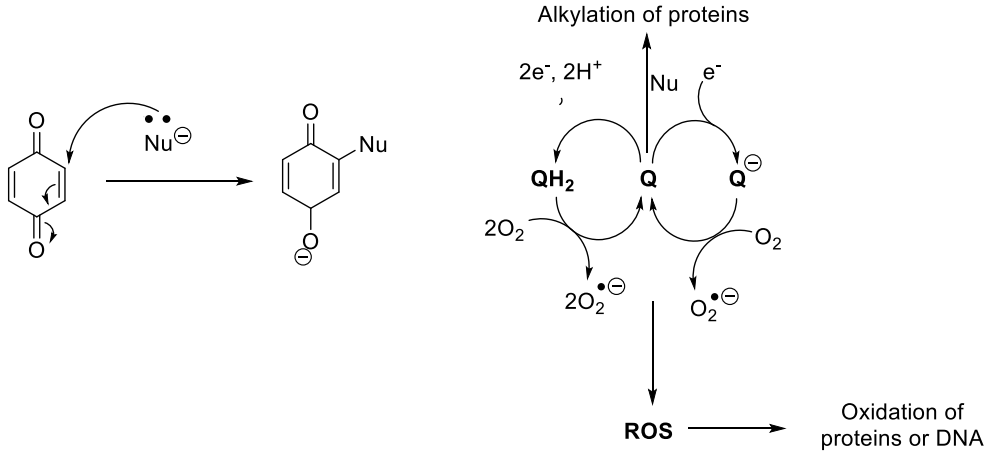

Figure 30. Possible toxicity mechanisms induced by quinones **[175].** *Left: quinones are able to react with nucleophiles by means of 1,4-addition (Michael reaction). Right: whole side-reactions by quinones involving Michael addition and reactions from reduced forms (Q^{-} or QH$_2$) with O$_2$ then resulting in ROS (reactive oxygen species) production.*

3.3.6. Going further in the analysis - Second generation electrochemical device

The device described above has the advantage of working in conditions where the entire algae suspension is affected by the illumination and the electrocatalytic cycle, especially via a forced convection regime. However, the presence of a large and reticulated electrode results in a high

capacitive current that can last for several hours, leading on the one hand to time-consuming studies and on the other to work with algae under pre-polarisation. In this context, a new device (see *Figure 31*) was developed in the form of a small-volume well (~ 500 µL) delimited with PDMS (Polydimethylsiloxane), whose bottom (radius ~ 0.5 cm) forms the working electrode, i.e. an ITO (Indium Tin Oxide) - Au layer [176].

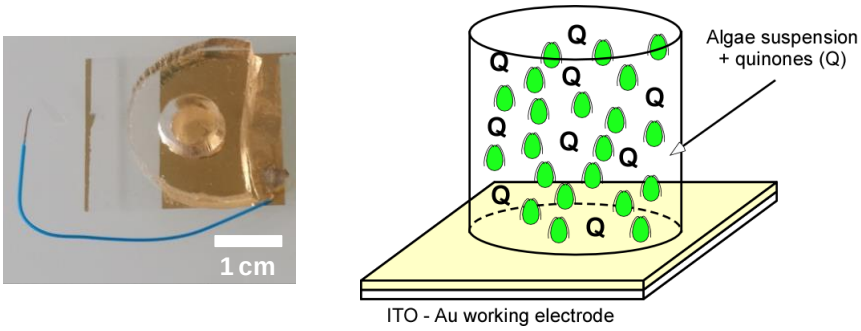

Figure 31. Second generation electrochemical device for extracting photosynthetic electrons from microalgae. *Left: picture of a typical ITO-Au well. Right: schematic view in presence of algae and quinones.*

This second-generation device was used to compare 2,6-DCBQ with 2,6-DMBQ, which is expected to be less active as an extracting quinone. The photocurrent behaviour was similar to that obtained in previous studies, with a rise in photocurrent, followed by stabilisation and then a slow decrease (see *Figure 32*).

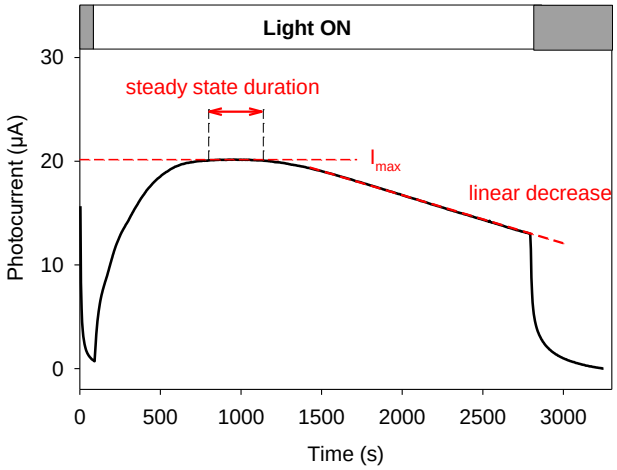

Figure 32. Representative chronoamperogram recorded from the second generation device *(WT algae at 2.10^7 cells. mL^{-1} with 100 µmol. L^{-1} 2,6-DCBQ under white light; P = 60 mW.cm^{-2}) at 380 mV vs Ag/AgCl.*

Thanks to the ease of use of this electrochemical set-up, it was possible to change the experimental parameters, in particular the concentration of quinones and algae, as well as the illumination conditions.

Concerning the illumination, continuous irradiance was compared with on/off light cycles. It can be seen that photoinhibition does really play a role in the photocurrent decay, but only to a moderate extent and for long periods (see *Figure 33*).

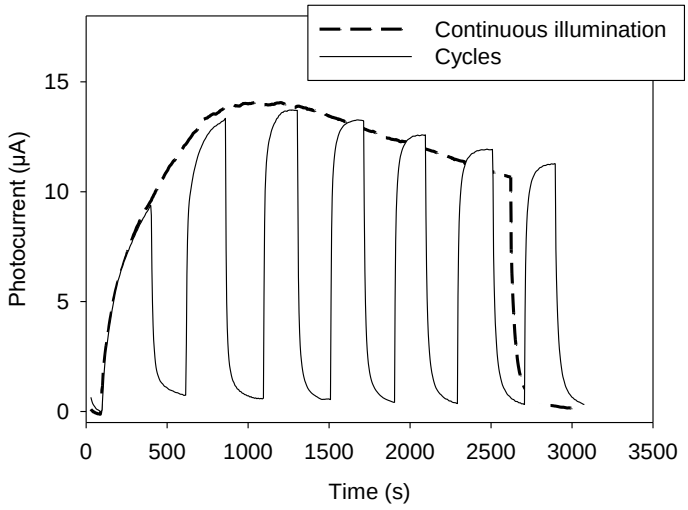

Figure 33. Effect of light on electrochemical experiments from microalgae and quinones. *Chronoamperograms recorded under the same conditions than above except for the light duration (dashed: continuous illuminations; solid: light on/off cycles).*

Concerning the steady state photocurrent, the concentration effect was found to follow a Michaelis-Menten relationship (see *Figure 34*), in agreement with the fact that the kinetically limiting process was the extraction of photosynthetic electrons by the quinones, which followed a similar relationship in the fluorescence measurements.

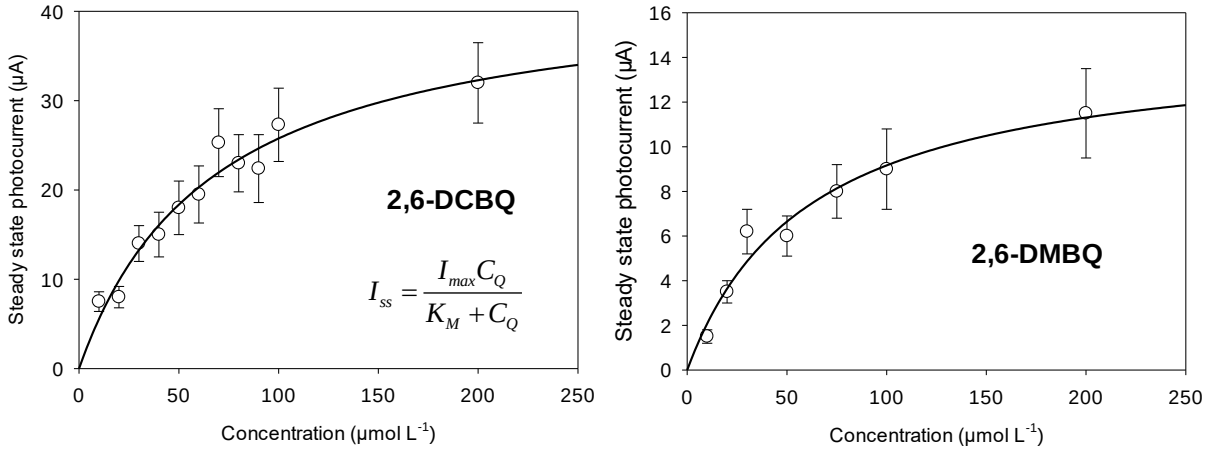

Figure 34. Steady state photocurrent recorded from WT algae as a function of quinone concentration *(left: 2,6-DCBQ; right: 2,6-DMBQ). Both shapes can be adequately fitted with a Michaelis-Menten like behaviour.*

These experiments confirm that 2,6-DCBQ is much more efficient than 2,6-DMBQ, in agreement with their redox potential. Another result of interest is the preliminary analysis of photocurrent stability,

which is an order of magnitude higher for 2,6-DMBQ. In other words, although on the insufficient basis of only two quinones, it would appear that a harvesting quinone would lead to a higher but less stable maximum photocurrent than a poorly electron accepting quinone.

These different behaviours and the second generation device have also been used to study a new strategy, i.e. mutagenesis. The main idea is to work on mutant algae whose PSII has been modified (see *Figure 35*), in this case by an additional 'pocket' to facilitate access to the quinone [177].

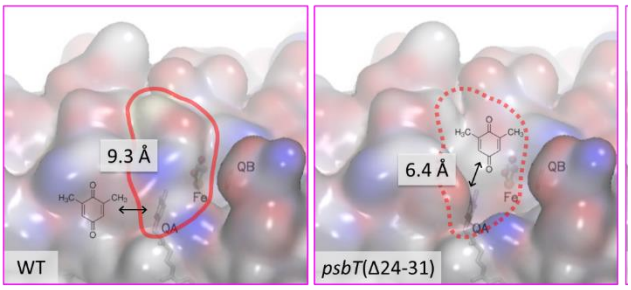

Figure 35. Surface structures of PSII built with the SWISS-MODEL workspace. *Left: no truncation. Right: upon truncation of PsbT. Red lines display the truncated region. The number shows the shortest distance measured between the conjugated ring of Q_A and the accessible surface of PSII.*

2,6-DMBQ was chosen as the candidate quinone because its poisoning effect is less pronounced than for 2,6-DCBQ and because it is a poor electron accepting quinone. It can be observed that if the work is performed in the presence of DCMU, an inhibitory molecule that can be embedded in the Q_B pocket and then suppress the endogenous electron flow, a residual photocurrent is still observed in the mutant compared with the WT algae, confirming that the additional access route is effective (see *Figure 36*).

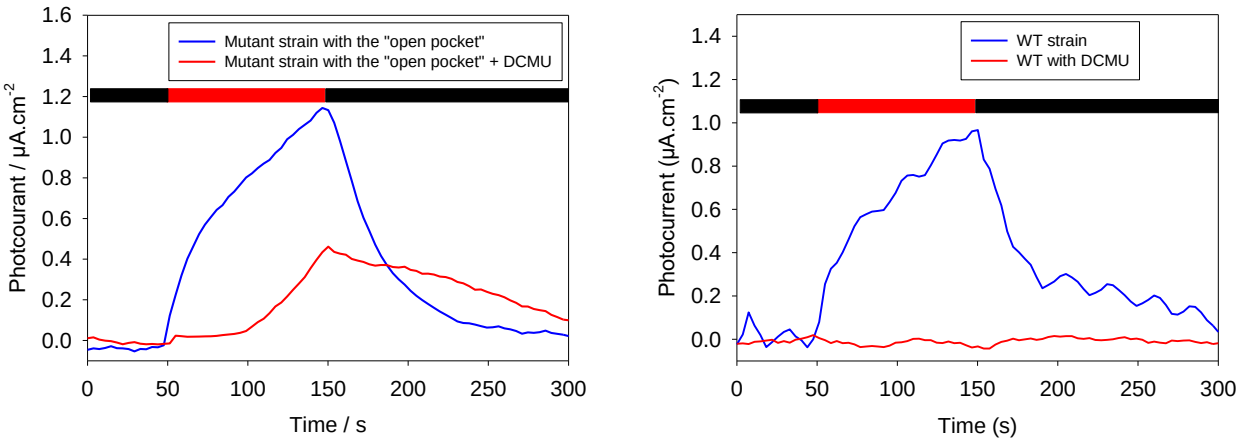

Figure 36. Chronoamperograms recorded from WT or mutant algae with 2,6-DMBQ *(30 µmol.L^{-1}) under a green actinic light (50 µmol photons.m^{-2}.s^{-1}). Left: mutant algae with or without DCMU pre-incubation. Right: WT algae with or without DCMU pre-incubation.*

This promising strategy nevertheless raises a series of questions. While the idea of modifying PSII to facilitate interaction with a "poor" quinone is a good one in principle, the new site must necessarily improve interaction with the quinone, otherwise it will be just another option on the chain, without facilitating the extraction of photosynthetic electrons. This requires other modifications, which have not yet been achieved, such as adjusting the size of the new pocket or increasing the lifetime of its reduced form.

It should be pointed out that all the conclusions and analyses of the results were obtained by fluorescence or electrochemical measurements performed independently. It was therefore essential to develop a new device that would enable the two types of information to be correlated in real time, i.e. data on the state of the photosynthetic chain (fluorescence) and photocurrent performance (electrochemistry).

3.3.7. Third generation device - Electrochemistry-fluorescence coupling

In order to simultaneously monitor the chlorophyll fluorescence emission of algae and the oxidation of the reduced form of the exogenous quinone, the new device was inspired by the former. The PDMS is now replaced by a glass cylinder attached by a specific cell to an ITO electrode (radius ~ 0.5 cm). An optical fibre allows illumination from beneath the electrode and measurement of the resulting fluorescence [178]. While electrochemical monitoring is carried out using a potentiostat, fluorescence measurements are obtained using a PAM (Pulse Amplitude Modulation) system. A continuous bubbling of air provides stirring, which also prevents the algae from sedimentation (see *Figure 37*).

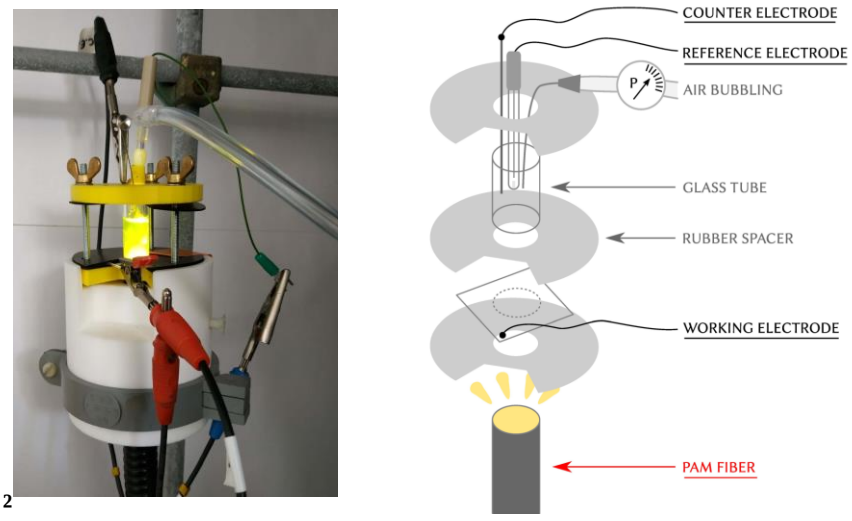

Figure 37. Third generation device allowing coupled fluorescence-amperometry measurements. *Left: photograph of the spectroelectrochemical cuvette. Right: scheme of the different components.*

Coupled signals can thus be collected from a mixture of WT microalgae and 2,6-DCBQ. The end of the experiment was reached either by adding DCMU or by switching off the actinic light (see *Figure 38*).

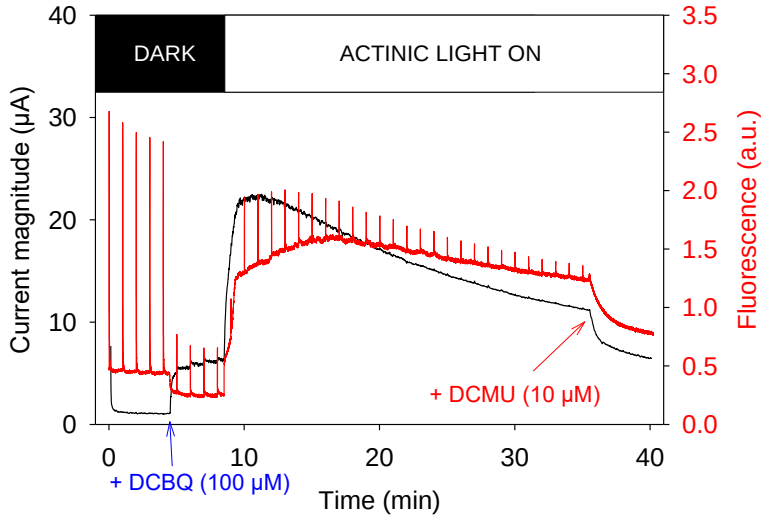

Figure 38. Representative "chronofluoroamperogram" recorded from a WT algae suspension *(2.10^7 cells.mL^{-1}) with 2,6-DCBQ (100 µmol.L^{-1}) under red actinic light (700 µmol photons.m^{-2}.s^{-1}); supersaturating pulse every 30 s.*

The typical current profile is observed when the fluorescence signals contain a peak every 30 s due to the application of the supersaturating pulse. This enables real-time measurement of fluorescence signals associated with actinic light and resulting from the supersaturating pulse. Unfortunately, it is impossible to determine a percentage of open centres (the continuous light makes it impossible to measure several F_0 values). However, it is possible to extract the photochemical efficiency (or quantum yield) of Φ_{PSII}, which corresponds to the ratio of photons transformed into photosynthetic electrons.

$$\Phi_{PSII} = \frac{F_{max} - F}{F_{max}} \qquad (\textbf{21})$$

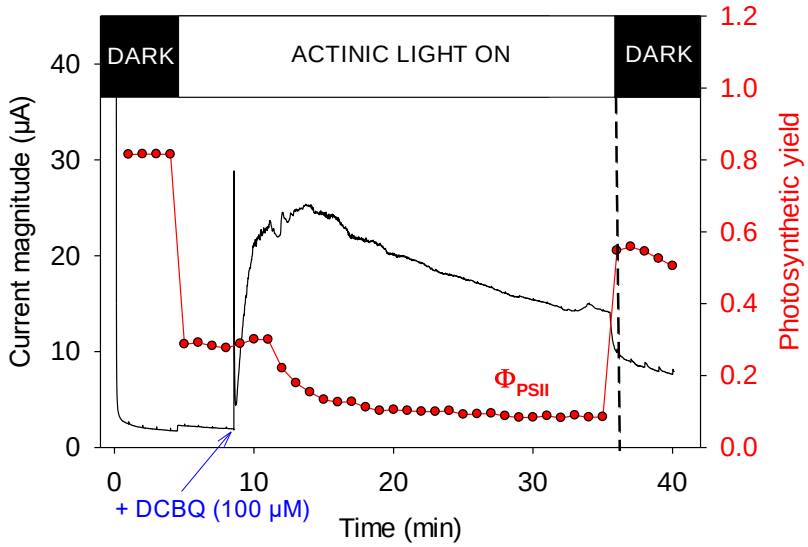

Figure 39. "chronofluoroamperogram" where the fluorescence signal is converted into PSII yield *(Φ_{PSII}) according to the formula described in the text.*

This enables the yield of the photosynthetic chain downstream of PSII to be correlated with the photocurrent. It can be seen that Φ_{PSII} increases as the photocurrent increases, which is expected since the addition of the quinone alleviates the chain and accelerates photon-electron conversion (see *Figure 39*). However, Φ_{PSII} fastly decreases until it reaches zero. This is because 2,6-DCBQ is also a fluorescence quencher. Its interaction with the chlorophyll antennae therefore diminishes the number of 'effective' photons and reduces photosynthetic yield. This result is interesting, but not sufficient to understand the fall in current. This is why NPQ can also be quantified from each fluorescence peak and an average of these peaks before illumination (see *Figure 40*).

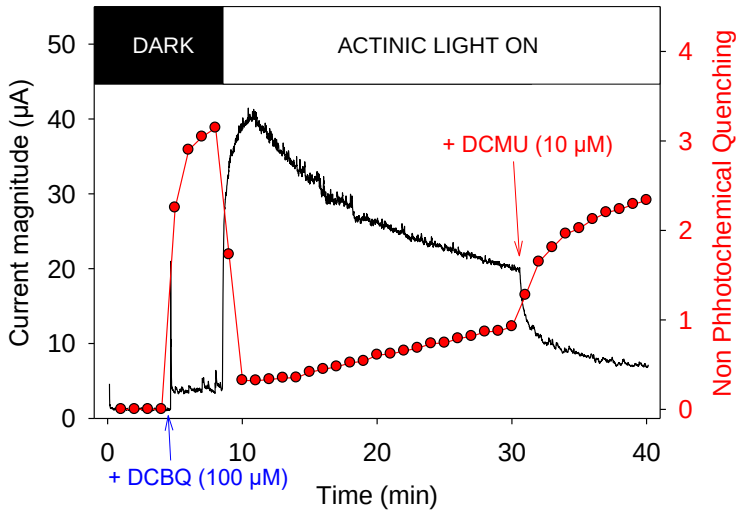

Figure 40. "chronofluoroamperogram" where the fluorescence signal is converted into non photochemical quenching *(NPQ) according to the formula described in the text.*

This shows that the NPQ mirrors the drop in photocurrent. Under electricity-generating conditions, this result confirms the fluorescence studies carried out previously, which identified kinetic quenching. This suggests that quinones are gradually no longer available to achieve the photosynthetic electron diverting. This does not rule out the previous hypothesis of the production of an unknown quenching molecule, but opens up the discussion to other possibilities, such as the fact that 2,6-DCBQs "accumulate" during the electrocatalytic cycle and, without being degraded, are involved in the quenching process.

In order to better understand these simultaneous measurements, modelling was done using different experimental conditions (fluorescence in the dark with quenching following 1st order kinetics, fall in current after addition of DCMU, rise in current after illumination; see *Figure 41*) [179].

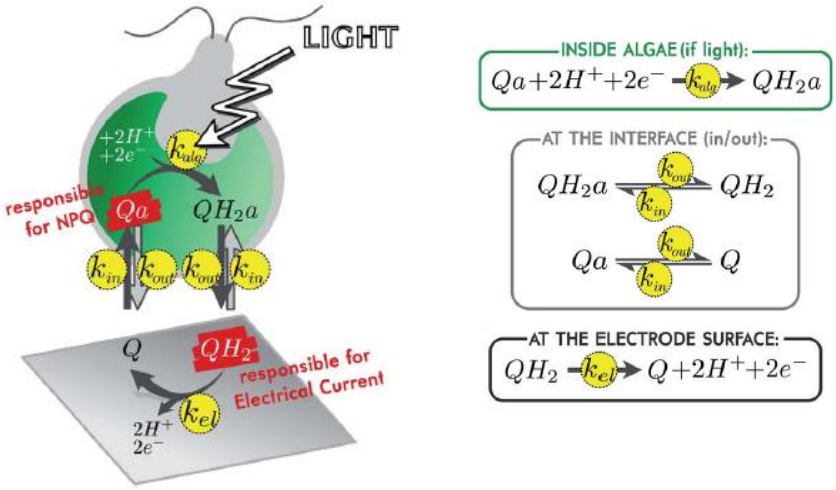

Figure 41. Scheme describing the steps involved in the production of photocurrent from microalgae*. Each step is labelled with one or two rate constants.*

After solving the system of four equations and four rate constants, the following results were obtained, enabling the experimental curves to be fitted with an excellent agreement ($R^2 > 0.99$).

$$\begin{aligned} k_{in} &= 1.13\times10^{-2}\ s^{-1} \\ k_{out} &= 9.49\times10^{-3}\ s^{-1} \\ k_{el} &= 6.02\times10^{-2}\ s^{-1} \\ k_{alg} &= 0.63\ s^{-1} \end{aligned} \qquad (\textbf{\textit{23}})$$

This shows that the rate-determining step in the whole process is really the interaction between the oxidised form of the quinone and the photosynthetic chain, but more importantly the rate of uptake/release of the redox mediator.

Based on these models, several assumptions on the photocurrent decay were mathematically incorporated into the system of equations to provide theoretical profiles of fluorescence and currents (see *Figure 42*).

- **« Trapping »**: quinones are lost within cell compartments and are gradually not able to be involved for diverting electrons

- **« Screening effect »**: NPQ due to quinones decreases the light intensity perceived by photosynthetic chains

- **« Toxicity »**: quinones alter photosynthetic chains by means of ROS production or Michael addition

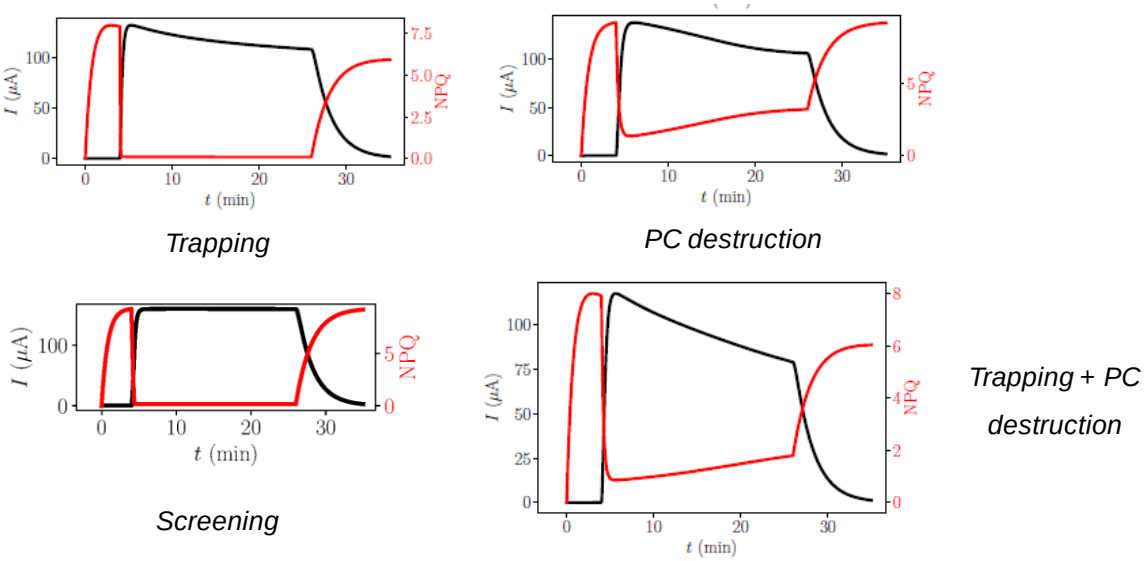

Figure 42. "chronofluoroamperogramms" simulated on the basis of the rate constants determined above. *One or more of these constants are modified to take into account possible toxicity mechanisms.*

As a result, the best conditions were found to be a mix between quinone trapping and photosynthetic chain destruction. In other words, the increase in NPQ may be related to the decrease of available photosynthetic chains for the electron rerouting. The amount of « pending » quinones therefore increases and they consequently quench Chl* instead of being involved in electron harvesting. Eventually, quinones are also lost in sequestered compartments thus preventing the final NPQ to recover its initial value. Unfortunately, same results are obtained whatever the mechanism considered (oxidative stress or Michael reaction).

3.3.8. Conclusion

At this stage of the project in the laboratory and in the field of electricity production from natural photosynthesis, the study of the microalgae-quinone tandem leads to the following conclusions. Firstly, quinones can act as effective redox mediators for the production of photocurrent from a suspension of *Chlamydomonas reinhardtii* microalgae. On the basis of the 2,6-DCBQ molecule, the decline in performance is related to the loss of the quinone in cellular compartments and its dual action since it is capable of generating toxicity mechanisms, the nature of which being still not clearly defined.

It is important to focus on the search for the best quinone, i.e. the one leading to the highest and most stable photocurrents. While previous studies have provided a better understanding of the biophotoelectrochemical system, they have not yet led to the definition of an identity card for the quinones to be selected. This is why it is necessary to firstly take advantage of the second generation device, which is very easy to use, to screen different structures based on their redox potential and their substituents (*Article n°1*) and then to consider other characterizations such as those related to ATP synthase (*Article n°1*) or photosystem I (*Article n°2*) with the idea of comparing the two model quinones (2,6-DCBQ and 2,6-DMBQ) on the basis of all these parameters (*Article n°3*).

Article n°1

A. Sayegh, L. Perego, M. Arderiu Romero, L. Escudero, J. Delacotte, M. Guille-Collignon, L. Grimaud, B. Bailleul, F. Lemaître *ChemElectroChem* **2021**, *8,* 2968-2978.

Finding Adapted Quinones for Harvesting Electrons from Photosynthetic Algae Suspensions

Article n°2

S. Ferté, M. Arderiu Romero, G. Shimakawa, B. Genty, B. Bailleul

How to probe photosystem I activity? A critical reappraisal of measurements of photosystem I yield

Article n°3

M. Arderiu Romero, M. Guille-Collignon, F. Lemaître, B. Bailleul

Analytical Fingerprint of the Interactions Between Quinones and Bioenergetic membranes in *Chlamydomonas reinhardtii*

REFERENCES

[1] Jackson, R.B., Friedlingstein P., Le Quéré, C., Abernethy, S., Andrew, R.M., Canadell, J.G., Ciais, P., Davis, S.J., Deng, Z., Liu, Z., Korsbakken, J.I., & Peters, G.P. (2022). Global fossil carbon emissions rebound near pre-COVID-19 levels. *Environ. Res. Lett.*, 17 (3), 031001.

[2] Masson, G., Bosch, E., Rechem, A., L'Epine, M., Kaizuka, I., Jäger-Waldau, A., & Donoso, J. (2023). Snapshot of Global PV Markets 2023 Task 1 Strategic PV Analysis and Outreach PVPS.

[3] Wang, S., Hausfather, Z., Davis, S., Lloyd, J., Olson, E.B., Liebermann, L., Núñez-Mujica, G.D., & McBride, J. (2023). Future demand for electricity generation materials under different climate mitigation scenarios, *Joule*, 7(2), 309-332.

[4] Nelson, N. (2011). Photosystems and global effects of oxygenic photosynthesis. *Biochim. Biophys. Acta Bioenerg.*, 1807 (8), 856-863.

[5] Ruben, S., Randall, M., Kamen, M., & Hyde, J.L. (1941). Heavy oxygen (O18) as a tracer in the study of photosynthesis. *J. Am. Chem.Soc.*, *63*(3), 877-879.

[6] Johnson M. P. (2016). Photosynthesis. *Essays Biochem.*, *60*(3), 255–273.

[7] L.T. Wey, P. Bombelli, X. Chen, J.M. Lawrence, C.M. Rabideau, S.J.L. Rowden, J.Z. Zhang and C.J. Howe (2019). The Development of Biophotovoltaic Systems for Power Generation and Biological Analysis. *Chem. Electro. Chem.*, 6(21): 5375–5386.

[8] Stirbet, A., Lazár, D., Guo, Y., & Govindjee, G. (2020). Photosynthesis: basics, history and modelling. *Ann. Bot.*, *126*(4), 511–537.

[9] Hill, R., & Bendall, F. (1960). Function of the Two Cytochrome Components in Chloroplasts: A Working Hypothesis. *Nature*, *186*(4719), 136–137.

[10] Shevela, D., Björn, L.O., & Govindjee, G. (2018). Z-Scheme of Electron Transport in Photosynthesis. Agrisera Educational Poster 2

[11] Döring, G., Renger, G., Vater, J., & Witt, H. T. (1969). Properties of the photoactive chlorophyll-aII in photosynthesis. *Zeitschrift fur Naturforschung. Teil B, Chemie, Biochemie, Biophysik, Biologie und verwandte Gebiete*, *24*(9), 1139–1143.

[12] Umena, Y., Kawakami, K., Shen, J. R., & Kamiya, N. (2011). Crystal structure of oxygen-evolving photosystem II at a resolution of 1.9 Å. *Nature*, *473*(7345), 55–60.

[13] Najafpour, M. M., Rahimi, F., Aro, E. M., Lee, C. H., & Allakhverdiev, S. I. (2012). Nano-sized manganese oxides as biomimetic catalysts for water oxidation in artificial photosynthesis: a review. *J. R. Soc. Interface*, *9*(75), 2383–2395.

[14] Suga, M., Akita, F., Yamashita, K., Nakajima, Y., Ueno, G., Li, H., Yamane, T., Hirata, K., Umena, Y., Yonekura, S., Yu, L. J., Murakami, H., Nomura, T., Kimura, T., Kubo, M., Baba, S., Kumasaka, T., Tono, K., Yabashi, M., Isobe, H., & Shen, J. R. (2019). An oxyl/oxo mechanism for oxygen-oxygen coupling in PSII revealed by an x-ray free-electron laser. *Science (New York, N.Y.)*, *366*(6463), 334–338.

[15] Barber J. (2004). Engine of life and big bang of evolution: a personal perspective. *Photosynth. Res.*, *80*(1-3), 137–155.

[16] Debus, R. J., Barry, B. A., Sithole, I., Babcock, G. T., & McIntosh, L. (1988). Directed mutagenesis indicates that the donor to P+680 in photosystem II is tyrosine-161 of the D1 polypeptide. *Biochem.*, *27*(26), 9071–9074.

[17] Metz, J. G., Nixon, P. J., Rögner, M., Brudvig, G. W., & Diner, B. A. (1989). Directed alteration of the D1 polypeptide of photosystem II: evidence that tyrosine-161 is the redox component, Z, connecting the oxygen-evolving complex to the primary electron donor, P680. *Biochem.*, *28*(17), 6960–6969.

[18] Shevela, D., Eaton-Rye, J. J., Shen, J. R., & Govindjee (2012). Photosystem II and the unique role of bicarbonate: a historical perspective. *Biochim. BBiophys. Acta*, *1817*(8), 1134–1151.

[19] Shevela, D., Kern, J.F., Govindjee, G., Whitmarsh, J., Messinger, J. (2021). Photosystem II. *eLS*, *2*(7), 1-16.

[20] Kok B. (1956). On the reversible absorption change at 705 mu in photosynthetic organisms. *Biochim. BiBiophys. Acta*, *22*(2), 399–401.

[21] Arnon, D. I., Whatley, F. R., & Allen, M. B. (1955). Vitamin K as a cofactor of photosynthetic phosphorylation. *Biochim. BBiophys. Acta*, *16*(4), 607–608.

[22] Caspy, I., Borovikova-Sheinker, A., Klaiman, D., Shkolnisky, Y., & Nelson, N. (2020). The structure of a triple complex of plant photosystem I with ferredoxin and plastocyanin. *Nat. Plants*, *6*(10), 1300–1305.

[23] Lima-Melo, Y., Kılıç, M., Aro, E. M., & Gollan, P. J. (2021). Photosystem I Inhibition, Protection and Signaling: Knowns and Unknowns. *Front. Plant Sci.*, *12*, 791124.

[24] Darrouzet, E., Cooley, J. W., & Daldal, F. (2004). The Cytochrome bc (1) Complex and its Homologue the b(6)f Complex: Similarities and Differences. *Photosynth. Res.*, *79*(1), 25–44 [25] Rieske, J. S., MacLennan, D. H., & Coleman, R. (1964). Isolation and properties of an iron-protein from the (reduced coenzyme Q)-cytochrome C reductase complex of the respiratory chain. *Biochem. Biophys. Res. Commun.*, *15*(4), 338–344.

[26] Mitchell P. (1975). The protonmotive Q cycle: a general formulation. *FEBS Lett.*, *59*(2), 137–139.

[27] Cramer, W. A., Hasan, S. S., & Yamashita, E. (2011). The Q cycle of cytochrome bc complexes: a structure perspective. *Biochim. BBiophys. Acta*, *1807*(7), 788–802.

[28] Stroebel, D., Choquet, Y., Popot, J. L., & Picot, D. (2003). An atypical haem in the cytochrome b(6)f complex. *Nature*, *426*(6965), 413–418.

[29] Malone, L. A., Qian, P., Mayneord, G. E., Hitchcock, A., Farmer, D. A., Thompson, R. F., Swainsbury, D. J. K., Ranson, N. A., Hunter, C. N., & Johnson, M. P. (2019). Cryo-EM structure of the spinach cytochrome b6 f complex at 3.6 Å resolution. *Nature*, *575*(7783), 535–539.

[30] Croteau, D., Alric, J., & Bailleul, B. (2023). The multiple routes of photosynthetic electron transfer in Chlamydomonas reinhardtii. Wollman, F.A., & Grossman, A. *The Chlamydomonas Sourcebook - third edition, 2, Elsevier, Organellar and Metabolic Processes*, 591-613.

[31] Nawrocki, W. J., Bailleul, B., Picot, D., Cardol, P., Rappaport, F., Wollman, F. A., & Joliot, P. (2019). The mechanism of cyclic electron flow. *Biochim. BBiophys. Acta. Bioenerg.*, *1860*(5), 433–438.

[32] Mitchell P. (1961). Coupling of phosphorylation to electron and hydrogen transfer by a chemi-osmotic type of mechanism. *Nature*, *191*, 144–148.

[33] Mitchell P. (1966). Chemiosmotic coupling in oxidative and photosynthetic phosphorylation. *Biol. Ev. Biol. Proc. Camb. Philos. Soc.*, *41*(3), 445–502.

[34] Boyer P. D. (2002). A research journey with ATP synthase. *J. Biol. Chem.*, *277*(42), 39045–39061.

[35] Allen J. (2002). Photosynthesis of ATP-electrons, proton pumps, rotors, and poise. *Cell*, *110*(3), 273–276.

[36] Hind, G., & Jagendorf, A. T. (1963). Separation of light and dark stages in photophosphorylation. *Proc. Natl. Acad. Sci. U.S.A., 49*(5), 715–722.

[37] Jagendorf, A. T., & Uribe, E. (1966). ATP formation caused by acid-base transition of spinach chloroplasts. *Proc. Natl. Acad. Sci. U.S.A.*, *55*(1), 170–177.

[38] Junge, W. (2004). Protons, proteins and ATP. *Photosynth. Res.*, *80*(1-3), 197-221.

[39] Bar-Even, A., Noor, E., & Milo, R. (2012). A survey of carbon fixation pathways through a quantitative lens. *J. Exp. Bot.*, *63*(6), 2325–2342.

[40] Miyake C. (2010). Alternative electron flows (water-water cycle and cyclic electron flow around PSI) in photosynthesis: molecular mechanisms and physiological functions. *PlantCell Physiol.*, *51*(12), 1951–1963.

[41] Asada K. (1999). THE WATER-WATER CYCLE IN CHLOROPLASTS: Scavenging of Active Oxygens and Dissipation of Excess Photons. *Annu. Rev. Plant Physiol. Plant Mol. Biol.*, *50*(1), 601–639.

[42] Croce, R., & van Amerongen, H. (2020). Light harvesting in oxygenic photosynthesis: Structural biology meets spectroscopy. *Science (New York, N.Y.)*, *369*(6506), 933-941.

[43] Croce, R., & van Amerongen, H. (2014). Natural strategies for photosynthetic light harvesting. *Nat. Chem. Biol.*, 1*0*(7), 492–501.

[44] Latimer, P., Bannister, T. T., & Rabinowitch, E. (1956). Quantum Yields of Fluorescence of Plant Pigments. *Science (New York, N.Y.)*, *124*(3222), 585–586.

[45] Weigert F. (1920). Über polarisiertes fluoreszenzlicht. *Verh D Phys Ges*, *23*,100-102

[46] Zaks, J., Amarnath, K., Sylak-Glassman, E. J., & Fleming, G. R. (2013). Models and measurements of energy-dependent quenching. *Photosynth. Res.*, *116*(2-3), 389–409

[47] Diner, B. A., & Rappaport, F. (2002). Structure, dynamics, and energetics of the primary photochemistry of photosystem II of oxygenic photosynthesis. *Annu. Rev. Plant Biol.*, *53*, 551–580

[48] Maxwell, K., & Johnson, G. N. (2000). Chlorophyll fluorescence-a practical guide. *J.Exp. Bot.*, *51*(345), 659–668.

[49] Murchie, E. H., & Lawson, T. (2013). Chlorophyll fluorescence analysis: a guide to good practice and understanding some new applications. *J. Exp. Bot.*, *64*(13), 3983–3998.

[50] Kalaji, H. M., Schansker, G., Ladle, R. J., Goltsev, V., Bosa, K., Allakhverdiev, S. I., Brestic, M., Bussotti, F., Calatayud, A., Dąbrowski, P., Elsheery, N. I., Ferroni, L., Guidi, L., Hogewoning, S. W., Jajoo, A., Misra, A. N., Nebauer, S. G., Pancaldi, S., Penella, C., Poli, D., & Zivcak, M. (2014). Frequently asked questions about in vivo chlorophyll fluorescence: practical issues. *Photosynth. Res.*, *122*(2), 121–158.

[51] Kautsky, H., Appel, W., & Amann, H. (1960). Die Fluoreszenzkurve und die Photochemie der Pflanz. *Biochemische Zeitschrift_*, *332*, 277–292.

[52] Kitajima, M., & Butler, W. L. (1975). Quenching of chlorophyll fluorescence and primary photochemistry in chloroplasts by dibromothymoquinone. *Biochim. BBiophys. Acta.*, *376*(1), 105–115.

[53] Trissl, H. W., Gao, Y., & Wulf, K. (1993). Theoretical fluorescence induction curves derived from coupled differential equations describing the primary photochemistry of photosystem II by an exciton-radical pair equilibrium. *Biophys. J.*, *64*(4), 974–988.

[54] Stahl, U., Tusov, V.B., Paschenko, V.Z., Voigta, J. (1989). Spectroscopic investigations of fluorescence behavior, role and function of the long-wavelength pigments of Photosystem I. *Biochim. Biophys. Acta.Bioenerg.*, *973*(2),198-204.

[55] Krüger, T. P., Wientjes, E., Croce, R., & van Grondelle, R. (2011). Conformational switching explains the intrinsic multifunctionality of plant light-harvesting complexes. *Proc. Natl. Acad. Sci. U.S.A.*, *108*(33), 13516–13521.

[56] Lazár D. (2013). Simulations show that a small part of variable chlorophyll a fluorescence originates in photosystem I and contributes to overall fluorescence rise. *J. Theor. Biol.*, *335*, 249–264.

[57] Schreiber, U., & Klughammer, C. (2021). Evidence for variable chlorophyll fluorescence of photosystem I in vivo. *Photosynth. Res.*, *149*(1-2), 213–231.

[58] Schreiber U. (2023). Light-induced changes of far-red excited chlorophyll fluorescence: further evidence for variable fluorescence of photosystem I in vivo. *Photosynth. Res.*, *155*(3), 247–270.

[59] Genty, B., Briantais, J-M., & Baker, N.R. (1989). The relationship between the quantum yield of photosynthetic electron transport and quenching of chlorophyll fluorescence. *Biochim. Biophys. Acta.*, *990*(1), 87-92.

[60] Genty B, Goulas Y, Dimon B, Peltier JM, Moya I. 1992. Modulation of efficiency of primary conversion in leaves, mechanisms involved at PSII. *In Research in Photosynthesis*, *4*, ed. N Murata, 603–610. Dordrecht: Kluwer Academic Publishers

[61] Joliot, P., & Joliot, A. (1992). Electron transfer between Photosystem II and the cytochrome b6f complex: mechanistic and structural implications. *Biochim.Biophys. Acta. Bioenerg.*, *1102*(1), 53-61.

[62] Govindjee, U. (2014). *Non-photochemical quenching and energy dissipation in plants, algae and cyanobacteria* (Vol. 40). B. Demmig-Adams, G. Garab, & W. Adams III (Eds.). Dordrecht: Springer Netherlands

[63] Ruban AV. (2016). Nonphotochemical Chlorophyll Fluorescence Quenching: Mechanism and Effectiveness in Protecting Plants from Photodamage. *Plant. Physiol.*, *170*(4),1903-16.

[64] Wraight, C. A., & Crofts, A. R. (1970). Energy-dependent quenching of chlorophyll alpha fluorescence in isolated chloroplasts. *Eur. J. Biochem.*, *17*(2), 319–327.

[65] Horton, P., Ruban, A. V., Rees, D., Pascal, A. A., Noctor, G., & Young, A. J. (1991). Control of the light-harvesting function of chloroplast membranes by aggregation of the LHCII chlorophyll-protein complex. *FEBS Lett.*, *292*(1-2), 1–4.

[66] Krause, G.H. (1988). Photoinhibition of photosynthesis. An evaluation of damaging and protective mechanisms. *Physiol. Plant.*, *74*, 566-574.

[67] Nilkens, M., Kress, E., Lambrev, P., Miloslavina, Y., Müller, M., Holzwarth, A. R., & Jahns, P. (2010). Identification of a slowly inducible zeaxanthin-dependent component of non-photochemical quenching of chlorophyll fluorescence generated under steady-state conditions in Arabidopsis. *Biochim. Biophysica Acta.*, *1797*(4), 466–475.

[68] Li, L., Aro, E. M., & Millar, A. H. (2018). Mechanisms of Photodamage and Protein Turnover in Photoinhibition. *Trends Plant Sci.*, *23*(8), 667–676.

[69] Ohad, I., Adir, N., Koike, H., Kyle, D. J., & Inoue, Y. (1990). Mechanism of photoinhibition in vivo. A reversible light-induced conformational change of reaction center II is related to an irreversible modification of the D1 protein. *J. Biol. Chem.*, *265*(4), 1972–1979.

[70] Ohad, I., Berg, A., Berkowicz, S. M., Kaplan, A., & Keren, N. (2011). Photoinactivation of photosystem II: is there more than one way to skin a cat? *Physiol. Plant.*, *142*(1), 79–86.

[71] Oguchi, R., Terashima, I., Kou, J., & Chow, W. S. (2011). Operation of dual mechanisms that both lead to photoinactivation of Photosystem II in leaves by visible light. *Physiol. Plant.*, *142*(1), 47–55.

[72] Zavafer A. (2021). A theoretical framework of the hybrid mechanism of photosystem II photodamage. *Photosynth. Res.*, *149*(1-2), 107–120.

[73] Hakala, M., Tuominen, I., Keränen, M., Tyystjärvi, T., & Tyystjärvi, E. (2005). Evidence for the role of the oxygen-evolving manganese complex in photoinhibition of Photosystem II. *Biochim. Biophys. Acta.*, *1706*(1-2), 68–80.

[74] Ohnishi, N., Allakhverdiev, S. I., Takahashi, S., Higashi, S., Watanabe, M., Nishiyama, Y., & Murata, N. (2005). Two-step mechanism of photodamage to photosystem II: step 1 occurs at the oxygen-evolving complex and step 2 occurs at the photochemical reaction center. *Biochem.*, *44*(23), 8494–8499.

[75] Danielius, R.V., Satoh, K., Van Kan, P.J.M., Plijter, P.J., Nuijs, A.M., & Van Gorkom, H.J. (1987). The primary reaction of photosystem II in the D1-D2-cytochrome b-559 complex. *FEBS Lett.*, *213*, (2), 241-244.

[76] Durrant, J.R., Giorgi, L.B., Barber, J., Klug, D.R., & Porter, G. (1990). Characterization of triplet states in isolated Photosystem II reaction centers: Oxygen quenching as a mechanism for photodamage. *Biochim. Biophys. Acta. Bioenerg.*, *1017*(2), 167-175.

[77] Jegerschöld, C., & Styring, S. (1996). Spectroscopic characterization of intermediate steps involved in donor-side-induced photoinhibition of photosystem II. *Biochem.*, *35*(24), 7794–7801.

[78] Kok B. (1956). On the inhibition of photosynthesis by intense light. *Biochim. BBiophys. Acta.*, *21*(2), 234–244.

[79] Klughammer, C., Schreiber, U. (1994). An improved method, using saturating light pulses, for the determination of photosystem I quantum yield via P700+-absorbance changes at 830 nm. *Planta*, *192*(2), 261–268.

[80] Klughammer, C., & Schreiber, U. (2016). Deconvolution of ferredoxin, plastocyanin, and P700 transmittance changes in intact leaves with a new type of kinetic LED array spectrophotometer. *Photosynth. Res.*, *128*(2), 195–214.

[81] Bailleul, B., Cardol, P., Breyton, C., & Finazzi, G. (2010). Electrochromism: a useful probe to study algal photosynthesis. *Photosynth. Res.*, *106*(1-2), 179–189.

[82] Ferté-Vogel, S. *Not published.*

[83] Oguchi, R., Terashima, I., & Chow, W. S. (2021). The effect of different spectral light quality on the photoinhibition of Photosystem I in intact leaves. *Photosynth. Res.*, *149*(1-2), 83–92.

[84] Takagi, D., Takumi, S., Hashiguchi, M., Sejima, T., & Miyake, C. (2016). Superoxide and Singlet Oxygen Produced within the Thylakoid Membranes Both Cause Photosystem I Photoinhibition. *Plant. Physiol.*, *171*(3), 1626–1634.

[85] Sonoike K. (2011). Photoinhibition of photosystem I. *Physiol. Plant.*, *142*(1), 56–64.

[86] Scheller, H. V., & Haldrup, A. (2005). Photoinhibition of photosystem I. *Planta*, *221*(1), 5–8.

[87] Bassi, R., & Dall'Osto, L. (2021). Dissipation of Light Energy Absorbed in Excess: The Molecular Mechanisms. *Annu. Rev. Plant Biol.*, *72*, 47–76.

[88] Kramer, D. M., Cruz, J. A., & Kanazawa, A. (2003). Balancing the central roles of the thylakoid proton gradient. *Trends. Plant Sci.*, *8*(1), 27–32.

[89] Rumberg, B., & Siggel, U. (1969). pH changes in the inner phase of the thylakoids during photosynthesis. *Die Naturwissenschaften*, *56*(3), 130–132.

[90] Tikkanen, M., Mekala, N. R., & Aro, E. M. (2014). Photosystem II photoinhibition-repair cycle protects Photosystem I from irreversible damage. *Biochim. Biophys. Acta.*, *1837*(1), 210–215.

[91] Joliot, P., & Johnson, G. N. (2011). Regulation of cyclic and linear electron flow in higher plants. *Proc. Natl. Acad. Sci. U.S.A.*, *108*(32), 13317–13322.

[92] Bonaventura, C., & Myers, J. (1969). Fluorescence and oxygen evolution from Chlorella pyrenoidosa. *Biochim. BBiophys. Acta.*, *189*(3), 366–383.

[93] Rochaix J. D. (2014). Regulation and dynamics of the light-harvesting system. *Annu. Rev. Plant Biol.*, *65*, 287–309

[94] Goldschmidt-Clermont, M. (2023). Chapter 24 - State transitions, Editor(s): Arthur R. Grossman, Francis-André Wollman. The Chlamydomonas Sourcebook (Third Edition), *Academic Press*, 787-805

[95] Zito, F., Finazzi, G., Delosme, R., Nitschke, W., Picot, D., & Wollman, F. A. (1999). The Qo site of cytochrome b6f complexes controls the activation of the LHCII kinase. *EMBO J.*, *18*(11), 2961–2969

[96] Allen, J., Bennett, J., Steinback, K.E., & Arntzen, C.J. (1981). Chloroplast protein phosphorylation couples plastoquinone redox state to distribution of excitation energy between photosystems. *Nature*, *291*(5810), 25–29

[97] Allen J. F. (2002). Plastoquinone redox control of chloroplast thylakoid protein phosphorylation and distribution of excitation energy between photosystems: discovery, background, implications. *Photosynth. Res.*, *73*(1-3), 139–148

[98] Wientjes, E., van Amerongen, H., & Croce, R. (2013). LHCII is an antenna of both photosystems after long-term acclimation. *Biochim. BBiophys. Acta.*, *1827*(3), 420–426

[99] Iwai, M., Wakao, S. & Niyogi, K.K. (2023). Chapter 25 - Photoprotection, Editor(s): Arthur R. Grossman, Francis-André Wollman, The Chlamydomonas Sourcebook (Third Edition). *Academic Press*

[100] Li, X. P., Gilmore, A. M., Caffarri, S., Bassi, R., Golan, T., Kramer, D., & Niyogi, K. K. (2004). Regulation of photosynthetic light harvesting involves intrathylakoid lumen pH sensing by the PsbS protein. *J.Biol. Chem.*, *279*(22), 22866–22874

[101] Ruban AV. (2016). Nonphotochemical Chlorophyll Fluorescence Quenching: Mechanism and Effectiveness in Protecting Plants from Photodamage. *Plant. Physiol.*, *170*(4),1903-16

[102] Ballottari, M., Truong, T. B., De Re, E., Erickson, E., Stella, G. R., Fleming, G. R., Bassi, R., & Niyogi, K. K. (2016). Identification of pH-sensing Sites in the Light Harvesting Complex Stress-related 3 Protein Essential for Triggering Non-Photochemical Quenching in Chlamydomonas reinhardtii. *J.Biol. Chem.*, *291*(14), 7334–7346

[103] Yamamoto, H. Y., Nakayama, T. O., & Chichester, C. O. (1962). Studies on the light and dark interconversions of leaf xanthophylls. *Arch. Biochem. Biophys.*, *97*(1), 168–173

[104] Troiano, J. M., Perozeni, F., Moya, R., Zuliani, L., Baek, K., Jin, E., Cazzaniga, S., Ballottari, M., & Schlau-Cohen, G. S. (2021). Identification of distinct pH- and zeaxanthin-dependent quenching in LHCSR3 from Chlamydomonas reinhardtii. *eLife*, *10*, e60383.

[105] Zhang, B., & Sun, L. (2019). Artificial photosynthesis: opportunities and challenges of molecular catalysts. *Chem. Soc. Rev.*, *48*(7), 2216–2264.

[106] Dau, H., Fujita, E., & Sun, L. (2017). Artificial Photosynthesis: Beyond Mimicking Nature. *ChemSusChem*, *10*(22), 4228–4235.

[107] El-Khouly, M., El-Mohsnawy, E., & Fukuzumi, S. (2017). Solar energy conversion: From natural to artificial photosynthesis. *J. Photochem. Photobiol. C: Photochem. Rev.*, *31*, 36-83.

[108] Zhang, J.Z., & Reisner, E. (2020). Advancing photosystem II photoelectrochemistry for semi-artificial photosynthesis. *Nat. Rev. Chem.*, *4*, 6–21.

[109] Kornienko, N., Zhang, J. Z., Sakimoto, K. K., Yang, P., & Reisner, E. (2018). Interfacing nature's catalytic machinery with synthetic materials for semi-artificial photosynthesis. *Nat.Nanotechnol.*, *13*(10), 890–899.

[110] Chen, M., & Blankenship, R.E. (2011). Expanding the solar spectrum used by photosynthesis. *Trends Plant Sci.*, *16*(8), 427–431.

[111] Grattieri, M., Beaver, K., Gaffney, E.M., Dong, F., & Minteer, S.D. (2020). Advancing the fundamental understanding and practical applications of photo-bioelectrocatalysis. *Chem. Comm.*, *56,* (61), 8553–8568.

[112] Strik, D.P., Timmers, R.A., Helder, M., Steinbusch, K.J., Hamelers, H.V., & Buisman, C.J. (2011). Microbial solar cells: applying photosynthetic and electrochemically active organisms. *Trends Biotechnol.*, *29*, (1), 41-49.

[113] Rosenbaum, M., He, Z. & Angenent, L. T. (2010). Light energy to bioelectricity: photosynthetic microbial fuel cells. *Curr. Opin. Biotechnol.*, *21*, 259–264.

[114] Danielle de Moura Torquato, L., & Grattieri, M. (2022). Photobioelectrochemistry of intact photosynthetic bacteria: Advances and future outlook. *Curr. Opin. Electrochem.*, *42*, 101018.

[115] Ahrling, K. A., & Peterson, S. (2003). Light-adaptation of photosystem II is mediated by the plastoquinone pool. *Biochem.*, *42*(25), 7655–7662.

[116] Ananyev, G., Renger, G., Wacker, U., & Klimov, V. (1994). The photoproduction of superoxide radicals and the superoxide dismutase activity of Photosystem II. The possible involvement of cytochrome b559. *Photosynth. Res.*, *41*(2), 327–338.

[117] Chen, G., Han, G., Göransson, E., Mamedov, F., & Styring, S. (2012). Stability of the S_3 and S_2 state intermediates in photosystem II directly probed by EPR spectroscopy. *Biochem.*, *51*(1), 138–148.

[118] Diner, B.A., Petrouleas, V. (1987). Light-induced oxidation of the acceptor-side Fe(II) of Photosystem II by exogenous quinones acting through the QB binding site. II. Blockage by inhibitors and their effects on the Fe(III) EPR spectra. *Biochim.Biophys. Acta. Bioenerg.*, *893*(2),138-148.

[119] Gleiter, H. M., Haag, E., Inoue, Y., & Renger, G. (1993). Functional characterization of a purified homogeneous Photosystem II core complex with high oxygen evolution capacity from spinach. *Photosynth. Res.*, *35*(1), 41–53.

[120] Haag, E., Gleiter, H. M., & Renger, G. (1992). Effects of photoinhibition on the PS II acceptor side including the endogenous high spin Fe (2+) in thylakoids, PS II-membrane fragments and PS II core complexes. *Photosynth. Res.*, *31*(2), 113–126.

[121] Halverson, K. M., & Barry, B. A. (2003). Sucrose and glycerol effects on photosystem II. *Biophys. J.*, *85*(2), 1317–1325.

[122] Izawa., S. (1980). Acceptors and donors and chloroplast electron transport. *Meth.Enzymol.*, *69*, 413-434.

[123] Joly, D., & Carpentier, R. (2007). The oxidation/reduction kinetics of the plastoquinone pool controls the appearance of the I-peak in the O-J-I-P chlorophyll fluorescence rise: effects of various electron acceptors. *J. Photochem. Photobiol. B, Biol.*, *88*(1), 43–50.

[124] Karukstis, K. K., Moision, R. M., Johansen, S. K., Birkeland, K. E., & Cohen, S. M. (1992). Alternative measures of photosystem II electron transfer inhibition in anthraquinone-treated chloroplasts. *Photochem. Photobiol.*, *55*(1), 125–13.2

[125] Lavergne, J. (1982). Interaction of exogenous benzoquinone with Photosystem II in chloroplasts. The semiquinone form acts as a dichlorophenyldimethylurea-insensitive secondary acceptor, *Biochim.Biophys. Acta. Bioenerg.*, *679*(1), 12-18.

[126] Petrouleas, V., & Diner, A.B. (1987). Light-induced oxidation of the acceptor-side Fe(II) of Photosystem II by exogenous quinones acting through the QB binding site. I. Quinones, kinetics and pH-dependence. *Biochim.Biophys. Acta.Bioenerg.*, *893*(2), 126-137.

[127] Bukhov, N. G., Sridharan, G., Egorova, E. A., & Carpentier, R. (2003). Interaction of exogenous quinones with membranes of higher plant chloroplasts: modulation of quinone capacities as photochemical and non-photochemical quenchers of energy in Photosystem II during light-dark transitions. *Biochim.Biophys. Acta.*, *1604*(2), 115–123.

[128] Pshybytko, N. L., Kruk, J., Kabashnikova, L. F., & Strzalka, K. (2008). Function of plastoquinone in heat stress reactions of plants. *Biochim. Biophys. Acta.*, *1777*(11), 1393–1399.

[129] Shevela, D., & Messinger, J. (2012). Probing the turnover efficiency of photosystem II membrane fragments with different electron acceptors. *Biochim. BBiophys. Acta.*, *1817*(8), 1208–1212.

[130] Viruvuru, V., & Fragata, M. (2008). Photochemical cooperativity in photosystem II. Characterization of oxygen evolution discontinuities in the light-response curves. *Phys. Chem. Chem. Phys.*, *10*(44), 6607–6614.

[131] Yanykin, D. V., Khorobrykh, A. A., Khorobrykh, S. A., & Klimov, V. V. (2010). Photoconsumption of molecular oxygen on both donor and acceptor sides of photosystem II in Mn-depleted subchloroplast membrane fragments. *Biochim. Biophys. Acta.*, *1797*(4), 516–523.

[132] Yu, S.-G., & Olof Björn, L. (1996). Differences in UV-B sensitivity between PSII from grana lamellae and stroma lamellae. *J. Photochem. Photobiol. B, Biol.*, *34*(1), 35–38.

[133] Forsman, J. A., & Eaton-Rye, J. J. (2021). The Interaction between PsbT and the DE Loop of D1 in Photosystem II Stabilizes the Quinone-Iron Electron Acceptor Complex. *Biochem.*, *60*(1), 53–63.

[134] Ananyev, G., Roy-Chowdhury, S., Gates, C., Fromme, P., & Dismukes, G. C. (2019). The Catalytic Cycle of Water Oxidation in Crystallized Photosystem II Complexes: Performance and Requirements for Formation of Intermediates. *ACS Catal.*, *9*(2),1396–140.

[135] Zavafer, A., Cheah, M. H., Hillier, W., Chow, W. S., & Takahashi, S. (2015). Photodamage to the oxygen evolving complex of photosystem II by visible light. *Sci. Rep.*, *5*, 16363.

[136] Dobrikova, A. G., & Apostolova, E. L. (2015). Damage and protection of the photosynthetic apparatus from UV-B radiation. II. Effect of quercetin at different pH. *J. Plant Physiol.*, *184*, 98–105.

[137] Nagao, R., Kitazaki, S., & Noguchi, T. (2018). Evaluation of photosynthetic activities in thylakoid membranes by means of Fourier transform infrared spectroscopy. *Biochim. Biophys. Acta. Bioenerg.*, *1859*(2), 129–136.

[138] Babcock, G. T., & Sauer, K. (1975). The rapid component of electron paramagnetic resonance signal II: a candidate for the physiological donor to photosystem II in spinach chloroplasts. *Biochim. Biophys. Acta.*, *376*(2), 329–344.

[139] Blubaugh, D. J., Atamian, M., Babcock, G. T., Golbeck, J. H., & Cheniae, G. M. (1991). Photoinhibition of hydroxylamine-extracted photosystem II membranes: identification of the sites of photodamage. *Biochem.*, *30*(30), 7586–7597.

[140] Ghanotakis, D. F., Babcock, G. T., & Yerkes, C. T. (1983). Exogenous versus endogenous acceptors in photosystem ii in inhibited chloroplasts. *Arch. Biochem. Biophys.*, *225*(1), 248–255.

[141] Gleiter, H. M., Nugent, J. H., Haag, E., & Renger, G. (1992). Photoinhibition affects the non-heme iron center in photosystem II. *FEBS Lett.*, *313*(1), 75–79.

[142] Gruszecki, W.I., Wardak, A., & Maksymiec, W. (1997). The effect of blue light o electron transport in photosystem II reconstituted in planar bilayer lipid membrane. *J. Photochem. Photobiol. B, Biol.*, *39*(3), 265-268.

[143] Vambutas, V., Beattie, D. S., & Moazzami, G. (1985). Anion (and cation) requirements of the coupled electron flow in spinach thylakoids. *J. Bioenerg. Biomembr.*, *17*(4), 225–237.

[144] Satoh, K., Oh-hashi, M., Kashino, Y., & Koike H. (1995). Mechanism of Electron Flow through the QB Site in Photosystem II. 1. Kinetics of the Reduction of Electron Acceptors at the QB and Plastoquinone Sites in Photosystem II Particles from the Cyanobacterium Synechococcus vulcanus. *Plant Cell Physiol.*, *36*(4), 597-605.

[145] Dau, H., Ivanov, B., Shevela, D., Armstrong, W. H., & Govindjee, G. (2021). Three overlooked photosynthesis papers of Otto Warburg (1883-1970), published in the 1940s in German and in Russian, on light-driven water oxidation coupled to benzoquinone reduction. *Photosynth. Res.*, *149*(3), 259–264.

[146] Baker, M. A., Lane, D. J., Ly, J. D., De Pinto, V., & Lawen, A. (2004). VDAC1 is a transplasma membrane NADH-ferricyanide reductase. *J.Biol. Chem.*, *279*(6), 4811–4819.

[147] Taylor, A. R., & Chow, R. H. (2001). A microelectrochemical technique to measure trans-plasma membrane electron transport in plant tissue and cells in vivo. *Plant CellEnviron.*, *24*(7), 749–754.

[148] Davey, M. S., Suggett, D. J., Geider, R. J., & Taylor, A. R. (2003). Phytoplankton plasma membrane redox activity: effect of iron limitation and interaction with photosynthesis. *J. Phycol.*, *39*(6), 1132–1144.

[149] Melgarejo, E., Carnicas, E., Niell, F. X., & Medina, M. Á. (2002). Effects of photoacclimation on plasma membrane ferricyanide reductase from the rhodophyta Gracilaria tenuistipitata. *Plant Sci.*, *162*(5), 753–759.

[150] Lynnes, J. A., Derzaph, T. L. M., & Weger, H. G. (1998). Iron limitation results in induction of ferricyanide reductase and ferric chelate reductase activities in Chlamydomonas reinhardtii. *Planta*, *204*(3), 360–365.

[151] McCormick, A.J., Bombelli, P., Bradley, R.W., Thorne, R., Wenzel, T., & Howe, C.J. (2015). Biophotovoltaics: oxygenic photosynthetic organisms in the world of bioelectrochemical systems. *Energy. Environ. Sci.*, *8*, 1092–1109.

[152] Sekar, N., & Ramasamy, R.P. (2015). Recent advances in photosynthetic energy conversion. *J. Photochem. Photobiol. C: Photochem. Rev.*, *22*, 19-33.

[153] Badura, A., Kothe, T., Schuhmann, W., & Rögner, M. (2011). Wiring photosynthetic enzymes to electrodes. *EnergyEnviron. Sci., 7*(4), 3263-3274.

[154] Grattieri, M. (2020). Purple bacteria photo-bioelectrochemistry: enthralling challenges and opportunities. *Photochem.Photobiol. Sci.*, *19*(4), 424-435.

[155] Zhang, J.Z., Bombelli, P., Sokol, K.P., Fantuzzi, A., Rutherford, A.W., Howe, C.J., & Reisner, E. (2018). Photoelectrochemistry of Photosystem II in *Vitro vs in Vivo*. *J. Am. Chem. Soc.*, *140*(1), 6-9.

[156] Goodenough U. W. (1992). Green yeast. *Cell*, *70*(4), 533–538.

[157] Rochaix J. D. (1995). Chlamydomonas reinhardtii as the photosynthetic yeast. *Annu. Rev. Genet.*, *29*, 209–230.

[158] Harris E. H. (2001). Chlamydomonas as a model organism. *Annu. Rev. Plant Physiol. Plant Mol. Biol.*, *52*, 363–406.

[159] Merchant, S. S., Prochnik, S. E., Vallon, O., Harris, E. H., Karpowicz, S. J., Witman, G. B., Terry, A., Salamov, A., Fritz-Laylin, L. K., Maréchal-Drouard, L., Marshall, W. F., Qu, L. H., Nelson, D. R., Sanderfoot, A. A., Spalding, M. H., Kapitonov, V. V., Ren, Q., Ferris, P., Lindquist, E., Shapiro, H., … Grossman, A. R. (2007). The Chlamydomonas genome reveals the evolution of key animal and plant functions. *Science (New York, N.Y.)*, *318*(5848), 245–250.

[160] Blaby, I. K., Blaby-Haas, C. E., Tourasse, N., Hom, E. F., Lopez, D., Aksoy, M., Grossman, A., Umen, J., Dutcher, S., Porter, M., King, S., Witman, G. B., Stanke, M., Harris, E. H., Goodstein, D., Grimwood, J., Schmutz, J., Vallon, O., Merchant, S. S., & Prochnik, S. (2014). The Chlamydomonas genome project: a decade on. *Trends Plant Sci.*, *19*(10), 672–680.

[161] Boynton, J. E., Gillham, N. W., Harris, E. H., Hosler, J. P., Johnson, A. M., Jones, A. R., Randolph-Anderson, B. L., Robertson, D., Klein, T. M., & Shark, K. B. (1988). Chloroplast transformation in Chlamydomonas with high velocity micro projectiles. *Science (New York, N.Y.)*, *240*(4858), 1534–1538

[162] Kindle K. L. (1990). High-frequency nuclear transformation of Chlamydomonas reinhardtii. *Proc. Natl. Acad. Sci. U.S.A.*, *87*(3), 1228–1232.

[163] Remacle, C., Cardol, P., Coosemans, N., Gaisne, M., & Bonnefoy, N. (2006). High-efficiency biolistic transformation of Chlamydomonas mitochondria can be used to insert mutations in complex I genes. *Proc. Natl. Acad. Sci. U.S.A.*, *103*(12), 4771–4776.

[164] Li, X., Zhang, R., Patena, W., Gang, S. S., Blum, S. R., Ivanova, N., Yue, R., Robertson, J. M., Lefebvre, P. A., Fitz-Gibbon, S. T., Grossman, A. R., & Jonikas, M. C. (2016). An Indexed, Mapped Mutant Library Enables Reverse Genetics Studies of Biological Processes in Chlamydomonas reinhardtii. *Plant Cell.*, *28*(2), 367–387.

[165] Li, X., Patena, W., Fauser, F., Jinkerson, R. E., Saroussi, S., Meyer, M. T., Ivanova, N., Robertson, J. M., Yue, R., Zhang, R., Vilarrasa-Blasi, J., Wittkopp, T. M., Ramundo, S., Blum, S. R., Goh, A., Laudon, M., Srikumar, T., Lefebvre, P. A., Grossman, A. R., & Jonikas, M. C. (2019). A genome-wide algal mutant library and functional screen identifies genes required for eukaryotic photosynthesis. *Nat. Genet.*, *51*(4), 627–635.

[166] Fauser, F., Vilarrasa-Blasi, J., Onishi, M., Ramundo, S., Patena, W., Millican, M., Osaki, J., Philp, C., Nemeth, M., Salomé, P. A., Li, X., Wakao, S., Kim, R. G., Kaye, Y., Grossman, A. R., Niyogi, K. K., Merchant, S. S., Cutler, S. R., Walter, P., Dinneny, J. R., Jinkerson, R. E. (2022). Systematic characterization of gene function in the photosynthetic alga Chlamydomonas reinhardtii. *Nat. Genet.*, *54*(5), 705–714.

[167] Jiang, W., Brueggeman, A. J., Horken, K. M., Plucinak, T. M., & Weeks, D. P. (2014). Successful transient expression of Cas9 and single guide RNA genes in Chlamydomonas reinhardtii. *Eukaryot. Cell.*, *13*(11), 1465–1469.

[168] Ferenczi, A., Pyott, D. E., Xipnitou, A., & Molnar, A. (2017). Efficient targeted DNA editing and replacement in Chlamydomonas reinhardtii using Cpf1 ribonucleoproteins and single-stranded DNA. *Proc. Natl. Acad. Sci. U.S.A.*, *114*(51), 13567–13572.

[169] Grossman, A.R. & Wollman, F.A. (2023). The Chlamydomonas Sourcebook. *Academic Press*, 3rd Edition.

[170] Longatte, G., Fu, H. Y., Buriez, O., Labbé, E., Wollman, F. A., Amatore, C., Rappaport, F., Guille-Collignon, M., & Lemaître, F. (2015). Evaluation of photosynthetic electrons derivation by exogenous redox mediators. *Biophys. Chem.*, *205*, 1–8.

[171] Longatte, G., Rappaport, F., Wollman, F. A., Guille-Collignon, M., & Lemaître, F. (2016). Mechanism and analyses for extracting photosynthetic electrons using exogenous quinones - what makes a good extraction pathway? *Photochem.Photobiol. Sci.*, *15*(8), 969–979.

[172] Longatte, G., Rappaport, F., Wollman, F.A., Guille-Collignon, M., & Lemaître, F. (2017). Electrochemical Harvesting of Photosynthetic Electrons from Unicellular Algae Population at the Preparative Scale by Using 2,6-dichlorobenzoquinone. *Electrochim. Acta.*, *236*, 337-342.

[173] Longatte, G., Guille-Collignon, M., & Lemaître, F. (2017). Electrocatalytic Mechanism Involving Michaelis-Menten Kinetics at the Preparative Scale: Theory and Applicability to Photocurrents from a Photosynthetic Algae Suspension with Quinones. *Chem. Phys. Chem.*, *18*(19), 2643–2650.

[174] Longatte, G., Sayegh, A., Delacotte, J., Rappaport, F., Wollman, F. A., Guille-Collignon, M., & Lemaître, F. (2018). Investigation of photocurrents resulting from a living unicellular algae suspension with quinones over time. *Chem. Sci. J.*, *9*(43), 8271–8281.

[175]. *Bolton*, J.L., Trush, M.A., Penning, T.M., Dryhurst, G., Monks, T.J. (2000). Role of quinones in *toxicology. Chem. Res.Toxicol., 13*(3), 135-160.

[176] Sayegh, A., Longatte, G., Buriez, O., Wollman, F.A., Guille-Collignon, M., Labbé, E., Delacotte, J., & Lemaître, F. (2019). Diverting photosynthetic electrons from suspensions of Chlamydomonas reinhardtii algae - New insights using an electrochemical well device. *Electrochim. Acta., 304*, 465-473.

[177] Fu, H. Y., Picot, D., Choquet, Y., Longatte, G., Sayegh, A., Delacotte, J., Guille-Collignon, M., Lemaître, F., Rappaport, F., & Wollman, F. A. (2017). Redesigning the Q_A binding site of Photosystem II allows reduction of exogenous quinones. *Nat. Commun.*, *8*, 15274.

[178] Beauzamy, L., Delacotte, J., Bailleul, B., Tanaka, K., Nakanishi, S., Wollman, F. A., & Lemaître, F. (2020). Mediator-Microorganism Interaction in Microbial Solar Cell: a Fluo-Electrochemical Insight. *Anal. Chem.*, *92*(11), 7532–7539.

[179] Beauzamy, L., Lemaître, F., & Derr, J. (2020). Underlying mechanisms in microbial solar cells: how modelling can help. *Sustain. Energy Fuels.*, *4*, 6004-6010.

Chapter II

Article n°1 - Finding Adapted Quinones for Harvesting Electrons From Photosynthetic Algae Suspensions

ChemElectroChem **2021**, *8,* 2968-2978
https://doi.org/10.1002/celc.202100757

Adnan Sayegh, Luca A. Perego, Marc Arderiu Romero, Louis Escudero, Jérôme Delacotte, Manon Guille-Collignon, Laurence Grimaud, Benjamin Bailleul, Frédéric Lemaître

Preliminary Section

The most obvious proxy of the efficiency of quinones as redox mediators of natural photosynthesis is the photocurrent produced by the biophotoelectrochemical system. This article therefore focuses on the investigation of several quinones (both commercial and synthesized in the laboratory) in relation to the *Chlamydomonas reinhardtii* microalgae. The ITO-based electrochemical device was built and used by Adnan Sayegh, a PhD student in the laboratory from 2015 to 2018. The organic syntheses were carried out by Luca Perego, a PhD student over the same period. I was involved in the fluorescence experiments and participated in the interpretations on redox potentials as well as on the first ATPsynthase experiments.

Graphical Abstract

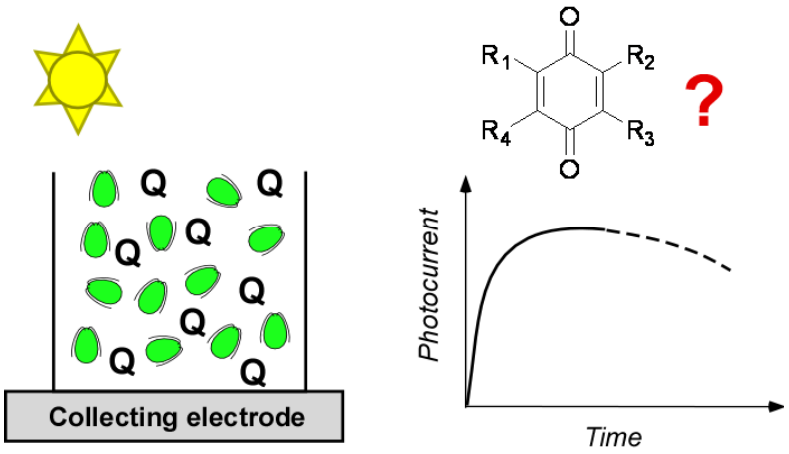

Performances of different quinones as redox mediators were investigated from suspensions of photosynthetic microalgae to produce photocurrents by using a miniaturized well-type Au/ITO electrochemical device. Some electrochemical aspects were considered (maximum photocurrent, stability) but side-effects of quinones were also studied (cytotoxic concentration, ATPsynthase). Correlations with redox potentials gave a first view to find the best compromise between bioelectricity production and toxicity.

ABSTRACT

Among all the chemical and biotechnological strategies implemented to extract energy from oxygenic photosynthesis, several concern the use of intact photosynthetic organisms (algae, cyanobacteria…). This means rerouting (fully or partially) the electron flow from the photosynthetic chain to an outer collecting electrode generating thus a photocurrent. While diverting photosynthetic electrons from living biological systems is an encouraging approach, this strategy is limited by the need to use an electron shuttle. Redox mediators that are able to interact with an embedded photosynthetic chain are rather scarce. In this respect, exogenous quinones are the most frequently used. Unfortunately, some of them also act as poisoning agents within relatively long timeframes. It thus raises the question of the best quinone. In this work, we use a previously reported electrochemical device to analyze the performances of different quinones. Photocurrents (maximum photocurrent, stability) were measured from suspensions of *Chlamydomonas reinhardtii* algae/quinones by chronoamperometry and compared to parameters like quinone redox potentials or cytotoxic concentration. From these results, several quinones were synthesized and analyzed in order to find the best compromise between bioelectricity production and toxicity.

Keywords : photosynthesis ; quinones ; electrochemistry ; *Chlamydomonas reinhardtii* algae ; photocurrent ; fluorescence ; ATPsynthase

1. Introduction

Photosynthesis is the fascinating process used by Nature to convert light into chemical energy. Mainly involved in plants and other organisms like algae and cyanobacteria, oxygenic photosynthesis relies on light absorption by chlorophyll antennae and photochemistry in reaction centers that triggers electron transfers along the photosynthetic chain (**Figure 1A**). It formally corresponds to a charge separation whose positive side induces the H_2O oxidation and the negative side eventually leads to the CO_2 reduction. This light-induced electron flow is obviously an inspiring mechanism in the current context of renewable energies and several strategies were recently considered to use photosynthesis as a light converter to electricity. This raises the question on how taking benefit from photosynthesis.[1] On the one hand, only the principle of the photosynthetic process (i.e. a charge separation induced by light illumination) can be retained. This is the scope of photovoltaics and artificial photosynthesis. On the other hand, natural photosynthesis (i.e. by using the already existing photosynthetic chain) can be directly used as an already available light converter. The first field has led to the best performances so far although the other one is a more recent and growing field.[2]

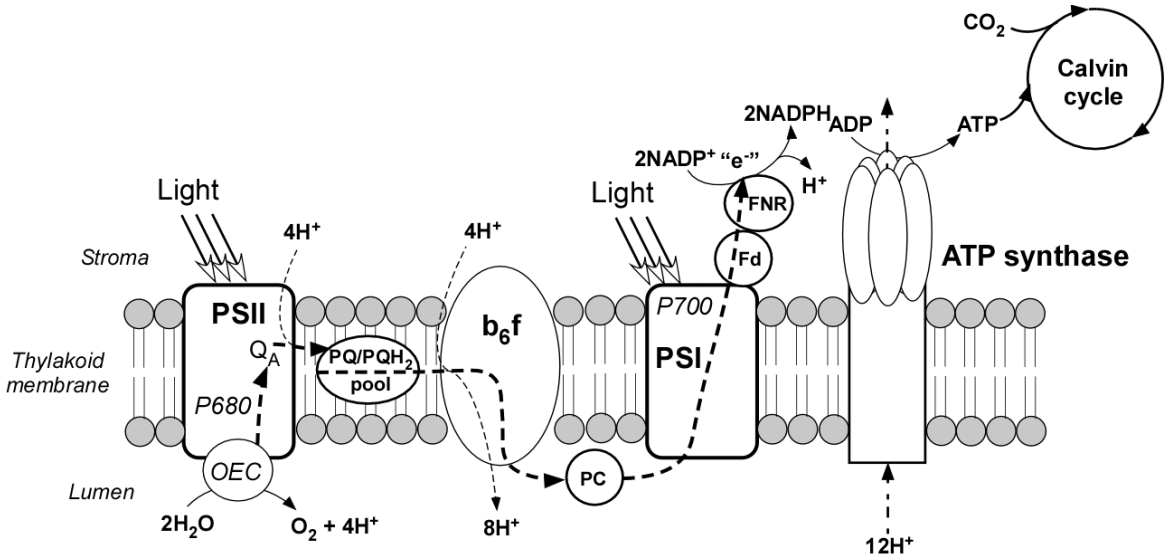

Figure 1A. *General scheme of the photosynthetic chain. Light is captured by light-harvesting complexes at the level of Photosystem II (PSII). Its subsequent excitation promotes energy transfer to P680 (that is the primary chlorophyll donor of PSII). The ensuing charge separation results in water oxidation by means of the Oxygen Evolving Complex (OEC) and reduction of the primary acceptor Q_A. Furthermore, electron transfer steps occur along the photosynthetic chain (oxido-reduction steps from plastoquinone (PQ) - plastoquinol (PQH_2) pool to plastocyanin (PC)) until the Photosystem I (PSI). A second excitation is then required and additional electron transfer pathways (Ferredoxin (Fd) $\rightarrow$ Ferredoxin-$NADP^+$ reductase (FNR)) eventually lead to the $NADP^+$ reduction. The resulting H^+ gradient triggers ATP production by means of ATP synthase. CO_2 is finally reduced through the Calvin cycle which uses the products of the photochemical phase of photosynthesis, NADPH and ATP.*

It is quite difficult to classify all the photobioelectrochemical systems using natural photosynthesis. The main strategies were reported in some excellent reviews[3] and especially very recent ones.[4] What the strategies have in common is to involve an outer collecting electrode to reroute the electrons resulting from the light excitation of the photosynthetic machinery. Advantages can be taken from fragments of the photosynthetic organisms like isolated photosystems (PSII and PSI; often designated as semi-artificial photosynthesis) or thylakoid membranes in a manner to favor the electron transfer with the electrode.[5] However, in the last decades, the use of intact photosynthetic organisms as "catalysts" was also considered due to the absence of extracting procedure and ability to be cultured. This corresponds to a broad field that is often termed as photosynthetic microbial fuel cells (PMFCs). Among them, those relying on a current production from water splitting reaction correspond to a promising subcategory named biophotovoltaics.[3g, 4a] Direct electron transfer can occur between the photosynthetic organism and the electrode but electron shuttles (soluble mediators like quinones, $Fe(CN)_6^{3-}$, phenazines or redox polymers…) also achieve mediated electron transfers that facilitate the exchanges between the collecting electrode and the biological target.[2b, 6]

In this context, we recently focused on a strategy devoted to the use of an algae suspension mixed with soluble redox mediators. Due to their PSII acceptor ability,[7] quinones are ideal candidates for this purpose.[6a, 8] In the past few years, we have indeed investigated the ability of several exogenous quinones to be reduced by a *Chlamydomonas reinhardtii* algae suspension.[9] Based on these results, photocurrents (~ 60 µA cm^{-2}) were recorded by implementing a corresponding spectroelectrochemical set-up involving a polarized carbon gauze electrode (surface area ~1 cm^2).[10] The current shape was globally consistent with the two expected complementary pathways (quinone (Q) reduction by illuminated algae and hydroquinone (QH_2) oxidation at the electrode surface; **Figure 1B**). Nevertheless, detailed modelings suggested deleterious side effects of quinones during the electron harvesting.[11] This poisoning behaviour was investigated by means of chronoamperometry and fluorescence measurements. The oxidizing power of the given quinones was supposed to be crucial but relatively few quinones were investigated.[12] All in all, these works pave the way for finding the best quinone in terms of chemical structure. However, although suitable for a preparative scale, the electrochemical set-up described above was not really adapted for systematic analyses of experimental parameters due to relatively long equilibration times before the experiment. This issue can be circumvented by using a miniaturized well-type Au/ITO electrochemical device.[13] In this work, such a gold electrochemical device is used to analyze the performances of different quinones as redox mediators in the context of photosynthetic electron diverting from *Chlamydomonas reinhardtii* cells. Effects of quinone incubation on the algae proliferation were also investigated by using other approaches. All together, these results gave an overview of the properties requested by the ideal quinones (redox potential, concentration…). Several quinones were therefore synthesized and their ability to produce the best current (magnitude and stability) was evaluated.

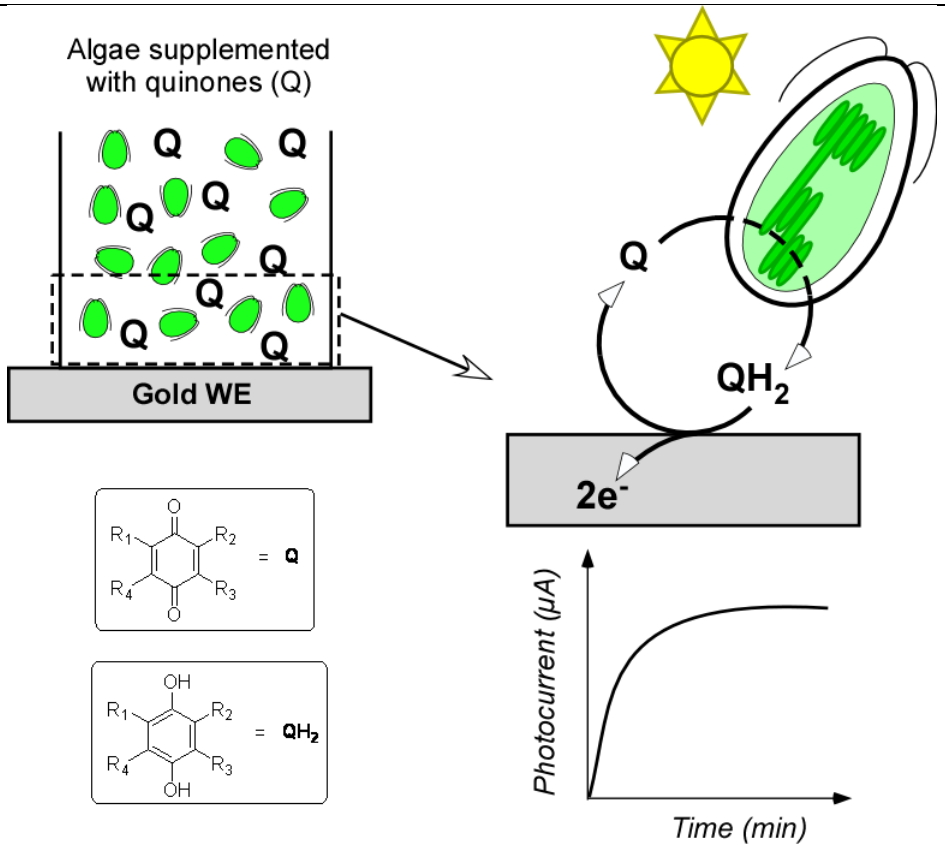

Figure 1B. Principle of the photocurrent production from the algae suspension. *Chlamydomonas reinhardtii algae are suspended in physiological medium supplemented with quinones (Q). It leads to the reduction of Q into hydroquinones (QH_2) by the photoexcited algae. The working gold electrode (reference and auxiliary electrodes are not shown for more clarity) is positioned at the bottom and poised at a potential value favoring the oxidation of QH_2 into Q and the subsequent production of photocurrent.*

2. Experimental

2.1. Cell culture and preparation

Two types of *Chlamydomonas reinhardtii* algae (wild-type or photosynthetic mutant) were used in this work. The wild type strain (hereafter referred as WT) derived from the 137c strain.[14] The Δ*petA* mutant lacks cytochrome b_6f that corresponds to the impairment of the photosynthetic chain.[15] In the absence of cytochrome b_6f (the quinol:plastocyanin oxidoreductase), the plastoquinol generated by light-induced turnovers of Photosystem II cannot be reoxidized by photosystem I. It therefore leads to the fast interruption of light-driven electron flow. In short, WT and ΔpetA were grown in Tris Acetate Phosphate aqueous medium (TAP = Tris base (20 mmol L^{-1}), NH_4Cl (7 mmol L^{-1}), $MgSO_4$ (0.83 mmol L^{-1}), $CaCl_2$ (0.45 mmol L^{-1}), K_2HPO_4 (1.65 mmol L^{-1}), KH_2PO_4 (1.05 mmol L^{-1}), CH_3CO_2H (0.3 mmol L^{-1})) at 25°C under rather dim light conditions (50 µE m^{-2} s^{-1}) prior to further measurements. From a cell suspension at $2x10^6$ cells mL^{-1}, algae are resuspended (after centrifugation at 4000 g) into Tris-minimal medium (= TAP without acetate) for further electrochemical or fluorescence experiments (final concentration of $2x10^7$ cells mL^{-1}).[9b, 13]

2.2. Chemical materials and solutions preparation

All chemicals (including quinones or hydroquinones) have been purchased from Sigma-Aldrich and have been used without further purification. Practically, quinones or hydroquinones were dissolved in absolute ethanol to make fresh mother solutions (10 mmol L^{-1}). Appropriate volumes of these solutions were thus directly added to the algae suspension (see text) for subsequent electrochemical (a well containing the cells; V = 500 µL) or fluorescence (a cuvette containing the algae suspension ; V = 2 mL) experiments.

2.3. Electrochemical experiments – Photocurrent recording

The ITO/Au electrochemical device for measuring photocurrents from a quinone-algae mixture was described elsewhere.[13] Briefly, a thin indium tin oxide (ITO) film (thickness 10 nm) followed by another film of gold (50 nm) are sputtered onto a glass slide (Deckglaser Menzel-Glaser microscope cover slides, Fisher Scientific; 24 mm x 48 mm x 170 µm). A well (9 mm diameter; volume ~ 500 µL) is delimited on the ITO/Au modified glass slide by using PDMS (polydimethyloxane RTV-615 ; Momentive Performance Materials France). Electrical connections were made by using a copper wire and a silver paint (Radiospares) covered by insulating glue. Platinum wire (30 x 1 mm) and Ag/AgCl (35 x 0.5 mm) wires were used as counter and reference (chloride anions ~7.9 mmol $L^{-1;}$ see above) electrodes, respectively.

Chronoamperometry experiments were carried out with aqueous solutions (well of V = 500 µL) containing quinones/algae mixtures in Tris-minimal medium within the PDMS well using a Parstat 2273 potentiostat (Princeton Applied Research). Appropriate volumes of quinones in absolute ethanol were added to the algae suspension and kept 5 seconds at open circuit voltage (OCV) for equilibration. Then the working electrode was polarized at 0.38 V vs Ag/AgCl. After stabilization of the baseline ("dark current"), the light source shutter was opened (actinic white light from a Scott KL1500 LCD halogen lamp at P = 60 mW cm^{-2}). The corresponding faradic photocurrent is then instantly measured. Light is turned off before the end of the experiment to allow the current to reach the baseline back. All plots and statistical analyses (average values ± s.e.m.) were performed using SIGMA Plot 10.0 software (Systat Software Inc., Richmond, CA, USA).

2.4. Spectroscopy measurements

2.4.1. Fluorescence experiments

The fluorescence measurements were carried out according the procedure described in previous works.[9-10,12] Briefly, fluorescence is measured by using a JTS-10 spectrophotometer (Biologic, Grenoble, France); an actinic red light (λ = 640 nm; I = 135 µE m^{-2} s^{-1}) is first applied during few seconds to induce photosynthesis. The steady state fluorescence under that illumination is called Fs. A short subsequent supersaturating pulse (250 ms; λ = 640 nm; I = 5000 µE m^{-2} s^{-1}) of exciting light is then applied to promote the full reduction of the quinone primary electro-acceptor Q_A to Q_A^-. The corresponding maximum fluorescence level (F_M) allows one to calculate the quantum yield of PSII chemistry as $\Phi_{PSII} = (F_M - Fs) / F_M$. Incubation periods were achieved under dark conditions and gentle stirring in order to avoid aggregation either in presence of quinones or in absence of quinones as a

control experiment. Fluorescence measurements have been performed every hour for each sample (V = 2 mL). Each experiment was repeated three times.

2.4.2. ATP synthase

The saturated light flash (6 ns) was provided by a laser dye (LDS 698) pumped by an ND-YAG second harmonic laser (Minilite Continuum). The interference filters at 520 ± 6 nm and 546 ± 6 nm have been used to measure absorption changes at desirable wavelengths. Cut-off filters (BG-39, Schott, Germany) was put in front of the measure and reference photodiodes to stop the actinic illumination. Electrochromic-Shift (ECS) measurements were calculated as the difference between the absorption changes at 520 and 546, to eliminate the contributions of the redox changes of the cytochrome *f* and flat contributions due to diffusion. Before the saturating laser flash was applied, cells were dark adapted for 1 min. The kinetics of ECS changes after a single turnover laser flash consisted in 3 phases. The first experimental point after the flash (300 µs, "a phase") corresponds to the electric field generated by photochemical events in the two photosystems. A second phase (~10-20 ms, called "b phase") followed, reflecting the activity of the cytochrome b_6f. The ECS decay (sometimes called "c phase") following the a and b phases reflects the consumption of the protons accumulated in the lumen by the activity of the CF1FO ATPase.

2.5. Synthesis of quinones

Three quinones used in this work were not purchased but synthesized according to the following procedures.

2.5.1. 2,5-Dichloro-3,6-dimorpholino-1,4-benzoquinone (DCMorBQ) [16]

A 50 mL round-bottom flask equipped with a magnetic stirrer was charged with a solution of chloranil (246 mg, 1.0 mmol) in 1,4-dioxane (10 mL). Morpholine (0.50 mL, 500 mg, 5.7 equiv) was then added. The reaction took place very quickly with a color change from yellow to yellow-brown. After stirring for 10 minutes at room temperature, methanol (10 mL) and water (1 mL) were added. After ageing in the mother liquor for 15 minutes, the precipitated solid was filtered and dried *in vacuo*. The title compound was thus obtained in the form of a brown solid (253 mg, 73% yield). ^{1}H NMR (300 MHz, $CDCl_3$): δ = 3.90–3.70 (m, 8H), 3.70–3.48 (m, 8H) ppm; ^{13}C NMR (75 MHz, $CDCl_3$): δ = 176.1, 148.1, 116.4, 67.7, 52.2 ppm.

2.5.2. 2,5-Dichloro-3,6-di-tert-butylthio-1,4-benzoquinone (DCThioBQ) [17]

A 50 mL round-bottom flask equipped with a magnetic stirrer was charged with chloranil (683 mg, 2.8 mmol), dichloromethane (12 mL), ethanol (12 mL), sodium 2-methyl-2-propanethiolate (690 mg, 6.2 mmol, 2.2 equiv), and acetic acid (480 µL, 8.4 mmol, 3.0 equiv). The resulting mixture was stirred overnight at room temperature, then diluted with dichloromethane (50 mL) and extracted with water (2 x 25 mL). The organic layer was dried over $MgSO_4$ and concentrated under reduced pressure. The title compound was thus obtained in the form of a dark brown solid (590 mg, 60% yield). ^{1}H NMR (300 MHz, $CDCl_3$): δ = 1.44 (s, 18H) ppm; ^{13}C NMR (75 MHz, $CDCl_3$): δ = 173.9, 151.4, 141.5, 53.5, 32.6 ppm.

2.5.3. 2,3-Dimethyl-5-phenyl-1,4-benzoquinone (DMPPBQ) [18]

A pressure-resistant tube (25 mL capacity, calculated reaction pressure: 5 bar, maximum allowed pressure: 20 bar) equipped with a magnetic stirrer was charged with 2,3-dimethylbenzoquinone (138.1 mg, 1.0 mmol), benzene (6.0 mL), palladium(II) acetylacetonate (15.2 mg, 0.050 mmol, 0.050 equiv), Ag_2CO_3 (827.5 mg. 3.0 mmol, 3.0 equiv), DMSO (0.25 mL, 3.50 mmol, 3.50 equiv), and pivalic acid (205.0 mg, 2.0 mmol, 2.0 equiv). The tube was sealed and the resulting mixture was stirred at 140 °C overnight. The reaction mixture was cooled to room temperature, transferred to a round-bottom flask and concentrated under reduced pressure. The residue was purified by flash chromatography on silica gel (eluent: toluene) to give the title compound in the form of yellow crystals (118.5 mg, 56% yield). ^{1}H NMR (300 MHz, $CDCl_3$): δ = 7.50–7.40 (m, 5H), 6.81 (s, 1H), 2.11 (s, 3H), 2.08 (s, 3H) ppm; ^{13}C NMR (75 MHz, $CDCl_3$): δ = 187.7, 186.9, 145.9, 141.4, 140.9, 133.4, 132.6, 129.9, 129.4, 128.5, 12.9, 12.3 ppm.

2.6. Threshold concentration of quinones for cell division

Suspended algae in Tris-minimal medium ($2x10^7$ cells mL^{-1}) are stirred under dim light (50 µE m^{-2} s^{-1}) in presence of exogenous quinones (from 10 to 100 µmol L^{-1}) over one hour. The suspension is then diluted in fresh TAP medium. Every 24 h, the algae concentration in both samples is measured (Malassez cell counting). The results are compared to a control experiment without adding quinones. In such a case, counting the cells every 24 h helps to determine the growing rate (defined as the increase in cell concentration every 24 h) as a function of time. The corresponding exponential increase of the growing rate allows one to extract a rate constant equal to 0.134 h^{-1} i.e. a doubling time of 5.2 h. Such a reference value allows one to extract the fraction of cells able to grow after being incubated with exogenous quinones.

3. Results and discussion

3.1. Photocurrents resulting from algae-quinones mixtures

Chronoamperometry measurements were performed using the well-shaped device reported in a previous work.[13] Photocurrents from *Chlamydomonas reinhardtii* algae suspension with several quinones (see **Figure 2A**) could therefore be recorded. A representative chronoamperogram (2,6-DCBQ / WT) is displayed in **Figure 2B**. Under illumination, the exogenous quinones interact with the photosynthetic chain within the algae suspension. This leads to the reduction of quinones (Q) and the subsequent formation of hydroquinones (QH_2) that are then oxidized at the gold electrode surface. Through this electrocatalysis pathway, the resulting current globally corresponds to the photosynthetic electron rerouting from the algae. This photocurrent increased until reaching a steady state value that eventually diminishes at long timeframes. Furthermore, the fast decrease of the photocurrent after turning light off shows that the electron harvesting results from the photosynthetic electron transfer chain (PETC).

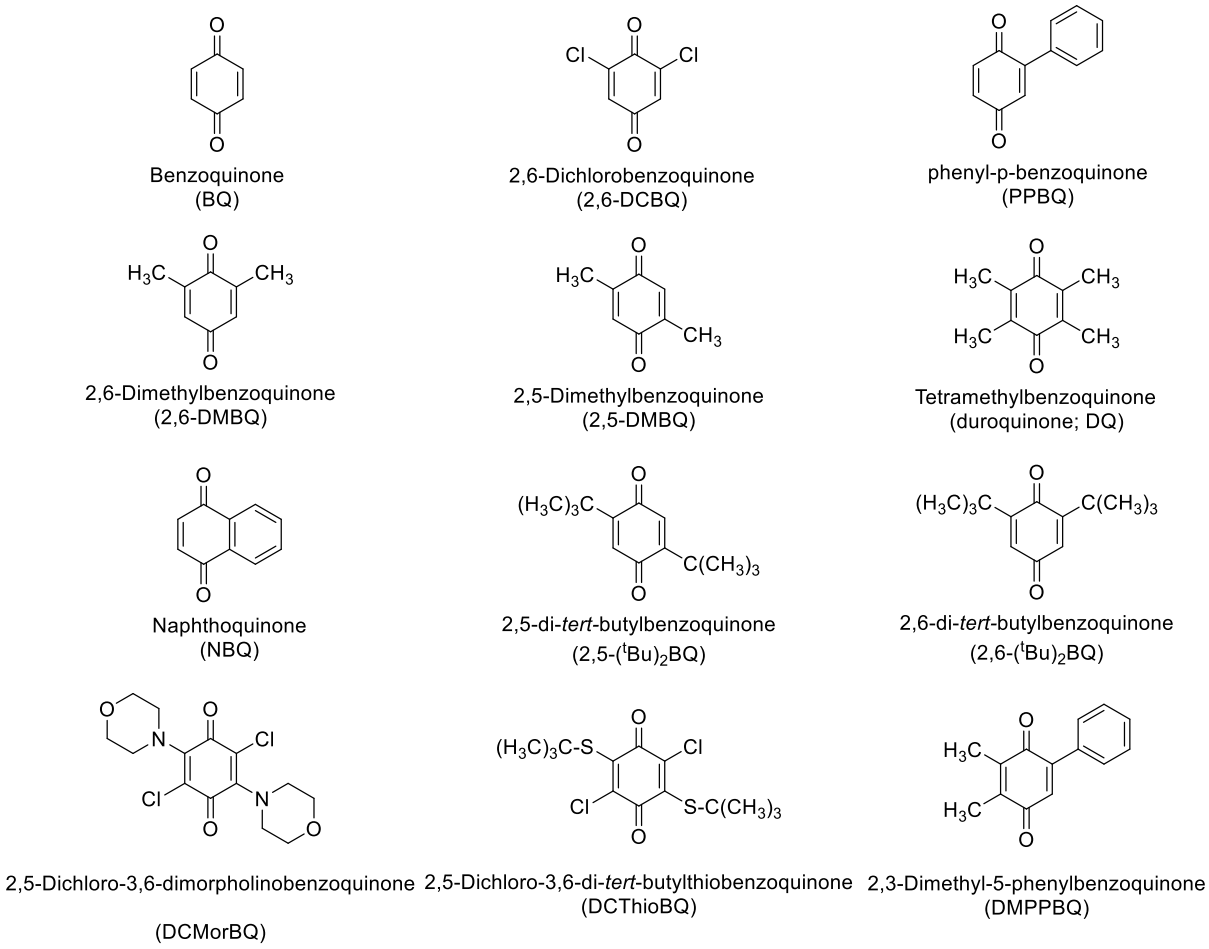

Figure 2A. Chemical structure of the quinones investigated in this work.

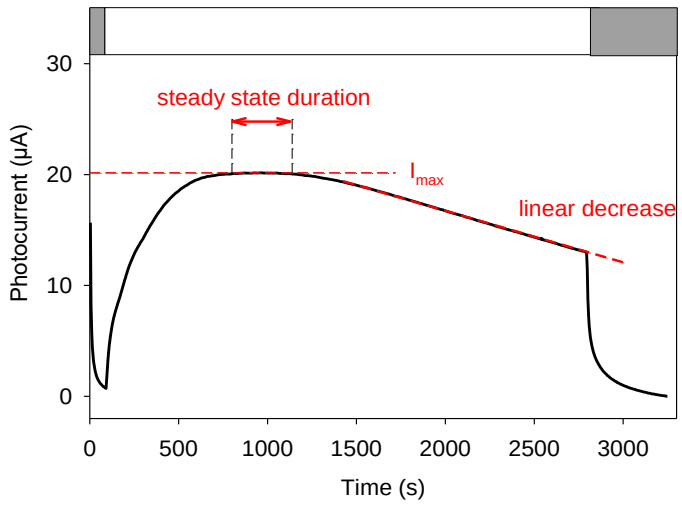

Figure 2B. Representative chronoamperometric trace (P = 60 mW cm^{-2}; E_W = 0.38 V vs Ag/AgCl) from a suspension of Chlamydomonas reinhardtii WT algae (2x10^7 cells mL^{-1}) with 2,6-DCBQ (100 µmol L^{-1}). *Light irradiance is displayed as a white rectangle. Before illumination, a background current is observed after electrode polarization, due to capacitive and faradic effects.[13] Once the baseline remaining stable (after ~90 s), the illumination of the algae-quinone solution is triggered. The main parameters (maximum photocurrent, steady state period, photocurrent decrease) are displayed.*

In order to provide some further insights into the research of the most appropriate quinones, we took benefit from previous works by screening several structures with this set-up (**Table 1**). Furthermore, two *Chlamydomonas reinhardtii* strains were investigated. The wild type (WT) strain corresponds to a fully functional photosynthetic electron transfer chain. The ΔpetA mutant lacks the b_6f complex so the electron flow is interrupted downstream of the plastoquinone pool.[15] As evidenced in **Table 1**, the best current is measured for WT algae with 2,6-DCBQ (I_{max} = (22.3 ± 3.9) µA, i.e. 35 µA cm^{-2}). This is consistent with the fact that 2,6-DCBQ is one of the most oxidizing agents (in terms of E° values for QH_2/Q at pH 7 and Q^-/Q) and therefore a good PSII acceptor. Furthermore, the recorded photocurrents are still lower with ΔpetA mutants. The differences are relatively small for the most efficient quinones (DCBQs and PPBQ) but very high for the two methylbenzoquinones. All in all, it suggests that the exogenous quinones readily act as PSII acceptors but can also interact downstream of the b_6f complex, for instance with PSI acceptors. This trend was already observed for 2,6-DMBQ in previous fluorescence experiments.[10a] In other words, some bad PSII acceptors can reroute the electron flow from another part downstream of the PETC. Furthermore, hindered quinones with electron donor groups (DQ; 2,5-(^{t}Bu)$_2$BQ; 2,6-(^{t}Bu)$_2$BQ) lead to low photocurrents according to a lower ability to accept electrons. **Figure 3** therefore show a quite good correlation between standard potentials with the maximum photocurrent. E°(QH_2/Q) at pH 7 displays the whole oxidizing power (**Figure 3A**) while E°(Q^-/Q) is more related to the first electron transfer between Q and the reduced species within the photosynthetic chain (**Figure 3B**). Whatever the considered standard potential is, the maximum photocurrent is globally correlated to the oxidizing properties of the considered quinone. Of note, BQ does not follow this trend. It shows that the redox potential may still not be a key parameter. Indeed, BQ is an unhindered quinone which can easily react as a Michael acceptor (see below).

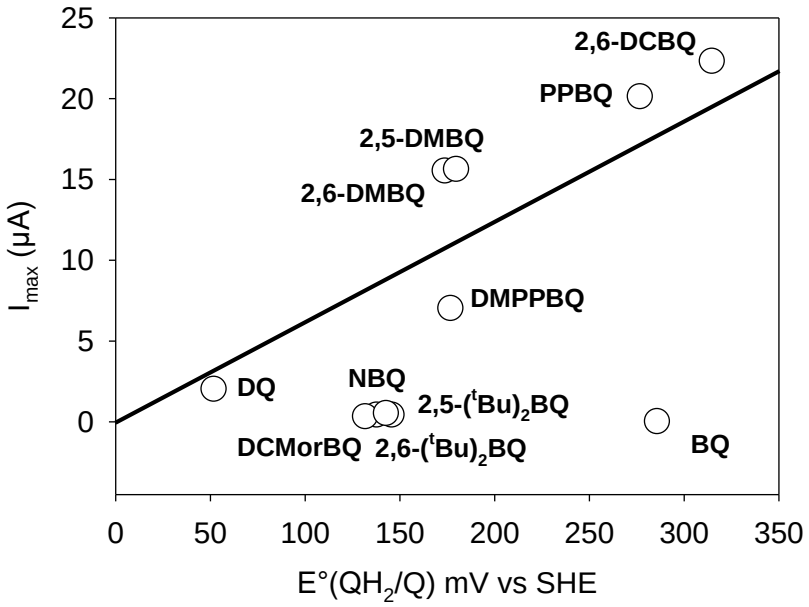

Figure 3A. Maximum photocurrents measured for different quinones (100 µmol L^{-1}) used with a WT algae suspension ($2x10^7$ cells mL^{-1}) within the well gold/ITO device as a function of E°(QH_2/Q) at pH 7.

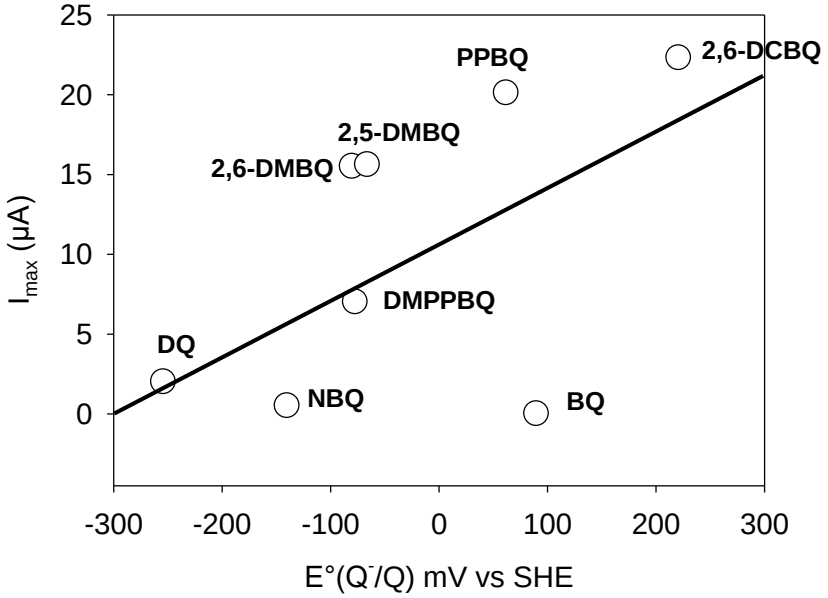

Figure 3B. Maximum photocurrents measured for different quinones (100 µmol L^{-1}) used with a WT algae suspension ($2x10^7$ cells mL^{-1}) within the well gold/ITO device as a function of E°(Q^-/Q).

Another interesting result is related to the stability of the photocurrent. Indeed, the photocurrents readily reach a steady state value before slowly decreasing (**Figure 2B**). This decrease depends on the quinone (**Table 1**) and cannot be predicted by the electrocatalysis process alone.

Quinone (Q)	Photocurrent (µA) WT	Photocurrent (µA) Δ*petA* mutant	I_{max}(WT)/ I_{max}(Δ*petA* mutant)	Decrease in photocurrent for WT (10^3 µA s^{-1})	Steady state duration (s)	E°'(QH_2/Q) pH 7 (mV vs SHE)	E°(Q^-/Q) (mV vs SHE)
2,6-DCBQ	22.3 ± 3.9	17.2 ± 3.0	1.3 ± 0.3	5.0 ± 0.8	190 ± 50	315 [31]	221 [32]
PPBQ	20.1 ± 3.5	12.6 ± 2.5	1.6 ± 0.4	2.1 ± 0.4	410 ± 40	277 [33]	62 [33]
2,5-DMBQ	15.6 ± 2.7	2.5 ± 0.5	6.2 ± 1.6	0.38 ± 0.15	810 ± 90	180 [31, 34]	-66 [34]
2,6-DMBQ	15.5 ± 2.8	2.1 ± 0.4	7.4 ± 1.9	0.53 ± 0.21	880 ± 90	174 [33]	-80 [32, 34]
DQ	2.0 ± 0.5	< 0.4	n.d.	< 0.2 [a]	> 1000 [b]	52 [33]	-254 [33]
2,6-(^{t}Bu)$_2$BQ	0.4 ± 0.1	n.d.	n.d.	< 0.2 [a]	> 1000 [b]	138 [c]	n.r.
2,5-(^{t}Bu)$_2$BQ	0.4 ± 0.1	n.d.	n.d.	< 0.2 [a]	> 1000 [b]	146 [35]	n.r.
NBQ	0.5 ± 0.1	0.4 ± 0.1	1.25 ± 0.4	< 0.2 [a]	> 1000 [b]	143 [31]	-140 [36]
BQ	~ 0	~ 0	n.d.	n.d.	n.d.	286 [33]	90 [33]
DCMorBQ	0.5 ± 0.1	n.d.	n.d.	< 0.2 [a]	> 1000 [b]	132 [c]	n.r.
DMPPBQ	5.8 ± 0.8	1.1 ± 0.4	5.5 ± 2.0	No decrease	1500	177 [c]	-77 [d]

Table 1. Average values of photocurrents *for different algae-quinone mixtures (C_Q = 100 µmol L^{-1}). [a]Because I_{max} is very low, the photocurrent appears quite stable overtime while slowly decreasing. The decrease is thus too low to be reliably extracted. [b]For the same reasons, the steady state duration can be only estimated. [c]Estimated by cyclic voltammetry. [d]Estimated by analogy with 2,3-DMBQ. n.d: not determined. n.r: not reported.*

This suggests concomitant poisoning effects due to quinones.[11a, 12] In our experiments, highly rerouting quinones (2,6-DCBQ or PPBQ) lead to moderate steady state photocurrent duration while low PSII accepting quinones (DMBQs, DQ) involve more stable photocurrents (**Table 1**).

Because a correlation is supposed between the "poisoning" effect of quinones (i.e. in terms of photocurrent decrease) and their oxidizing properties, the effects of quinones were also investigated in absence of electrocatalysis.

3.2. Effects of quinones on the algae without electrocatalysis

3.2.1. Algae incubation with exogenous quinones – Effects on Φ_{PSII}

An interesting way to investigate the unexpected effects of quinones is to estimate the quantum yield of PSII chemistry (Φ_{PSII}) by fluorescence measurements. This corresponds to the fraction of absorbed light by PSII chlorophylls used in photochemistry (i.e being converted in photosynthetic electron flow from PSII).[19] Briefly, induction fluorescence curves are the usual analytical tool to calculate this parameter. To obtain these curves, chlorophyll fluorescence emission is measured during illumination of the algae suspension. Indeed, light is captured by PSII that leads to a charge separation (P680-pheo-$Q_A \rightarrow$ P680$^+$-pheo-Q_A^-) and especially the reduction of the primary acceptor Q_A into Q_A^- (**Figure 1A**). Under steady state actinic light, a fraction of Q_A is reduced and a fraction of Q_A is oxidized, which gives an intermediate value of fluorescence (F_S; see **Figure 4A**). A supersaturating pulse then induces the full reduction of Q_A and the maximum level of fluorescence (F_M). Φ_{PSII} thus corresponds to the fluorescence yield $(F_M-F_S)/F_M$.

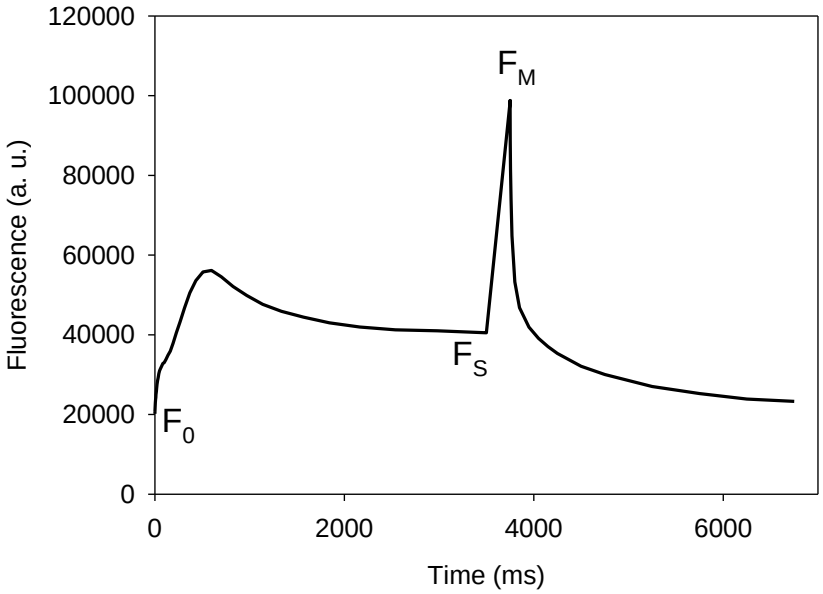

Figure 4A. Representative fluorescence induction curve (WT cells; 2.10^7 cells mL^{-1}; I° = 135 µE m^{-2} s^{-1}). The initial fluorescence (F_0) corresponds to the dark-adapted state. After illumination, the fluorescence varies until a steady state level (F_S) where the Q_A/Q_A^- ratio is constant. The surpersaturating and short light pulse fully reduces Q_A into Q_A^-. It helps to reach the maximum fluorescence emission (F_M).

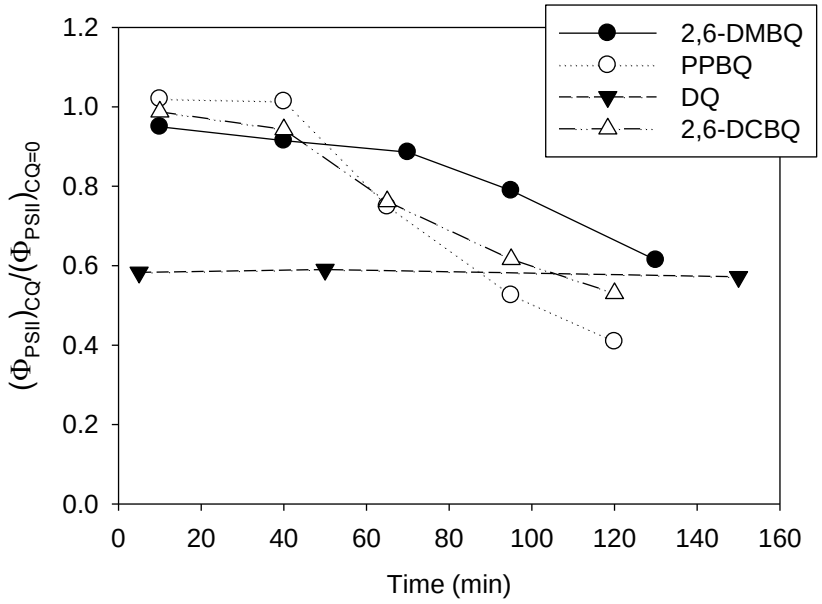

Figure 4B. Normalized Φ_{PSII} values as a function of incubation time for an algae suspension (2.10^7 cells mL^{-1}) incubated with quinones at a concentration of 100 µmol L^{-1}.

In these experiments, WT algae suspensions were incubated with four representative quinones (at 100 µmol L^{-1}), the fluorescence was followed during a 4 s illumination and the values of Φ_{PSII} were measured at the end of this light period (**Figure 4A**). As displayed in **Figure 4B**, the quantum efficiency of PSII is altered after incubation with quinones for three of them (2,6-DCBQ, PPBQ, 2,6-DMBQ). Conversely, Φ_{PSII} remains constant for DQ although the initial value is already diminished due to the quinone. Furthermore, no effect was observed with the hydroquinone forms. The decrease for 2,6-DCBQ, 2,6-DMBQ and PPBQ is globally consistent with previous experiments where the quinones have been shown to act in different ways. First, quinones are known to perform non-photochemical quenching of chlorophyll fluorescence.[20] They indeed interact with excited chlorophyll, decrease the lifetime of the exciton in PSII antenna and thus decrease the available light for charge separation. Furthermore, the production of additional quenchers during the incubation was already observed in the PPBQ case for previous works.[12] Second, quinones can react as Michael acceptors and alter the microorganism.[21] The case of DQ is more difficult to rationalize because the Φ_{PSII} value did not significantly vary but remained quite low compared to the case without quinones. This intrinsic moderate ability to harvest photosynthetic electrons from the beginning to the end of the incubation is consistent with an inhibiting behavior. The quinone may thus be maintained at the extraction site without being reduced due to its low redox potential. It would result in an "inverted" zone where the quinone interrupts the chain and decreases the fraction of Q_A.[9b] More generally, it is worth mentioning that the quite fast quenching behavior of quinones makes difficult the observation of the expected increase of Φ_{PSII} that can be measured only under peculiar conditions.[22]

As a first conclusion, the decrease in Φ_{PSII}, especially for PPBQ, may result from a combined role of quinones in terms of toxicity and quenching. Therefore, the Φ_{PSII} value did not properly correlate the photocurrent values. In order to go further, the ATP synthase activity and the cell growth after quinone incubation were monitored.

3.2.2. ATP synthase activity

During photosynthesis, electron transfer along the photosynthetic chain gives birth to a vectorial relocation of protons from the stroma to the lumenal space of the thylakoids. This displacement of protons across the membrane induces the creation of an electrochemical proton gradient ($\Delta\mu_H^+$) or proton motive force (pmf) that includes two components: a proton concentration gradient (ΔpH) and an electric field (Δψ). The $\Delta\mu_H^+$ has a key role in photosynthesis by providing the energy required for the synthesis of ATP produced by ATP synthase.[23] The ΔpH plays the role of modulator of the rate of electron transfer and sets off de-excitation of surfeit light in the bosom of photosynthetic light harvesting complexes.[24] The presence of this electric field induces a slight shift in the energy levels of some photosynthetic pigments present in the thylakoid membrane. This consequently changes their absorption spectra, due to the Stark effect, and induces an electrochromic Shift (ECS).[25] The light-induced variation of the absorption spectrum provides information on the proton motive force across the membrane and, therefore, the functioning of ATP synthase.[26] Effectively, in the majority of photosynthetic systems and especially in *Chlamydomonas*, the ECS signal is linear as a function of the intensity of the electric field.

The kinetic analysis of the ECS signal following a saturating laser flash makes it possible to bring out three different phases. This data treatment is possible by using repetitive flash spectroscopy to synchronize photosynthetic samples for kinetic resolution and signal to noise ratio improvements.[27] Saturating laser flashes allow the excitation of all photosystems at a time, but are too short to allow two charge separations in the same photosystem. The first very faster rise “a phase” of the ECS signal (in pink in **Figure 5A**) corresponds to a rapid increase of the electric field created by the charge separation in PSI and PSII which time scale range is below the kinetic measurement resolution; it corresponds to less than 100 µs. This phase is followed by a slower rising phase (called "b phase" and lasting few tens of ms) (in blue in **Figure 5A**) correlated with the turnover of the complex b_6f which couples electron movement from plastoquinol to plastocyanin and the pumping of extra protons across the thylakoid.[27] Finally, after the end of this “b phase”, there is a decrease in the electric field (“c phase”). In native chloroplasts, this ECS decay (in green in **Figure 5A**) lies in the charge leakage mostly due to the consumption of the proton gradient by the ATP synthase that reduces the electric field. Therefore, the variation in relaxation time of the ECS signal provides information on the level of activity of the corresponding enzyme (*e.g.*, “a phase” on number of active photosystems, “b phase” on activity of cytochrome b_6f and “c phase” on ATP synthase activity, respectively).

We measured the flash-induced ECS kinetics in the presence of various quinones in order to look at their effect on the ATP synthase activity. The addition of exogenous quinones clearly slowed down the relaxation of ECS (“c phase”; **Figure 5B**) with the highest effect measured with 2,6-DCBQ. Conversely, DQ does not induce any disturbance. The results obtained are generally in line with previous studies, namely that DQ has almost no disturbance effect unlike quinones such as 2,6-DCBQ and to a lesser extent 2,6-DMBQ. This slow-down of ATPase activity can be explained if 1 / it is inhibited directly by quinones or 2 / if quinones indirectly affect the pmf ($\Delta\mu H^+$) present before the flash since there is an ATPase activation threshold by the pmf.[28] Here, the ECS increase and relaxation in response to a few ms pulse of saturating light allows one to discriminate between these two options.

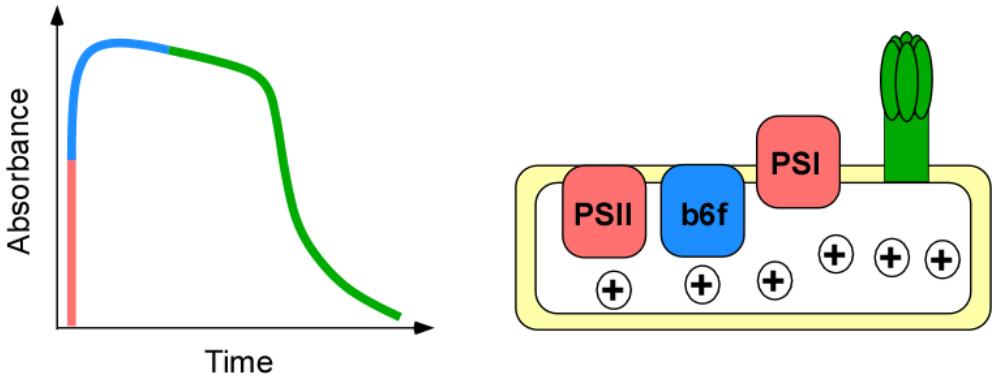

Figure 5A. Schematized kinetics of the Electro-Chromic Shift (ECS) as measured in *Chlamydomonas reinhardtii* algae upon excitation with a supersaturating laser pulse. Three phases can thus be evidenced in pink ("a phase"), blue ("b phase") and green (slow decay phase) that correspond to different enzyme activity (pink: PSII and PSI, blue: b_6f, green: ATP synthase).

At the end of such a pulse, the electric field generated is ~5 fold higher than after a flash (**Figure S1 vs Figure 5B**) and all treatments show a comparably fast initial decay of the electric field, which demonstrates that the ATPase is not intrinsically inhibited by exogenous quinones. Instead, for the quinones which slowdown the ATPase activity after a flash, a typical pulse-induced ECS relaxation at low dark pmf is obtained, comprising a fast and a slow phase.[29] This validates the second hypothesis, where the slower "c phase" reflects a weaker pmf in the dark (ie before the flash), which is in equilibrium with the ATP/ADP ratio in the chloroplast. This may represent a lower ATP concentration under these conditions because respiration is inhibited by quinones. Among the investigated quinones, the most harvesting quinone (2,6-DCBQ, PPBQ) are the more active towards the relaxation phase while poor accepting quinones (2,6-DMBQ, DQ) lead to moderate effects.

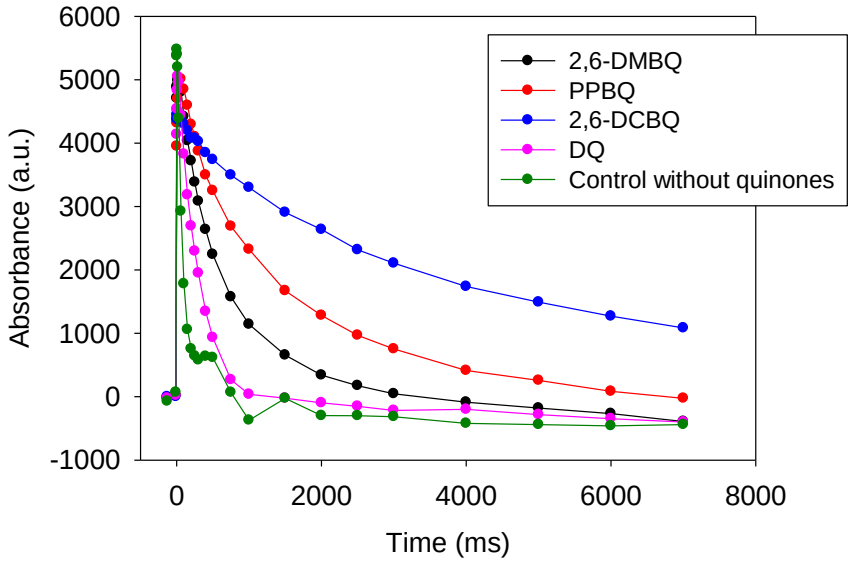

Figure 5B. Monitoring of the status of ATP synthase for algae suspensions at $2x10^7$ cells mL^{-1}: laser flash-induced ECS kinetics in the presence of various quinones (DQ, 2,6-DMBQ, 2,6-DMBQ, PPBQ; concentration of 100 µmol L^{-1}) and in the control. Time 0 corresponds to the laser flash.

Another (indirect) effect can be observed on those flash-induced ECS kinetics and relate to the extent of "b phase". Indeed, it is a common observation that in oxic conditions, wild type cells do not show a "b phase" because it is bypassed by the fast relaxation of ECS by the ATPase activity. However, in the presence of 2,6-DMBQ, 2,6-DCBQ or PPBQ, the "c phase" becomes several orders of magnitude slower than the "b phase" (few seconds vs 10-20 ms). The "b phase" is thus expected to appear but is still not observed. This probably shows that the b_6f is decorrelated from the rest of the photosynthetic chain and confirms that these quinones completely bypass the photosynthetic chain.

3.2.3. Cell growth

An interesting way to observe the poisoning effect of quinones is to estimate their effect on the algae proliferation during their culture. To do so, wild-type algae were incubated with different quinone concentrations under experimental conditions used for chronoamperometry (micromolar range; one hour). Their growth rate and doubling time are then compared to a control experiment, i.e., without any quinone incubation. It consequently allows us to deduce the fraction of cells capable of growing after incubation with quinones. As a result, we define two threshold concentrations: CC_{20} and CC_{80} which correspond to quinone concentrations where 80 and 20% of cells still grow, respectively. Quinones leading to a fast current decrease thus correspond to CC values much less than 100 µmol.L^{-1} (**Table 2**).

Quinone	CC80 (µmol L^{-1})	CC20 (µmol L^{-1})
2,6-DCBQ	20	10
PPBQ	20	10
2,6-DMBQ	50	40
DQ	> 100	> 100
BQ	80	70
2,6-(^{t}Bu)$_2$BQ	> 100	> 100
2,5-(^{t}Bu)$_2$BQ	> 100	> 100
DCMorBQ	> 100	> 100
DCThioBQ	< 10	< 10
DMPPBQ	> 100	> 100

Table 2. Threshold concentrations for estimating the poisoning effect of some quinones. *CC_{20} and CC_{80} correspond to quinone concentrations where 80 and 20% of cells still grow, respectively.*

As an example, 2,6-DCBQ is a quinone that prevents the cell growth at relatively low concentrations. A similar effect was recently observed in the case of cyanobacteria.[6b] The results are in agreement with a redox potential-activity relationship. The less oxidizing quinones (i.e., with low

redox potential; DMBQ, DQ) did not lead to a significant poisoning whereas the most oxidizing quinones (DCBQ, PPBQ) show low CC values where they may act as poisons. Among the considered quinones, a correlation can be established between the ability to reroute photosynthetic electrons and a poisoning behavior. While this does not concern algae, this fact was already observed for quinones towards hepatocytes and was attributed to the ability of electrophilic quinones to form addition products with GSH.[30] Moreover, the hydroquinone forms have no effect on the cell growth under the same conditions. Furthermore, sterically hindered quinones (for methyl substituents for DQ or *tertio*-butyl substituants for (^{t}Bu)$_2$BQ) are clearly non-toxic in the usual concentration used in chronoamperometry. The electron-donor groups obviously involve a very low redox potential that does not fit the requirements for harvesting photosynthetic electrons. However, it paves the way for using hindered quinones whose redox potential will be high enough to extract electrons from the photosynthetic chain.

3.3. Investigation of other quinones

From the above-mentioned results, we see that electron harvesting and poisoning behaviours are both related to oxidising (i.e., with a high redox potential) and/or poorly substituted quinones. As a result, we chose to work with quinones bearing both electron-withdrawing and donor groups as a compromise. This is the case of 2,5-dichloro-3,6-dimorpholine-1,4-benzoquinone (DCMorBQ), 2,5-dichloro-3,6-di-*tert*-butylthio-1,4-benzoquinone (DCThioBQ) and 2,3-dimethyl-4-phenyl-1,4-benzoquinone (DMPPBQ).

DCMorBQ corresponds to a quinone moiety bearing two electron-withdrawing chloride atoms and two electron-donating morpholine groups. As shown by cyclic voltammetry experiments, DCMorBQ is less oxidising than 2,6-DCBQ (**Figure S2)**. A first interesting result is related to the absence of effects of DCMorBQ towards algae proliferation for a concentration of 100 µmol L^{-1}. Unfortunately, chronoamperometry experiments evidenced that the photocurrent recorded for 2x10^7 cells mL^{-1} and 100 µmol L^{-1} of DCMorBQ is less than 1 µA **(Figure 6**).

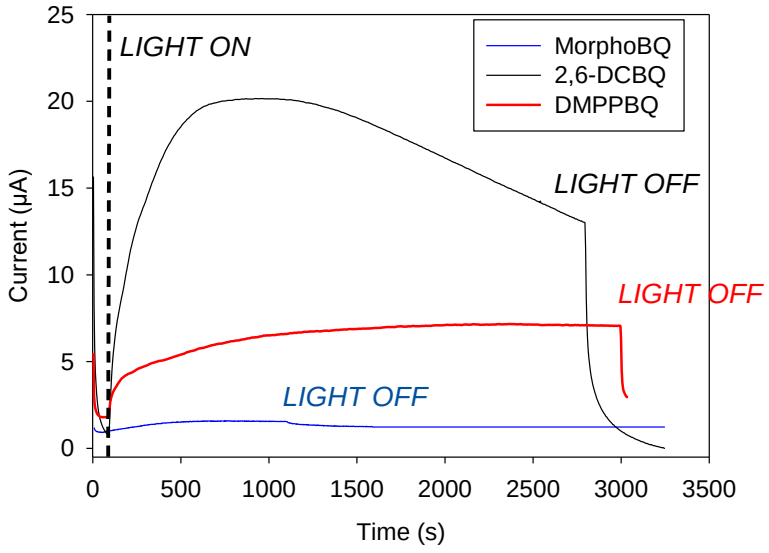

***Figure 6. Representative chronoamperograms from a suspension** of Chlamydomonas reinhardtii algae (2x10^7 cells mL^{-1}) under illumination with 2,6-DCBQ, MorphoBQ and DMPPBQ (100 µmol L^{-1}).*

It means that adding two morpholine groups to 2,6-DCBQ makes the resulting quinone not able to harvest electrons from the PETC. Induction fluorescence experiments (**Figure S3)** suggest that DCMorBQ would inhibit electron transfer with the PETC because the fluorescence level under actinic light did not significantly change after applying the supersaturating pulse (ie $\Phi_{PSII} \sim 0$). This result would be consistent with an irreversible interaction between DCMorBQ and the Q_B pocket by means of nitrogen donor atoms that lead to a complete reduction of Q_A in the light.

In a similar idea, DCThioBQ corresponds to 2,5-DCBQ substituted with two *tert*-butylthiolate groups. Unfortunately, cyclic voltammetry evidences that the redox potential of DCThioBQ is not significantly altered by comparison with 2,5-DCBQ (**Figure S4**). Furthermore, due to the thioether group, DCThioBQ is easily adsorbed on gold electrode. Finally, even at low concentrations (10 µmol L^{-1}), DCThioBQ prevents algae proliferation and even induces degradation of algae (the green color rapidly turns red). Therefore, no chronoamperometry experiment was achieved with this inappropriate quinone.

As mentioned above, functionalizing the DCBQ moiety did not lead to convincing results. As a consequence, the third quinone we considered was formally a structural mix between a rerouting (PPBQ) and a non-poisoning quinone (DMBQ), i.e. 2,3-dimethyl-4-phenyl-1,4-benzoquinone (DMPPBQ). Interestingly, this quinone resembles plastoquinone where a phenyl group replaces the isoprenyl side chain. From an electrochemical point of view, the redox behaviour of DMPPBQ is similar to that of 2,3-DMBQ (2,3-dimethyl-benzo-1,4-quinone) as evidenced in cyclic voltammetry (**Figure S5)**. It allowed us to find that its oxidizing properties in terms of $E°(QH_2/Q)$ is similar to DMBQs. Like DQ or DCMorBQ, no effect of DMPPQ towards algae proliferation was observed for a concentration of 100 µmol L^{-1}. These preliminary results suggest that DMPPQ may combine appropriate properties for rerouting photosynthetic electrons without leading to significant poisoning effects at a concentration of 100 µmol L^{-1}. As a result, this trend is confirmed by chronoamperometry measurements that evidence a stable photocurrent (5.8 ± 0.8 µA) over the time period considered in our studies (**Figure 6**). Among the investigated quinones, DMPPBQ gives the best result in terms of stable photocurrent: it corresponds to a significant photocurrent with the best stability. In other words, all the quinones leading to a higher photocurrent (2,6-DCBQ, PPBQ, DMBQs) concomitantly imply a decrease in stability.

3.4. Discussion

In this work, we screened different quinones from highly (DCBQ, PPBQ) to moderately oxidizing ones (DMBQs, DQ). It obviously raises the question of the ideal exogenous quinone to harvest photosynthetic electrons from algae suspensions. While it may not be a definitive trend, we observed a relationship between the oxidizing properties of the considered quinone and the stability of the photocurrent (**Table 2**). **Figure 7A** thus depicted the maximum photocurrents obtained with quinones at 100 µmol.L^{-1} as a function of the stability of such a photocurrent. This confirms that the most rerouting quinones are also the most poisoning ones because the harvesting effect of a high concentration (100 µmol.L^{-1}) is fastly countered by the side effects of the considered quinone (see also **Figure S6**). As a result, a high redox potential will globally lead to high but unstable photocurrents due to quinone toxicity. Conversely, a low redox potential should lead to a stable but quite low photocurrent.

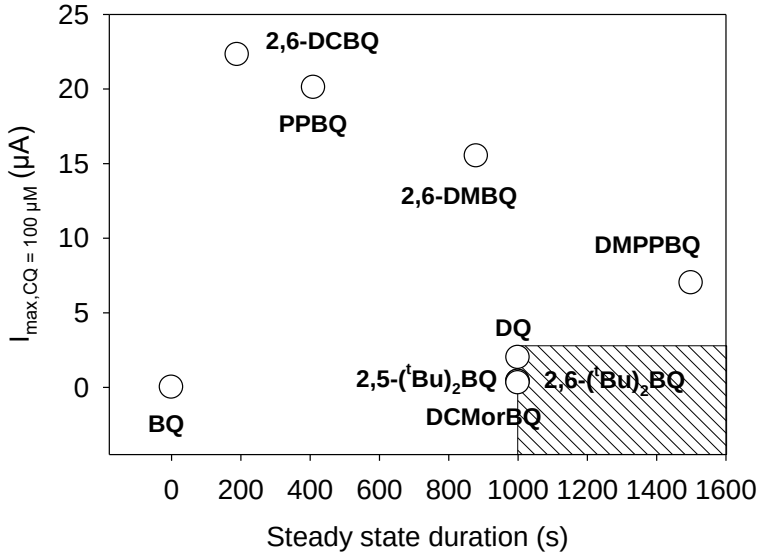

Figure 7A. Maximum photocurrents measured for different quinones *(100 µmol L^{-1}) from a suspension of Chlamydomonas reinhardtii algae (2x10^7 cells mL^{-1}) as a function of the steady state duration. The dashed zone corresponds to the uncertainties of steady state stability due to the low measured photocurrents.*

A second interesting analysis is to consider concentration ranges where the maximum photocurrent remains stable. **Figure 7B** shows the stable maximum photocurrents (measured at CC20) as a function of a nearly non toxic concentration (i.e. CC20). It is worth mentioning that similar photocurrents for 2,6-DCBQ, PPBQ, 2,6-DMBQ and DMPPBQ are observed provided that the highest non toxic quinone concentrations were used. This evidenced a "shift effect' related to the tuning of quinone concentration. For instance, 2,6-DMBQ and 2,6-DCBQ correspond to very different quinones in terms of structure and redox potential but give similar performances if used at 10 and 40 µmol L^{-1}, respectively.

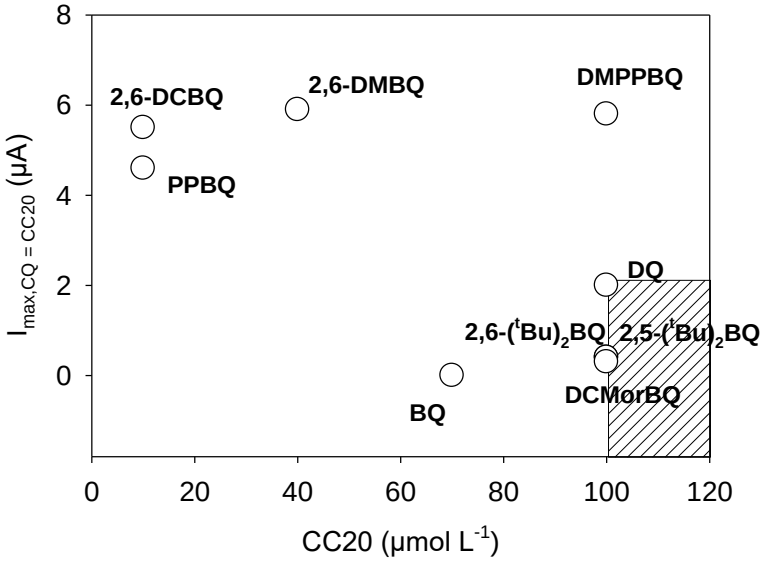

Figure 7B. Maximum stable photocurrents measured for a quinone concentration equal to CC20*, i.e. a quinone concentration range where incubation of quinones prevent 20% of cells to grow.*

Furthermore, the comparison of intrinsic oxiding ability of quinones (resulting from E° values and calculated by the ratio of the maximum stable photocurrent to the highest non toxic concentration) is well respected within non toxic quinone concentration ranges (**Figure 7C**). This confirms the role of quinone concentration and its side effect beyond toxic threshold concentrations.

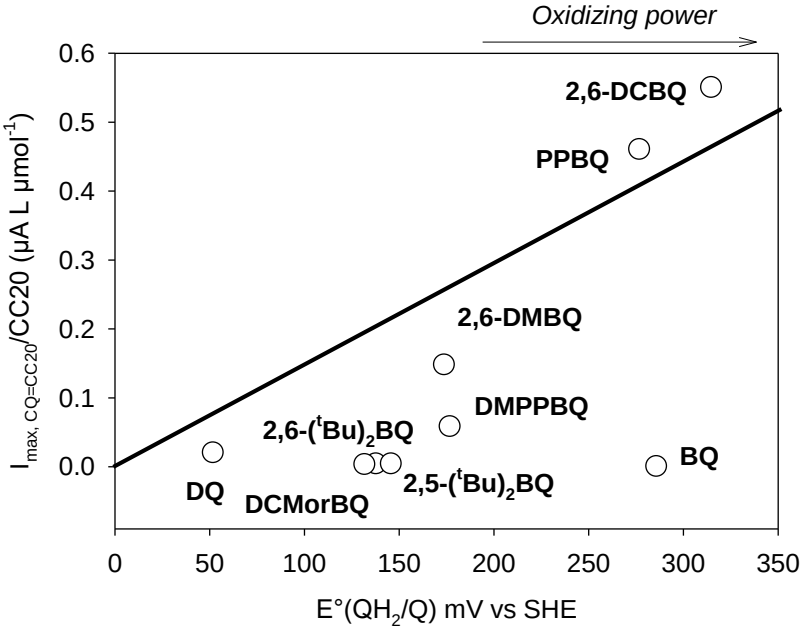

Figure 7C. Ratio of the maximum stable photocurrent (for CC20) to CC20 as a function of E°(QH$_2$/Q) values.

All in all, the choice of the appropriate quinone for rerouting photosynthetic electrons from *Chlamydomonas reinhardtii* algae relies on some different parameters that should require a whole compromise. 1/ The redox potential reflects the oxidizing properties of the quinone that may lead to high but unstable photocurrents. This can be tuned by the subtituents of the quinone and their electronic effects. 2/ The substituents of the quinone also play a role if considering that they can alter the organism by means of Michael additions. A non-hindered quinone like BQ seems to easily react with nucleophiles. Most importantly, steric hindrance and electronic effects can be interconnected since substituted quinones with electrodonating groups both prevent electron harvesting and side effects. 3/ Performances can be tuned by adjusting the quinone concentration. Below a toxic threshold concentration, no poisoning occurs so similar performances for two quinones can be reached by adjusting the quinone concentration close to its highest non toxic value.

Therefore, both quinone structure and concentration might finely tune their harvesting electron performances. Quinones both substituted with electron-donating and withdrawing groups thus appear as an interesting strategy. From this, DMPPBQ corresponds to significant stable performances without no concentration limits in the range of considered concentrations herein. As a result, DMPPBQ currently represents the best compromise with the best non-toxic concentration/photocurrent parameters couple.

4. Conclusion

In this article, we used a previously reported gold electrochemical device for investigating photosynthetic electron harvesting from algae suspensions by exogenous quinones. From this screening, we observed that the most rerouting quinones both lead to high but unstable maximum photocurrents. Beyond some now « usual » quinones (DCBQ, DMBQ, PPBQ), we have started investigating substituted and hindered quinones. Among them, DMPPBQ gave an interesting and stable photocurrent. However, taking into account the intrinsic performances of quinones and their toxicity makes the comparison more difficult to select the best candidate. Considering concentration ranges where the quinone is not toxic, DMPPBQ is consequently the best candidate and paves the way for future optimizations of the strategies involving quinones as redox mediators.

Acknowledgements

This work has been supported in part by CNRS (UMR 8640, UMR7141), Ecole Normale Supérieure, French Ministry of Research, Faculté des Sciences et Ingénierie - Sorbonne Université and the "Initiative d'Excellence" program from the French State (Grant "DYNAMO", ANR-11-LABX-0011-01). M.G.-C. thanks Institut Universitaire de France Fellowship Program.

REFERENCES

[1] X. G. Zhu, S. P. Long, D. R. Ort, *Annu. Rev. Plant Biol.* **2010**, *61*, 235-261.

[2] a) R. E. Blankenship, D. M. Tiede, J. Barber, G. W. Brudvig, G. Fleming, M. Ghirardi, M. R. Gunner, W. Junge, D. M. Kramer, A. Melis, T. A. Moore, C. C. Moser, D. G. Nocera, A. J. Nozik, D. R. Ort, W. W. Parson, R. C. Prince, R. T. Sayre, *Science* **2011**, *332*, 805-809; b) K. L. Saar, P. Bombelli, D. J. Lea-Smith, T. Call, E.-M. Aro, T. Mueller, C. J. Howe, T. P. J. Knowles, *Nat. Energy* **2018**, *3*, 75-81.

[3] a) M. Rosenbaum, Z. He, L. T. Angenent, *Curr. Opin. Biotechnol.* **2010**, *21*, 259-264; b) C. F. Meunier, X.-Y. Yang, J. C. Rooke, B.-L. Su, *ChemCatChem* **2011**, *3*, 476-488; c) A. Badura, T. Kothe, W. Schuhmann, M. Roegner, *Energy Environ. Sci.* **2011**, *4*, 3263-3274; d) D. P. B. T. B. Strik, R. A. Timmers, M. Helder, K. J. J. Steinbusch, H. V. M. Hamelers, C. J. N. Buisman, *Trends Biotechnol.* **2011**, *29*, 41-49; e) R. A. Voloshin, V. D. Kreslavski, S. K. Zharmukhamedov, V. S. Bedbenov, S. Ramakrishna, S. I. Allakhverdiev, *Biofuel Res. J.* **2015**, *2*, 227-235; f) N. Sekar, R. P. Ramasamy, *J. Photochem. Photobiol. C* **2015**, *22*, 19-33; g) A. J. McCormick, P. Bombelli, R. W. Bradley, R. Thorne, T. Wenzel, C. J. Howe, *Energy Environ. Sci.* **2015**, *8*, 1092-1109.

[4] a) J. Tschörtner, B. Lai, J. O. Krömer, *Front. Microbiol.* **2019**, *10*, article866; b) L. T. Wey, P. Bombelli, X. L. Chen, J. M. Lawrence, C. M. Rabideau, S. J. L. Rowden, J. Z. Zhang, C. J. Howe, *ChemElectroChem* **2019**, *6*, 5375-5386; c) F. Milano, A. Punzi, R. Ragni, M. Trotta, G. M. Farinola, *Adv. Funct. Mater.* **2019**, *29*; d) J. Z. Zhang, E. Reisner, *Nat. Rev. Chem.* **2020**, *4*, 6-21; e) M. Grattieri, K. Beaver, E. M. Gaffney, F. Y. Dong, S. D. Minteer, *Chem. Commun.* **2020**, *56*, 8553-8568.

[5] a) M. Kato, J. Z. Zhang, N. Paul, E. Reisner, *Chem. Soc. Rev.* **2014**, *43*, 6485-6497; b) R. Tel-Vered, I. Willner, *ChemElectroChem* **2014**, *1*, 1778-1797; c) J. O. Calkins, Y. Umasankar, H. O'Neill, R. P. Ramasamy, *Energy Environ. Sci.* **2013**, *6*, 1891-1900; d) M. Rasmussen, A. Shrier, S. D. Minteer, *Phys. Chem. Chem. Phys.* **2013**, *15*, 9062-9065; e) M. Rasmussen, S. D. Minteer, *Phys. Chem. Chem. Phys.* **2014**, *16*, 17327-17331; f) J. Z. Zhang, P. Bombelli, K. P. Sokol, A. Fantuzzi, A. W. Rutherford, C. J. Howe, E. Reisner, *J. Am. Chem. Soc.* **2018**, *140*, 6-9.

[6] a) K. Hasan, Y. Dilgin, S. C. Emek, M. Tavahodi, H.-E. Akerlund, P.-A. Albertsson, L. Gorton, *ChemElectroChem* **2014**, *1*, 131-139; b) E. R. Clifford, R. W. Bradley, L. T. Wey, J. M. Lawrence, X. L. Chen, C. J. Howe, J. Z. Zhang, *Chem. Sci.* **2021**, *12*, 3328-3338.

[7] S. Izawa, *Methods Enzymol.* **1980**, *69*, 413-434.

[8] M. Grattieri, Z. Rhodes, D. P. Hickey, K. Beaver, S. D. Minteer, *ACS Catal.* **2019**, *9*, 867-873.

[9] a) G. Longatte, H.-Y. Fu, O. Buriez, E. Labbe, F.-A. Wollman, C. Amatore, F. Rappaport, M. Guille-Collignon, F. Lemaitre, *Biophys. Chem.* **2015**, *205*, 1-8; b) G. Longatte, F. Rappaport, F. A. Wollman, M. Guille-Collignon, F. Lemaitre, *Photochem. Photobiol. Sci.* **2016**, *15*, 969-979.

[10] a) H.-Y. Fu, D. Picot, Y. Choquet, G. Longatte, A. Sayegh, J. Delacotte, M. Guille-Collignon, F. Lemaitre, F. Rappaport, F.-A. Wollman, *Nat. Commun.* **2017**, *8*; b) G. Longatte, F. Rappaport, F.-A. Wollman, M. Guille-Collignon, F. Lemaitre, *Electrochim. Acta* **2017**, *236*, 327-332.

[11] a) G. Longatte, M. Guille-Collignon, F. Lemaitre, *ChemPhysChem* **2017**, *18*, 2643-2650; b) L. Beauzamy, F. Lemaitre, J. Derr, *Sustain. Energ. Fuels* **2020**, *4*, 6004-6010.

[12] G. Longatte, A. Sayegh, J. Delacotte, F. Rappaport, F.-A. Wollman, M. Guille-Collignon, F. Lemaitre, *Chem. Sci.* **2018**, *9*, 8271-8281.

[13] A. Sayegh, G. Longatte, O. Buriez, F.-A. Wollman, M. Guille-Collignon, E. Labbe, J. Delacotte, F. Lemaitre, *Electrochim. Acta* **2019**, *304*, 465-473.

[14] a) A. R. Grossman, S. J. Karpowicz, M. Heinnickel, D. Dewez, B. Hamel, R. Dent, K. K. Niyogi, X. Johnson, J. Alric, F. A. Wollman, H. Y. Li, S. S. Merchant, *Photosynth. Res.* **2010**, *106*, 3-17; b) S. S. Merchant, S. E. Prochnik, O. Vallon, E. H. Harris, S. J. Karpowicz, G. B. Witman, A. Terry, A. Salamov, L. K. Fritz-Laylin, L. Marechal-Drouard, W. F. Marshall, L. H. Qu, D. R. Nelson, A. A. Sanderfoot, M. H. Spalding, V. V. Kapitonov, Q. H. Ren, P. Ferris, E. Lindquist, H. Shapiro, S. M. Lucas, J. Grimwood, J. Schmutz, P. Cardol, H. Cerutti, G. Chanfreau, C. L. Chen, V. Cognat, M. T. Croft, R. Dent, S. Dutcher, E. Fernandez, H. Fukuzawa, D. Gonzalez-Ballester, D. Gonzalez-Halphen, A. Hallmann, M. Hanikenne, M. Hippler, W. Inwood, K. Jabbari, M. Kalanon, R. Kuras, P. A. Lefebvre, S. D. Lemaire, A. V. Lobanov, M. Lohr, A. Manuell, I. Meir, L. Mets, M. Mittag, T. Mittelmeier, J. V. Moroney, J. Moseley, C. Napoli, A. M. Nedelcu, K. Niyogi, S. V. Novoselov, I. T. Paulsen, G. Pazour, S. Purton, J. P. Ral, D. M. Riano-Pachon, W. Riekhof, L. Rymarquis, M. Schroda, D. Stern, J. Umen, R. Willows, N. Wilson, S. L. Zimmer, J. Allmer, J. Balk, K. Bisova, C. J. Chen, M. Elias, K. Gendler, C. Hauser, M. R. Lamb, H. Ledford, J. C. Long, J. Minagawa, M. D. Page, J. M. Pan, W. Pootakham, S. Roje, A. Rose, E. Stahlberg, A. M. Terauchi, P. F. Yang, S. Ball, C. Bowler, C. L. Dieckmann, V. N. Gladyshev, P. Green, R. Jorgensen, S. Mayfield, B. Mueller-Roeber, S. Rajamani, R. T. Sayre, P. Brokstein, I. Dubchak, D. Goodstein, L. Hornick, Y. W. Huang, J. Jhaveri, Y. G. Luo, D. Martinez, W. C. A. Ngau, B. Otillar, A. Poliakov, A. Porter, L. Szajkowski, G. Werner, K. M. Zhou, I. V. Grigoriev, D. S. Rokhsar, A. R. Grossman, *Science* **2007**, *318*, 245-251; c) L. Houille-Vernes, F. Rappaport, F.-A. Wollman, J. Alric, X. Johnson, *Proc. Natl. Acad. Sci. USA* **2011**, *108*, 20820-20825.

[15] B. Rimbault, D. Esposito, D. Drapier, Y. Choquet, D. Stern, F. A. Wollman, *Mol. Gen. Genet.* **2000**, *264*, 486-491.

[16] a) D. Buckley, H. B. Henbest, P. Slade, *J. Chem. Soc.* **1957**, 4891-4900; b) V. K. Tandon, S. Kumar, N. N. Mishra, P. K. Shukla, *Eur. J. Med. Chem.* **2012**, *56*, 375-386.

[17] T. Kitagawa, J. Toyoda, K. Nakasuji, H. Yamamoto, I. Murata, *Chem. Lett.* **1990**, 897-900.

[18] S. Zhang, F. J. Song, D. B. Zhao, J. S. You, *Chem. Commun.* **2013**, *49*, 4558-4560.

[19] a) B. Genty, J. M. Briantais, N. R. Baker, *Biochim. Biophys. Acta* **1989**, *990*, 87-92; b) K. Maxwell, G. N. Johnson, *J. Exp. Bot.* **2000**, *51*, 659-668; c) E. H. Murchie, T. Lawson, *J. Exp. Bot.* **2013**, *64*, 3983-3998.

[20] a) K. K. Karukstis, S. C. Boegeman, J. A. Fruetel, S. M. Gruber, M. H. Terris, *Biochim. Biophys. Acta* **1987**, *891*, 256-264; b) K. K. Karukstis, S. M. Gruber, J. A. Fruetel, S. C. Boegeman, *Biochim. Biophys. Acta* **1988**, *932*, 84-90.

[21] a) A. Brunmark, E. Cadenas, *Chem. Biol. Interact.* **1988**, *68*, 273-298; b) X. W. Guo, H. Mayr, *J. Am. Chem. Soc.* **2014**, *136*, 11499-11512; c) T. J. Monks, R. P. Hanzlik, G. M. Cohen, D. Ross, D. G. Graham, *Toxicol. Appl. Pharmacol.* **1992**, *112*, 2-16.

[22] L. Beauzamy, J. Delacotte, B. Bailleul, K. Tanaka, S. Nakanishi, F. A. Wollman, F. Lemaitre, *Anal. Chem.* **2020**, *92*, 7532-7539.
[23] P. Mitchell, *Nature* **1961**, *191*, 144-&.
[24] A. Kanazawa, D. M. Kramer, *Proc. Natl. Acad. Sci. USA* **2002**, *99*, 12789-12794.
[25] H. T. Witt, *Biochim. Biophys. Acta* **1979**, *505*, 355-427.
[26] B. Bailleul, P. Cardol, C. Breyton, G. Finazzi, *Photosynth. Res.* **2010**, *106*, 179-189.
[27] P. Joliot, R. Delosme, *Biochim. Biophys. Acta* **1974**, *357*, 267-284.
[28] F. Buchert, B. Bailleul, T. Hisabori, *Biochim. Biophys. Acta Bioenerg.* **2017**, *1858*, 966-974.
[29] P. Joliot, A. Joliot, *Biochim. Biophys. Acta Bioenerg.* **2008**, *1777*, 676-683.
[30] a) G. A. Moore, L. Rossi, P. Nicotera, S. Orrenius, P. J. Obrien, *Arch. Biochem. Biophys.* **1987**, *259*, 283-295; b) P. J. Obrien, *Chem. Biol. Interact.* **1991**, *80*, 1-41; c) L. Rossi, G. A. Moore, S. Orrenius, P. J. Obrien, *Arch. Biochem. Biophys.* **1986**, *251*, 25-35.
[31] C. Preston, C. Critchley, *Photosynth. Res.* **1988**, *16*, 187-202.
[32] P. R. Rich, D. S. Bendall, *Biochim. Biophys. Acta* **1980**, *592*, 506-518.
[33] V. Petrouleas, B. A. Diner, *Biochim. Biophys. Acta* **1987**, *893*, 126-137.
[34] Y. Song, G. R. Buettner, *Free Radical Biol. Med.* **2010**, *49*, 919-962.
[35] W. Flaig, Beutelsp.H, H. Riemer, E. Kalke, *Justus Liebigs Ann. Chem.* **1969**, *719*, 96-111.
[36] K. Ollinger, G. D. Buffinton, L. Ernster, E. Cadenas, *Chem. Biol. Interact.* **1990**, *73*, 53-76.

SUPPORTING INFORMATION

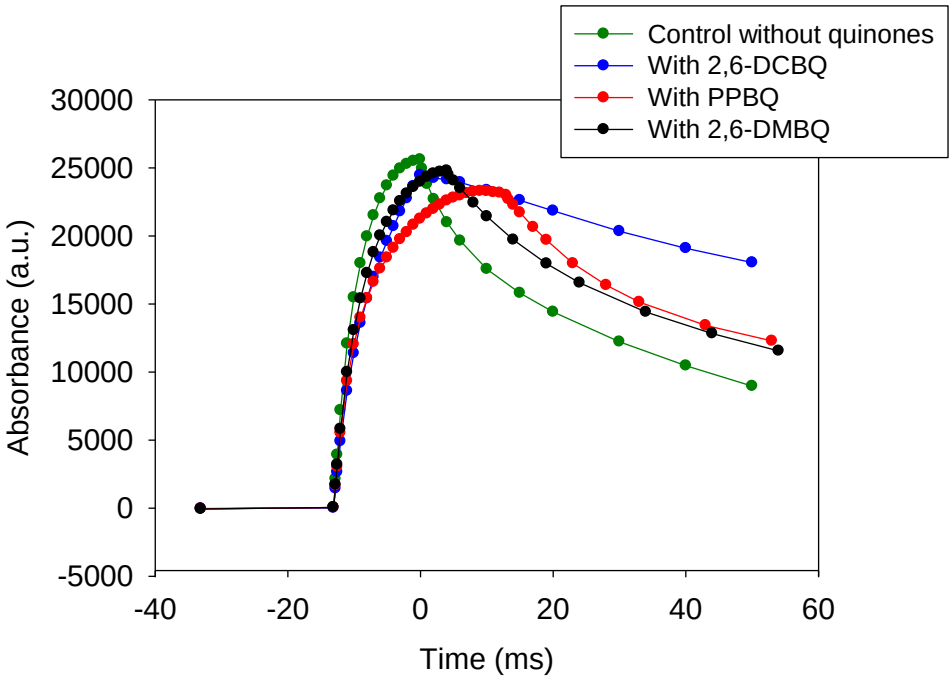

Figure S1. *Pulse-induced ECS kinetics for algae suspensions (2x10^{7} cells mL^{-1}) in the presence of various quinones (2,6-DMBQ, 2,6-DMBQ, PPBQ; concentration of 100 µmol L^{-1}) and in the control.*

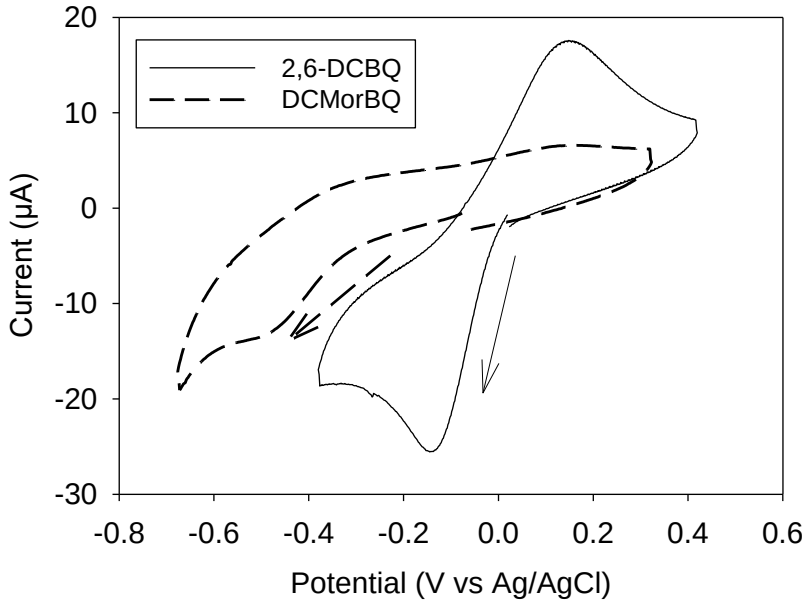

Figure S2. *Cyclic voltamogramms of DCMorBQ (dashed line) and 2,6-DCBQ (solid line) in tris-minimal medium (500 µmol L^{-1}) with the Au-ITO device used in the chronoamperometry experiments. v = 100 mV s^{-1}. The arrows indicate the initial scanning direction from the starting potential value.*

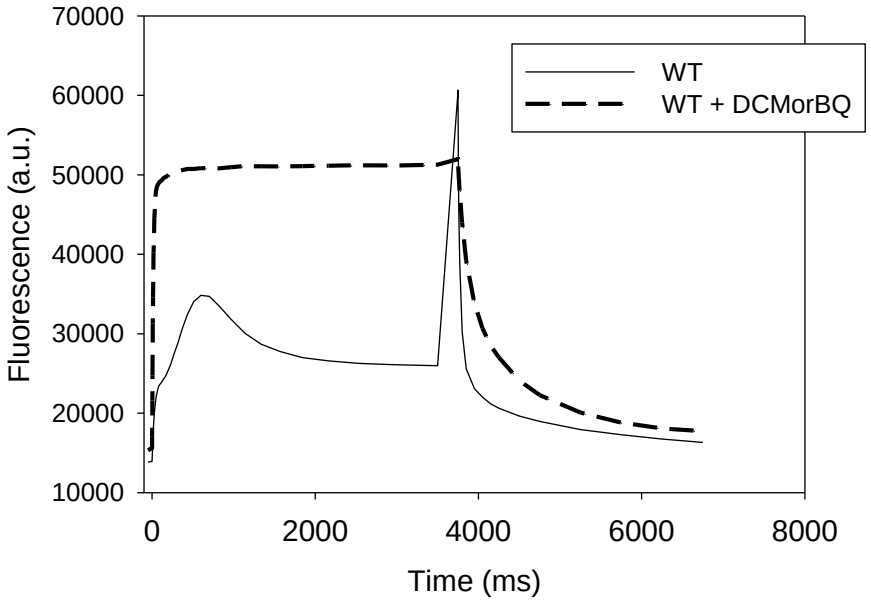

Figure S3. *Fluorescence induction curves for a suspension of Chlamydomonas reinhardtii (2x10^7 cells. mL^{-1}; solid line) with DCMorBQ (100 µmol L^{-1}). I° = 135 µmol photons m^2 s^{-1}.*

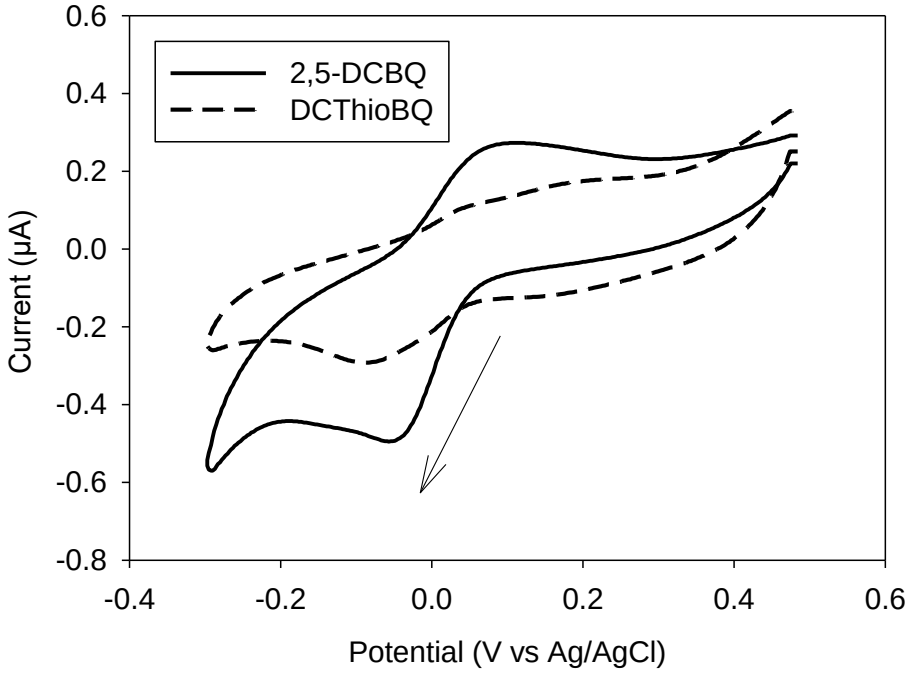

Figure S4*. Cyclic voltamogramms of DCThioBQ (dashed line) and 2,5-DCBQ (solid line) in tris-minimal medium (100 µmol L^{-1}) with the Au-ITO device used in the chronoamperometry experiments. v = 100 mV s^{-1}. The arrow indicates the initial scanning direction from the starting potential value.*

A)

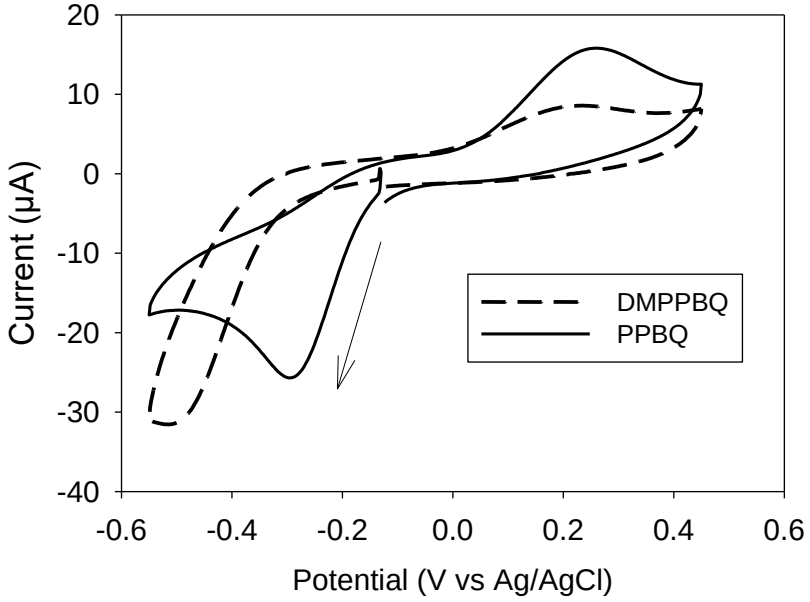

B)

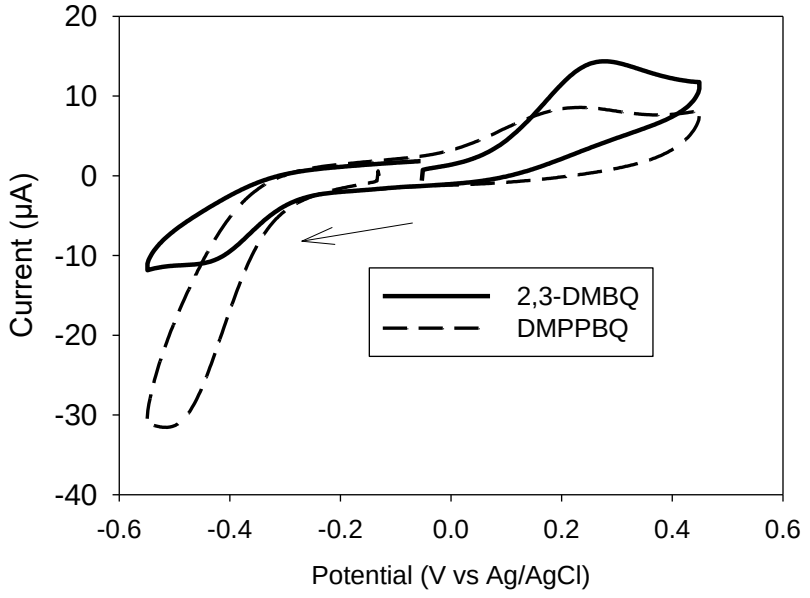

***Figure S5**. Cyclic voltamogramms of A) DMPPBQ (dashed line; 500 µmol L^{-1}) and PPBQ (solid line; 100 µmol L^{-1}) or B) DMPPBQ (dashed line; 500 µmol L^{-1}) and 2,3-DMBQ (solid line; 100 µmol L^{-1}) in tris-minimal medium with the Au-ITO device used in the chronoamperometry experiments. v = 100 mV s^{-1}. The arrows indicate the initial scanning direction from the starting potential value.*

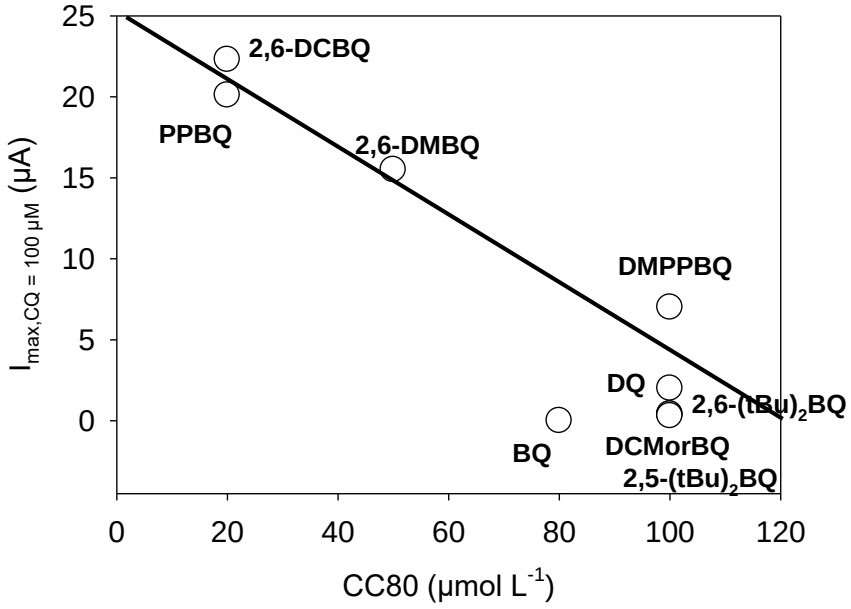

***Figure S6**. Maximum photocurrents recorded for a quinone concentration of 100 µmol L^{-1} as a function of CC80, i.e. a quinone concentration range where incubation of quinones prevent 80% of cells to grow*

Chapter Conclusion

This first article shows that the behavior of quinones towards microalgae is rather complex. While most quinones act as redox mediators, as they are reduced by the photosynthetic chain, the structure-activity relationship is not easy to determine.

It is now clear (except for BQ) that maximum current production and/or the PSII acceptor property is related to the redox potential of quinones (whether QH_2/Q or $Q^{\cdot-}/Q$ couples are considered). All the results for numerous quinones are summarized *in Figure 1*.

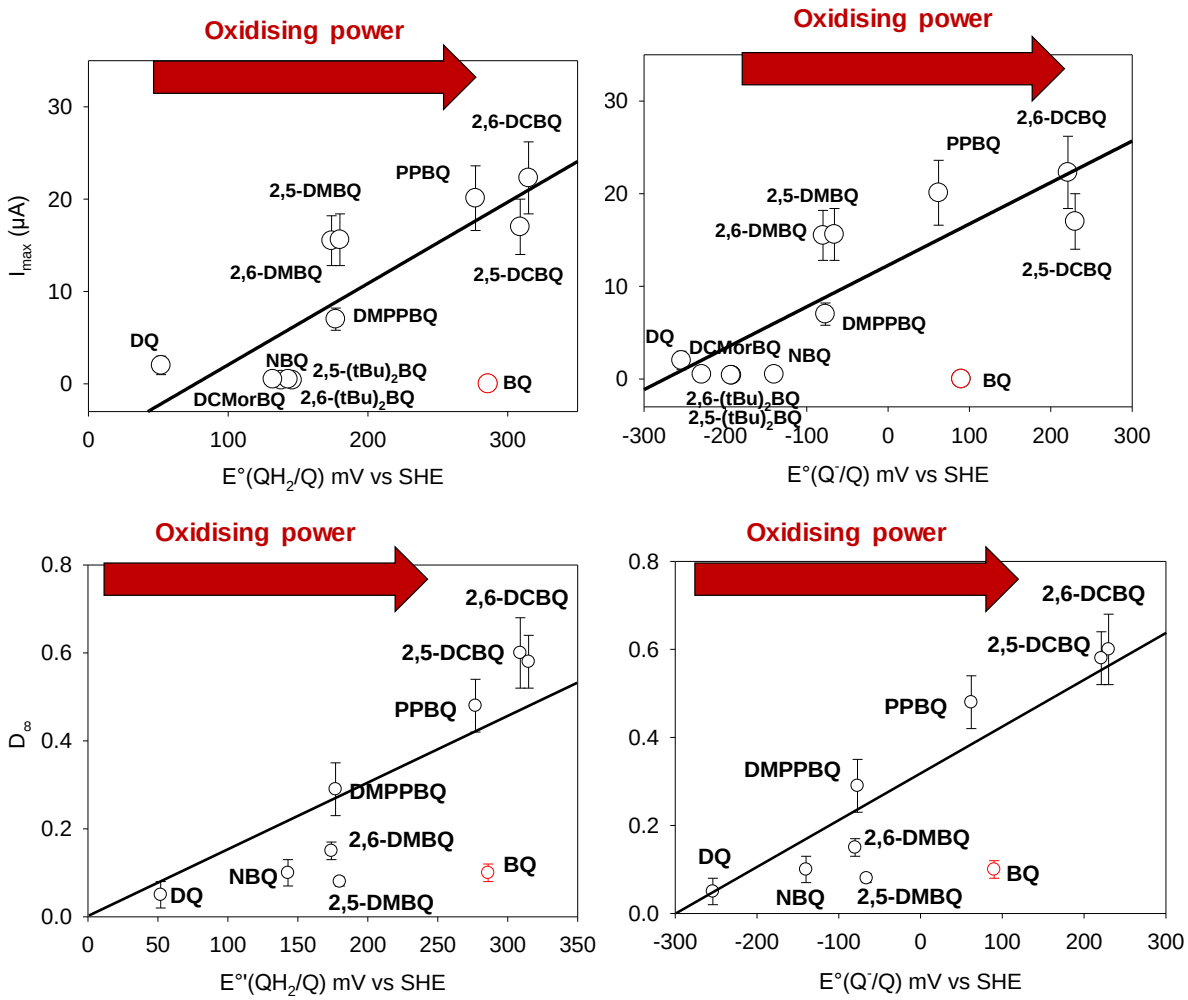

Figure 1. Summary of the main results mentionned in article n°1 *: $I_{max} = f(E°)$; $D_\infty = f(E°)$ for different quinones.*

The poisoning effect (current decay, antiproliferative effect) also seems to lead to clear trends. First of all, the lower the duration and stability, the higher the maximum photocurrent.

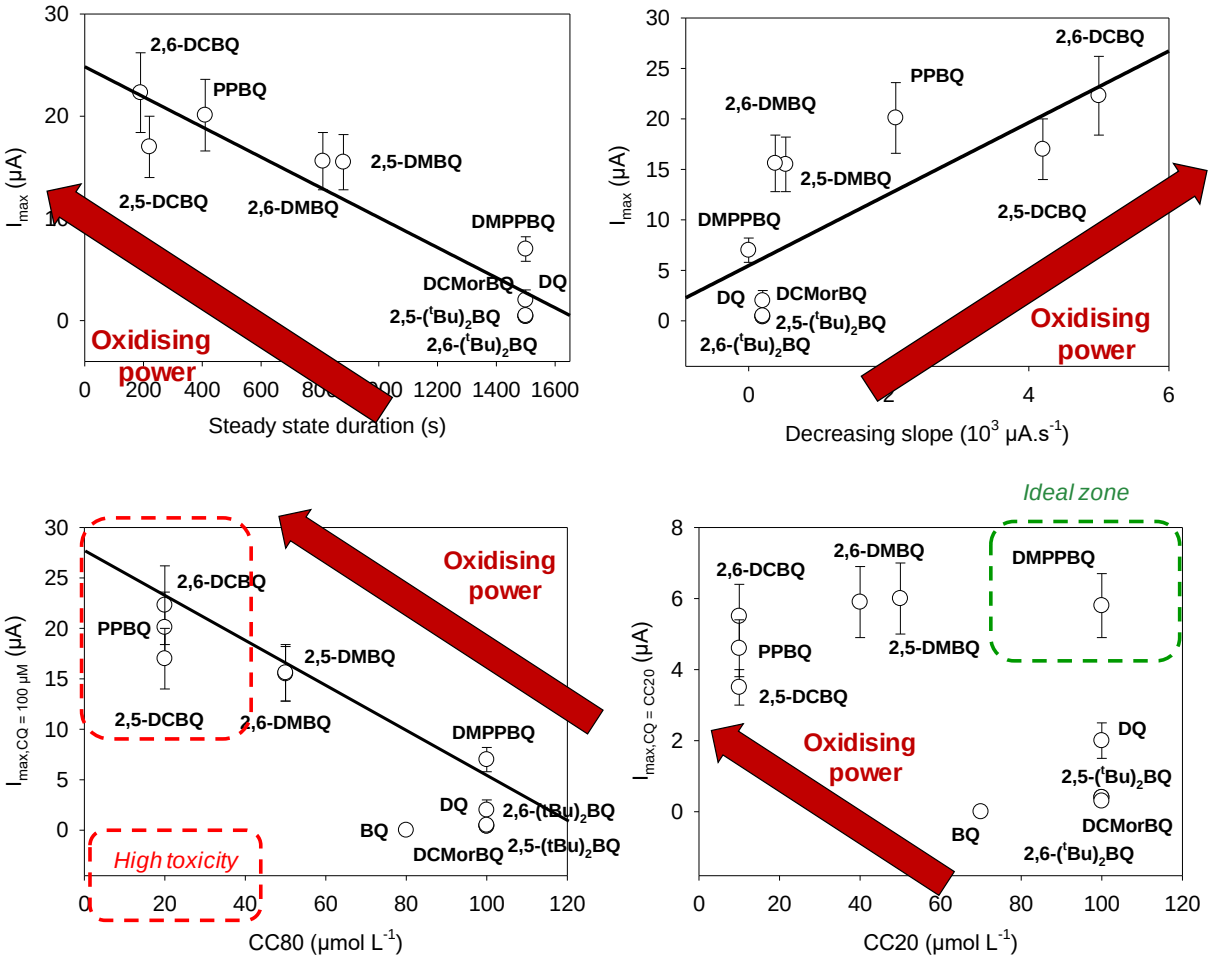

Figure 2. Summary of the main results mentionned in article n°1*. Top: I_{max} = f(steady state duration) ; I_{max} = f(decrease in current). Bottom: I_{max} = f(CC80) with CC80 the (threshold where 20% of cells still grow); I_{max} = f(CC20) with CC20 the (threshold where 80% of cells still grow). I_{max} was measured for different quinones at 100 µmol. L^{-1} except for the bottom right graph where I_{max} was measured for CC20.*

In other words, the most rerouting quinones (i.e. with a high E° value and a corresponding increase in I_{max}) lead to the most transient behaviours (current current stability decreases in terms of plateau length and decay rate). Second, cell proliferation studies point in the same direction since a toxic effect is observed and more significant for the most oxiding quinones.

Despite the fact that the poisoning mechanism remains unclear, these results suggest that the ideal quinone (diverting + low poisoning) may only be a compromise, and that the main criterion should therefore be to find a quinone with a "moderate" E°. Finally, the comparison of maximum photocurrent values for the same stability period (i.e. for the highest non-toxic concentration) is highly interesting. On the one hand, it confirms the previous trend. On the other hand, it highlights a levelling of performance according to the "E°" criterion. In other words, a diverting quinone at low concentration (e.g. 2,6-DCBQ) can have the same effect (in terms of photocurrent magnitude and stability) as a less diverting quinone at higher concentration (e.g. 2,6-DMBQ). However, this

"homothetic " effect should lead to the same maximum current value for all quinones (see *Figure 2*). This is not the case, and shows that simple "E°" is not the only factor to consider, even if it is essential.

Steric hindrance could be an important issue. A good example is DMPPBQ (a trisubstituted molecule with a mixture of electron-withdrawing and electron-donating groups). This molecule has an intermediate E° which is close to that of DMBQs (which are less hindered), but provides better performance (maximum current, stability, CC80). Unfortunately, the number of substituents of a quinone also has a major impact on the E° value.

The fact that E° is a key criterion, and that steric hindrance may be a factor, could suggest that the side effects of quinones are due to electrophilic quinone reactivity in parallel with electron extraction. In principle, reasoning in terms of E° could rule out questions relating to oxidative stress. Indeed, in the case of ROS production, the reduced species (Q^- or QH_2) would interact with O_2. In such a context, it would be quinones with low E° values (i.e. with high reducing power) that would lead to higher poisoning through superoxide anion $O_2^{\bullet-}$ production. The results show that this would not be the case. However, this mechanism cannot be definitively discarded, because even if superoxide anion production is thermodynamically not favored with strongly oxidizing quinones. This does not mean that superoxide anion would not be formed. From a kinetic point of view, intermediate E° values (DMBQs for example) are still enough to lead to a relatively high $O_2^{\bullet-}$ formation rate constant (~10 $mol^{-1}.L.s^{-1}$) and an equilibrium constant that remains moderate (~10^{-2}).

All in all, the current indicators are still too broad to fully understand the interactions between quinones and the photosynthetic chain. As also mentionned in the article, complementary parameters (ATP synthase, PSII yield) may offer a better overview of the quinone effects. Particularly, the detailed activity of ATPsynthase and interactions/connections with the respiratory chain represent new areas for investigation. Similarly, changes in PSI activity also need to be better understood. While the ways of studying the respiratory chain or ATPsynthase are reasonably well established, it is necessary to focus on the issues and biases involved in PSI-related measurements.

Chapter III

Article n°2 - How to Probe Photosystem I Activity? Critical Reappraisal of Methods to Measure Photosystem I Activity

Suzanne Ferté-Vogel, Marc Arderiu Romero, Ginga Shimakawa, Bernard Genty, Benjamin Bailleul

Preliminary Section

To investigate photosynthesis, the most powerful and widely used approach consists in measuring photosystem II activity by the means of chlorophyll fluorescence. It can sometimes be important to have robust measurement of PSI activitie to calculate the electron transfer through photosystem I, visualize the accumulation of stromal reductants downhill PSI or to investigate PSI photoinhibition or PSI inhibition by various factors. In the frame of my PhD, it was important not to restrain myself to PSII measurements but instead to have a comprehensive view of the photosynthetic electron transfer chain. I got involved in a critical reappraisal of the PSI measurements used in the last quarter of century. In this chapter, I will present the work I participated to which aimed to determine the best way to investigate PSI activity, using absorption difference spectroscopy. By comparing two methods based on absorption difference spectroscopy (Electro-Chromic Shift and P_{700} redox changes) to measure the PSI acitivity, we were aiming to find the most accurate and robust approach to investigate PSI yields. This work was led by a former PhD student at IBPC, Suzanne Ferté. My contribution was to perform additional experiments (started during my M2 internship and ended at the beginning of my PhD) and participating in the interpretation of the resuts and in the writing of the manuscript.

Abstract

Photosystem I (PSI) works in series with photosystem II to convert light into chemical energy in oxygenic photosynthesis. Accurate assessments of PSI activity are detrimental to the understanding of most modes of photosynthetic regulation, especially the cyclic electron flow round PSI. The most widely used observable to study PSI activity is the absorption change that occurs with the oxidation-reduction of P*700,* the special pair of PSI reaction centre. Here, we develop a model linking the PSI yield to the redox state of P*700* before and after a multiple turnover saturating light pulse. The PSI yield appears to be equal to the amount of PSI oxidized during the pulse divided by the total amount of PSI oxidized at the end of the pulse. In the green alga *C. reinhardtii*, estimates from this method agree with results obtained by an alternative method based on the electro-chromic shift of photosynthetic pigments. In contrast, currents modes of calculation systematically underestimate PSI yield -by as much as tenfold in our dataset- because they don't take into consideration the over-reduction of the PSI acceptor side by the multiple turnover pulse itself. Notably, the new calculation does not require the normalization by the signal corresponding to fully oxidized P700, which is problematic especially in plants. It should provide a more robust way to study PSI activity, cyclic electron flow and the regulation of the photochemical phase of photosynthesis. We also propose a simple correction to reassess published data.

Abbreviations list

ATP, adenosine triphosphate; CEF, cyclic electron flow around PSI; cyt b*6f*, cytochrome b_6f; DBMIB, dibromo-6-isopropyl-3-methyl-1,4-benzoquinone; DCMU, 3-(3,4-dichlorophenyl)-1,1-dimethylurea; ECS, electro-chromic shift; HA, hydroxylamine; LEF, linear electron flow; MV, methyl viologen; NADPH, nicotinamide adenine dinucleotide phosphate; pmf, proton motive force; PSI, photosystem I; PSII, photosystem II; Y(I), PSI yield; $Y(I)_{ECS}$, PSI yield based on ECS; $Y(I)_{P700}$, PSI yield based on P_{700} pulse method; Y(NA), PSI acceptor-side limitation; $Y(NA)_{P700}$, PSI acceptor-side limitation based on P_{700} pulse method; Y(ND), PSI donor-side limitation.

1. Introduction

In oxygenic photosynthesis, the photosynthetic electron transfer chain comprises two photosystems. Photosystem II (PSII) and photosystem I (PSI) work in series to allow linear transfer of electrons generated from the oxidation of water in PSII to reduce $NADP^+$ into nicotinamide adenine dinucleotide phosphate (NADPH) downstream of PSI. The electron transfer from PSII to PSI involves the plastoquinone pool diffusing in the thylakoid membrane, the lumen-soluble plastocyanins (or cytochrome c_6) and a plastoquinol-plastocyanin oxidoreductase called cytochrome b_6f (cyt b_6f). The electron transfer is coupled to the translocation of protons across the thylakoid membrane, giving rise to an electrochemical proton gradient or proton motive force (pmf). The pmf comprises both an electric (Δψ) and an osmotic (ΔpH) component and fuels the synthesis of adenosine triphosphate (ATP) by the CF1-F0 ATP synthase. The methods used to measure the linear electron flow from water to NADPH mostly rely on measurements of PSII because it is the most convenient photosynthetic complex to probe. The PSII chlorophyll fluorescence yield is high enough to allow the energy conversion in PSII to be calculated (Kautsky et al., 1960; Duysens, 1963; reviewed in Baker, 2008). The oxidation of water, the final electron donor, occurs in the oxygen evolving complex of PSII so it is also possible to measure O_2 evolution as a powerful alternative assay. Fluorescence and oxygen based methodologies have been cross-validated (Genty et al., 1992) and are now well established and widely used by the community of photosynthesis researchers. However, measuring PSII activity alone is not sufficient to view the complexity of photosynthetic function and regulatory flexibility. For instance, in addition to the linear electron flow involving the two photosystems, several modes of alternative electron flow can play an important role in providing some flexibility in terms of ATP/NADPH ratios (Eberhard et al., 2008). In cyanobacteria, terrestrial plants and green algae, it has been shown that electron transfer from reduced PSI acceptors back to the inter-photosystem chain at the plastoquinone pool or at the b_6f level can occur, allowing PSI to operate independently from PSII (Arnon et al., 1958; reviewed thoroughly in Bendall and Manasse, 1995, and in Shikanai, 2007). This gives rise to a cyclic electron flow (CEF) around PSI, which is thought to play a crucial role in photosynthetic regulation by increasing the ATP/NADPH balance (Allen, 2002). Since CEF does not produce any quantifiable net product, the most accurate way to measure CEF in physiological conditions is to compare PSII and PSI activities (Fan et al., 2016). The CEF participates, together with other alternative electron flows, in the protection of both photosystems under excess light by regulating cyt b_6f and PSII activities (Endo and Asada, 2008; Chaux et al., 2015). The over-reduction of PSI acceptors when the Calvin-Benson-Bassham cycle performs poorly (as in conditions like chilling or low CO_2 availability) results in severe photo-inhibition of PSI (Havaux and Davaud, 1994; Terashima et al., 1994; reviewed in Sonoike, 2011 and in Scheller and Haldrup, 2005) through the oxidative destruction of the iron-sulfur clusters (Sonoike et al., 1995). Photosynthetic organisms can respond to this harmful situation by slowing down cyt b_6f activity, through "photosynthetic control" (Rumberg and Siggel, 1969; Foyer et al, 2012; Joliot and Johnson, 2011). To fully understand the complexity of photosynthetic regulation by investigating this important process requires measurements of the PSI energy conversion efficiency, and of its acceptor-side and donor-side limitations, i.e. the loss of PSI efficiency due to lack of PSI acceptors or donors, respectively. However, measurements of PSI activity are not as straightforward as for PSII.

PSI is a protein complex embedded in the thylakoid membrane which catalyzes the electron transfer from the special pair P_{700} to the PSI [4Fe-4S] centers and to the stromal soluble electron carrier ferredoxin (Golbeck, 2007). Two PSI cofactors are involved in the first stable charge separation: P_{700} and the first stable acceptor, called A hereafter, which corresponds to the PSI iron-suflur proteins (Malkin and Bearden, 1971; Oh-Oka et al., 1991). To perform a stable charge separation, defined here as transferring an electron from P_{700} to A, a PSI center needs P_{700} to be reduced and A to be oxidized. These [P_{700} A] PSI centers are thus considered to be open as they are ready to perform a charge separation as soon as the next photon is absorbed. Because of the high maximal quantum yield of PSI, close to 1 (Nelson, 2009), the fraction of open PSI centers can be considered as the quantum yield of PSI. In 1972, Hiyama and Ke showed *in vitro* that the absorption spectrum of P_{700} changes depending on its redox state (Hiyama and Ke, 1972). The same is true *in vivo* and absorption variation at 705 and 820 nm are mainly due to P_{700} redox state changes (Harbinson and Woodward, 1987). Historically, this property has been used to differentiate between the fractions of PSI with a reduced or oxidized P_{700} that were originally considered as open and closed centers, respectively (Harbinson et al., 1989; Harbinson and Foyer, 1991). Indeed, centers with oxidized P_{700} are closed as they will not be able to perform a charge separation. They are denoted [P_{700}^+ A] and called donor-side limited centers because the oxidation of P_{700} in the light reflects a bottleneck in the electron transfer upstream of PSI (on the donor side).

In 1994, Klughammer and Schreiber acknowledged that the fraction of PSI with a reduced P_{700} overestimates the fraction of open PSI in conditions of over-reduction of the acceptor-side of PSI. Indeed, the [P_{700} A^-] centers are closed despite a reduced P_{700}. Those centers are called acceptor-side limited centers because the reduction of both cofactors in the light reflects a bottleneck in the electron transfer downstream of PSI (on the acceptor side). The difficulty stems from the distinction between open [P_{700} A] and acceptor-side limited [P_{700} A^-] centers ([P_{700}^+ A^-] centers, rare and usually neglected, would be considered as donor-side limited in this view). Since acceptor-side limited centers cannot perform charge separation and oxidize P_{700} on the next photon, an advanced method was proposed where open centers were considered as centers with P_{700} reduced but photo-oxidizable upon a multi-turnover saturating light pulse (Klughammer and Schreiber, 1994). The authors of the original paper did not provide a theoretical framework supporting their mode of calculation of PSI yield and acknowledged that since "an alternative, proven method for ΦI determination is lacking, only indirect evidence for the correctness and general applicability of the proposed approach can presently be given" (Klughammer and Schreiber, 1994). Despite this, the P_{700} pulse method has been widely used to investigate many aspects of photosynthesis, e.g. PSI photo-inhibition (e.g. Brestic et al., 2015; Zivcak et al., 2015), photosynthetic control (e.g. Weis et al., 1987), ferredoxin oxidation pathways (e.g. Voss et al., 2008), responses to cold temperatures (e.g. Suzuki et al., 2011; Wang et al., 2013) or cyclic electron flow (e.g. Laisk et al., 2010; Talts et al., 2007; DalCorso et al., 2008; Kono et al., 2014; Kou et al., 2015). Commercial measurement devices have been developed on this basis, like the Dual-Pam distributed by Walz (Germany) and the P_{700} pulse method has become the standard methodology to probe PSI activity.

In this work, we propose a simple model for the PSI redox changes induced by muti-turnover light pulses which expresses the PSI yield (the fraction of PSI open centers) as the amount of PSI oxidized

during the pulse divided by the total amount of PSI oxidized at the end of the pulse. We test our model by comparing its outputs to PSI yields calculated based on the stable electric field (stabilized charge separation) induced by a single PSI turnover flash and measured by the Electro-Chromic Shift (ECS) of photosynthetic pigments.

2. Methods

2.1. Strains, growth and sampling

Chlamydomonas reinhardtii wild type laboratory strain T222 and the pc3.1$^+$ mutant strain were obtained from the Chlamystation (http://chlamystation.free.fr/). *Arabidopsis thaliana* Col-0 was a kind gift from Dr Fredy Barneche and Menuu Singla (Ecole Normale Supérieure, Paris, France). The dinoflagellate *Amphidinium carterae* (RCC1522) was obtained from the Roscoff Culture Collection (http://roscoff-culture-collection.org/). Chlamydomonas cells were grown in Tris-acetate-phosphate (TAP) medium (Harris, 2009) at 25°C under continuous light provided by white LEDs and were harvested when the cell density was between 2 and 6 million cells per mL. The light irradiance was 30 µmol photons m^{-2} s^{-1} for the wild type and 10 µmol photons m^{-2} s^{-1} for the light-sensitive pc3.1$^+$. *A. thaliana* was grown at 22°C with an 8-hr light/16-hr dark photoperiod at a light intensity of 100 µmol photons m^{-2} s^{-1}. Leaves were harvested at the rosette stage (5 weeks after germination). *Am. carterae* was grown in enriched seawater/artificial water (Berges et al., 2001) at 19°C under a 12-hr photoperiod at a light intensity of 30 µmol photons m^{-2} s^{-1} using fluorescent tubes. Cells were harvested in the exponential growth phase when the cell density was between 80 000 and 200 000 cells per mL.

For photosynthetic measurements, liquid cultures of *C. reinhardtii* or *Am. carterae* were concentrated by centrifugation (4 min at 3500 rpm) and resuspended in their supernatant to a density of ~10^7 or 10^6 cells mL^{-1}, respectively. Ficoll® was added to prevent drifts in the absorption measurements due to sedimentation of the cells. Concentrated samples were then stirred at 350 rpm under 10 µmol photons m^{-2} s^{-1} white light for at least 30 min before starting measurements.

2.2. *Inhibitors/chemicals*

Hydroxylamine (HA), (3,4-dichlorophenyl) -1,1-dimethylurea (DCMU), methylviologen (MV), dibromo-6-isopropyl-3-methyl-1,4-benzoquinone (DBMIB), glucose and glucose oxidase were obtained from Sigma Aldrich. DCMU and DBMIB were diluted in ethanol. HA, MV, glucose and glucose oxidase were diluted in distilled water. PSII was inhibited with 10 µM DCMU and 100 to 500 µM HA (for each experiment, the minimal concentration to reach maximal fluorescence in the dark was determined and used). When necessary, anoxic conditions were induced by addition of 20 mM glucose and glucose oxidase (~280 U mL^{-1}) in brimful, tightly closed cuvettes. MV at a concentration of 4 mM was added to the microalgae sample or infiltrated into leaves 4 min before measurements to allow it to fully infiltrate the stroma. To compare leaf samples with and without MV, we used two pieces of the same leaf, sampled symmetrically across the leaf axis. MV did not seem to release acceptor-side limitation in the dinoflagellate *Am. carterae.*

2.3. In vivo spectroscopy

All spectroscopic measurements were performed using a Joliot Type Spectrophotometer (JTS-10, Biologic, Grenoble, France) so fluorescence and absorption difference were measured on the same sample. The actinic continuous light and the saturating pulse (5000 µmol photons m^{-2} s^{-1}, corresponding to ~2200 photons per PSI per second) were provided by orange LEDs (630 nm) and the saturating laser flash was provided by a dye laser (690 nm) pumped with a Nd: YAG laser (6 ns duration, 532 nm).

For fluorescence, detection pulses were provided by a white LED with a blue filter (470 nm). Reference and measuring photodiodes were protected from actinic light with a BG39 Schott filter (Mainz, Germany) and an LPF650+RG665 Schott filter, respectively. PSII maximal quantum yield was calculated as Fv/Fm = (Fm – F_0)/Fm, where F_0 is the fluorescence level in the dark-adapted (for 1 min) sample and Fm is the maximal fluorescence levels obtained after a saturating light pulse in dark-adapted sample. These measurements were performed to verify that after DCMU and HA treatment, all PSII centers were closed, i.e. Fv/Fm = 0.

To correct for artefacts, all data shown for absorption change measurements (both P_{700} and ECS) are the differences between the measurement in the presence of the actinic light (laser flash, background actinic light or saturating pulse) and the measurement in the absence of actinic light. P_{700} redox changes were measured as the difference in the absorbance changes at 705 and 735 nm to correct for contributions from scattering and plastocyanin absorption changes. For leaves, the 810-870 nm region is preferred for probing P_{700} to minimize leaf absorption and artefacts due to changes in the fluorescence yields. This was not the case for the protocol used here as we used DCMU and HA to fully close all PSII centers. In these conditions, we found that 705-735 nm and 810-870 nm gave similar results (not shown) but we chose the near far-red region for higher signal-to-noise ratios. The light-detecting diodes were protected from scattered actinic light with an RG695 Schott filter (Mainz, Germany). We calculated $Y(I)_{P700}$, $Y(NA)_{P700}$ and Y(ND) as described in Klughammer and Schreiber (1994). To normalize the output, we realized that the maximal absorption change corresponding to the oxidation of 100% of P_{700} was not reached with common protocols described in the literature (i.e. using far-red light or a saturating DCMU concentration). The absorption change corresponding to 100% P_{700} oxidation was reached by adding a saturating laser flash to a few ms of a saturating pulse in the presence of the cyt b_6f inhibitor DBMIB (1 µM) and the PSI electron acceptor MV.

Electro-chromic shift (ECS) signals were measured as the difference in the absorbance changes at 520 and 546 nm for *C. reinhardtii* and *A. thaliana* or at 563 nm for *Am. carterae*. These wavelengths were chosen to eliminate absorption changes related to c-type cytochromes. The detection wavelengths were provided by a white LED with appropriate interferential filters (10 nm full width at half-maximum, Edmund Optics). The measuring and reference photodiodes were protected from scattered and transmitted actinic light by a BG39 Schott filter (Mainz, Germany). All ECS data were normalized to the ECS increase produced by a single-turnover saturating flash in the presence of DCMU and HA in dark-adapted cells, and results are therefore expressed as charge separation per PSI. The fraction of open PSI centers, $Y(I)_{ECS}$, was calculated as the ratio between the ECS increase induced by the saturating flash in the condition of interest and that in dark-adapted samples. $Y(NA)_{ECS}$ was calculated by subtracting Y(ND), estimated from P700 measurements, from $Y(I)_{ECS}$.

3. Results

Let us consider a situation where the fractions of open centers, donor-side limited and acceptor-side limited centers are $[P_{700}\ A]$, $[P_{700}^{+}\ A]$ and $[P_{700}\ A^{-}]$ respectively. Again, if $[P_{700}^{+}\ A^{-}]$ centers are present, they will be considered like $[P_{700}^{+}\ A]$ because the P700 observable cannot distinguish them. By convention:

$$[P_{700}\ A] + [P_{700}^{+}\ A] + [P_{700}\ A^{-}] = 1 \qquad \text{(Equation 1)}$$

Let us consider a multiple turnover pulse, lasting few ms and intense enough to close all PSI, i.e. the ratioof open centers at the end of the pulse, noted $[P_{700}\ A]_p$, is null. It follows that, if we call $[P_{700}^{+}\ A]_p$ and $[P_{700}\ A^{-}]_p$ the fractions of donor-side limited and acceptor-side limited centers at the end of the pulse,

$$[P_{700}^{+}\ A]_p + [P_{700}\ A^{-}]_p = 1 \qquad \text{(Equation 2)}$$

In equation 1, $[P_{700}^{+}\ A]$ can be measured through P700 redox state and only $[P_{700}\ A^{-}]$ is unknown. It will be useful to introduce the ratio $[P_{700}\ A^{-}]/[P_{700}\ A^{-}]_p$ by combining the equations (1) and (2):

$$[P_{700}\ A] = 1- [P_{700}^{+}\ A] - [P_{700}\ A^{-}]/\ [P_{700}\ A^{-}]_p.(1- [P_{700}^{+}\ A]_p) \qquad \text{(Equation 3)}$$

In the hypothesis chosen by Klughammer and Schreiber, $[P_{700}\ A^{-}]_p = [P_{700}\ A^{-}]$ which gives: $[P_{700}\ A] = [P_{700}^{+}\ A]_p - [P_{700}^{+}\ A]$. Experimentaly, this will be measured as (Pm'-P)/(Pm-P0) (see Figure 1C). In the previous method by Harbinson & Foyer, the acceptor side limitation was not taken into account; therefore, equation 1 gives $[P_{700}\ A] = 1 - [P_{700}^{+}\ A]$ which can be assessed experimentaly as (Pm-P)/(Pm-P0) (see Figure 1). Instead, we will consider the possibility that the acceptor side increases during the pulse and will develop a simple kinetic model to evaluate the increase in acceptor side limitation, i.e. $[P_{700}\ A^{-}]/\ [P_{700}\ A^{-}]_p$.

In our model, acceptor side limitation increases as much as the donor side limitation does during the pulse, i.e. $[P_{700}\ A^{-}]/\ [P_{700}\ A^{-}]_p = [P_{700}^{+}\ A]/[P_{700}^{+}\ A]_p$, which, once replaced in equation 3, leads to:

$$[P_{700}\ A] = 1- [P_{700}^{+}\ A] - [P_{700}^{+}\ A]/\ [P_{700}^{+}\ A]_p.(1- [P_{700}^{+}\ A]_p) = ([P_{700}^{+}\ A]_p - [P_{700}^{+}\ A])/[P_{700}^{+}\ A]_p \qquad \text{(Equation 4)}$$

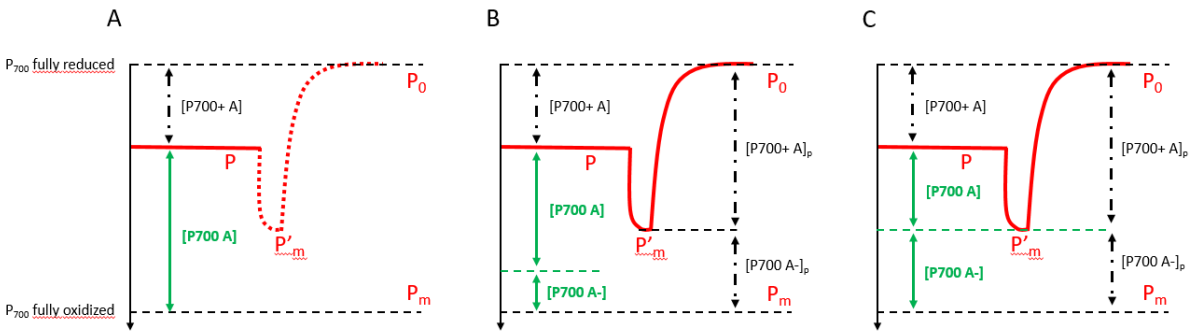

Figure 1 Comparison of 3 methods to quantify PSI yield. *In all panels, the red curves represent the P700 redox changes starting from a given stationary light condition (P). After an extra oxidation of P700 after a saturating pulse (P'm), a relaxation in the dark allows the full reduction of P700 (P0). The full oxidation of P700 (Pm) is obtained in the light in conditions of PSII inhibition (see Methods). A: Based on (Harbinson & Foyer, 1989), the proportion of open PSI centers [P700 A] is calculated as (Pm – P)/Pm. B: Based on the model described in this work, [P700 A] is calculated as (P'm – P)/(P'm-P0). C: Based on the method described in (Klughammer & Schreiber, 1994), [P700 A] is calculated as (P'm – P)/(Pm-P0).*

In our model, the fraction of open PSI centers is calculated from the experimental data as (Pm'-P)/(Pm'-P0). In order to test experimentally our model as well as the ones proposed previously, we looked for an alternative method. We first wondered why not using a single turnover flash instead of a multiple turnover pulse? The single turnover flash, which can be produced with a laser, is routinely favored in photophysiology studies (e.g. Junesch and Graber, 1987; Delosme et al., 1994). It would have the advantage of allowing all open PSI to perform one - and only one - charge separation without perturbing the state of the acceptor side. Unfortunately, the P_{700} oxidation-reduction kinetics following a laser flash cannot easily discriminate an open center from an acceptor-side limited center. Indeed, in both cases, a charge separation will occur in the sub-microsecond range and will be followed by a fast rereduction of P_{700}^+. Indeed, the re-reduction of P_{700}^+ by plastocyanin or other secondary donors like cytochrome c_6 is fast ($t_{1/2}$ ≈ 5 µs if the secondary donor is already fixed, otherwise $t_{1/2}$ ≈ 200 µs, Hippler et al., 1997) and has similar kinetics as the charge recombination between P_{700}^+ and Fx^-, when A (the pool of iron sulfur clusters) is reduced (Warren et al., 1990). P_{700} is therefore unsuited as a variable for distinguishing between open centers and acceptor-side limited centers after a single turnover flash. However, there is at least one clear difference between a charge separation stabilized by the electron transfer from secondary donors to P_{700} and a charge separation followed by a charge recombination: in the first case, a positive charge remains in the lumen, but in the second case the charge is cancelled. The electric field across the thylakoid can be probed *in vivo* by monitoring the electro-chromic shift (ECS) of the photosynthetic pigments (Witt, 1979; Bailleul et al., 2010). This phenomenon which is a special case of the Stark effect (Stark, 1914) stems from the shift in the absorption spectrum of some of the photosynthetic pigments embedded in the thylakoid membrane when photosynthetic activity generates an electric field (a component of the pmf) across the thylakoid. ECS can therefore in principle indicate the proportion of PSI centers that are open by quantifying the stable electric field generated by a saturating single turnover flash. It has the advantage of clearly

distinguishing charge recombination events occurring in acceptor-side limited centers (the electric field relaxes in hundreds of µs) and stabilized charge separation in open centers (the electric field remains stable).

We aimed to test the validity of our P_{700}-based calculation of PSI yield by comparing it to an ECS-based estimation (see also Methods). For initial validation studies, we decided to use the green alga *Chlamydomonas reinhardtii* instead of higher plant leaves, because it is easier to use chemicals with liquid cell cultures as samples are more homogeneous and results readily reproducible. In all experiments, (3,4-dichlorophenyl)-1,1-dimethylurea (DCMU) and hydroxylamine (HA) were added to the cells in order to fully inhibit PSII. Importantly, in these conditions the flash-induced ECS only reflects the contribution from PSI. The PSI yield based on ECS is readily measured as the flash-induced ECS normalized to its equivalent in dark-adapted samples (where the PSI yield is one).

We first varied the fraction of open PSI centers, or PSI yield, by modulating the light intensity. In these conditions, the PSI yield is determined by the rate of photon absorption by PSI and the rate of the CEF around PSI. After photosynthesis reached its steady-state rate, we measured the PSI yield with the ECS-based method, denoted hereafter Y(I)*ECS*, and compared it with the three modes of calculation of PSI yield based on P_{700} redox state: the initial calculation from (Harbinson & Foyer, 1991), (Pm-P)/(Pm – P0), the one proposed by (Klughammer and Schreiber, 1994), (Pm'-P)/(Pm-P0), and its calculation as (Pm'-P)/(Pm'-P0), based on our theoretical model. As expected, the PSI yield measured with ECS decreased with increasing light irradiance reflecting the fact that CEF saturates under relatively low irradiance (Fig 2A/B/C).

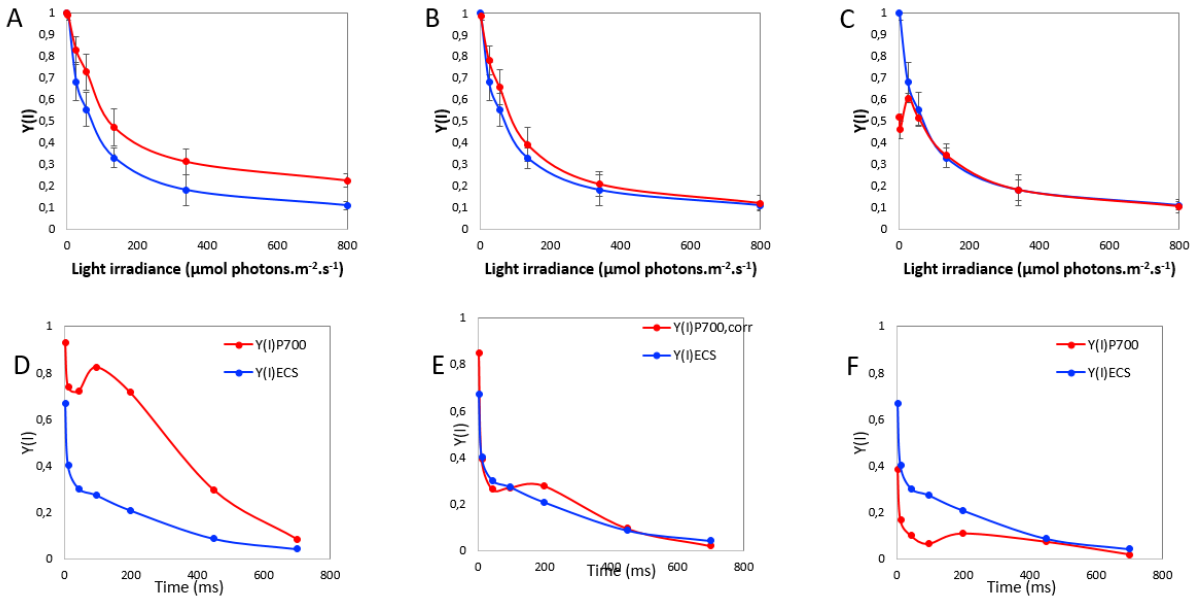

Figure 2. Comparison of PSI yield in oxic conditions, in the absence of PSII activity. *A/B/C: Light dependence of PSI yield. D/E/F: kinetics of PSI yield at the dark-to-light transition (800 µmol photons.m^{-2}. s^{-1}) The red points correspond to the PSI yield calculated with the method from Harbinson & Foyer (A, D), from the method described in this manuscript (B, E) and with the method from Klughammer and Schreiber (panel C, F). In all panels, the blue points correspond to the PSI yield calculated with the ECS method. All data represent the mean ± SD from 3 independent biological replicates.*

This was also the case for the Y(I) calculated from P_{700} with our model (Fig 2B) but not for the two other methods where significant differences with ECS were found, an overestimation of Y(I) under high light for the Harbinson & Foyer method (Fig 2A) and an under-estimation of Y(I) in low light for the Klughammer & Schreiber method (Fig 2C), i.e. in the dark and at 3 µmol photons m^{-2} s^{-1}, the lowest irradiance tested which corresponds to ~2 photons per PSI per second (see Methods). The discrepancy was larger during the first second of a dark-to-light transition (Fig 2 D/E/F), where the Y(I) based on ECS decreased from its dark-adapted vaue (1) to a value close to its dark-adapted value in the light (Fig 2D/E/F). Again, the P_{700}-based Y(I) based on our model follows the one from ECS (Fig 2E) but the PSI yield measured by Harbinson & Foyer and Klughammer & Schreiber methods are always higher and lower, respectively, than the one measured with ECS (Figure 2D/F).

In the absence of acceptor-side limited centers, which can be created by using the artificial PSI acceptor methylviologen (MV), all reduced P_{700} are photo-oxidizable. In these conditions, there should be no acceptor side limitation, Y(I) should be equal to the fraction of reduced P*700* before the pulse and should be correctly assessed with the three P_{700}-based methods. As expected, in the presence of MV the ECS method and the three P_{700}-based methods give similar results (Sup Figure 1). The agreement between P_{700} and ECS estimations of PSI yield in the absence of acceptor-side limitation was also observed recently in cyanobacteria using phenazine methosulfate as a PSI electron acceptor (Figure 3 in Viola et al., 2019). This consistency between results strongly suggests that there is no intrinsic error or artefact in the methods used, and that the discrepancy in steady state light or during dark to light transitions is related to the estimation of the acceptor side limitation by the Harbinson & Foyer and Klughammer & Schreiber methods. To further confirm the causal link between the discrepancy and the level of reduced PSI acceptors, we took the opposite approach by creating conditions in which the acceptor-side limitation is known to be especially high. In anoxic conditions, the reductants produced by glycolysis and the Krebs cycle cannot be re-oxidized by the mitochondrial respiration chain. This reducing power diffuses in the cell via membrane shuttles and results in a reducing pressure in the chloroplast stroma (Hoefnagel et al., 1998). What is more, chloroplast oxidases, like plastid terminal oxidase (Bennoun, 1983; Houilles-Verne et al., 2011; Nawroki et al., 2019) or flavodirion proteins (Chaux et al., 2017), cannot deal with this reducing pressure in the absence of their substrate O_2. Consequently, anoxia leads to enhanced reducing pressure on PSI acceptors. In dark-adapted anoxic cells, the discrepancy was even higher than in oxic conditions as the $Y(I)_{ECS}$ remained equal to 1 (Figure 5), as well as the estimation from Harbinson & Foyer or our model. In contrast, the Y(I) estimated by the Klughammer & Schreiber method decreased to a value of ~0.3 (Fig 5). Again, we compared the estimations of Y(I) based on P_{700} or ECS in transitory situations at different times after the onset of different light irradiances. Here again, our estimation of Y(I) based on P_{700} gave the best results, with a good agreement with the ECS estimation (Fig 3B, one representative experiment but see Fig 4, later). The discrepancies of the two other P_{700}-based assessment with the ECS method became larger in anoxic conditions, where the Harbinson & Foyer and the Klughammer & Schreiber methods, respectively over-estimated and under-estimated the (I) (Fig 3A/C). It should be noted that assays with MV cannot be done in anoxic conditions, because O_2 is the final electron acceptor in the MV-mediated electron transfer from PSI.

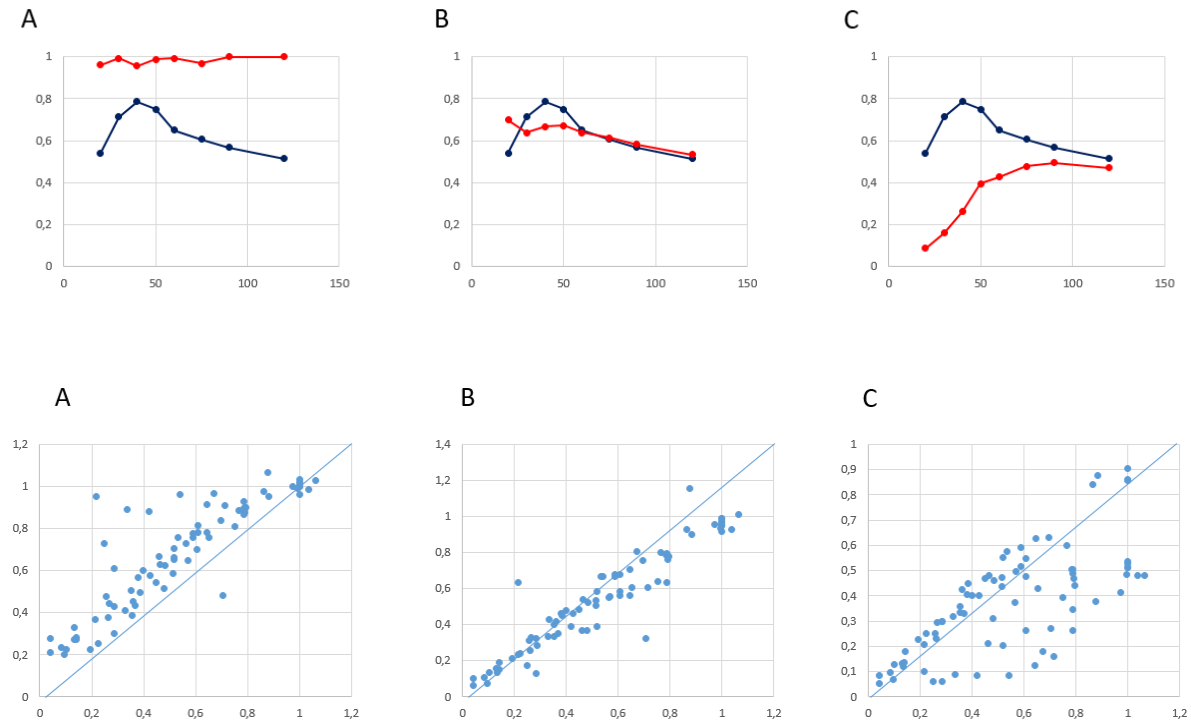

Figure 4. Comparison of PSI yield in oxic conditions, in the absence of PSII activity. *Comparison of Y(PSI) based on P700 and ECS methods, based on data from Figure 2 and 3 (3 other dark-to light kinetics in both oxic and anoxic conditions were added). The different panels correspond to the method from Harbinson & Foyer (A), to the method described in this manuscript (B) and to the method from Klughammer and Schreiber (panel C). All data represent the mean ± SD from 3 independent biological replicates.*

Figure 4 sums up all the data presented in Figures 2 and 3 where the ECS and P_{700} methods were compared. We used a color code reflecting the amount of acceptor side limitation and based on the ratio (P'm-P0)/(Pm-P0). When all the data are taken together, it is clear that the Harbinson & Foyer and Klughammer & Schreiber methods tend to overestimate and underestimate, respectively, the Y(I) whereas the calculation based on our simple model gives a good agreement with the Y(I) estimated from the flash-induced ECS. Interestingly, there is a good agreement between all methods when the acceptor side limitation is low (darker blue points), whereas the discrepancy increases with the high acceptor side limitation for the Harbinson & Foyer and Klughammer & Schreiber methods (darker red points). The overestimation of Y(I) by the Harbinson & Foyer method when there is an acceptor side limitation is straightforward, since this method considers that all centers with P_{700} reduced is open. The underestimation by Klughammer & Schreiber method in those conditions supports our initial concern that the multiple turnover pulse over-reduces PSI acceptors during the pulse, leading to an overestimation of the acceptor-side limitation at the expense of the PSI yield.

As postulated in the Introduction, this might be the result of using a multiple turnover pulse. If several charge separations are necessary before reaching the maximal oxidation of P_{700}, then several electrons will be transferred to the PSI acceptor side. The fraction of closed PSI centers due to reduction of the acceptor, [P_{700} A^-], at the end of the pulse will be overestimated compared to before

the pulse. Therefore, the measured Y(I) based on Klughammer & Schreiber method will be lower than the actual PSI yield, Y(I). The number of charge separations can be measured by monitoring the electric field or ECS generated during the multiple turnover pulse and comparing it to the one generated by one saturating laser flash. In dark-adapted oxic *Chlamydomonas* during the pulse, 4 PSI turnovers occur before maximal P_{700} oxidation is reached (Figure 5B) which corresponds to 50% of P_{700} (Figure 5A and B). The 4 electrons transferred might have reduced the acceptor side of PSI and generated some [P_{700} A^-] centers, preventing the full oxidation of P_{700}. When tested in the presence of MV, one more charge separation can occur (Figure 5C) and this allows almost all P_{700} to be oxidized during the pulse (Figure 4A and B). As a control, we used a plastocyanin mutant which can only perform one charge separation because its P_{700} cannot be reduced. In this case, the pulse-induced ECS increase confirms that only one charge separation occurs (Figure 5C), that all P_{700} is oxidized during the pulse (Figure 5A and B), and that the ECS and P_{700} methods give the same result (Figure 5A). This demonstrates that the P_{700} pulse bias comes from the use of a multiple turnover pulse, which makes the fraction of [P_{700} A^-] at the end of the pulse higher than that before the pulse.

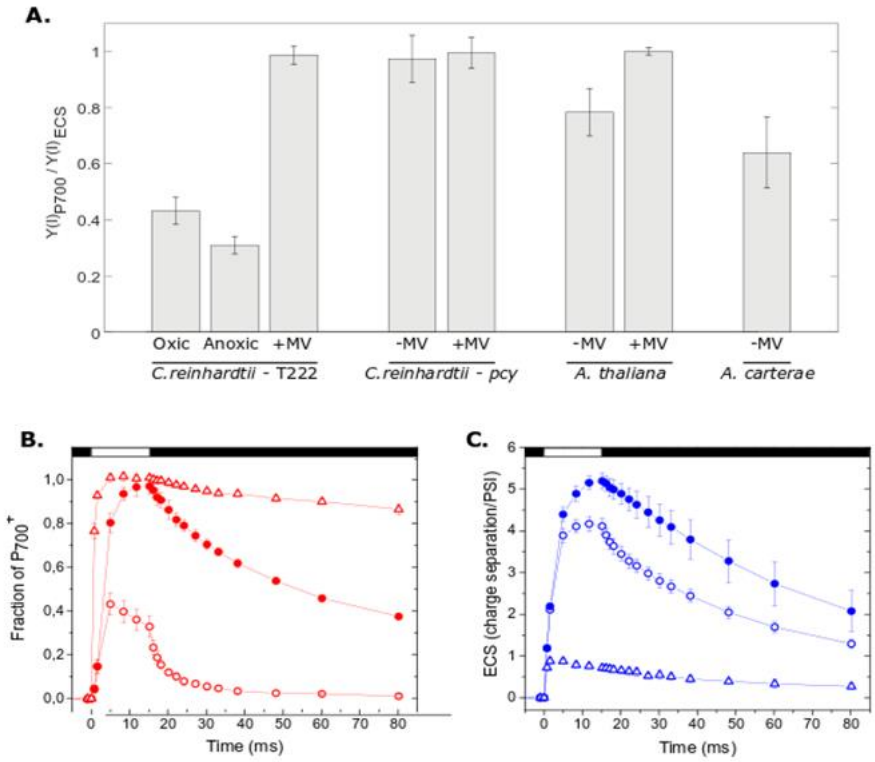

Figure 5. Comparison of estimated fractions of open PSI centers in dark-adapted photosynthetic organisms according to ECS and the 3 different P_{700} methods. *(**A**) ECS and P_{700} based PSI yields in Chlamydomonas reinhardtii, the higher plant Arabidopsis thaliana and the dinoflagellate Amphidinium carterae. T222, wild type; pcy, plastocyanin mutant in oxic conditions; MV methylviologen. (**B** and **C**) Kinetics of P_{700} (**B**) and ECS (**C**) during and after the saturating light pulse in Chlamydomonas wild-type with (closed circles) and without (open circles) MV and in the plastocyanin mutant (triangles). Error bars correspond to the standard deviation of 3 biological replicates.*

We investigated whether the discrepancy measured in *C. reinhardtii* is also observed in other photosynthetic species. In the dark, the fraction of open PSI centers should not depend on the activity of other photosynthetic complexes, so we could compare different strains and species, independently modifying the donor and acceptor pool size by adding chemicals. We measured $Y(I)_{ECS}$ and $Y(I)_{P700}$ in dark-adapted leaves of *Arabidopsis thaliana* and in the dinoflagellate *Amphidinium carterae*. In both cases, we observed the same trend: $Y(I)_{ECS}$ was higher than $Y(I)_{P700}$. Like in *C. reinhardtii*, there was no discrepancy in *A. thaliana* in the presence of MV (Figure 4). Equivalent data with MV in the dinoflagellate *Am. carterae* was not obtained because we did not detect any effect of MV in this species.

4. Discussion

4.1. Generalities

Comparing the PSI parameters estimated based on the P_{700} pulse method with an alternative approach based on ECS allowed us to demonstrate that the P_{700} pulse method underestimates the PSI yield when a significant $Y(NA)_{P700}$ is measured, i.e. when there is an acceptor-side limitation at the end of the pulse. The underestimation went as high as a factor 10 in our dataset (Figure 5B). When a multiple turnover pulse is used and the initial pool of PSI donors is large, several electrons will be transferred to the PSI acceptors during the pulse. The amount by which the PSI yield is underestimated is proportional to $Y(NA)_{P700}$, a dependency that we were able to predict with the following simple assumption. The multiple turnover pulse generates both acceptor-side and donor-side limited PSI centers at a ratio which remains the same as before the pulse. This assumption simply means that the "capacity" for oxidation of PSI acceptors and the "capacity" for reduction of PSI donors do not change within the few ms of the pulse.

Early approaches to assessing PSI yield based on P_{700} measurements considered that all PSI with reduced P_{700} were open (Harbinson and Foyer, 1991). The P_{700} pulse method was developed as an improvement on those approaches, allowing open and acceptor-side limited PSI centers to be distinguished. In conditions where all P_{700} are photo-oxidizable, i.e. Y(NA) is 0, both approaches prove right. As soon as there is a fraction of acceptor-side limited centers, both methods prove wrong and the K&S method cannot be considered as an improvement on the Harbinson and Foyer (H&F) method. This can be clearly visualized in Figure 5D, which displays the relative error of Y(I) estimated by the P_{700} pulse method and by the H&F method, as a function of the true acceptor-side limitation, i.e. the fraction of $[P_{700}\ A^-]$ centers or Y(NA). In both cases, the relative error is proportional to the acceptor-side limitation, but the H&F method naturally overestimates Y(I) whereas the K&S method underestimates it. The slope depends on the (true) PSI yield. For a Y(I) of 0.5, the relative errors made by the H&F and K&S methods mirror each other. However, a major difference is that the dependency between the error and the acceptor-side limitation increases with Y(I) in the case of K&S method (the slope is $(1\text{-}Y(I))^{-1}$, see Appendix 1), but decreases with Y(I) in the case of H&F method (the slope is $Y(I)^{-1}$, see Appendix 1).

4.2. An internal contradiction in the P_{700} pulse method

For all photo-oxidizable P_{700} to be oxidised despite being rapidly reduced by plastocyanin or other secondary donors like cytochrome c6 ($t_{1/2}$ ≈ 5 µs if the secondary donor is already fixed, otherwise $t_{1/2}$ ≈ 200 µs, Hippler et al., 1997), according to Klughammer and Schreiber "the light pulses must be sufficiently long to allow several PSI turnovers, such that the immediate donor pool is emptied during a pulse". When all secondary donors are oxidized, the P_{700} reduction rate does indeed become limited by the rate of electron transfer through cyt b_6f ($t_{1/2}$ ≈ 10 ms), slowing down the re-reduction of P_{700} by 2 to 3 orders of magnitude. A sufficiently strong light pulse would therefore allow all photo-oxidizable P_{700} to be probed. However, an explicit assumption of this method is that "at least during the early phase of a saturation pulse, the oxidation of the donor side is more pronounced than the reduction at the acceptor side. For this reason, it appears unlikely that a reaction center in the state P_{700} A is converted into the state $P_{700}A^-$ during the first milliseconds of a saturating light pulse". These two hypotheses are clearly contradictory. PSI photochemistry and charge conservation dictate that electrons extracted on the donor side are transferred to the acceptor side. If several photochemical events are allowed to oxidize several secondary donors, then several electrons will be transferred through PSI, modifying the redox state of the acceptors. For this reason, we are concerned that the pulse-method could overestimate the acceptor-side limitation, $Y(NA)_{P700} > Y(NA)$, and underestimate the fraction of open PSI centers $Y(I)_{P700} < Y(I)$, when the pool of PSI donors is large.

The good news is that as the underestimation of the PSI yield with the P_{700} pulse method is proportional to the $Y(NA)_{P700}$ a correction can be made. The correct value for Y(I) can be calculated from the parameters derived from the P700 pulse method: $Y(I) = Y(I)_{P700} / (1-Y(NA)_{P700})$. When such correction is done, the comparison between the corrected PSI yield and $Y(I)_{ECS}$ are in very close agreement (Fig 5C), i.e. the ratio becomes 1 as expected, except for the data points for which the $Y(NA)_{P700}$ is higher than 0.8. For those data points, the correction is very prone to small errors as both $Y(I)_{P700}$ and $(1-Y(NA)_{P700})$ are small numbers.

Revisiting 25 years of research base on the P_{700} pule method, covering many aspects of photosynthesis, will be a challenge. The values of PSI yield measured in dark-adapted photosynthetic samples are good examples of the errors that have been recorded and propagated in the literature. It is clear that given the ambient redox potential in a dark-adapted chloroplast, P_{700} should be fully reduced (the redox potential of P_{700} being in the 375 to 525 mV range, Ke 2001) and A should be fully oxidized (the redox potential of iron-sulfur centers being in the -520 to -705 mV range, Golbeck and Bryant, 1991; Golbeck, 1993). Therefore the PSI yield in the dark should be equal to 1. This is not what the P_{700} pulse method shows. We obtained $Y(I)_{P700}$ values of ~0.8 in *A. thaliana* leaves, ~0.5 in *C. reinhardtii* and ~0.6 in *Am. carterae*. In the literature, $Y(I)_{P700}$ is 0.8 in dark-adapted *A. thaliana* leaves (Kono et al., 2018), 0.8-0.9 in sunflower leaves (Klughammer and Schreiber, 1994; Sejima et al., 2014), 0.7 in barley leaves (Pfündel et al., 2008), 0.5 in pea leaves (Schansker et al., 2003), 0.8 in wheat leaves (Brestic et al., 2015; Zivcak et al., 2015), 0.3-0.42 in *Jatropha curcas L* (Ranjan et al., 2014), 0.65 in *Microsorum punctatum* and 0.55 in *Paraleptochillus decurrens* (Wang et al., 2013). Similar low values of $Y(I)_{P700}$ in dark-adapted photosynthetic organisms have been documented in the angiosperm *Ipomoea nil* and in the cyanobacterium *Synechococcus elongatus* PCC 7942 (Shimakawa et al., 2019).

The literature regarding CEF, and especially the deduced role of the *A. thaliana* proton gradient regulator 5 (PGR5) and proton gradient regulator-like 1 (PGRL1) proteins in this process, might have also been strongly affected by the errors inherent in the P_{700} pulse method. Indeed, one of the main arguments in favor of a role of these proteins in CEF comes from the measurement of a lower $Y(I)_{P700}$ and a higher $Y(NA)_{P700}$ in the *pgrl1* and *pgr5* mutants compared to the wild type (e.g. DalCorso et al., 2008; Kono et al., 2014; Kou et al., 2015). These observations have been interpreted as the signature of a lower CEF rate, leading to acceptor-side limitation. The limitations of the K&S method demonstrated here invalidate this conclusion. It would be wise to reappraise the literature on CEF in a timely way and correct any relevant data as we propose here. Going forward this would increase the robustness and precision of experimental data and give a more accurate view of how the light phase of photosynthesis is regulated in all its diversity.

The later overestimates the acceptor-side limitation and therefore underestimates the fraction of PSI open centers by up to ten-fold in our dataset. The overestimation is proportional to the factor (1-[P_{700} A^-]) calculated at the end of the pulse, as expected based on our theoretical calculations. A simple formula can therefore be applied to erroneous measurements of Y(I) in the literature. Future work using the approach described in this work, together with the reappraisal of the litterature about cyclic electron flow around PSI, should improve our current models of the regulation of photosynthesis.

This calculation differs from the one proposed by (Klughammer and Schreiber, 1994). Moreover, we use an alternative method. Estimates of the fraction of PSI open centers by measuring ECS generated by a single turnover flash agree very well with the estimates from our P_{700}-based calculation but strongly differ from the mode of calculation of PSI yield based on (Klughammer and Schreiber, 1994), which is currently used.

Acknowledgements

We would like to thank Fredy Barnèche and Meenu Singla for their technical help growing *Arabidopsis thaliana.* We would also like to thank Francis-André Wollman, Stefano Santabarbara, Helmut Kirchhoff, Anja Krieger-Liszkay and Pierre Sétif for fruitful discussions and Anja Krieger-Liszkay for access to the Dual-PAM. B.B. and S.F. acknowledge financial support from the European Research Council (ERC) under the European Union Horizon 2020 research and innovation program (grant agreement no. 715579). We also thank the Roscoff culture collection for providing the strain of *Am. carterae*.

References

Allen, J. F. (2002). Photosynthesis of ATP—electrons, proton pumps, rotors, and poise. *Cell*, *110*(3), 273-276.

Arnon, D. L., Whatley, F. R., & Allen, M. B. (1958). Assimilatory power in photosynthesis. *Science*, *127*(3305), 1026-1034.

Bailleul, B., Cardol, P., Breyton, C., & Finazzi, G. (2010). Electrochromism: a useful probe to study algal photosynthesis. *Photosynth. Res.*, *106*(1-2), 179.

Baker, N. R. (2008). Chlorophyll fluorescence: a probe of photosynthesis in vivo. *Annu. Rev. Plant Biol.*, *59*, 89-113.

Bendall, D. S., & Manasse, R. S. (1995). Cyclic photophosphorylation and electron transport. *Biochim.Biophys. Acta Bioenerg*., *1229*(1), 23-38.

Bennoun, P. (1983). Effects of mutations and of ionophore on chlororespiration in Chlamydomonas reinhardtii. *FEBS Lett.*, *156*(2), 363-365.

Berges, J. A., Franklin, D. J., & Harrison, P. J. (2001). Evolution of an artificial seawater medium: improvements in enriched seawater, artificial water over the last two decades. *J. Phycol.*, *37*(6), 1138-1145.

Brestic, M., Zivcak, M., Kunderlikova, K., Sytar, O., Shao, H., Kalaji, H. M., & Allakhverdiev, S. I. (2015). Low PSI content limits the photoprotection of PSI and PSII in early growth stages of chlorophyll b-deficient wheat mutant lines. *Photosynth. Res.*, *125*(1-2), 151-166.

Buchert, F., Bailleul, B., Hisabori, T. (2017). A γ-subunit point mutation in Chlamydomonas reinhardtii chloroplast F1Fo-ATP synthase confers tolerance to reactive oxygen species. *Biochim. Biophys. ActaBioenerg.*, *1858*(12), 966-974.

Chaux, F., Peltier, G., Johnson, X. (2015). A security network in PSI photoprotection: regulation of photosynthetic control, NPQ and O2 photoreduction by cyclic electron flow. *Front.Plant Sci.*, *6*, 875.

Chaux, F., Burlacot, A., Mekhalfi, M., Auroy, P., Blangy, S., Richaud, P., Peltier, G. (2017). Flavodiiron proteins promote fast and transient O2 photoreduction in Chlamydomonas. *Plant Physiol.*, *174*(3), 1825-1836.

DalCorso, G., Pesaresi, P., Masiero, S., Aseeva, E., Schünemann, D., Finazzi, G., ... & Leister, D. (2008). A complex containing PGRL1 and PGR5 is involved in the switch between linear and cyclic electron flow in Arabidopsis. *Cell*, *132*(2), 273-285.

Delosme, R., Béal, D., Joliot, P. (1994). Photoacoustic detection of flash-induced charge separation in photosynthetic systems. Spectral dependence of the quantum yield. *Biochim. Biophys. Acta Bioenerg.*, *1185*(1), 56-64.

Duysens, L. N. M. (1963). Mechanism of the two photochemical reactions in algae as studied by means of fluorescence. Studies on microalgae and photosynthetic bacteria, 353-372.

Eberhard, S., Finazzi, G., Wollman, F. A. (2008). The dynamics of photosynthesis. *Annu. Rev. Genet.*, *42*, 463-515.

Endo, T., Asada, K. (2008). Photosystem I and photoprotection: cyclic electron flow and water-water cycle. In *Photoprotection, Photoinhibition, Gene Regulation, and Environment* (pp. 205-221). Springer, Dordrecht.

Fan, D. Y., Nie, Q., Hope, A. B., Hillier, W., Pogson, B. J., Chow, W. S. (2007). Quantification of cyclic electron flow around Photosystem I in spinach leaves during photosynthetic induction. *Photosynth. Res.*, *94*(2-3), 347.

Fan, D. Y., Fitzpatrick, D., Oguchi, R., Ma, W., Kou, J., Chow, W. S. (2016). Obstacles in the quantification of the cyclic electron flux around Photosystem I in leaves of C3 plants. *Photosynth. Res.*, *129*(3), 239-251.

Foyer, C. H., Neukermans, J., Queval, G., Noctor, G., Harbinson, J. (2012). Photosynthetic control of electron transport and the regulation of gene expression. *Journal of Experimental Botany*, *63*(4), 1637-1661.

Genty B, Goulas Y, Dimon B, Peltier JM, Moya I. 1992. Modulation of efficiency ofprimary conversion in leaves, mechanisms involved at PSII. In Research in Photosynthesis, Volume 4, ed. N Murata, pp. 603–10. Dordrecht: Kluwer Academic Publishers.

Golbeck, J. H., & Bryant, D. A. (1991). Current topics in bioenergetics. In Light-Driven Reactions in Bioenergetics (Vol. 16).

Golbeck, J. H. (1993). The structure of photosystem I: Current Opinion in Structural Biology 1993, 3: 508–514. *Curr. Opin. Struct. Biol.*, *3*(4), 508-514.

Golbeck, J. H. (Ed.). (2007). Photosystem I: the light-driven plastocyanin: ferredoxin oxidoreductase (Vol. 24). Springer Science & Business Media.

Harbinson, J., Woodward, F. I. (1987). The use of light-induced absorbance changes at 820 nm to monitor the oxidation state of P-700 in leaves. *Plant Cell Environ.*, *10*(2), 131-140.

Harbinson, J., Genty, B., Baker, N. R. (1989). Relationship between the quantum efficiencies of photosystems I and II in pea leaves. *Plant Physiol.*, *90*(3), 1029-1034.

Harbinson, J., Foyer, C. H. (1991). Relationships between the efficiencies of photosystems I and II and stromal redox state in CO2-free air: evidence for cyclic electron flow in vivo. *Plant Physiol.*, 97(1), 41-49.

Harris, E. H. (2009). The chlamydomonas sourcebook (Vol. 1, pp. 119-157). D. B. Stern, & G. B. Witman (Eds.). San Diego, CA: Elsevier.

Havaux, M., Davaud, A. (1994). Photoinhibition of photosynthesis in chilled potato leaves is not correlated with a loss of photosystem-II activity. *Photosynth. Res.*, *40*(1), 75-92

Hippler, M., Drepper, F., Farah, J., Rochaix, J. D. (1997). Fast electron transfer from cytochrome c 6 and plastocyanin to photosystem I of Chlamydomonas reinhardtii requires PsaF. *Biochem.*, *36*(21), 6343-6349.

Hiyama, T., Ke, B. (1972). Difference spectra and extinction coefficients of P700. *Biochim. Biophys.a ActaBioenerg.*, *267*(1), 160-171.

Hoefnagel, M. H., Atkin, O. K., Wiskich, J. T. (1998). Interdependence between chloroplasts and mitochondria in the light and the dark. *Biochim.Biophys. ActaBioenerg.*, *1366*(3), 235-255.

Houille-Vernes, L., Rappaport, F., Wollman, F. A., Alric, J., Johnson, X. (2011). Plastid terminal oxidase 2 (PTOX2) is the major oxidase involved in chlororespiration in Chlamydomonas. *Proc. Natl. Acad.Sci.*, *108*(51), 20820-20825.

Izawa, S. (1980). Acceptors and donors and chloroplast electron transport. In Methods in Enzymology (Vol. 69, pp. 413-434). Academic Press

Joliot, P., Johnson, G. N. (2011). Regulation of cyclic and linear electron flow in higher plants. *Proc.Natl. Acad.Sci. U.S.A.*, *108*(32), 13317-13322.

Joliot, P., Delosme, R. (1974). Flash-induced 519 nm absorption change in green algae. *Biochim. Biophys. Acta Bioenerg.*, *357*(2), 267-284.

Junesch, U., Gräber, P. (1987). Influence of the redox state and the activation of the chloroplast ATP synthase on proton-transport-coupled ATP synthesis/hydrolysis. *Biochim.Biophys. ActaBioenerg.*, *893*(2), 275-288.

Kautsky H, Appel W, Amann H (1960) Die Fluoreszenzkurve und die Photochemie der Pflanze. Biochem Z 332:277–292

Ke, B. (2001). The primary electron donor of photosystem I—P700. Photosynthesis: Photobiochemistry and Photobiophysics, 463-478.

Klughammer, C., & Schreiber, U. (2016). Deconvolution of ferredoxin, plastocyanin, and P700 transmittance changes in intact leaves with a new type of kinetic LED array spectrophotometer. *Photosynth. Res.*, *128*(2), 195-214.

Klughammer, C., Schreiber, U. (1994). An improved method, using saturating light pulses, for the determination of photosystem I quantum yield via P700+-absorbance changes at 830 nm. *Planta*, *192*(2), 261-268.

Kono, M., Noguchi, K., Terashima, I. (2014). Roles of the cyclic electron flow around PSI (CEF-PSI) and O2-dependent alternative pathways in regulation of the photosynthetic electron flow in short-term fluctuating light in Arabidopsis thaliana. *PlantCell Physiol.*, *55*(5), 990-1004.

Kou, J., Takahashi, S., Fan, D. Y., Badger, M. R., Chow, W. S. (2015). Partially dissecting the steady-state electron fluxes in Photosystem I in wild-type and pgr5 and ndh mutants of Arabidopsis. *Front. Plant Sci.*, *6*, 758.

Laisk, A., Talts, E., Oja, V., Eichelmann, H., Peterson, R. B. (2010). Fast cyclic electron transport around photosystem I in leaves under far-red light: a proton-uncoupled pathway? *Photosynth. Res.*, *103*(2), 79-95.

Malkin, R., Bearden, A. J. (1971). Primary reactions of photosynthesis: photoreduction of a bound chloroplast ferredoxin at low temperature as detected by EPR spectroscopy. *Proc. Natl. Acad.Sci. U.S.A.*, *68*(1), 16-19.

Nawrocki, W. J., Tourasse, N. J., Taly, A., Rappaport, F., Wollman, F. A. (2015). The plastid terminal oxidase: its elusive function points to multiple contributions to plastid physiology. *Annu. Rev. Plant Biol.*, *66*, 49-74.

Nelson, N. (2009). Plant photosystem I–the most efficient nano-photochemical machine. *J. Nanosci. Nanotechnol.*, *9*(3), 1709-1713.

Oh-Oka, H., Itoh, S., Saeki, K., Takahashi, Y., Matsubara, H. (1991). FA/FB protein from the spinach photosystem I complex: Isolation in a native state and some properties of the iron-sulfur clusters. *Plant Cell Physiol.*, *32*(1), 11-17.

Rumberg, B., Siggel, U. (1969). pH changes in the inner phase of the thylakoids during photosynthesis. *Sci. Nat.*, *56*(3), 130-132.

Scheller, H. V., Haldrup, A. (2005). Photoinhibition of photosystem I. *Planta*, *221*(1), 5-8.

Shikanai, T. (2007). Cyclic electron transport around photosystem I: genetic approaches. *Annu. Rev. Plant Biol.*, *58*, 199-217.

Sonoike, K. (2011). Photoinhibition of photosystem I. *Physiologia Plantarum*, *142*(1), 56-64.

Sonoike, K., Terashima, I., Iwaki, M., Itoh, S. (1995). Destruction of photosystem I iron-sulfur centers in leaves of Cucumis sativus L. by weak illumination at chilling temperatures. *FEBS Lett.*, 3*62*(2), 235-238.

Stark, J. (1914). Beobachtungen über den Effekt des elektrischen Feldes auf Spektrallinien. I. Quereffekt. *Ann.Phys.*, *348*(7), 965-982.

Suzuki, K., Ohmori, Y., Ratel, E. (2011). High root temperature blocks both linear and cyclic electron transport in the dark during chilling of the leaves of rice seedlings. *Plant Cell Physiol.*, *52*(9), 1697-1707.

Talts, E., Oja, V., Rämma, H., Rasulov, B., Anijalg, A., Laisk, A. (2007). Dark inactivation of ferredoxin-NADP reductase and cyclic electron flow under far-red light in sunflower leaves. *Photosynth. Res.*, *94*(1), 109-120.

Terashima, I., Funayama, S., Sonoike, K. (1994). The site of photoinhibition in leaves of Cucumis sativus L. at low temperatures is photosystem I, not photosystem II. *Planta*, *193*(2), 300-306.

Voss, I., Koelmann, M., Wojtera, J., Holtgrefe, S., Kitzmann, C., Backhausen, J. E., Scheibe, R. (2008). Knockout of major leaf ferredoxin reveals new redox-regulatory adaptations in Arabidopsis thaliana. *Physiol. Plant.*, *133*(3), 584-598.

Wang, J. H., Li, S. C., Sun, M., Huang, W., Cao, H., Xu, F., ... & Zhang, S. B. (2013). Differences in the stimulation of cyclic electron flow in two tropical ferns under water stress are related to leaf anatomy. *Physol. Plant.*, *147*(3), 283-295.

Warren, P. V., Parrett, K. G., Warden, J. T., Golbeck, J. H. (1990). Characterization of a photosystem I core containing P700 and intermediate electron acceptor A1. *Biochem.*, *29*(28), 6545-6550.

Weis, E., Ball, J. T., Berry, J. (1987). Photosynthetic control of electron transport in leaves of Phaseolus vulgaris: evidence for regulation of photosystem 2 by the proton gradient. In Progress in photosynthesis research (pp. 553-556). Springer, Dordrecht.

Witt, H. T. (1979). Energy conversion in the functional membrane of photosynthesis. Analysis by light pulse and electric pulse methods: The central role of the electric field. *Biochim.Biophys. ActaBioenerg.*, *505*(3-4), 355-427.

Zivcak, M., Brestic, M., Kunderlikova, K., Sytar, O., Allakhverdiev, S. I. (2015). Repetitive light pulse-induced photoinhibition of photosystem I severely affects CO2 assimilation and photoprotection in wheat leaves. *Photosynth. Res.*, *126*(2-3), 449-463.

SUPPORTING INFORMATION

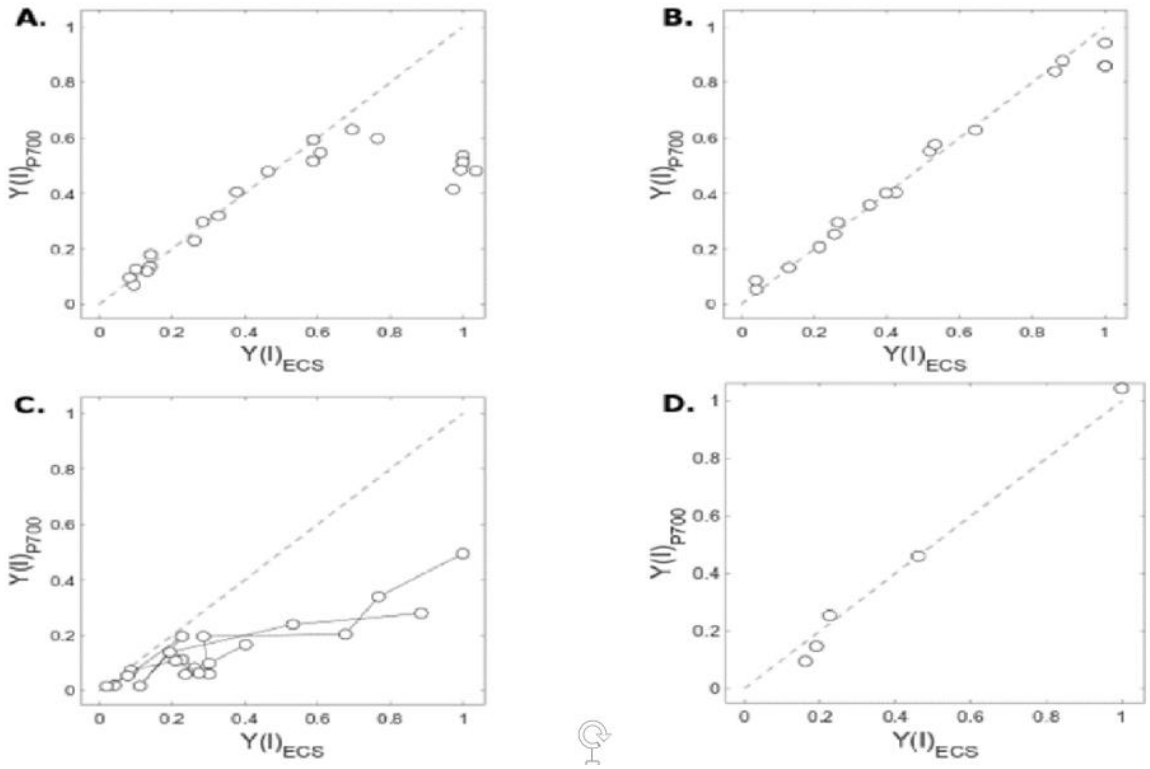

Sup Figure 1. Comparison of estimated fractions of PSI open centers in C. reinhardtii in oxic conditions according to ECS and P_{700} methods. *Experiments were carried out in the presence of DCMU and HA. (**A** and **B**) $Y(I)_{P700}$ plotted as a function of $Y(I)_{ECS}$. Values were determined in the absence (**A**) or presence (**B**) of MV under steady-state illumination. Data points correspond to those shown in Figure 1B and 1C plus two other independent biological replicates. (**C** and **D**) $Y(I)_{P700}$ as a function of $Y(I)_{ECS}$. Values were determined in the presence absence (**A**) or presence (**B**) of MV during the dark-to-light transition at the onset of a 800 µmol photons m^{-2} s^{-1} light irradiance.*

Chapter Conclusion

In this chapter, we have shown that previous methods based on P_{700} measurements, in particular the method proposed by Klughammer and Schreiber in 1994, fail in calculating PSI yield. In particular, the Klughammer and Schreiber method presents a bias because it systematically underestimates the PSI yield. The underestimation is proportional to the acceptor side limitation at the end of the pulse. Thanks to the comparison of P_{700} measurements with ECS measurements perfomed in parallel, we were able to propose a correction of the P_{700} data. With this correction, we believe that correct estimatations of the quantum yield of PSI are possible, and importantly, that already produced data can be revisited on this basis.

Based on the results presented in this chapter, one could conclude that the best approach to measure PSI activity would be to use ECS measurements. However, ECS measurements measure the additive effects of PSII and PSI, which are not so easy to deconvolute. P_{700} measurement are easy to perform, there are accessible commercial instruents allowing to do so and and those measurements do not require the purchase of an expensive laser (contrary to ECS).

For this reason, I will favor the use of P_{700} measurements and the corrected calculations proposed in this work, in the next chapter which aims at investigating the effects of various external quinones on the different photosynthetic complexes.

Chapter IV

Article n°3 - Analytical Fingerprint of the Interactions Between Quinones and Bioenergetic membranes in *Chlamydomonas reinhardtii*

Marc Arderiu Romero, Manon Guille-Collignon, Benjamin Bailleul, Frédéric Lemaître

This work was presented as a poster at the annual meeting of the French Photosynthesis Society (Journées de la Société Française de Photosynthèse; 22nd-23rd June 2023).

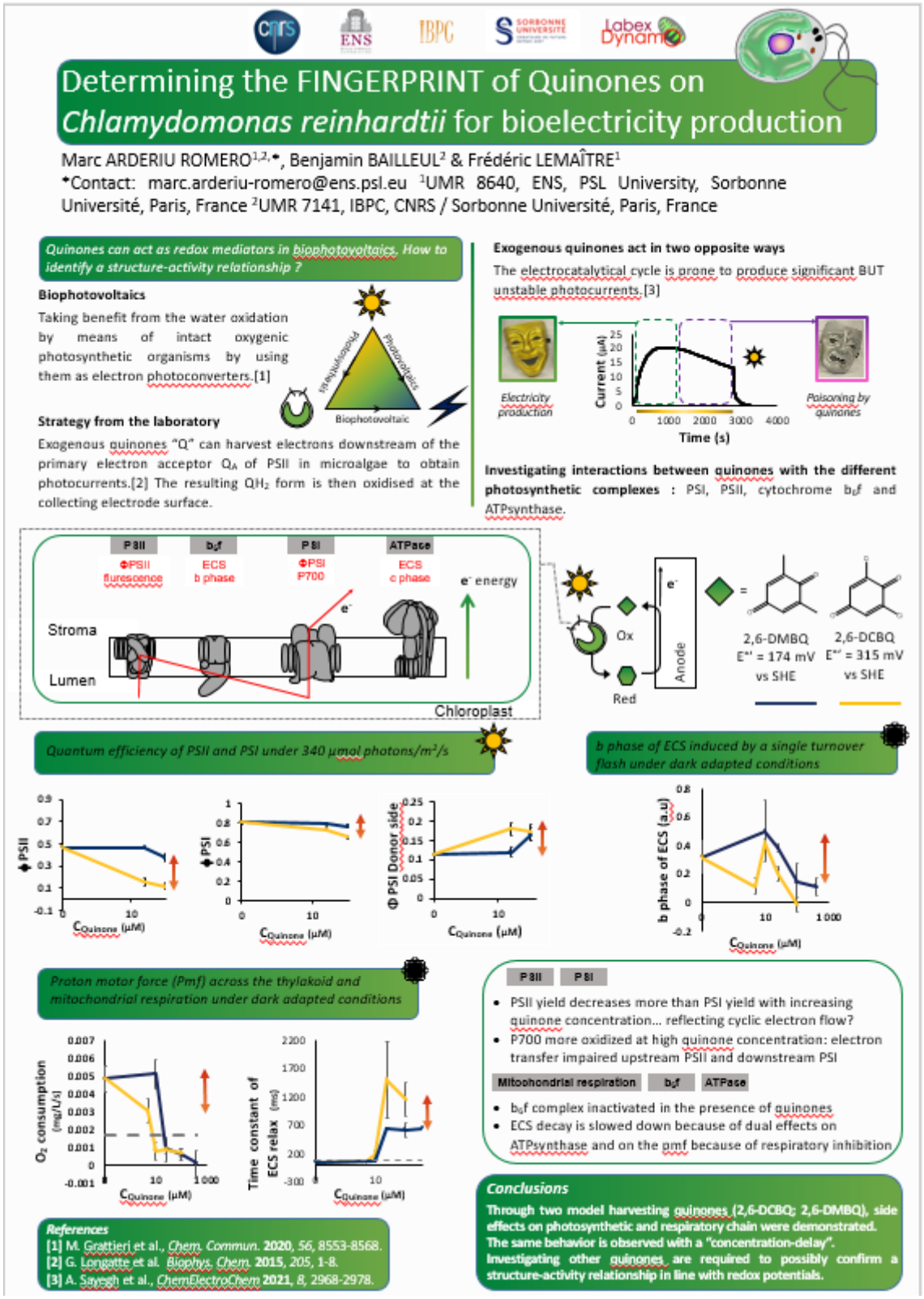

Abstract

The use of intact photosynthetic organisms (e.g. microalgae or cyanobacteria) for biotechnological approaches is a promising avenue to extract sustainable energy from oxygenic photosynthesis. More particularly, exogenous quinones can act as electron shuttles to reroute part of the photosynthetic electron flow of living cells to an outer collecting electrode. This encouraging approach is however hampered by reported poisoning effects of exogenous quinones on the cell bioenergetics. In order to better understand those poisoning effects, we investigated the modes and sites of interaction of two model quinones (2,6-DCBQ and 2,6-DMBQ) with the respiratory and photosynthetic electron transfer chains of the green alga *Chlamydomonas reinhardtii*. By considering different analytical tools (chlorophyll *a* fluorescence, transient absorption spectrometry, O_2 consumption rate), the two exogenous quinones are shown to hamper the photosynthetic electron transfer from photosystem II (PSII) to the cytochrome b_6f and in turn enhance cyclic electron flow around PSI and, at longer term, PSII damage. In addition, the investigated quinones initiate the suppression of mitochondrial respiration, illustrated by the decrease of O_2 consumption. This results in the diminution of the ATP exchanges between mitochondrion and chloroplast responsible for the generation of the proton motive force across the thylakoid in darkness, and in turn affects the performances of the CF1FO ATPase. For all those effects, 2,6-DCBQ was more effective than 2,6-DMBQ (the half-inhibition concentration was 2-to-5 fold lower for DCBQ) according to its higher redox potential and partition coefficient values. This work provides a new framework for the study of biophotovoltaic devices using photosynthetic organisms and quinones as mediators and could be extended to find the best candidates combining efficient bioelectricity production and limited toxicity.

Keywords: photosynthesis; quinones; electron transfer; *Chlamydomonas reinhardtii*, green algae

Abbreviations

2,6-DCBQ = 2,6-Dichloro-1,4-benzoquinone; 2,6-DMBQ = 2,6-Dimethyl-1,4-benzoquinone; DCMU = 3,4-dichlorophenyl-1,1-dimethylurea; ATP = adenosine triphosphate; CEF = cyclic electron flow around PSI; b_6f = cytochrome b_6f; ECS = electro-chromic shift; LEF = linear electron flow; NADPH = nicotinamide adenine dinucleotide phosphate; PSI = photosystem I; PSII = photosystem II; Y_I = PSI yield; Y_{NA} = PSI acceptor-side limitation; Y_{ND} = PSI donor-side limitation; PETC, photosynthetic electron transport chain; PMF = Proton Motive Force; LogP = partition coefficient (logarithmic scale); Y_{II} = PSII yield ; F_v/F_m = PSII maximal quantum yield; NPQ = non-photochemical quenching.

1. Introduction

Organic compounds of the "1,4-benzoquinone" type (often referred to simply as "quinones", which is the term for the class of molecules to which they belong) are conjugated and cyclic structures containing the cyclohexadienedione moiety (*Scheme 1*). From an electrochemical point of view, quinones are often referred to as the hydroquinone/quinone redox couple (QH_2/Q), since the quinone form Q can be reduced as follows: $Q + 2e^- + 2H^+ = QH_2$. The electrochemical behaviour of quinones in aqueous media is highly complicated and can be described using a 9-species square scheme involving protonation/deprotonation and electron transfer steps (*Scheme 1*).[1, 2] Furthermore, the oxidizing power of quinones makes them an excellent electron relay. Therefore, these are important molecules in biology, as they are involved in electron transfer chains within thylakoid membranes (photosynthesis) or inner mitochondrial membranes (respiration).[3 , 4] Such oxidizing properties are also used in organic reactions,[5] while the semi-quinone form (Q^-) has conversely a reducing behaviour and is prone to react with O_2.[6] Of note, quinones are also promising molecules in batteries.[7] Finally, quinones are excellent electrophiles and can undergo 1,4-addition, resulting in the formation of a hydroquinone-type derivative.[8]

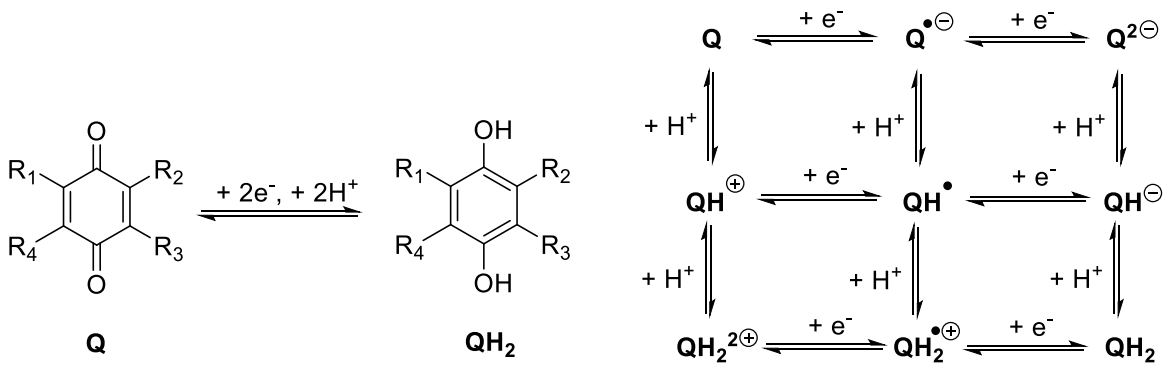

Scheme 1. *Left: electrochemical reaction involving the hydroquinone (QH_2)/quinone (Q) redox couple. Right: detailed electrochemical behavior of quinones in line with a nine-member square scheme.*

The action and reactivity of a quinone is also directly related to the number and nature of its four substituents. The oxidising power will be enhanced or attenuated depending on the presence of electrowithdrawing or electrodonating groups. The ease of reacting with a nucleophile is in turn linked to steric hindrance. It should also be noted that the quinones involved in biology are sequestered in membranes by means of a substituent based on a long aliphatic chain.[3]

In the context of bioelectricity production from photosynthetic organims, quinones are ones of the most used molecules to act as electron shuttles.[9 , 10] Indeed, these soluble mediators are known to interact with the photosynthetic electron transfer chain (PETC) (*Figure 1*). Competing with embedded endogenous quinones (i.e. plastoquinone or ubiquinone pools in thylakoids and inner mitochondrial membranes, respectively), they can partially or totally short-circuit the photosynthetic electron flow by being reduced to QH_2. This hydroquinone form will then be released to be oxidised to the Q quinone form at the surface of a collecting electrode, generating an electric photocurrent.[11] A wide range of structures have been tested against isolated PSII, thylakoid membranes or whole photosynthetic organisms.[12 , 13-15] However, the nature of the interactions involved is not so easy. While the action of photosynthetic electron extraction has been clearly demonstrated, the site of electron transfer is not necessarily unique (PSII, PSI...).[16] For example, quinones can become

incorporated into the Q_B pocket in PSII and then be reduced by the embedded quinone Q_A^-.[17] They can also interact with the downstream plastoquinone pool.[18] Furthermore, the instability of the photocurrents obtained (on isolated PSII or thylakoides membranes, from living photosynthetic organisms) suggests side effects of quinones, which would make them dual agents, capable of both alleviating the photosynthetic chain and impairing the metabolism of the considered organism.[10, 19] These issues are progressively being addressed in the literature but certain trends are emerging, such as the fact that the most oxidising quinones are also those that lead to the highest and most transient currents.[13] However, the measurement of photocurrent produced by a mixture of photosynthetic organisms and quinones is not a sufficient basis for an in-depth description of the effect(s) of the quinone(s). Other behaviours have been identified through fluorescence measurements, such as the ability of quinones to interact with light-harvesting antennae (non-photochemical quenching), which in turn reduces the quantum yield of PSII even though quinones have a diverting effect.[20, 21] Nevertheless, the actual range of interactions provided by quinones still remain unclear.

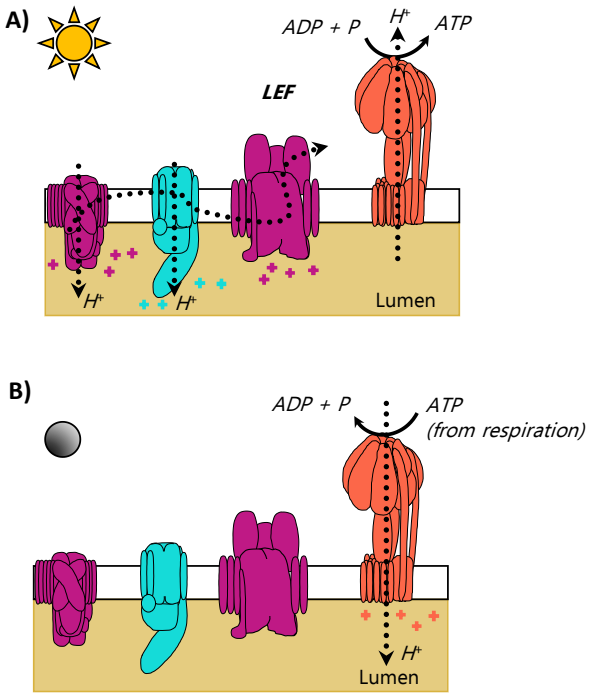

Figure 1. Schematic overview of the photosynthetic electron transport chain in Chlamydomonas reinhardtii under steady state light adapted (A) dark adapted (B) conditions. *Dotted black arrows indicate linear electron flow across the PETC and proton transport. Black dashed arrows indicate ATP transport. Black solid arrows indicate chemical reactions. Colored positive signs correspond to charge separations to their identical color complexes. Key complexes are shown from left to right (PSII; b_6f; PSI and ATPase respectively).*

This is why we chose to consider here two quinones with opposite structural properties, i.e. 2,6-DCBQ (2,6-dichloro-1,4-benzoquinone with Cl as an electron withdrawing group, EWG) and 2,6-DMBQ (2,6-methyl-1,4-benzoquinone with CH_3 as an electron donor group, EDG). From the model compounds, the changes in various experimental parameters providing information on each photosynthetic complex, as well as the activity (O_2 consumption, ATP production) of the respiratory chain, were investigated with the aim to define the first elements of a fingerprint for the action of a given quinone on bioenergetic membranes.

2. Methods

2.1. Cell culture and preparation

The T222 wild type laboratory strain of *Chlamydomonas reinhardtii* (hereafter referred to as WT) [22] was obtained from the Chlamystation (http://chlamystation.free.fr/). WT was grown in acetate phosphate aqueous medium (TAP = Tris base (20 mmol L^{-1}), NH_4Cl (7 mmol L^{-1}), $MgSO_4$ (0,83 mmol L^{-1}), $CaCl_2$ (0,45 mmol L^{-1}), K_2HPO_4 (1,65 mmol L^{-1}), KH_2PO_4 (1,05 mmol L^{-1}), CH_3CO_2H (0,3 mmol L^{-1}) [23] at 25°C under continuous dim light conditions (50 µmol photons m^{-2} s^{-1}) provided by white LEDs. From a cell suspension between 1 and $2*10^6$ cells mL^{-1}, algae are resuspended (after centrifugation at 4000g, 4 minutes) in their supernatant, while adding Ficoll® (to avoid drifts in the absorption measurements due to fast sedimentation of the cells) for future spectroscopy measurements (to a final concentration of $2*10^7$ cells mL^{-1}). Concentrated samples were then stirred at 300 rpm under very dim light conditions (10 µmol photons m^{-2} s^{-1} white light) before starting further measurements under light adapted or dark adapted conditions.

2.2. Inhibitors/Chemicals and solution preparation

2,6-Dichloro-1,4-benzoquinone (2,6-DCBQ), 2,6-Dimethyl-1,4-benzoquinone (2,6-DMBQ), (3,4-dichlorophenyl)-1,1-dimethylurea (DCMU), Antimicyn A (AA) have been purchased from Sigma Aldrich (Saint-Quentin-Fallavier, France) and diluted into ethanol to obtain fresh mother solutions (10 mmol L^{-1} for the quinones, 5 mmol L^{-1} for AA). PSII inhibition was obtained with 10 µmol L^{-1} DCMU and respiration was strongly inhibited at 5 µmol L^{-1} Antimicyn A. 2 mL of cell suspension was then used in plastic cuvettes for fluorescence or transient absorption measurements in the Joliot-Type Spectrometer (see below) or 500 µL was insered in the cuvette of the Clark electrode for respiration measurements.

2.3. Spectroscopic measurements

The Joliot-Type Spectrophotometer (JTS-10, Biologic, Grenoble, France) allows to perform both fluorescence and absorption difference measurements on the same sample.

Fluorescence induction is measured as follows: basal detecting pulses are provided by a white led filtered by a blue interference filter (470 nm). Actinic red light (AL; 340 µmol photons m^{-2} s^{-1}) as well as the saturating pulse (5000 µmol photons m^{-2} s^{-1}, corresponding to 2200 photons PSI^{-1} s^{-1}) are provided by orange leds (630 nm). The reference and measuring photodiodes are protected from actinic illumination by a BG39 Schott and a LPF650 + RG665 Schott filters respectively (Mainz, Germany). F_0 was measured after dark-adaptation for 1 minute, F was measured in the presence of a background continuous actinic light, once a steady-state is reached. F_m and F_m' were measured at the end of a 250 ms pulse of saturating light on dark-adapted or light-adapted samples, respectively. Fluorescence-based parameters were calculated as in reference [24]. PSII maximal quantum yield was measured as $F_v/F_m = (F_m - F_0)/F_m$, the PSII quantum yield in the light as $Y_{II} = (F_m'-F)/F_m'$ and the non-photochemical quenching as $NPQ = (F_m - F_m')/F_m'$.

To evaluate the photosensitivity of PSII as a function of the concentration of exogenous quinones, we used a fluorescence imaging system allowing to measure the above parameters in several samples concomitantly (e.g. 96 well plates).[25] The apparatus uses green actinic light (532 nm, 230 µmol

photons m^{-2} s^{-1}) and green saturating pulses (250 ms duration, 2100 µmol photons m^{-2} s^{-1}). The fluorescence is detected by the camera thanks to a high pass filter (> 680 nm, Schott) which cut the green actinic light. This setup was used for *Figures S1, S2* and *S3*.

For transient absorption changes measurements, we have used the same actinic light and saturating pulses. We also used single saturating laser flashes (6 ns, 520 nm) provided by a laser dye medium (LDS 698, 690 nm) pumped by an ND-YAG second harmonic laser (Minilite Continuum). Electrochromic shift (ECS) was measured as the difference of absorbance changes at 520 nm and 546 nm (to eliminate contributions from cytochrome *f*, P_{700} and scattering). The detecting light was provided by a white light filtered by interferential filters at the appropriate wavelength (520 +/- 6 nm or 546 +/- 6 nm). Both reference and measurement photodiodes are protected by cutoff filters (BG39 Schott filter, Mainz, Germany). All ECS data are normalized to the ECS increase produced 150 µs after a saturating laser flash under dark adapted conditions, which allows all photosystems to perform one charge separation.

P_{700} redox changes were measured as the difference between absorption changes at 705 nm and 735 nm, which eliminates most of the contribution from plastocyanins, ferredoxins and scattering. Photodiodes are protected by RG695 Schott filters. Normalization of the data is given by the change of absorption between dark-adapted sample (P_{700} fully reduced) and under strong illumination in the presence of 10 µmol L^{-1} DCMU (allowing almost complete oxidation of P_{700}). P_0 corresponds to the absorption signal in dark-adapted sample, P was measured in the presence of a background continuous actinic light, once a steady-state is reached. P_m and P_m' were measured at the end of a 20 ms pulse of saturating light on dark-adapted or light-adapted samples, respectively. Then Y_{NA} and Y_{ND} were calculated as a modified calculation of that reported in reference [26], where Y_I and Y_{ND} are calculated as $(P_m' - P)/(P_m - P_0)$ and $P/(P_m-P_0)$, respectively. Y_{NA} is calculated as $1 – Y_{ND} – Y_I$.

2.4. Respiration measurements

Chlamydomonas reinhardtii oxygen evolution rate was measured in a closed lid Clark O_2 electrode chamber (Hansatech) under high stirring at 20°C. All experiments began with a 2' period in darkness, followed by the addition of the according compound. Respiration rate (or oxygen consumption) was measured in the dark by calculating the rate of oxygen consumption over time (during 5'), 15' after adding the quinones. Controls were made for partial loss of respiration with 5 µmol L^{-1} Antimicyn A addition. Values obtained were normalized by the cell concentration to yield values expressed in nmol O_2 $cell^{-1}$ s^{-1}.

2.5. Calculations

Advanced Chemistry Development (ACD/Labs) Software V11.02 (© 1994-2023 ACD/Labs) has been used to calculate all theoretical modelling for both LogP values of DCBQ and DMBQ. All plots, fittings and statistical analyses were performed using SIGMA Plot 10.0 software (Systat Software Inc., Richmond, CA, USA) or OriginPro, Version 2021 (OriginLab Corporation, Northampton, MA, USA).

3. Results and discussion

3.1. Quinones structure and properties

In order to study the interaction between the PETC and quinones in the absence of electrocatalysis, we used a previously tested set-up, which is already established in the literature about quinones.[21, 27] In order to draw a clear-cut correlation between the effects on the algal photosynthesis (and bioenergetics in general) and the quinones chemistry, two extreme cases have been selected (*Figure 2*). In this respect, 2,6-DCBQ (with two Cl as EWGs) is considered to be one of the most oxidizing agents (in terms of E°' values for both QH_2/Q and Q^-/Q pairs) and therefore a good PSII acceptor (for instance the redox potential of the Q_A^-/Q_A acceptor in PSII is – 200 mV vs SHE). Conversely, 2,6-DMBQ has a more moderately oxidizing profile due to the CH_3 as EDGs. Even as electron withdrawing groups seem to correlate with oxidizing properties, it is worth considering the possible link between the steric hindrance of different substituents that could prevent the electron harvesting ability. This is why we only considered quinones substituted in 2- and 6- positions here. Furthermore, previous investigations in the laboratory suggests that quinones may be inactive by being sequestered within cell compartments or able to directly interact with excited chlorophylls (e. g. non-photochemical quenching).[20, 28] This is consistent with relatively lipophilic quinones, as confirmed by their partition coefficient "LogP" values higher than 1. Indeed, such a parameter corresponds to the repartition of a given species between a polar (water) and an apolar organic solvent (octal) and gives an estimation of the lipophilicity of the molecule.

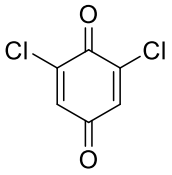

2,6-DCBQ
E°'(QH_2/Q) at pH 7
= + 315 mV vs SHE
E°(Q^-/Q) = + 221 mV vs SHE
LogP = 1.73

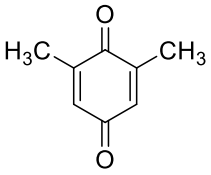

2,6-DMBQ
E°'(QH_2/Q) at pH 7
= + 174 mV vs SHE
E°(Q^-/Q) = -80 mV vs SHE
LogP = 1.22

Figure 2. *Structures and some physico-chemical properties of the two quinones (2,6-DCBQ and 2,6-DMBQ) investigated in this work.*

In our work, according with the previous investigations, a window of quinone concentration between 5 and 400 µmol L^{-1} has been selected. This indeed makes it possible to work between sub-toxic threshold and lipidic membrane trapping concentrations, and to study side effects at optimal photocurrent concentrations and to draw correlations between opposite quinone concentrations. Having previously seen how initially stable photocurrents diminish over time, all measurements have been taken less than one hour after algae were incubated with either quinones or inhibitors.

3.2. Algae incubation with exogenous quinones – effects on respiration and photosynthesis

First of all, the effect of quinone addition was investigated on the two energy-producing organelles. The photosynthesis activity in the chloroplast is followed through the yield of photosystem II (Y_{II}, the fraction of absorbed photons giving rise to photochemistry in PSII, i.e. initiating electron flux through PSII) and the respiratory activity (*Figure 1*) in the mitochondrion through O_2 consumption

measurements (see *Methods*). More particularly, a continuous diminution of Y_{II} over time was already observed in quinone-*Chlamydomonas reinhardtii* mixtures.[13] In our case, the measurement period (less than one hour after algae were incubated) remains consistent with a time range where the Y_{II} does not fluctuate significantly.

Furthermore, a continuous decrease of O_2 consumption was globally observed with increasing quinone concentration. In the presence of 10 µmol L^{-1} 2,6-DMBQ, no effect was observed but a sharp decrease of respiration occurred when concentration was increased to 25 µmol L^{-1} and an almost complete inhibition of respiration was obtained at 100 or 400 µmol L^{-1} (*Figure 3A*). The same behavior was observed with the 2,6-DCBQ except that the decrease of respiration occurred at lower quinone concentration (< 10 µmol L^{-1}). As a control, the respiration rate in the presence of the cytochrome bc_1 complex, Antimycin A (AA), is shown as grey dotted line (here and in other Figures) and corresponds to the residual activity of the Alternative Oxidase. These results indicate that both quinones inhibit the respiratory activity of *Chlamydomonas reinhardtii* which exhibits greater sensitivity to 2,6-DCBQ. To probe the effect of those quinones on the PETC, the activity of PSII in dark- and light- adapted cells was also monitored.

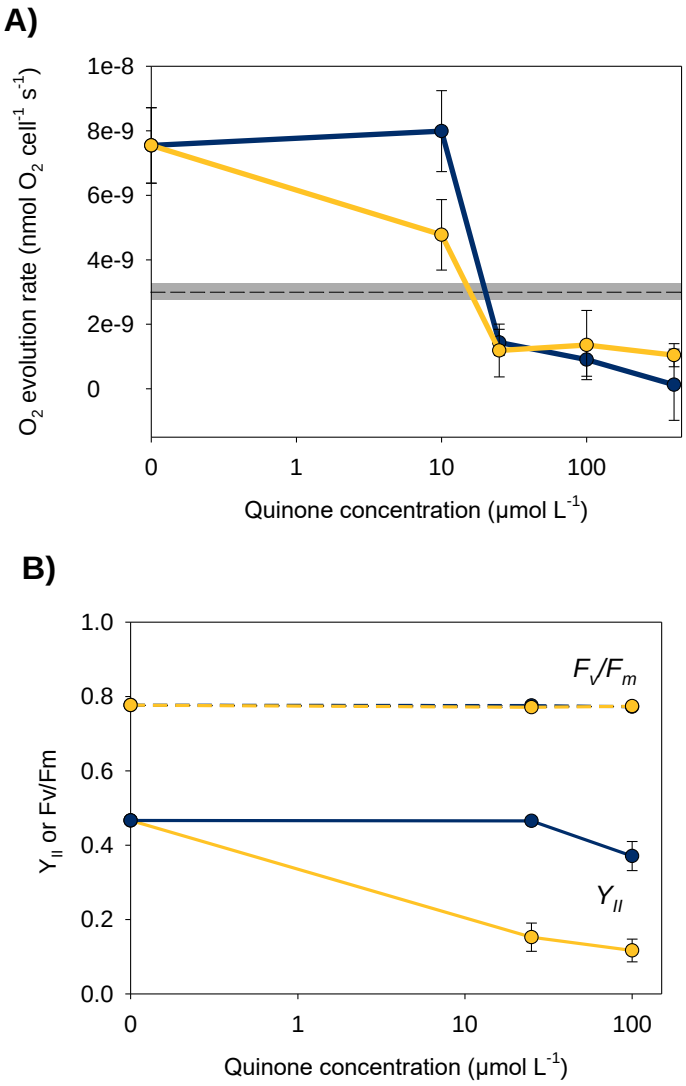

Figure 3. Chlamydomonas reinhardtii oxygen evolution rate over time in dark adapted conditions and quantum efficiency of PSII under steady state actinic light (WT cells; 2*10^7 cells mL^{-1}; I° = 340 µmol photons m^{-2} s^{-1}) and

***dark adapted conditions**. A) O_2 evolution rate (nmol cell^{-1} s^{-1}) measurements 15' after the addition of quinones or respiration inhibitors (AA) as a proxy for the respiration activity of the algae under dark adapted conditions. The grey dotted line and shadow correspond to Antimicyn A (5 µmol L^{-1}) inhibitor control (see Methods). B) Fluorescence measurements of PSII quantum efficiency (Y_{II}) after 40' in steady state actinic light (i.e. the % of photons which are used for photochemistry; continuous lines). Fluorescence measurements of PSII maximal quantum efficiency (F_v/F_m) after 40' in dark adapted conditions (dotted lines). Blue circles correspond to 2,6-DMBQ. Yellow circles correspond to 2,6-DCBQ. Data correspond to the mean ± S.D. of ten independent biological replicates for each kind of experiment.*

In the presence of an actinic background light (340 µmol photons m^{-2} s^{-1}, orange light, see *Methods*), the PSII yield was ~0.47 (i.e. 47 % of the photons absorbed are converted into photochemistry and electron transfer) in the control cells but decreased to values below 0.2 for concentrations of 25 or 100 µmol L^{-1} of 2,6-DCBQ (*Figure 3B*). Once again, 2,6-DMBQ showed a lower influence on PSII activity since no effect was seen at 25 µmol L^{-1} and only a slight decrease in Y_{II} was measured at 100 µmol L^{-1}. The results are consistent with previous photobioelectrochemical results showing a differentiated action of quinones, both in terms of structure (Cl = EWG; CH_3 = EDG) and concentration (100 µmol L^{-1} > 25 µmol L^{-1}).[11, 13] More particularly, a continuous diminution of Y_{II} over time was already observed in presence of exogenous quinones beyond one hour of incubation under dark conditions.[13] Such a decrease reveals *a posteriori* that the electron diverting by external quinones is more than counterbalanced by their toxicity towards the LEF. It has been indeed previously reported that quinones may act as Michael acceptors poisoning the algae.[29-31] As for respiration, our present data therefore indicate that both quinones influence PSII activity and linear electron flow (LEF) but with a greater sensitivity to DCBQ. Additionnally, this effect was not due to possible PSII damages since the maximum quantum yield of PSII (F_v/F_m) under dark conditions remained ~ 0.78 in the control as well as in the two treatments for the rather short illumination used here, in all tested concentrations. This clearly indicates that a step of the LEF is impaired in the presence of 25 or 100 µmol L^{-1} 2,6-DCBQ (and to a lower extent at 100 µmol L^{-1} 2,6-DMBQ), that is not in line with PSII capacity to perform photochemistry. Finally, in the present study, a decrease of the maximal yield of PSII (F_v/F_m) is observed after prolonged period of high light illumination. Compared to the situation in the absence of quinones (F_v/F_m decreases by ~20%), the loss of F_v/F_m was further enhanced in the presence of 10 µmol L^{-1} 2,6-DCBQ and more, or in the presence of 25 µmol L^{-1} 2,6-DMBQ and more (*Figure S1*). Comparing to dark conditions experiments, this also suggests photoinhibition effects.

3.3. Effect of exogenous quinones on PSI activity

As already mentioned elsewhere, both quinones are able to harvest photosynthetic electrons at the level of PSII acceptors *in Chlamydomonas reinhardtii*.[21, 27] Furthermore, quinones are known to dissipate excess of light energy as heat, by interacting with excited chlorophylls and bringing them back to the ground state, a phenomenon commonly known as non-photochemical quenching (NPQ).[32, 33] As evidenced in *Figure S2*, NPQ significantly increases as a function of quinone concentration. A linear relationship is observed for concentrations higher than 10 µmol L^{-1} as expected with previous measurements on this system.[19-21] However, such a quenching behavior has been shown not to be a limiting factor.[28] Considering there is little to no difference on the rise of NPQ for both 2,6-DCBQ and 2,6-DMBQ after light illumination (*Figure S3*), we have to assume other possible points of action on the PETC, which can explain the impairment of LEF and the enhanced photosensitivity. In this

respect, the study of redox changes of the special pair of PSI, P700, presents itself as an ideal candidate to observe the location of the electron flow impairment (*Figure 4A*). Indeed, a bottleneck uphill PSI would slow down the electron flow towards $P700^+$ and result in an oxidized P700 (donor-side limited PSI), whereas a bottleneck downhill PSI would impair the reoxidation of PSI acceptors (A) and result in the reduction of P700 (acceptor-side limited PSI). We measured the performance of PSI through the calculation of the PSI yield (the fraction of absorbed photons giving rise to photochemistry in PSI), and the donor and acceptor-side limitations of PSI (Y_I, Y_{ND} and Y_{NA} respectivey, see Methods).[26] The maximum quantum yield of PSI being close to 1,[34], PSI yield can be considered as the proportion of open PSI centers.

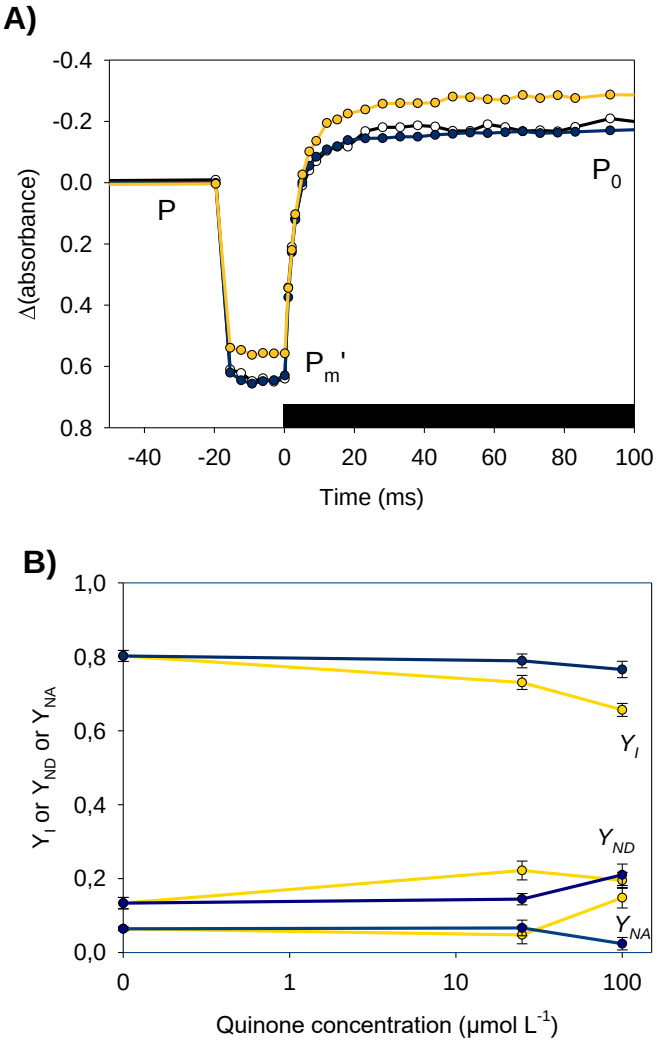

Figure 4. Chlamydomonas reinhardtii quantum efficiencies of PSI under steady state actinic light conditions (WT cells; 2*10^7 cells mL^{-1}; I° = 340 µmol photons m^{-2} s^{-1}). *A) Representative P_{700} absorbance kinetics. P is the basal state (arbitrary fixed at 0) corresponding steady state light adapted conditions (340 µmol photons m^{-2} s^{-1}; orange rectangle). P denotes the amount of closed centers [P_{700}^+A] under steady state actinic light. From this baseline, positive and negative values indicate P_{700}^+ (oxidized) and P_{700} (reduced) centers respectively. P_m' is reached after applying a saturating pulse (5000 µmol photons m^{-2} s^{-1}; red rectangle). P_0 is related to the total amount of PSI oxidized after the end of the pulse (black rectangle). P_m (P_{700} full oxidation) is obtained in the presence of DCMU and is not displayed for more clarity. B) The activity of PSI "Y_I" as a function of quinone concentration was calculated from these absorbance levels. Y_{NA} and Y_{ND} are derived from Y_I (see Methods). Y_I = PSI quantum efficiency, i.e. the % of protons that are converted in PSI charge separation; Y_{NA} = PSI donor side limitation; Y_{ND} = PSI acceptor side limitation. Blue, yellow and white circles correspond to 2,6-DMBQ (100 µmol L$^-$*

[1]), 2,6-DCBQ (100 µmol L^{-1}) and control conditions (no quinone) respectively. Black circles correspond to a control without quinone incubation. Data correspond to the mean ± S.D. of ten independent biological replicates.

In *Figure 4B* we can see how PSI yield diminishes after 40 minutes under steady state actinic light (340 µmol photons m^{-2} s^{-1}) in the presence of quinones. The impact of quinones on PSI yield is smaller than that on PSII yield, which probably indicates the stimulation of Cyclic Electron Flow (CEF) around PSI. CEF is an alternative pathway that does not involve PSII and plays an important role in photosynthesis regulation. Comparing PSI and PSII yields in the light is indeed routinely used to determine CEF [35] and here, Y_{II} decreases by ~2/3 when PSI yield decreases only by ~20% for 2,6-DCBQ at 100 µmol L^{-1}. The detailed analysis of P_{700} kinetics reveals that the slight decrease of Y_I comes with a slight increase of Y_{ND} (P_{700} is more oxidized) in the presence of each quinone, in accordance with the fact that the rate of electron transfer from PSII is diminished (*Figure 3B*). This is true for the highest concentration (100 µmol L^{-1}) of 2,6-DMBQ and already at 25 µmol L^{-1} 2,6-DCBQ in agreement with the quinones redox potential (*Figure 4C and 4D*). At this stage, the quinone seems to impair LEF uphill of PSI and, given the stimulation of CEF, most likely at the level of the PSII to plastoquinone electron transport which is not shared by CEF. This would explain the decrease of Y_{II}, the increase of Y_{ND} as well as the increased ratio of PSI/PSII activities (Y_I/ Y_{II}). It is to note that at the highest concetration (100 µmol L^{-1}) of 2,6-DCBQ, the Y_I decreases significantly and this is accompanied by the apparition of a limitation on the acceptor side of PSI (increased Y_{NA}) which could indicate that quinones become toxic for CEF also at very high concentrations.

3.4. Effect of exogenous quinones on proton transport across thylakoids

To give a more detailed and complete view of the interaction between quinones and the PETC, the generation of the proton motive force across the thylakoid was also investigated. During oxygenic photosynthesis, the light-induced electron transfer in the PETC is coupled to the translocation of protons across the thylakoidal membrane from the stroma to the lumen (*Figure 1*). This movement generates an electrochemical proton gradient ($\Delta\mu_H^+$) or proton motive force (PMF), composed of both an electric field (Δψ) and a proton gradient ΔpH (*Figure 5A*). The PMF will subsequently power the synthesis of adenosine triphosphate (ATP) from adenosine diphosphate (ADP) and inorganic phosphate (P) by the CF_1F_O ATPsynthase (*Figure 1*). The generation of PMF (more exactly its electric component) and its consumption by the CF_1F_O can be probed by the so called electrochromic shift (ECS). In the presence of the electric field (Δψ) generated by photosynthetic activity, some of the photosynthetic pigments embedded in the thylakoid membrane will see their absorption spectra modified (Stark effect; *Figure 5B*).[36-38] In this regard, this light-induced variation of absorption provides a quantitative measurement of the electric component of the PMF because ECS works in practice as an *in vivo* voltmeter.

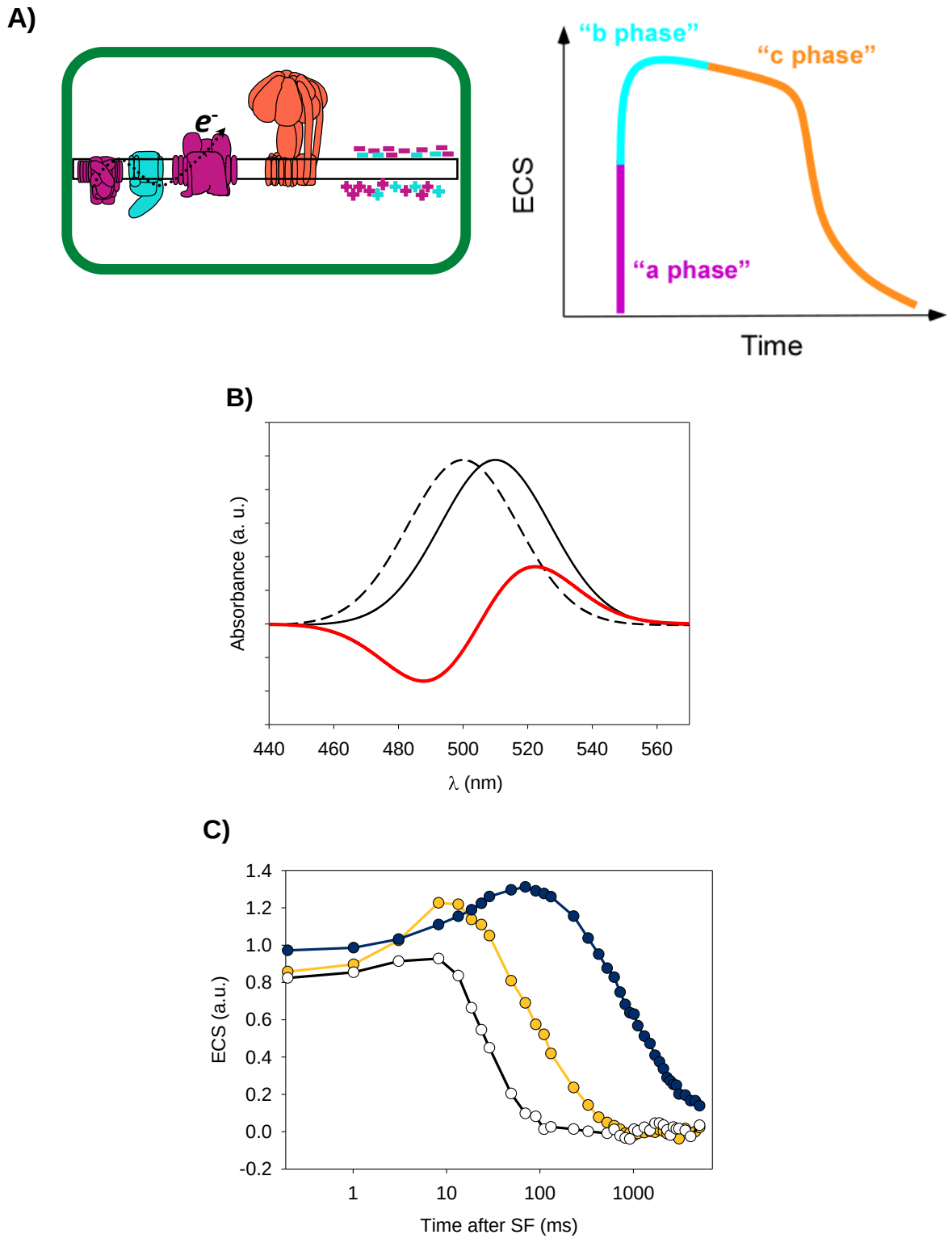

Figure 5. Chlamydomonas reinhardtii experimental – like linear Electro-Chromic Shift (ECS) kinetics upon excitation with a saturating laser flash under dark adapted conditions*. A) Representation of an electrochemical proton gradient $\Delta\mu_H^+$ on the photosynthetic chain, charges coded according to their origin (PSI/PSII in purple and cytochrome b_6f in turquoise). ATPase is colored in orange. (B) The presence of the electric field (Δψ) is caused by the translocation of protons across the thylakoid membrane. It therefore produces a change in the absorption spectra of photosynthetic pigments (dashed line: no electrical field; solid line: with an electrical field) due to the Stark effect. Such a difference (red line) at a specific wavelength according to the species is visible at 520 nm for Chlamydomonas reinhardtii). Of note, the absorption changes are effectively proportional to the activity of the*

photosynthetic electron transport chain complexes (PSI, PSII, cytochrome b_6f and ATPase). C) Three different phases occur after applying a saturating flash (SF): the fast rise phase or "a" phase (purple), the "b phase" (light blue) and the "c phase" (orange). D) Flash induced ECS (referred as "single turnover") traces for 2,6-DMBQ (25 µmol L^{-1}; blue trace) or 2,6-DCBQ (10 µmol L^{-1}; yellow trace) or no quinone incubation control (black trace). Please note that the curve is given on a logarithmic scale.

The ECS kinetics following a saturating laser flash (SF; *Figure 5C*) was used to probe the effect of exogenous quinones on each photosynthetic complex (PSI, PSII, b_6f, ATPase).[39] Indeed, the photosystems and b_6f generate an electric field *after a saturating laser flash*, by generating/moving positive charges (protons, oxidized plastocyanin) inside the lumen. This happens in two phases. First, 150 µs after the flash, all photosystems I and II have performed one - and only one - charge separation increasing the electric field by as much ("a phase", purple). Then a second phase ("b phase", ~10 ms, blue) corresponds to the electron transfer from plastoquinols to plastocyanin catalyzed by the cytochrome b_6f (*Figure 5C*) and coupled to the pumping of two protons. Finally, the last phase of ECS kinetics ("c phase", red) corresponds to the ATPase-catalyzed consumption of the flash-induced proton motive force, resulting in the relaxation of the ECS (*Figure 5A*).

The flash-induced ECS kinetics was measured after 15 minutes of incubation with various concentrations of the two quinones (2,6-DCBQ; 2,6-DMBQ; *Figure 5C*). No significant difference was observed regarding the "a phase" indicating that PSI and PSII functions were not altered by the incubation with exogenous quinones (*Figures 5C* and *6A*). This is in line with the unaffected F_v/F_m value (*Figure 3B*) and the conservation of active PSI (not shown) after short illumination. In contrast, the kinetics of the "c" phase was affected by the two quinones (*Figures 5D and 6B*) indicating a slow down of the proton export through the CF_1F_0 Atpase. The effect on the "b" phase was not easy to assess. Indeed, when the "c" phase is fast, i.e. the CF_1F_0 is highly active, the "b" phase appears shortcuted leading to under-estimations of its amplitude and rate (Buchert et al, 2021). For this reason, we report only the amplitude of the "b" phase when the half-time of ECS relaxation ("c" phase) was greater than 100 ms (*Figure 6C*). The analysis of the "b" phase suggested an inhibition of the plastoquinol to plastocyanin electron transfer catalyzed by the cytochrome b_6f turnover. To confirm this inhibition and explore also the amplitude of the "b" phase under low quinone concentration, we searched for a condition when the "c" phase was artificially slowed-down. This is the case in the presence of the cytochrome bc_1 inhibitor, Antimycin A (AA), which slows down the ATPsynthase because of chloroplast-mitochondrial ATP exchange (see [40] and below). The amplitude of the "b" phase was shown to be half that of the "a" phase, as expected theoretically, in the control conditions and under low concentration of exogenous quinone. Furthermore, the inhibition of the « b phase » is greater in the presence of Antimycine A at a given quinone concentration. But most importantly, the inhibition of the "b" phase under high concentration of exogenous quinone, was confirmed, indicating that 2,6-DCBQ and 2,6-DMBQ inhibit the electron transfer from plastoquinol to plastocyanin, which is coupled to proton pumping giving rise to the "b" phase[40]. Again, the poorest accepting quinone (2,6-DMBQ) lag in its inactivation of the "b" and "c" phases compared to 2,6-DCBQ (*Figure 6B and 6C*).

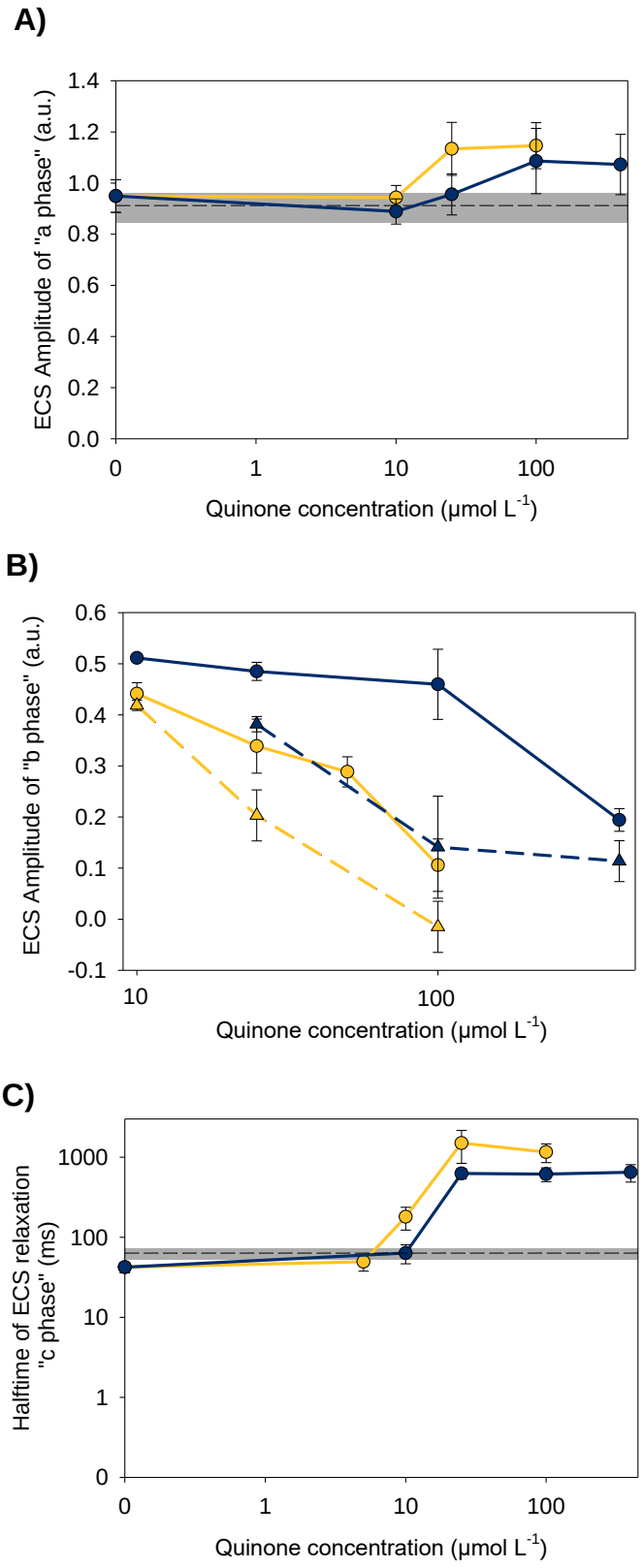

Figure 6. Dark adapted ATPase electrochromic shift (ECS) laser flash single turnover kinetics as a function of quinone concentration*. Blue circles correspond to 2,6-DMBQ (0-400 µmol L^{-1}). Yellow circles correspond to 2,6-DCBQ (0-100 µmol L^{-1}). A) Maximal amplitude of "a phase". B) Maximal amplitude of "b phase" without (circles and straight line) or with (triangles and dotted line) Antimicyn A (5 µmol L^{-1}). C) ECS "c phase" relaxation (calculated as $t_{1/2}$ values). The grey dotted line and shadow in A) and C) correspond to Antimicyn A (5 µmol L^{-1}) inhibitor control (see Methods). The amplitude of the "b phase" is underestimated when the ECS relaxation is too*

fast (when the duration of the "c phase" becomes comparable with the duration of the "b phase", i.e. few tens of ms). This is the reason why we discarded all "b phase" calculations in panel B when the $t_{1/2}$ of "phase c" (panel C) was lower than 100 ms. Data correspond to the mean ± S.D. of at least three independent biological replicates relaxation after a saturating laser flash under dark adapted conditions (WT cells; $2*10^7$ cells mL^{-1}).

Nevertheless, a decrease in the relaxation time of ECS is ambiguous to interpret[41]. This could either mean that i) the CF_1F_O ATPase is directly affected by quinones and it is no longer able to pump protons across the thylakoidal membrane in the presence of exogenous quinones, ii) the CF_1F_O ATPase is in the "inactivated" form because of a decrease in the dark-adapted PMF.[40, 42] Indeed, it is known that ATPase can be in an active or inactive form depending on whether the dark-adapted PMF is above or below a threshold value, respectively.[40, 42, 43] Discriminating between a direct (degradation) or indirect (PMF regulation) effect of exogenous quinones is possible thanks *to the use of multiple turnover pulses*.[41] This can be explained by a simple analogy (but see [38] for further explanation) : one can estimate the water volume contained in an opaque bottle through the volume of water to be added till it spills out (which is equal to the initialy "empty" volume of the bottle). Here, the amount of positive charges (mostly protons) to be pumped in the lumen before protons leak out of the membrane informs us about the pedestal of PMF present in the dark and can be measured through ECS. In brief, the highest the amplitude of the ECS increase during a saturating pulse of light, the lowest the PMF pre-existing before the pulse.

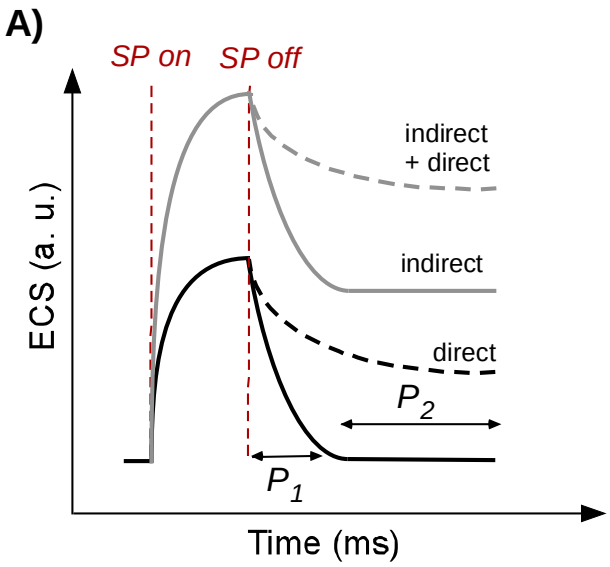

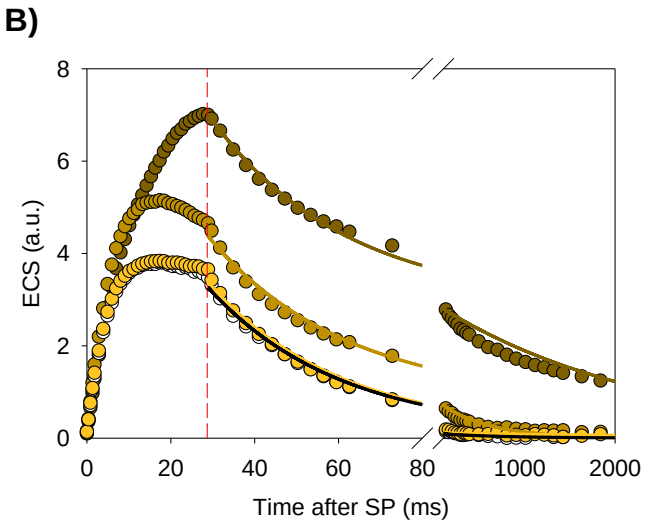

Figure 7. ECS "multiple turnover" strategy to distinguish direct/indirect effects on ATPase in PETC*. A) Schematic ECS kinetics durinf a "multiple turnover" pulse and its two-phased relaxation from dark adapted and quinone incubated cells in line with the action mechanism of ATPase deactivation. Black solid line corresponds to control conditions. Different curves are expected depending on the nature of the effect on the ATPase: indirect (gray solid line); direct (black dashed line) or both direct and indirect (gray dashed line). The two phases of relaxation (exponential decay according to $A_i exp(-k_i t)$) are indicated by double arrows. The slow (left; P_2) and fast (right; P_1) phases are referred to (A_2, t_2) and (A_1, t_1) parameters respectively (where A_i is the maximal amplitude and t_i is the half-time according to $t_i = ln2/k_i$). B) Typical experimental trace of ECS multiple turnover under dark adapted conditions (WT cells; $2*10^7$ cells mL^{-1}). Dark yellow circles correspond to 2,6-DCBQ (100 µmol L^{-1}). Medium yellow circles correspond to 2,6-DCBQ (25 µmol L^{-1}). Yellow circles correspond to 2,6-DCBQ (5 µmol L^{-1}). Black circles correspond to control solutions without quinones. Associated color relaxation curves correspond to their respective fits. Time zero corresponds to saturating pulse (SP; 5000 µmol photons m^{-2} s^{-1}) start. Red dotted line indicates saturating pulse on and off. The period of interest (0-80 ms) is displayed with a linear scale for more clarity. The rest (200 – 2000 ms) is depicted on a compacted scale after a break (80-200 ms).*

Indeed, a decrease in the intrinsic capacity of ATPase to consume the electric field should lead to a slowdown of the whole ECS relaxation phase (black dashed line in *Figure 7A*). An indirect effect through the decrease of the PMF below the threshold of ATPase activation would, at the contrary, result in a greater amplitude of the pulse-induced ECS and a biphasic decay of ECS (gray solid line in *Figure 7A*). A combination of direct and indirect effect would result both in a slowdown of the fast phase and an increase of the amplitude of the slow phase.

In the control condition, the ECS increase upon a multiple turnover pulse is ~4 times bigger than after a single turnover flash. The pulse-induced ECS kinetics in the presence of various concentrations of 2,6-DCBQ show both an increase in the total amplitude of the ECS rise (up to 8 charge separations per photosystems at 100 µmol L^{-1} 2,6-DCBQ) and the apparition of two phases in the relaxation (significant at 25 µmol L^{-1}, even more pronounced at 100 µmol L^{-1}). The slow phase lasts few seconds, whereas the fast phase is finished in 100 ms and does not seem to be affected by exogenous quinones (*Figure 7B*). This points to an indirect effect of the exogenous quinones on the activity of the CF_1F_O ATPase, through the "a" decrease of the PMF in the dark.

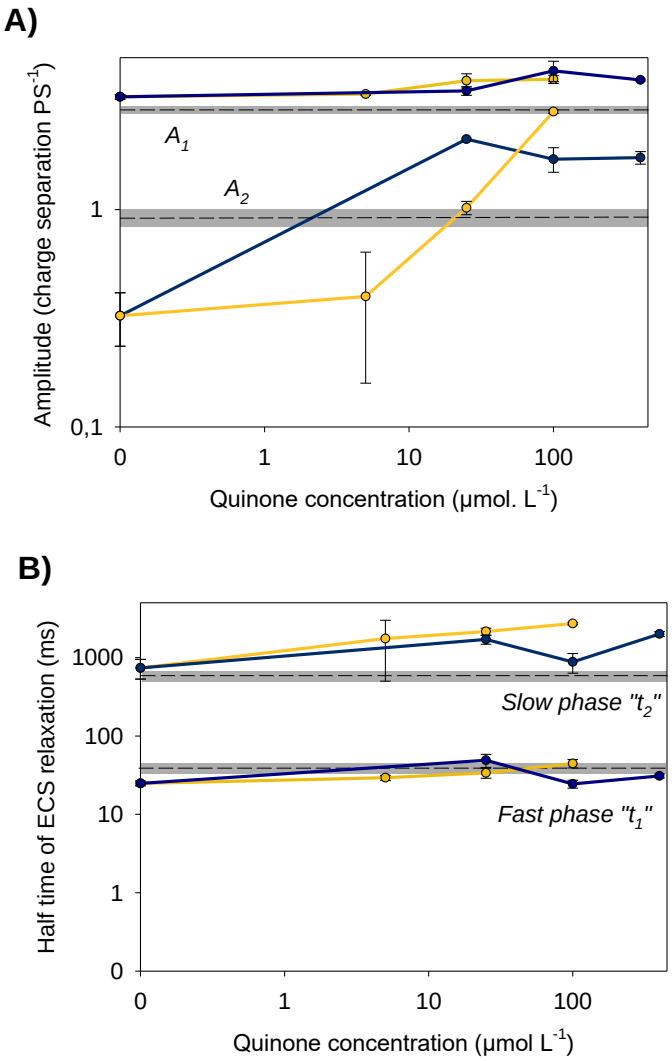

Figure 8. Kinetic data from Electrochromic shift (ECS) multiple turnover measurements *in presence of quinones. A) Top: ECS multiple turnover relaxation "fast phase" (P_1) maximal amplitude (A_1) 15' after addition of quinones normalized to the maximal amplitude of ECS single turnover (i.e. one saturating flash; see above) "a phase". Bottom: ECS multiple turnover relaxation "slow phase" (P_2) maximal amplitude (A_2) 15' after addition of quinones, normalized to the maximal amplitude of ECS single turnover "a phase". B) Top: ECS multiple turnover "slow phase" (P_2) relaxation time (t_2) 15' after addition of quinones. Bottom: ECS multiple turnover "fast phase" (P_1) relaxation constant (t_1) 15' after addition of quinones. Blue and yellow traces correspond to 2,6-DMBQ and 2,6-DCBQ respectively. The grey dotted line and shadow correspond to Antimicyn A inhibitor control (5 µmol L^{-1}; see Methods). All data correspond to the mean ± S.D. of three independent biological replicates relaxation and result from experiments with saturating light pulses (5000 µmol photons m^{-2} s^{-1}) under dark adapted conditions (WT cells; $2*10^7$ cells mL^{-1}).*

A more quantitative analysis of the ECS relaxation was performed after a multiple turnover pulse (*Figure 8*) by deconvoluting the ECS relaxation as a biexponential decay (a fast exponential component of amplitude A_1 and half-life time t_1 and a slow exponential component of amplitude A_2 and half-life time t_2). After analysis, the fast phase of ECS decay did not seem to be severely affected by the exogenous quinones, ranging from 20 ms (control value) to 40 ms (value obtained with 5 µmol L^{-1} Antimycin A; *Figure 8B*). Conversely, the amplitude and kinetics of the slow phase was strongly dependent on the presence of exogenous quinones (*Figures 8A and 8B*). At 100 µmol L^{-1} 2,6-DCBQ, the

amplitude of this slow phase was ~3 charge separations per PS, almost equivalent to the total ECS increase in control conditions (*Figure 8A*).

The presence of a PMF in the dark in control conditions is a robust observation in plants, green algae or diatoms which has been explained by the energetic coupling of the PETC and the respiratory chain (*Figure 1*).[41, 42, 44, 45] Indeed, the CF_1F_O ATPase being reversible, it can synthesize or hydrolyze ATP depending on the extent of the PMF and on the [ATP]/[ADP][P] ratio. In the dark, the only source of ATP is the mitochondrial respiration and the presence of a PMF in the dark has been interpreted as the hydrolysis of ATP generated in the mitochondrion. In agreement with this interpretation, the addition of Antimycin A (an inhibitor of the complex III and of the classical respiratory pathway) increases the amplitude of the slow phase (*Figure 8A*) which indicates a PMF decrease in the dark below the threshold of ATPase activation. The effect of Antimycin A is incomplete since the alternative respiratory pathway, involving complex I and the Alternative Oxidase, is still active in those conditions and still provides ATP.[40] In this view, the A_2 increase in the presence of the two exogenous quinones reflects the decrease of the PMF "pedestal" in the dark which is in line with the inhibition of O_2 evolution rate in the dark with 2,6-DCBQ and 2,6-DMBQ (*Figure 3A*). When the mitochondrial respiration is plotted as a function of the amplitude of the slow phase, a monotonous relationship is observed across all treatments, i.e. Antimycin A, 2,6-DCBQ and 2,6-DMBQ (*Figure 9*) which further indicates that changes in CF_1F_0 performances are entirely due to the indirect effect of respiratory inhibition on the PMF, independently of the nature of the respiratory inhibitor.

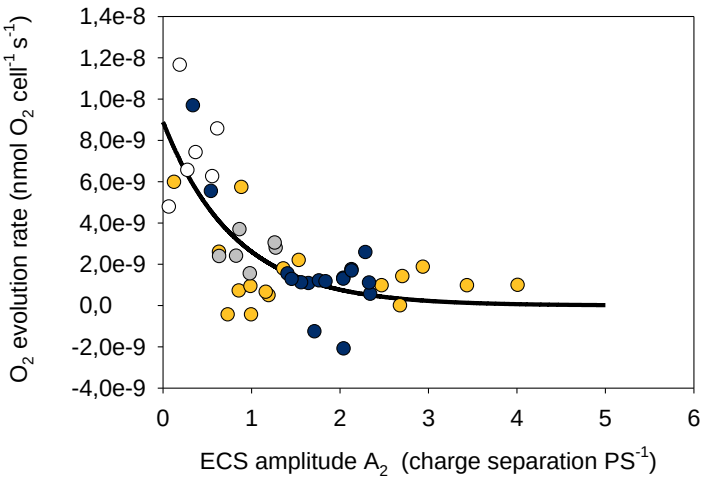

Figure 9. Comparison of Chlamydomonas reinhardtii O_2 evolution rate and ATPase relaxation kinetics in the presence of quinones. *Correlation of O_2 evolution rate activity to the maximal amplitude of ECS multiple turnover slow phase for all quinone (2,6-DCBQ; yellow/2,6-DMBQ; blue) concentrations (0-400 µmol L^{-1}) or with no quinones control (empty dot) and AA control (grey dot). The solid line corresponds to a monoexponential decay.*

Taken the data altogether as a composite, a good agreement is obtained for the hypothesized scenario in which, for short time incubations with quinones, the highest the inhibition of O_2 consumption the lowest ATP is hydrolyzed by the CF_1F_O ATPase, the lowest the dark-adapted "pedestal" PMF and the highest the amplitude of the slow phase of ECS relaxation after a saturating pulse of light. Both 2,6-DCBQ and 2,6-DMBQ action modes align with their respective oxidizing/lipophilic properties, and their shifted action upon the algae, albeit the full inhibition of the

respiratory chain occurs immediately after incubation without any time delay whereas the suppression of the dark PMF takes 5 to 15 minutes to occur (*data not shown*). It could reflect the delay between the decrease in mitochondrial ATP production and the consumption of the ATP pool in the cell. Moreover, 2,6-DMBQ does not follow a monotonous decrease of the PMF pedestal. At high 2,6-DMBQ concentrations of, the ECS decay reaccelerates after extended incubations (*data not shown*) which suggests the activation of fermentation pathway under long anaerobic periods to provide ATP as previously observed in *Chlamydomonas.*[46]

4. Conclusion

Previously, studies have tentatively tried to elucidate the action mechanisms of quinones on the bioenergetic processes of *Chlamydomonas reinhardtii*.[13, 47] In the present work (*Figure 10*), by using two canonical exogenous quinones, with a high (2,6-DCBQ) or moderate (2,6-DMBQ) redox potential, we have tempted to structure a first rationale of their effect on the PETC of the algae as in [48]. In this respect, this study has combined previously loosely connected results for the activity of exogenous quinones on PSII and ATPase activities [13] and added measurements of PSI activity (and the extent of its donor- and acceptor-side limitations) as well as the activity of the respiratory chain and inter-organelle energetic interactions. Beyond the NPQ[21] and recently evidenced interactions with chlorophyll,[49] the global concentration-dependent action of quinones (*Figure 10*) seems to consist in i) an inhibition of electron transfer between PSII and the cytochrome b_6f and an increase in PSII photosensitivity, ii) the stimulation of Cyclic Electron Flow around PSI and electron rerouting towards oxidized external quinones, iii) the inhibition of mitochondrial respiration and resulting decrease in the PMF across the thylakoids and iv) in turn an inactivation of the chloroplastic ATPase visualized by a slower relaxation of the PMF generated by a single turnover flash. Yet, several gaps still need to be uncovered. While these experiments indicate that the electron transfer between PSII and the cytochrome b_6f is impaired, there is no clear picture as to the mechanism of this impairement (e.g. inhibition at the level of the quinone exchange at the Q_B site or decreased mobility of the plastoquinols in between the two complexes) while the PQ pool is also an expected site of interaction.[18] Additionally, we have shown that incubation of *Chlamydomonas* cells with external quinones leads to the PMF decrease and the inactivation of the CF_1F_O ATPase, it would be of interest to study the effect of quinones on ATPase under light adapted conditions. Once a better understanding of the interaction of external quinones with the PETC is reached, the role of PSI as electron pool for quinone harvesting will be worth being revisited.

Making the analysis of the quinone structure – activity interaction on the PETC only in the presence of two quinones might not be sufficient, as it has been previously conveyed that i) PSII yield and photocurrent do not properly correlate, giving rise to differentiated action modes amongst quinones and ii) maximum current values do not converge for all quinones with increasing concentrations.[13] All in all, a rationale for choosing a broader range of quinones to establish a quinone fingerprint including the following values must be established: redox potential, LogP, NPQ, size, stability, effect on the ATPase, on the respiratory chain and on PSI/PSII activity. It would be important to extend the approach used in this work to a larger group of quinones or other potential mediators. Also, given the differences in time incidences, it would be interesting to work in longer and shorter time spans.

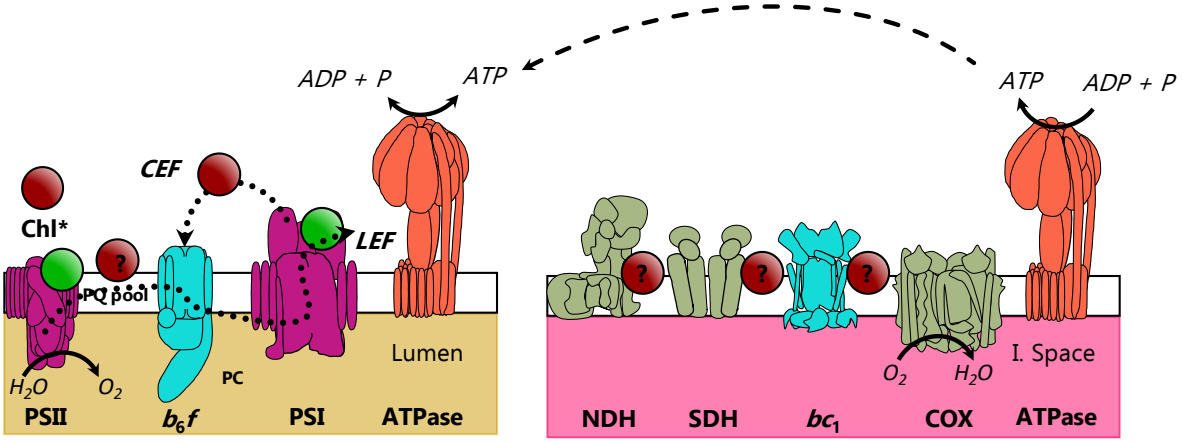

Figure 10. Schematic overview of the quinone effect on the photosynthetic electron transport chain (PETC) in Chlamydomonas reinhardtii chloroplasts and ATPase activity in mitochondria. *Black dashed arrows indicate ATP transport. Green dots indicate harvesting quinone effects (2,6-DCBQ, 2,6-DMBQ). Undesired quinone effects are shown with a red degraded dot on the suspected site of action.*

Acknowledgements

This work has been supported in part by CNRS (UMR 8640, UMR 7141), Ecole Normale Supérieure, French Ministry of Research, Faculté des Sciences et Ingénierie – Sorbonne Université and the "Initiative d'Excellence" program from the French State (Grant "DYNAMO", ANR-11-LABX-011-01). M.G.-C. thanks Institut Universitaire de France Fellowship Program. B.B. acknowledge financial support from the European Research Council (ERC) under the European Union Horizon 2020 research and innovation program (grant agreement no. 715579).

References

[1] G.T. Krayz, S. Bittner, A. Dhiman, J.Y. Becker, Electrochemistry of Quinones with Respect to their Role in Biomedical Chemistry, Chem. Rec, 21 (2021) 2332-2343.
[2] E. Laviron, Electrochemical Reactions With Protonations At Equilibrium .10. The Kinetics Of The Para-Benzoquinone Hydroquinone Couple On A Platinum-Electrode, J. Electroanal. Chem., 164 (1984) 213-227.
[3] M.M. Braasch-Turi, J.T. Koehn, D.C. Crans, Chemistry of Lipoquinones: Properties, Synthesis, and Membrane Location of Ubiquinones, Plastoquinones, and Menaquinones, Int. J. Mol. Sci., 23 (2022) 12856.
[4] D. Deamer, Electrochemical energy for living systems, Curr. Opin. Electrochem., 29 (2021) 100742.
[5] A.E. Wendlandt, S.S. Stahl, Quinone-Catalyzed Selective Oxidation of Organic Molecules, Angew. Chem. Int. Ed., 54 (2015) 14638-14658.
[6] Y. Song, G.R. Buettner, Thermodynamic and kinetic considerations for the reaction of semiquinone radicals to form superoxide and hydrogen peroxide, Free Radical Biol. Med., 49 (2010) 919-962.
[7] P. Symons, Quinones for redox flow batteries, Curr. Opin. Electrochem., 29 (2021) 100759.
[8] J.L. Bolton, M.A. Trush, T.M. Penning, G. Dryhurst, T.J. Monks, Role of quinones in toxicology, Chem. Res. Toxicol., 13 (2000) 135-160.
[9] M. Grattieri, K. Beaver, E.M. Gaffney, F.Y. Dong, S.D. Minteer, Advancing the fundamental understanding and practical applications of photo-bioelectrocatalysis, Chem. Commun., 56 (2020) 8553-8568.
[10] N.S. Weliwatte, M. Grattieri, S.D. Minteer, Rational design of artificial redox-mediating systems toward upgrading photobioelectrocatalysis, Photochem. Photobiol. Sci., 20 (2021) 1333-1356.
[11] A. Sayegh, G. Longatte, O. Buriez, F.A. Wollman, M. Guille-Collignon, E. Labbe, J. Delacotte, F. Lemaitre, Diverting photosynthetic electrons from suspensions of Chlamydomonas reinhardtii algae - New insights using an electrochemical well device, Electrochim. Acta, 304 (2019) 465-473.
[12] K. Hasan, Y. Dilgin, S.C. Emek, M. Tavahodi, H.-E. Akerlund, P.-A. Albertsson, L. Gorton, Photoelectrochemical Communication between Thylakoid Membranes and Gold Electrodes through Different Quinone Derivatives, ChemElectroChem, 1 (2014) 131-139.
[13] A. Sayegh, L.A. Perego, M.A. Romero, L. Escudero, J. Delacotte, M. Guille-Collignon, L. Grimaud, B. Bailleul, F. Lemaitre, Finding Adapted Quinones for Harvesting Electrons from Photosynthetic Algae Suspensions, ChemElectroChem, 8 (2021) 2968-2978.
[14] E.R. Clifford, R.W. Bradley, L.T. Wey, J.M. Lawrence, X.L. Chen, C.J. Howe, J.Z. Zhang, Phenazines as model low-midpoint potential electron shuttles for photosynthetic bioelectrochemical systems, Chem. Sci., 12 (2021) 3328-3338.
[15] J.Z. Zhang, P. Bombelli, K.P. Sokol, A. Fantuzzi, A.W. Rutherford, C.J. Howe, E. Reisner, Photoelectrochemistry of Photosystem II &ITin Vitro&IT vs&IT in Vivo&IT, J. Am. Chem. Soc., 140 (2018) 6-9.
[16] H.Y. Fu, D. Picot, Y. Choquet, G. Longatte, A. Sayegh, J. Delacotte, M. Guille-Collignon, F. Lemaitre, F. Rappaport, F.A. Wollman, Redesigning the Q(A) binding site of Photosystem II allows reduction of exogenous quinones, Nat. Commun., 8 (2017).

[17] K. Satoh, H. Koike, T. Ichimura, S. Katoh, Binding Affinities Of Benzoquinones To The Q(B) Site Of Photosystem-Ii In Synechococcus Oxygen-Evolving Preparation, Biochim. Biophys. Acta, 1102 (1992) 45-52.
[18] K. Satoh, M. Ohhashi, Y. Kashino, H. Koike, Mechanism Of Electron Flow-Through The Qb Site In Photosystem-II .1. Kinetics Of The Reduction Of Electron-Acceptors At The Q(B) And Plastoquinone Sites In Photosystem-II Particles From The Cyanboacterium Synechococcus-Vulcanus, Plant Cell Physiol., 36 (1995) 597-605.
[19] G. Longatte, A. Sayegh, J. Delacotte, F. Rappaport, F.A. Wollman, M. Guille-Collignon, F. Lemaitre, Investigation of photocurrents resulting from a living unicellular algae suspension with quinones over time, Chem. Sci., 9 (2018) 8271-8281.
[20] L. Beauzamy, J. Delacotte, B. Bailleul, K. Tanaka, S. Nakanishi, F.A. Wollman, F. Lemaitre, Mediator-Microorganism Interaction in Microbial Solar Cell: a Fluo-Electrochemical Insight, Anal. Chem., 92 (2020) 7532-7539.
[21] G. Longatte, H.Y. Fu, O. Buriez, E. Labbe, F.A. Wollman, C. Amatore, F. Rappaport, M. Guille-Collignon, F. Lemaitre, Evaluation of photosynthetic electrons derivation by exogenous redox mediators, Biophys. Chem., 205 (2015) 1-8.
[22] S.D. Gallaher, S.T. Fitz-Gibbon, A.G. Glaesener, M. Pellegrini, S.S. Merchant, Chlamydomonas Genome Resource for Laboratory Strains Reveals a Mosaic of Sequence Variation, Identifies True Strain Histories, and Enables Strain-Specific Studies, Plant Cell, 27 (2015) 2335-2352.
[23] E.H. Harris, The Chlamydomonas sourcebook: a comprehensive guide to biology and laboratory use, Academic Press, San Diego, 1989.
[24] B. Genty, J.M. Briantais, N.R. Baker, The relationship between the quantum yield of photosynthetic electron-transport and quenching of chlorophyll fluorescence, Biochim. Biophys. Acta, 990 (1989) 87-92.
[25] X. Johnson, G. Vandystadt, S. Bujaldon, F.A. Wollman, R. Dubois, P. Roussel, J. Alric, D. Beal, A new setup for in vivo fluorescence imaging of photosynthetic activity, Photosynth. Res., 102 (2009) 85-93.
[26] C. Klughammer, U. Schreiber, An Improved Method, Using Saturating Light-Pulses, For The Determination Of Photosystem-I Quantum Yield Via P700+-Absorbency Changes At 830 Nm, Planta, 192 (1994) 261-268.
[27] G. Longatte, F. Rappaport, F.A. Wollman, M. Guille-Collignon, F. Lemaitre, Mechanism and analyses for extracting photosynthetic electrons using exogenous quinones - what makes a good extraction pathway?, Photochem. Photobiol. Sci., 15 (2016) 969-979.
[28] L. Beauzamy, F. Lemaitre, J. Derr, Underlying mechanisms in microbial solar cells: how modeling can help, Sustain. Energy Fuels, 4 (2020) 6004-6010.
[29] A. Brunmark, E. Cadenas, Oxidation of quinones by H2O2: formation of epoxy- and hydroxyquinone adducts and electronically excited states, Basic Life Sci., 49 (1988) 81–86.
[30] X.W. Guo, H. Mayr, Quantification of the Ambident Electrophilicities of Halogen-Substituted Quinones, J. Am. Chem. Soc., 136 (2014) 11499-11512.
[31] T.J. Monks, R.P. Hanzlik, G.M. Cohen, D. Ross, D.G. Graham, Quinone Chemistry And Toxicity, Toxicol. Appl. Pharmacol., 112 (1992) 2-16.

[32] K.K. Karukstis, S.C. Boegeman, J.A. Fruetel, S.M. Gruber, M.H. Terris, Multivariate-Analysis Of Photosystem-Ii Fluorescence Quenching By Substituted Benzoquinones And Naphthoquinones, Biochim. Biophys. Acta, 891 (1987) 256-264.
[33] K.K. Karukstis, S.M. Gruber, J.A. Fruetel, S.C. Boegeman, Quenching of chlorophyll fluorescence by substituted anthraquinones, Biochim. Biophys. Acta, 932 (1988) 84-90.
[34] N. Nelson, Plant Photosystem I - The Most Efficient Nano-Photochemical Machine, J. Nanosci. Nanotechnol., 9 (2009) 1709-1713.
[35] D.Y. Fan, D. Fitzpatrick, R. Oguchi, W.M. Ma, J.C. Kou, W. Chow, Obstacles in the quantification of the cyclic electron flux around Photosystem I in leaves of C3 plants, Photosynth. Res., 129 (2016) 239-251.
[36] B. Bailleul, P. Cardol, C. Breyton, G. Finazzi, Electrochromism: a useful probe to study algal photosynthesis, Photosynth. Res., 106 (2010) 179-189.
[37] J. Stark, Beobachtungen über den Effekt des elektrischen Feldes auf Spektrallinien. I. Quereffekt Ann. Phys. (Berlin), 348 (1914).
[38] H.T. Witt, Energy-Conversion In The Functional Membrane Of Photosynthesis - Analysis By Light-Pulse And Electric Pulse Methods - Central Role Of The Electric-Field, Biochim. Biophys. Acta, 505 (1979) 355-427.
[39] P. Joliot, R. Delosme, Flash-Induced 519nm Absorption Change In Green-Algae, Biochim. Biophys. Acta, 357 (1974) 267-284.
[40] F. Buchert, B. Bailleul, P. Joliot, Disentangling chloroplast ATP synthase regulation by proton motive force and thiol modulation in Arabidopsis leaves, Biochim. Biophys. Acta Bioenerg., 1862 (2021) 148434.
[41] M. Long, A. Peltekis, C. Gonzalez-Fernandez, H. Hegaret, B. Bailleul, Allelochemicals of Alexandrium minutum: Kinetics of membrane disruption and photosynthesis inhibition in a co-occurring diatom, Harmful Algae, 103 (2021) 101997.
[42] P. Joliot, A. Joliot, Quantification of the electrochemical proton gradient and activation of ATP synthase in leaves, Biochim. Biophys. Acta Bioenerg., 1777 (2008) 676-683.
[43] F. Buchert, B. Bailleul, T. Hisabori, A gamma-subunit point mutation in &ITChlamydomonas reinhardtii &ITchloroplast F1Fo-ATP synthase confers tolerance to reactive oxygen species, Biochim. Biophys. Acta Bioenerg., 1858 (2017) 966-974.
[44] P. Bennoun, Chlororespiration Revisited - Mitochondrial-Plastid Interactions In Chlamydomonas, Biochim. Biophys. Acta Bioenerg., 1186 (1994) 59-66.
[45] B. Bailleul, N. Berne, O. Murik, D. Petroutsos, J. Prihoda, A. Tanaka, V. Villanova, R. Bligny, S. Flori, D. Falconet, A. Krieger-Liszkay, S. Santabarbara, F. Rappaport, P. Joliot, L. Tirichine, P.G. Falkowski, P. Cardol, C. Bowler, G. Finazzi, Energetic coupling between plastids and mitochondria drives CO2 assimilation in diatoms, Nature, 524 (2015) 366-369.
[46] X. Johnson, J. Alric, Central Carbon Metabolism and Electron Transport in Chlamydomonas reinhardtii: Metabolic Constraints for Carbon Partitioning between Oil and Starch, Eukaryot. Cell, 12 (2013) 776-793.
[47] V.V. Terentyev, A.K. Shukshina, A.A. Chetverkina, Action of 2,6-Dichloro-1,4-benzoquinone on the O-2-Evolving Activity of Photosystem II in Chlamydomonas reinhardtii Cells with and without Cell Wall: Inhibitory Effect of Its Oxidized Form, Cells, 12 (2023).

[48] L. Dow, F. Stock, A. Peltekis, D. Szamosvari, M. Prothiwa, A. Lapointe, T. Bottcher, B. Bailleul, W. Vyverman, P.G. Kroth, B. Lepetit, The Multifaceted Inhibitory Effects of an Alkylquinolone on the Diatom Phaeodactylum tricornutum, ChemBioChem, 21 (2020) 1206-1216.
[49] T.K. Baikie, L.T. Wey, J.M. Lawrence, H. Medipally, E. Reisner, M.M. Nowaczyk, R.H. Friend, C.J. Howe, C. Schnedermann, A. Rao, J.Z. Zhang, Photosynthesis re-wired on the pico-second timescale, Nature, 615 (2023) 836-840.

SUPPORTING INFORMATION

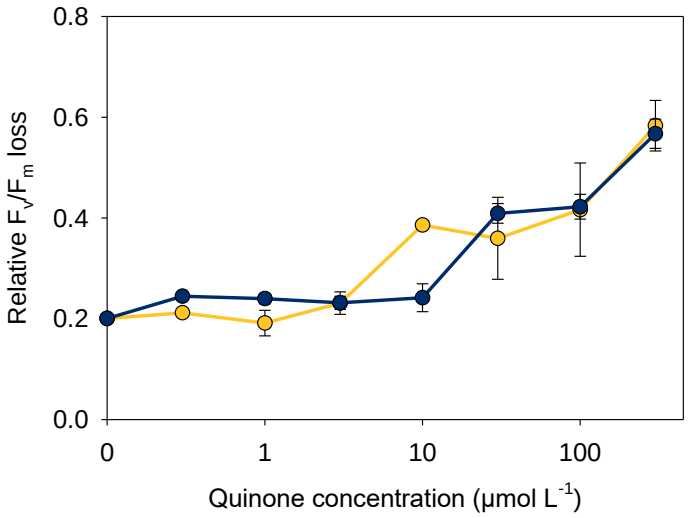

***Figure S1. Chlamydomonas reinhardtii PSII maximal quantum yield (F_v/F_m) loss**. Measured after 40 minutes under actinic light adapted conditions (340 µmol photons m^{-2} s^{-1}) followed by 5 minutes under dark incubation with quinones. The blue circles correspond to 2,6-DMBQ. The yellow circles correspond to 2,6-DCBQ. Data correspond to the mean ± S.D. of five independent biological replicates.*

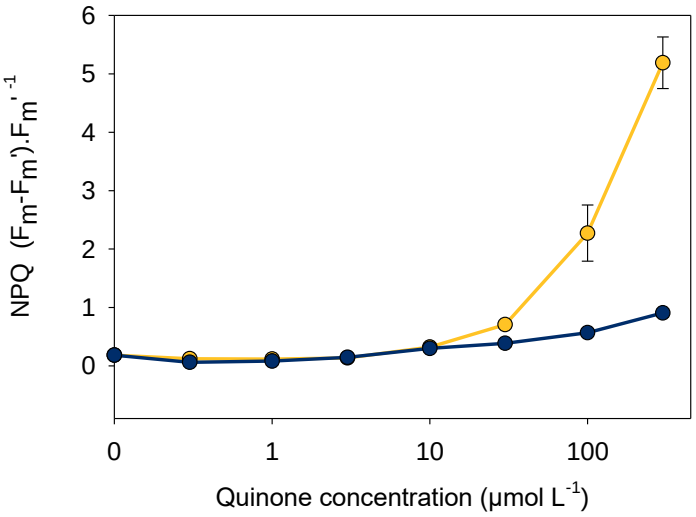

***Figure S2. NPQ measured from Chlamydomonas reinhardtii cells ($2*10^7$ cells mL^{-1}) in the presence and absence of exogenous quinones**. After a few seconds of actinic light (green light; 450 µmol photons m^{-2} s^{-1}), F_m and F_m' were measured in the dark with a saturating pulse in the absence or presence of various quinone concentrations (2,6-DCBQ in yellow; 2,6-DMBQ in blue) respectively. Data are mean ± S.D. of 5 independent replicates.*

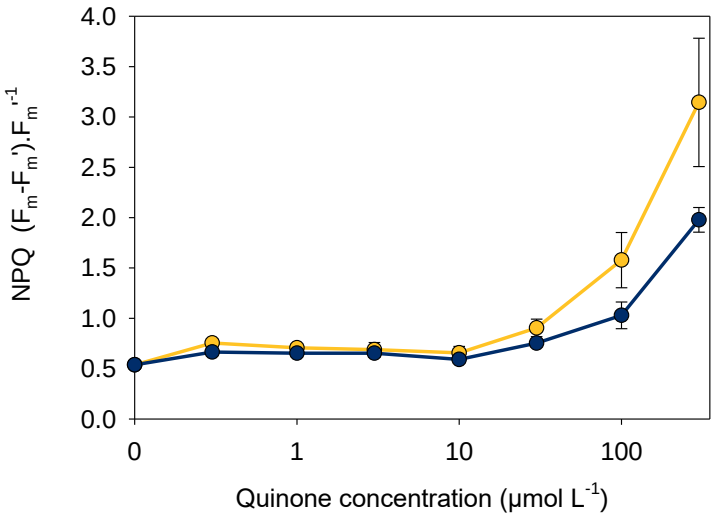

Figure S3. NPQ after long illumination of Chlamydomonas reinhardtii cells (2*10^7 cells mL^{-1}) in the presence and absence of exogenous quinones*. After 40 minutes of illumination with a green actinic light (450 µmol photons m^{-2} s^{-1}), F_m and F_m' were measured in the dark with a saturating pulse in the absence or presence of various quinone concentrations (2,6-DCBQ in yellow; 2,6-DMBQ in blue) respectively. Data are mean ± S.D. of 5 independent replicates.*

GENERAL CONCLUSION

In the course of this work, the effect of exogenous quinones on the photosynthetic chain of the microalga Chlamydomonas reinhardtii was investigated using various analytical methods.

Firstly, photocurrent responses showed that the structure of the harvesting quinone undoubtedly plays a role in its magnitude and stability. In this context, a correlation with the oxidizing power of quinones (standard potential of the reduced quinone/oxidized quinone couple) could be observed over the range of quinones probed. Moreover, the antiproliferative effect of quinones also supports this finding, suggesting that the efficiency of electron diverting and the poisoning effect of quinones belong together. This suggests that equivalences between quinones can be found by adjusting the tandem "E°' vs. concentration". However, other effects can be highlighted, such as NPQ-generating capacity and lipophilicity, which may play a role in performance. It is therefore essential to define as many parameters as possible to describe in detail the effect of a given quinone on the chain.

In this respect, the activity of PSI, downstream of PSII and the b6f complex but upstream of ATP synthase, can provide additional information, especially as the quantum yield of PSI is little altered by NPQ. This analysis, far more challenging than that based on fluorescence measurements for PSII, requires a critical viewpoint in order to set up a reliable and robust procedure.

This is not the only method of analysis, and a detailed look at ATP synthase and respiratory chain activity can, along with the other parameters mentioned above, give rise to a "corpus" of key parameters providing an overall view (with desired vs undesired effects) of quinones with regard to their impact on the photosynthetic chain. Thus, by means of two model quinones, one with a high redox potential (2,6-DCBQ) and the other with a moderate redox potential (2,6-DMBQ), it was possible to suggest a global, concentration-dependent effect of the quinone, which would inhibit the b6f complex and have a dual effect on the photosynthetic and respiratory chains.

On the basis of only two quinones, it is not meaningful to make these results general, as they need to be verified and then extended to other, judiciously chosen structures. It raises the question of the most encouraging structure knowing that other parameters including lipophilicity can play a role. For instance, unpublished data treatement from NPQ measurements evidenced a possible correlation between the partition coefficient P (i.e. $[Q]_{octanol}/[Q]_{water}$) with the « lost » quinone concentration C_{sat} or the pseudo-partition coefficient k’.

$$k' = \frac{C_{quinones,\text{lost}}}{C_Q} \qquad C_{sat} = \frac{n_{quinones,membranes,\max}}{V_{total}}$$

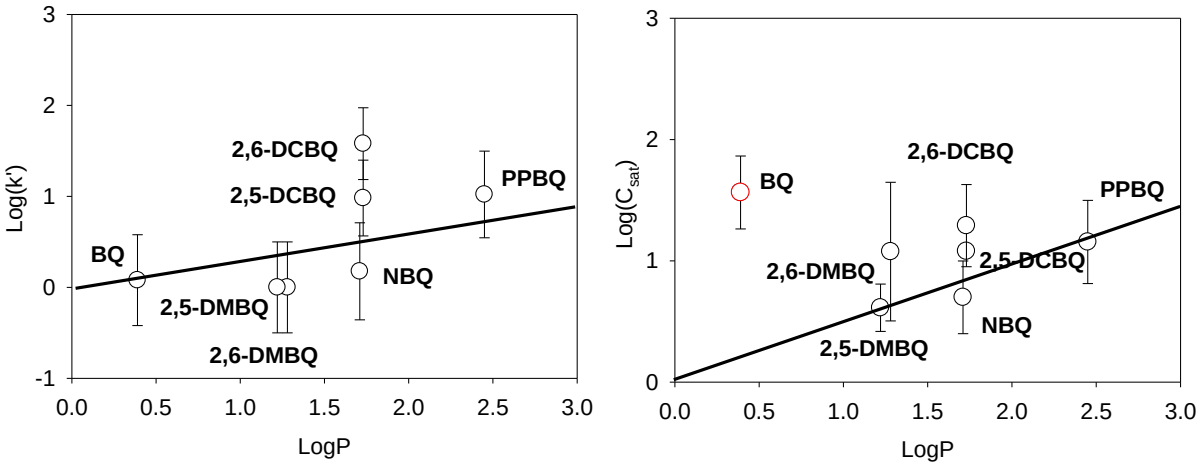

Correlation between theoretical logP values and parameters calculated from NPQ measurements (left : k' ; right : C_{sat}) for different quinones in presence of ΔPetA Chlamydomonas reinhardtii algae.

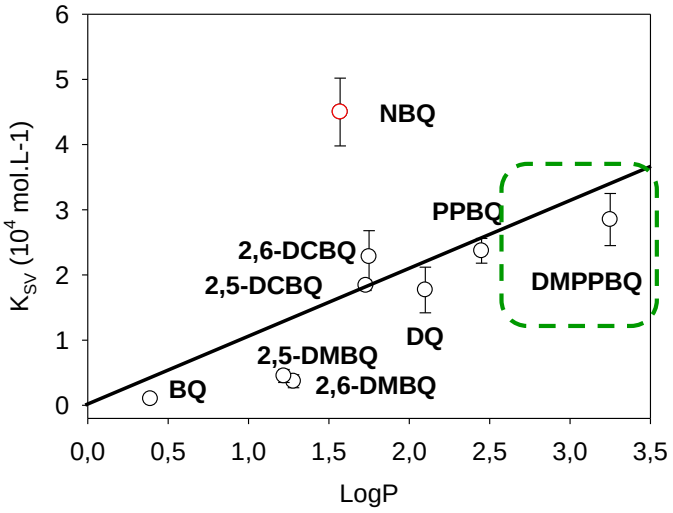

Correlation between theoretical logP values and the Stern-Volmer's constant calculated from NPQ measurements (left : k' ; right : C_{sat}) for different quinones in presence of ΔPetA Chlamydomonas reinhardtii algae. DMPPQ is to date the best compromise is outlined in green.

Assuming that « P » a relevant parameter in this case, the results are globally consistent with quinone lipophilicities so the most lipophilic quinones are good quenchers as well and are preferably sequestered in cell compartments. All the required parameters to describe the interactions of a quinone towards the photosynthetic chain are summarized below.

What should be a quinone ID ?

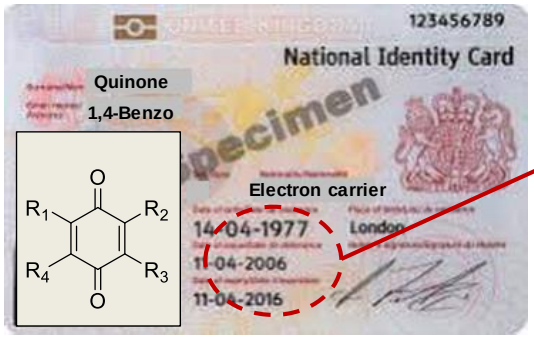

- Redox potential (Q^{-}/Q ? QH_2/Q ? QH/Q ?)
- Log P (Q and QH_2)
- Steric hindrance / Michael acceptor (Y/N)
- NPQ
- Size
- Stability
- ATP Synthase
- Respiratory chain
- PSII

Representative scheme of all the values that should be required to define the « ID » or fingerprint of quinone interactions towards the photosynthetic chain.

The use of computational methods to predict the lipophilicity, standard potential of quinones, electrophilicity or steric hindrance (and even by means of artificial intelligence), will undoubtedly contribute to a judicious pre-selection of quinones to target. On the long term, having brought close to the question of the ideal quinone for entire *Chlamydomonas* cells, leads to discussing the ways for the fabrication of the entire fuel cell. The nature of the cathode, the anode, the mediator and other suitable organisms needs further discussion. But more particularly, the choice of the appropriate photosynthetic organism still remains under debate. For instance, cyanobacteria have less membranes to cross than microalgae, which would favor the entry and exit of mediators. Conversely, in the case of cyanobacteria, the respiratory and photosynthetic chains are much more closely connected (common complex) than a simple exchange of ATP, which could suggest more pronounced deleterious effects of quinones.

In this regard, a new way could be reached by both considering changes of mediators and living organisms. In this way, nitrite anions are secreted by diatoms under high light conditions. This opens up an interesting pathway, originally conceived by Fabrice Rappaport at IBPC, since in this case exogenous nitrate anions can be reduced to nitrite via an excess of electrons from another pathway than the already established PSII pathway, that is, an excess of PSI electrons. This does not exclude the study of other organisms, such as algae without cell walls, *Chlamydomonas* mutants and thylakoid and chloroplast subunits available in the IBPC collection, which could also be interesting to explore.

RÉSUMÉ

La stratégie consistant à utiliser la chaîne photosynthétique comme convertisseur de la lumière en électricité est un espoir pour basculer vers des énergies adaptées aux besoins humains respectueux de l'environnement. A cet égard, il existe deux façons de procéder soit en s'inspirant du principe de la photosynthèse et créer ex nihilo une photopile soit en utilisant les organismes photosynthétiques vivants et en déviant le flux électronique parcourant la chaîne photosynthétique.

Ce travail s'intéresse à la seconde option et met en jeu des microalgues modéles *Chlamydomonas reinhardtii*. L'idée est d'opérer en présence de quinones comme médiateurs redox qui peuvent alors jouer le rôle de navettes d'électrons entre les algues et une électrode collectrice. Si les quinones sont effectivement capables de jouer ce rôle, de nombreux effets indésirables semblent limiter les performances d'un tel système en termes d'intensité et de stabilité du photocourant.

C'est pourquoi ce travail sera consacré à une étude de type structure-activité de différentes quinones en lien avec leurs performances de photocourant. Le photocourant n'est cependant que l'observable d'un phénomène global et complexe et c'est pourquoi, à travers deux quinones modèles, les interactions plus spécifiques avec la chaîne photosynthétique (PSII, PSI, ATPsynthase) mais aussi la chaîne respiratoire, seront étudiées et discutées.

ABSTRACT

The idea of using the photosynthetic chain as a converter of light into electricity is a hopeful way of switching to environmentally-friendly energies adapted to human needs. In this respect, there are two approaches: either by building on the principle of photosynthesis and creating a solar cell ex nihilo, or by using living photosynthetic organisms and diverting the electron flow through the photosynthetic chain.

This work focuses on the second possibility, using *Chlamydomonas reinhardtii* model microalgae. The idea is to use quinones as redox mediators, which can then act as electron shuttles between the algae and a collecting electrode. While quinones are indeed suitable for this role, a number of side effects appear to limit the performance of such a system in terms of photocurrent intensity and stability.

This work will therefore focus on a structure-activity analysis of various quinones in relation to their photocurrent performance. Photocurrent, however, is only the observable of a global and complex phenomenon, and this is why, through two model quinones, the more specific interactions with the photosynthetic chain (PSII, PSI, ATPsynthase) but also the respiratory chain, will be studied and discussed.